Factors Affecting Glucose Uptake in Tissue-engineered Human Skeletal Muscle

by

Megan Elizabeth Kondash

Department of Biomedical Engineering
Duke University

Date:_____

Approved:

_____
George A. Truskey, Supervisor

_____
Nenad Bursac

_____
David Katz

_____
Timothy Koves

_____
William Kraus

Dissertation submitted in partial fulfillment of
the requirements for the degree of Doctor
of Philosophy in the Department of
Biomedical Engineering in the Graduate School
of Duke University

2019

ABSTRACT

Factors Affecting Glucose Uptake in Tissue-engineered Human Skeletal Muscle

by

Megan Elizabeth Kondash

Department of Biomedical Engineering
Duke University

Date:_____

Approved:

_____
George A. Truskey, Supervisor

_____
Nenad Bursac

_____
David Katz

_____
Timothy Koves

_____
William Kraus

An abstract of a dissertation submitted in partial fulfillment of the requirements for the degree of Doctor of Philosophy in the Department of Biomedical Engineering in the Graduate School of Duke University

2019

Copyright by
Megan Elizabeth Kondash
2019

Abstract

Tissue-engineered skeletal muscle myobundles offer a promising approach for developing a human *in vitro* model of healthy and diseased muscle for drug development and testing. Their three-dimensional structure offers a better model of the organization of native skeletal muscle than monolayer culture does, and their amenability to an array of functional measures provides a multifaceted account of the tissue's health. One such functional measure is the metabolic state of the myobundle, which in an *in vitro* model of healthy skeletal muscle should reflect the metabolism of native muscle. However, skeletal muscle cultured *in vitro* is exposed to artificially high levels of nutrients meant to promote cell growth, and it exhibits altered glucose uptake, with high rates of glycolysis and a dampened insulin response. Inflammation is closely linked with skeletal muscle metabolic dysfunction, and the field could benefit from a human tissue-engineered myobundle model of inflammation to elucidate mechanisms of disease progression and to examine drug safety and efficacy in inflamed muscle.

We first characterized the glucose uptake and insulin response of tissue-engineered myobundles in the basal state and in response to treatment with metformin and an HDAC inhibitor. We then imparted greater physiological relevance to the system via altered culture conditions and examined the impact on myobundle metabolic and contractile function. Finally, we validated the ability of pro-inflammatory cytokine

exposed-myobundles to recapitulate key aspects of inflammation-mediated skeletal muscle dysfunction.

We found that myobundles exhibit insulin sensitivity similar to that of *in vivo* skeletal muscle, but insulin responsiveness is substantially lower, in accordance with other *in vitro* studies. Metformin treatment stimulated a robust increase in basal glucose uptake, and treatment with the HDAC inhibitor 4-PBA enhanced myobundle contractile function and insulin responsiveness. We showed that altering myobundle culture conditions to provide more physiologic nutrient availability was sufficient to metabolically reprogram the myobundles to a less glycolytic state. To model an inflammation-mediated disease state, we exposed myobundles to pro-inflammatory cytokines and found that the inflamed myobundles exhibited contractile dysfunction, a robust secretion of pro-inflammatory cytokines, and increased basal glucose uptake while still retaining a functional response to metformin treatment. Overall, this work validates the suitability of a tissue-engineered skeletal muscle model for detecting metabolic perturbations mediated by drug treatment, nutrient availability, and inflammatory conditions.

Dedication

I dedicate this dissertation to my family.

Contents

Abstract iv

List of Tables xiii

List of Figures xiv

Acknowledgements xvii

1. Introduction 1

1.1 Background and significance 1

1.1.1 Microphysiological systems 1

1.1.2 Skeletal muscle function 4

1.1.2.1 Contractile force production 4

1.1.2.2 Fiber types 6

1.1.2.3 Metabolism 9

1.1.3 Inflammation in skeletal muscle 12

1.1.3.1 Role of inflammation in skeletal muscle regeneration 12

1.1.3.2 Chronic inflammation-associated skeletal muscle dysfunction 13

1.1.4 Tissue-engineered skeletal muscle 17

1.1.4.1 Cell source considerations 18

1.1.4.2 Scaffolding and extracellular matrix 24

1.1.4.3 Optimizing tissue-engineered skeletal muscle force production 27

1.1.4.4 Expanding the relevance of the tissue-engineered muscle model 33

1.1.4.5 Metabolism 35

1.2 Specific aims and hypotheses 41

2. Glucose Uptake and Insulin Response in Tissue-engineered Human Skeletal Muscle 43

2.1 Introduction 43

2.2 Materials and Methods 44

2.2.1 Isolation and monolayer culture of primary myoblasts and myotubes 44

2.2.2 Myobundle formation and culture 46

2.2.3 Media-based glucose uptake assay 47

2.2.4 2-deoxyglucose uptake quantification assay 48

2.2.5 EC_{50} curve fitting 49

2.2.6 Contractile function measurements 49

2.2.7 Electrical stimulation 50

2.2.8 Drug and inhibitor treatment 51

2.2.9 qRT-PCR 51

2.2.10 Normalization and statistical analysis 52

2.3 Results 53

2.3.1 Media-based glucose uptake assay 53

2.3.2 2-deoxyglucose uptake assay 55

2.3.3 Effect of lowering amino acid and insulin content 60

2.3.4 Effect of treatment with metformin on myotube and myobundle 2-DG uptake 62

2.3.5 Characterization of myobundle insulin response 64

2.3.6 Effect of electrical stimulation on myobundle 2-DG uptake 66

2.3.7 Effect of altered ECM content on myobundle 2-DG uptake 68

2.3.8 Effect of altered culture conditions on myobundle 2-DG uptake 69

2.3.9 Effect of Akt and HDAC inhibitors on myotube and myobundle 2-DG uptake and contractile function 72

2.4 Discussion 77

2.5 Conclusions 86

2.6 Chapter acknowledgements 87

3. Low Amino Acid and Growth Factor Reduced Conditions Promote a Metabolic Shift in Tissue-engineered Human Skeletal Muscle 88

3.1 Introduction 88

3.2 Materials and Methods 91

3.2.1 Primary human myogenic cell isolation and culture 91

3.2.2 Formation and culture of myobundles 92

3.2.3 Contractile force and kinetics measurement 92

3.2.4 Quantification of 2-deoxyglucose (2-DG) uptake 93

3.2.5 Immunofluorescence staining of 3D myobundles 94

3.2.6 Nuclei quantification assay 95

3.2.7 L-lactate quantification assay 95

3.2.8 Seahorse XFe24 metabolic phenotype assay 95

3.2.9 qRT-PCR 96

3.2.10 Statistical analysis 97

3.3 Results 98

3.3.1 Effect of LAAGFR conditions on myobundle 2-DG uptake at two weeks post-differentiation and time course studies 98

3.3.2 Effect of LAAGFR conditions on myobundle 2-DG uptake and cell quantity at one week post-differentiation 101

3.3.3 Analysis of individual variable effects 102

3.3.4 Characterization of metabolic phenotype of myobundles cultured in LAAGFR and Baseline conditions 104

3.3.5 Gene expression of myobundles cultured in LAAGFR and Baseline conditions 108

3.3.6 Contractile function of myobundles cultured in LAAGFR and Baseline conditions 111

3.4 Discussion 113

3.5 Conclusions 117

3.6 Chapter acknowledgements 117

4. A Tissue-engineered Human Skeletal Muscle Model of Inflammation 119

4.1 Introduction 119

4.2 Materials and Methods 121

4.2.1 Isolation of primary cord blood-derived monocytes and differentiation to monocyte-derived macrophages (MDM) 121

4.2.2 Polarization of MDMs in 2D culture 122

4.2.3 Flow cytometry 123

4.2.4 Immunofluorescence in 2D cultures and 3D myobundles 123

4.2.5 Isolation and culture of primary myoblasts 124

4.2.6 Myobundle formation and culture 125

4.2.7 Contractile function measurements 126

4.2.8 Cytokine arrays 127

4.2.9 2-deoxyglucose uptake quantification assay 128

4.2.10 Statistical analysis 129

4.3 Results 129

4.3.1 Optimization of differentiation conditions for monocyte-derived macrophages 129

4.3.2 Polarization of MDMs to a pro-inflammatory state using LPS and IFNγ 132

4.3.3 Polarization of MDMs to a pro-inflammatory state using TNFα and IFNγ 134

4.3.4 Impact of un-polarized MDMs on myobundle function 135

4.3.5 Polarization of MDM myobundles with LPS and IFNγ at one week post-differentiation 135

4.3.6 Polarization of MDM myobundles with LPS, IFNγ, and TNFα at ten days post-differentiation 142

4.3.7 Polarization of MDM myobundles with TNFα and IFNγ to model sterile inflammation 144

4.3.8 Inflammatory cytokine treatment of myobundles without MDMs using GM-CSF, TNFα, and IFNγ to model sterile inflammation 147

4.3.9 Treatment of inflammatory cytokine-treated myobundles with metformin 156

4.4 Discussion 160

4.5 Conclusions 167

4.6 Chapter acknowledgements 167

5. Conclusions 169

5.1 Key findings 169

5.2 Dissertation summary 170
5.3 Future directions 173
Appendix A: Protocol for myogenic cell isolation from surgical waste sample 176
Appendix B: Protocol for standard size myobundle formation 180
Appendix C: Custom low amino acid base media formulation 187
Appendix D: Protocol for preparing custom low amino acid base media formulation 189
Appendix E: LAAGFR and Baseline complete media formulations 191
Appendix F: Protocol for 2-deoxyglucose uptake quantification assay 192
Appendix G: Protocol for immunostaining myobundles 199
Appendix H: Protocol for nuclei quantification of myobundles 201
Appendix I: Protocol for preparing myobundles for 96-well plate 206
Appendix J: Protocol for Seahorse measurements using myobundles for 96-well plate 207
Appendix K: Protocol for preparing myobundles for cryosectioning 213
Appendix L: Protocol for isolation of CD14+ monocytes from umbilical cord blood 216
Appendix M: Protocol for staining macrophages for flow cytometry 224
References 226
Biography 265

List of Tables

Table 1. Primer sequences used for qRT-PCR. 52

Table 2. Primer sequences used for qRT-PCR. 97

Table 3. Baseline and LAAGFR culture conditions. 98

Table 4. Components of the base DMEM, αMEM, and LAA media compared with plasma amino acid reference values[273]. 104

Table 5. Flow cytometry analysis of time course of macrophage marker expression by MDMs derived using M-CSF and GM-CSF. 130

Table 6. Flow cytometry analysis of macrophage marker expression by MDMs differentiated using 10 and 50 ng/mL GM-CSF. 131

Table 7. Flow cytometry analysis of macrophage marker expression by adherent and non-adherent MDMs. 131

Table 8. Flow cytometry analysis of macrophage marker expression by un-polarized MDMs and MDMs polarized using LPS and IFNγ 133

Table 9. Flow cytometry analysis of macrophage marker expression by MDMs polarized using TNFα and/or IFNγ. 134

Table 10. Compiled cytokine response by pro-inflammatory cytokine-treated myobundles without MDMs. 153

Table 11. Effect of inflammatory cytokine treatment on myobundle insulin responsiveness. 156

Table 12. Custom low amino acid (LAA) base media formulation compared to DMEM and α-MEM. 187

Table 13. LAAGFR and Baseline complete media formulations 191

List of Figures

Figure 1. Media-based assay for measuring glucose uptake. 55

Figure 2. 2-deoxyglucose-based assay for measuring glucose uptake. 56

Figure 3. 2-DG uptake quantification assay optimization and validation. 60

Figure 4. Effect of lowering amino acid and insulin content. 61

Figure 5. Effect of metformin treatment on myotubes in monolayer culture and myobundles. 63

Figure 6. Characterization of insulin sensitivity and dose response in myobundles. 65

Figure 7. Effect of electrical stimulation on 2-DG uptake and insulin response. 67

Figure 8. Effect of altering ECM components on myobundle function 69

Figure 9. Effect of altering media components and culture conditions on basal and insulin-mediated 2-DG uptake 71

Figure 10. Effect of Akt inhibitor on basal and insulin-mediated 2-DG uptake by myobundles. 72

Figure 11. Effect of the specific HDAC4 and 5 inhibitor LMK235 on basal and insulin-mediated 2-DG uptake by myotubes. 74

Figure 12. Effect of the general HDAC inhibitor 4-PBA on 2-DG uptake and contractile function 76

Figure 13. Compilation of insulin responsiveness in 2-D and 3-D. 86

Figure 14. Basal 2-DG uptake in myobundles cultured in LAAGFR or Baseline conditions, tested at 2 weeks post-differentiation. 99

Figure 15. Time course of 2-DG uptake and contractile function of myobundles. 100

Figure 16. Myobundles cultured in LAAGFR conditions exhibit decreased basal glucose without differences in cellularity. 101

Figure 17. Amino acid content of the base media is primarily responsible for lowered basal glucose uptake. 103

Figure 18. Myobundles cultured in LAAGFR conditions exhibit shift toward decreased glycolysis. 106

Figure 19. Positive correlation of 2-DG uptake rates and L-lactate production. 107

Figure 20. Miniaturized myobundles used for Seahorse testing. 107

Figure 21. LAAGFR formulation and culture conditions are linked to decreased glucose transporter expression. 109

Figure 22. Gene expression of myosin heavy chain isoforms. 111

Figure 23. Myobundles cultured in LAAGFR conditions exhibit functional changes in fatigue resistance, without an impact on tetanic force production or twitch kinetics. 113

Figure 24. Expression of the M1 marker CD80 after polarization with LPS and IFNγ 133

Figure 25. Impact of non-polarized MDMs on contractile function of myobundles. 135

Figure 26. Impact of polarization with LPS and IFNγ on contractile function of MDM myobundles tested at 7 days post-differentiation. 137

Figure 27. Cytokine concentrations in the media of MDM myobundles. 141

Figure 28. Impact of polarization with LPS and IFNγ and TNFα on contractile function of MDM myobundles tested at 10 days post-differentiation. 143

Figure 29. Impact of polarization with IFNγ and TNFα on contractile function and sarcomeric structure of MDM myobundles tested at 10 days post-differentiation. 146

Figure 30. Impact of treatment with GM-CSF and IFNγ and TNFα on contractile function and sarcomeric structure of myobundles without MDMs tested at 10 days post-differentiation. 149

Figure 31. Cytokine concentrations in the media of myobundles treated with GM-CSF, IFNγ, and TNFα. 152

Figure 32. Effect of inflammatory cytokine treatment on 2-DG uptake by myobundles. 155

Figure 33. Effect of metformin treatment on contractile function of inflamed myobundles. 157

Figure 34. Effect of metformin on 2-DG uptake by inflamed myobundles. 159

Acknowledgements

I would like to communicate my gratitude to Dr. George Truskey for giving me the opportunity to join his lab, and for his teaching, support, insight and mentorship. With his guidance, I have learned a great deal about carrying out solid, well-considered scientific investigation. I thank Dr. Kam Leong for his kind mentoring. I am grateful to the members of my committee, Dr. Nenad Bursac, Dr. David Katz, Dr. Tim Koves, and Dr. William Kraus for their feedback and guidance during my time at Duke.

I would like to recognize my colleagues for their support and help with scientific questions as well as contributions towards a positive environment in the lab. Specifically, I want to thank my direct collaborators, Anandita Ananthakumar, Catherine Oliver, Dr. Brittany Davis, Dr. Xu Zhang, Samantha Lasater, Varun Prasad, Dr. Lauran Madden, Kendall Liang, and Dr. Smruthi Suryaprakash. Finally, I would like to acknowledge the 3,348 myobundles that made this work possible.

I thank my parents, Bruce and Janice, for their support and guidance throughout my life and during my time at Duke. Their advice and perspective gave me the momentum to carry on during challenging times.

I am incredibly grateful to my husband AJ for his constant, unwavering support during our time in graduate school. He has accompanied me for countless late-night lab trips, acted as my practice audience and editor, and can spout off terms including 'fibrinogen', '2-deoxyglucose', and 'sarcomeric alpha-actinin' like nobody's business.

1. Introduction

Portions of this chapter were previously published in the following form and are re-used here with permission from the publisher: Kondash, M.E., Davis, B.N.J., Truskey, G.A. 2017. Optimizing 3D Models of Engineered Skeletal Muscle. Engineering 3D Tissue Test Systems. K.J.L. Burg, D. Dreau and T. Burg. Boca Raton, FL, CRC Press, 321-350 doi: 10.1201/9781315118260-19[1].

1.1 Background and significance

1.1.1 Microphysiological systems

The drug discovery pipeline is an expensive and inefficient process, with each new drug coming at the cost of $1.8 billion[2] and accompanied by high rates of attrition during clinical trials. A drug in phase 1 clinical trials has only a 10.4% chance of reaching FDA approval, and only 50% of drugs which reach phase 3 clinical trials are eventually approved[3]. This high rate of late-stage attrition in phase 3 trials is especially costly and is due primarily to efficacy issues[3]. If attrition could be reduced by using improved pre-clinical methods, the average cost per new drug could be dramatically lowered, sustaining continued drug innovation.

Microphysiological systems (MPS) include organoids, which are three-dimensional tissue-engineered constructs which are designed to replicate certain key functional aspects of organs[4,5]. Their purpose is to provide an *in vitro* platform for testing drug safety and efficacy that better recapitulates *in vivo* physiology than do standard *in*

vitro cell cultures grown in two dimensional cultures, thereby improving the quality of pre-clinical data[6]. Whereas two-dimensional cell cultures typically feature one cell type grown on a plastic surface, three-dimensional MPS offer organ-like structures with cell-cell and cell-ECM interactions and frequent incorporation of more than one cell type. Examples of organs being modeled for drug testing using three-dimensional MPS functional units include skeletal muscle[7,8], vasculature[9], liver[10], kidney[11], and brain[12]. In contrast to two-dimensional *in vitro* culture systems, MPS offer tissue-level functional measures that can serve as markers of tissue health and they provide a more complex system in which to examine drug effects, while still maintaining the ability to tightly regulate the system.

Microphysiological systems constructed using human cells also offer an advantage over *in vivo* pre-clinical animal models. Rodents and other species do not provide an entirely accurate model of human function. For example, there is a poor correlation between the expression of mouse and human genes following an acute inflammatory stress, which can have an impact on liver-specific drug metabolism[13]. Further, there are known immunological signaling pathway discrepancies between the two species[14]. Interspecies differences in function play a role in the appearance of unexpected side effects of drugs during clinical trials.

In the case of some drugs, animal models have failed to predict drug-induced mitochondrial toxicity that occurs once the drug is in clinical trials[15]. A specific example

of the potential for varied drug responses across species is evident in the screening process of cerivastatin. Cerivastatin is a synthetic statin that is structurally distinct from previously-approved 'natural' fermentation-derived statins produced as secondary metabolites of fungi[16,17]. In pre-clinical animal trials, cerivastatin exhibited widely variable species-dependent side effects that were largely attributed to interspecies differences in metabolism of the drug. Despite a high sensitivity of dogs to the drug, it was determined to be safe for humans at therapeutic levels[18]. Once on the market, cerivastatin caused rhabdomyolysis, severe or fatal breakdown of skeletal muscle tissue, in a small percentage of patients[16,] potentially due to statin-induced ubiquinone deficiency in the muscle leading to defects in cellular respiration[18]. Rhabdomyolysis was notably observed in patients who were concurrently undergoing treatment with gemfibrozil, which increases the plasma concentration of cerivastatin[19], or in those receiving the highest approved dose of cerivastatin[20]. This incident underlines the species-dependent response that a drug may elicit, drug-drug interactions, and the resulting uncertainty about which results to apply to potential human responses, strengthening the argument for the use of human cells for screening studies.

When engineered human myobundles were cultured with either cerivastatin or lovastatin (a statin that has not caused safety concerns and remains on the market), the engineered muscle exhibited toxicity to cerivastatin at doses 100x less than those at which lovastatin toxicity was observed, a result that is in accord with clinical reports[7].

Importantly, engineered human muscle provides a drug screening platform that enables testing of drugs and drug interactions on the same patient, to determine which treatment regimens will yield the highest safety and efficacy for that particular patient.

Microphysiological systems are also useful for disease modeling in specific organs. These platforms offer a distinct advantage over disease state modeling in two-dimensional culture due to their functional capacity. They are especially useful for modeling rare diseases in which there is a limited patient population, constraining the potential for clinical trials. Diseases that have been modeled using MPS made from patient-derived cells include Hutchinson-Gilford Progeria Syndrome[21] and Timothy Sydrome[22]. Alternatively, disease models can be created by inducing a disease state in healthy tissue, which can be useful for studying disease progression.

Skeletal muscle is responsible for movement and force generation in the human body, comprises nearly 40% of the body's total mass[23], and is exposed to drugs in the blood stream as a result of its rich vascular network[24]. As such, it is a highly relevant organ for modeling using microphysiological systems, which must recapitulate certain crucial aspects of *in vivo* muscle function.

1.1.2 Skeletal muscle function

1.1.2.1 Contractile force production

Structurally, skeletal muscle consists of muscle fibers surrounded by connective tissue, called the endomysium. Muscle fibers are bundled in parallel into structures

called fascicles. These fascicles are also surrounded by connective tissue, called the perimysium, and transmit force production to joints via tendons. Each muscle fiber is the product of multiple myogenic cells fusing to form one multinucleated cell, within which exist thousands of the contractile functional unit of muscle, the sarcomere. Each sarcomere is approximately 3 μm in length[25] and is composed of two major proteins, myosin (thick filament) and actin (thin filament). At the level of the sarcomere, according to the sliding filament theory, contraction occurs when the actin slides past the myosin, thereby shortening the sarcomere[26]. According to the cross-bridge theory[27], when calcium is released from the sarcoplasmic reticulum in response to a stimulus such as an action potential from a motor neuron, it attaches to troponin, causing a conformational change that moves tropomyosin, exposing the actin binding site for the myosin head. The energy from the release of the inorganic phosphate group formed when the ATP was hydrolyzed enables the myosin head to bind more strongly to the actin, and the release of the ADP allows it to pivot, pulling the actin with it. More ATP must bind to the myosin head and be hydrolyzed to allow it to release the actin and change its conformation to begin the cycle again. This myosin-actin cycling results in sarcomere shortening and muscle contraction[28]. The pace of this cycling process relies on the speed at which the ATPase can hydrolyze ATP. The cycle ends when calcium is sequestered back within the sarcoplasmic reticulum and the myosin-binding sites are no longer exposed.

Skeletal muscle exhibits a force-length relationship whereby force production is dependent on the level of overlap between the actin and myosin filaments. Maximal force production occurs at an ideal length of the sarcomere at which there is maximal overlap of actin and myosin. If the sarcomere is longer or shorter, there are portions of the myosin filament which cannot form cross-bridges[29].

The type of stimulus which the skeletal muscle receives determines the type of contraction produced. A single stimulus will produce a single contraction, called a twitch contraction. If another stimulus is applied before the muscle has relaxed, the contractions will sum, and as more stimuli are applied, the muscle eventually produces a tetanic contraction, in which the muscle is producing maximal force and does not produce more force regardless of additional stimuli. With continued stimulation, the force output of the muscle begins to decline, a phenomenon known as high-frequency fatigue[30]. Fatigue has a variety of proposed contributors, including impaired calcium release and sensitivity with sustained contraction[31,32], depletion of ATP[33], and production of reactive oxygen species (ROS)[34].

1.1.2.2 Fiber types

Skeletal muscle is composed of a range of fiber types, characterized functionally by differences in metabolic and contractile phenotypes which make each fiber type more suitable for a certain type of movement. Broadly, type II fast twitch fibers are responsible for quick, strong contractions such as jumping, while type I slow twitch

fibers are used for long-term less energy-intensive processes such as maintaining posture. It is important to note that despite detailed classification parameters, skeletal muscle phenotypes do not fall into distinct categories; muscle fibers are heterogeneous and are often hybrids which co-express multiple MHC isoforms, creating a spectrum of contractile and metabolic properties[35]. It is also possible for changes in metabolic phenotype to occur without changes in contractile properties[36]. However, for the sake of clarifying differences in fiber type properties, we will focus on defining adult fiber types as type I, type IIA, and type IIX. The fiber type IIB has been observed in other mammals, but not in humans[37]. Type I fibers containing MHC encoded for by the MYH7 gene, type IIA fibers contain MHC encoded for by the MYH2 gene, and type IIX fibers contain MHC encoded for by the MYH1 gene[38].

Type I fibers are typically characterized in terms of contractile function by lower maximum force output, low ATPase activity leading to slower contraction kinetics[39,40], and greater fatigue resistance due to lower ATP expenditure during contraction[36]. The contractile function of type I fibers corresponds to the metabolic properties of the fibers. Type I fibers exhibit the highest levels of mitochondrial content and oxidative enzymes, and use oxidative metabolism of glucose and fatty acids to produce the ATP needed to supply their energy demands[41]. Type I fibers are additionally characterized by the smallest fiber diameter[42]. Type IIX fibers represent the opposite end of the spectrum; they exhibit high maximum force production, high ATPase activity which leads to fast

contraction kinetics[39,40], and are the least fatigue resistant of the fiber types. Type IIX fibers have a high glycolytic enzyme presence which allows them to produce ATP through glycolysis at a faster rate than type I fibers. Type IIA fibers have similar contraction kinetics as type IIX fibers[39,40], but have a greater mitochondrial content than type IIX fibers and fatigue resistance comparable to that of type I fibers, with a metabolic phenotype intermediate to that of type I and type IIX[36]. Glycogen content is greater in fast twitch fibers[43] and lipid content is greater in slow twitch fibers[44], reflecting the differences in ATP production methods in the two fiber types.

When the fiber type composition of the vastus lateralis in humans was measured, it was found to be 50-55% type I fibers, 30-35% type IIA fibers, and 10-20% type IIX fibers[45]. There is a great deal of plasticity in fiber type, with shifts in fiber type enrichment resulting from exercise[46,47], and disease[48].

In addition to those that are prevalent in adult skeletal muscle, certain myosin heavy chain isoforms are only expressed during development and muscle fiber regeneration[49]. These include MYH3-encoded embryonic MHC and MYH8-encoded neonatal MHC. During early development in humans, embryonic, perinatal, and type I fibers are all present in primary generation fibers[50], with secondary generation fibers expressing only embryonic and neonatal isoforms[51]. Prior to birth, the expression of embryonic and neonatal isoforms declines and the type I isoform reemerges[52].

Interestingly, after injury to adult muscle, embryonic and neonatal MHC isoforms are again detectable in regenerating myofibers[53].

1.1.2.3 Metabolism

Glucose uptake and metabolism

Glucose enters skeletal muscle cells primarily via two glucose transporters, GLUT1 and GLUT4, which allow selective movement of glucose down its concentration gradient into the cell. GLUT1 is responsible for constitutive, basal glucose uptake in skeletal muscle and is expressed at relatively low levels[54], while GLUT4 is responsible for insulin- or contraction-stimulated glucose uptake. Type I fibers are responsible for the majority of glucose uptake in the body due to their increased expression of GLUT4[55]. In healthy skeletal muscle, insulin activates the translocation of GLUT4 from an intracellular recycling loop to the plasma membrane. Signaling occurs via insulin binding with the insulin receptor, resulting in tyrosine phosphorylation of insulin receptor substrate-1 (IRS-1) followed by activation of phosphatidylinositol 3-kinase (PI3K) which results in the activation of phosphoinositide-dependent protein kinase 1 (PDK1), leading to phosphorylation of Akt[56]. Akt phosphorylates and inhibits AS160/TBC1D4, which releases GLUT4 vesicles to translocate to the plasma membrane[57].

Alternatively, GLUT4 translocation can be stimulated via contraction-mediated, insulin independent pathways under the control of AMP-activated protein kinase (AMPK)[58]. During prolonged exercise in humans, GLUT4 translocates to the sarcolemma[59], which is coupled with increased glucose uptake[60]. There is evidence that

there are two separate pools of GLUT4; one that responds to insulin stimulation, and another that responds to exercise[61,62], which would explain the additive effects of insulin stimulation and exercise on glucose uptake. When skeletal muscle is trained by consistent exercise, it undergoes several changes that influence glucose metabolism. These include increased GLUT4 expression and increased mitochondrial biogenesis[54], which is likely linked to the fiber type shift from type IIX to type IIA that can occur with endurance and high-intensity resistance training[63,64]. Together, these changes produce in trained muscle an increased oxidative capacity[65] coupled with a greater level of insulin responsiveness[66].

Glucose as a fuel source can be obtained from the bloodstream or from muscle glycogen stores, especially during intense exercise[67]. Once inside the cell, glucose is phosphorylated and undergoes glycolysis to produce pyruvate, resulting in the net production of 2 ATP[68]. At this point, the pyruvate can be converted to lactate as the end-product of anaerobic glycolysis, a process which occurs mostly under exercise conditions in skeletal muscle in the body, when ATP demands are outpacing the rate of oxidative metabolism[69]. Lactate production prevents the buildup of pyruvate from inhibiting further glycolysis and regenerates NAD+[68]. Alternatively, pyruvate can enter the mitochondria, where it is converted to acetyl-CoA and can enter into the TCA cycle, which, coupled to oxidative phosphorylation in the electron transport chain, produces

32 ATP[68]. Glucose metabolism is generally low in skeletal muscle at rest, with fat as the preferred fuel source during resting conditions[70].

Fat metabolism

Energy is derived from fat through the process of oxidative metabolism. Fatty acids are activated to fatty acyl-CoA and transported into the mitochondria, a process enabled by the carnitine shuttle. Once inside the mitochondria, fatty acids undergo β-oxidation to produce acetyl-CoA, which proceeds through the TCA cycle[68]. During the resting state, fat oxidation is responsible for 55-70% of energy production in skeletal muscle[71,72].

Amino acid metabolism

Although skeletal muscle produces the majority of its ATP from carbohydrates and fat[71], protein-based energy production comprises about 5-15% of total energy production[45,73]. Skeletal muscle is responsible for about 50% of the body's branched chain amino acid catabolism[74,75]. Leucine can be converted to acetyl-CoA and undergoes oxidation in the tricarboxylic acid (TCA) cyle[75], while valine is converted into succinyl-CoA and can either be used in the TCA cycle or enter the electron transport chain[76], and isoleucine can be converted to either acetyl CoA or succinyl-CoA[76].

Metabolic flexibility

In the fasted, resting state, skeletal muscle derives the majority of its energy from the oxidation of fat. During low-intensity exercise, free fatty acids remain the primary energy source, with a small increase in the contribution of plasma glucose. As exercise intensity increases, the primary energy source switches to muscle glycogen, with lower

and relatively comparable contributions of plasma glucose, muscle triglycerides, and plasma free fatty acids[71,72]. After a meal, as glucose and insulin levels rise, fuel preferences shift from fat to glucose oxidation to efficiently use available nutrients[77,78]. The ability of skeletal muscle to respond appropriately to external stimuli such as nutrient availability and exercise by switching fuel sources is vital, and dysfunction in this process may be central to the development of insulin resistance[77,79,80].

1.1.3 Inflammation in skeletal muscle

1.1.3.1 Role of inflammation in skeletal muscle regeneration

Immediately after injury, satellite cells, the quiescent muscle progenitor cells that express Pax7 and reside in the satellite cell niche between the sarcolemma and the basal lamina of the muscle fibers, become activated and begin to proliferate. This activated state is associated with the expression of myogenic regulatory factors MyoD and Myf5. A portion of the population continues to express Pax7, eventually downregulating MyoD expression and returning to repopulate the satellite cell niche[81]. However, most of the satellite cells cease to express the satellite cell marker Pax7 and go on to differentiate fully[82].

When skeletal muscle cells are injured, necrosis follows as part of the destruction phase, and the release of intracellular components, such as creatine kinase, into the bloodstream recruits neutrophils and eosinophils to the damaged tissue. Neutrophil numbers slowly decline and phagocytic M1 pro-inflammatory macrophages become the

most prevalent immune cell in the tissue during the repair phase occurring between 24-48 hours post-injury[83], engaging in the phagocytosis of necrotic cells and cellular debris. At around 2 days post-injury, anti-inflammatory M2 macrophages begin to accumulate in the tissue, with numbers peaking at around 4 days post-injury[84]. Immune cells appear to be crucial in muscle repair, as inhibiting macrophage presence in injured muscle impairs the ability of the fibers to regenerate[85,86].

During the early phase of immune response to injury, immune cells produce an array of pro-inflammatory cytokines, including IFNγ and TNFα. These cytokines recruit more immune cells to the site and polarize macrophages to the M1 state. Other cytokines produced during this stage of inflammation include IL-6 and IL-1[84]. In addition to influencing the immune cells themselves, these cytokines play a role in the muscle regeneration process by inducing progenitor cell proliferation. For example, TNFα is a crucial instigator of satellite cell activation, stimulating progression to early differentiation via p38 MAPK activation[87], which induces MyoD expression[88]. IL-6 and IFNγ have also been shown to mediate myoblast proliferation[89,90]. As the repair process progresses, anti-inflammatory M2 macrophages become prevalent and secrete anti-inflammatory cytokines, such as IL-10, which promote myoblast differentiation[85].

1.1.3.2 Chronic inflammation-associated skeletal muscle dysfunction

Metabolic dysfunction

Obesity-associated inflammation involves long-term, low-level immune system activation and is linked to the development of metabolic dysregulation, including

insulin resistance and the development of type 2 diabetes[91]. This cluster of conditions which includes obesity, inflammation, insulin resistance, type 2 diabetes, and cardiovascular disease, is known as the metabolic syndrome. The majority of studies linking obesity to inflammation and metabolic dysfunction have primarily investigated the role of adipose tissue in propagating a pro-inflammatory environment. In the context of obesity, adipose tissue recruits pro-inflammatory M1 macrophages, resulting in an accumulation of 10x greater macrophage quantities in the tissue[92] and the release of a wide array of pro-inflammatory cytokines, including IL-4, IL-5, IL-6, IL-8, IL-10, IL-12, IL-13, GM-CSF, IFNγ, and TNFα, which are all present at elevated serum levels in obese individuals[93-97]. The general state of systemic inflammation leads to metabolic dysfunction in multiple body systems, including skeletal muscle.

In addition to experiencing the effects of adipose tissue-induced systemic inflammation, skeletal muscle itself may become inflamed during obesity. Levels of pro-inflammatory cytokines TNFα, IFNγ, and IL-1β are increased in skeletal muscle in obesity[98]. Evidence shows that similarly to adipose tissue, skeletal muscle can experience increased pro-inflammatory macrophage infiltration with obesity[99,100], though changes in macrophage content of muscle adipose tissue are more dramatic[99]. In conjunction with paracrine signaling from adjacent immune cells, skeletal muscle cells have the capacity to produce hundreds of myokines which can produce autocrine as well as systemic effects[101,102]. Most of these myokines have been studied in the context of exercise, in

which exercise-induced cytokine release has the potential to produce anti-inflammatory effects[102]. For example, after exercise, skeletal muscle produces substantial levels of IL-6, which can increase basal and insulin-stimulated glucose uptake in skeletal muscle[103]. However, IL-6 also has pro-inflammatory effects, and in the context of long-term chronic inflammation associated with obesity, many of the cytokines produced by muscle may have autocrine effects that lead to continued pro-inflammatory cytokine release and further immune cell recruitment[104,105]. The pro-inflammatory effects of TNFα and IFNγ occur via activation of the NF-κB and JNK pathways and activation of the JAK/STAT1 pathway, respectively. These pathways have all been implicated in impaired insulin signaling[98].

Skeletal muscle insulin resistance and the development of type 2 diabetes are intricately linked; when present in conjunction with excessive caloric intake there is evidence that insulin resistance in skeletal muscle is the earliest detectable metabolic defect in the progression of Type 2 diabetes. The disease state in insulin resistance can be characterized by defects in insulin signaling, specifically decreased tyrosine and increased serine phosphorylation of IR and IRS-1, and decreased activation of PI3K and its downstream target Akt, as well as defects in glucose transport, specifically GLUT4 translocation and resultant insulin-stimulated glucose uptake rates, and defects in glucose metabolism, including decreased glucose phosphorylation and decreased glycogen synthesis[106].

Skeletal muscle also undergoes fiber type shifts with obesity that lead to changes in fuel selection preferences. The muscle of obese subjects exhibits increased glycolytic type II fibers and decreased oxidative type I fibers compared to controls[107,108]. The resulting phenotype is a more glycolytic tissue with impaired oxidative capacity. There is some debate over whether this shift contributes to the pathogenesis of further metabolic dysfunction[107] or whether it is a protective mechanism to restore metabolic homeostasis[109].

Contractile dysfunction

Skeletal muscle proteins are in a constant cycle of degradation and synthesis. In a chronic inflammatory state, this balance is disrupted and the rate of protein degradation exceeds that of synthesis, resulting in muscle atrophy. In many muscle wasting diseases, the primary culprit of atrophy is an increased rate of protein degradation via the ubiquitin-proteasome system[110] and autophagy[111,112] and some downregulation of anabolic processes. In skeletal muscle, protein synthesis is upregulated by the PI3K-Akt-mTOR signaling pathway, which stimulates anabolic programs[113]. The opposing force is mediated by the myostatin-Smad3 pathway, which negatively regulates skeletal muscle growth[114]. TNFα and chronic IL-6 exposure have both been shown to induce catabolic effects on skeletal muscle[115].

IL-6 has also been associated with impaired muscle strength specifically in sarcopenic obesity[116], the co-presentation of fatigue and muscle weakness with obesity[117]. This state of sarcopenia is due to a decline in muscle mass, but also a decline in muscle

function, with decreases in fiber cross-sectional area as well as impaired intrinsic fiber contractility[118,119]. Inflammation-associated changes in the specific force of skeletal muscle are independent of catabolism and may be due to oxidative stress induced by inflammatory cytokines. In addition to its catabolic effects, TNFα has been suspected to reduce the specific force of skeletal muscle via nitric oxide and reactive oxygen species-mediated myofibrillar alterations[120].

1.1.4 Tissue-engineered skeletal muscle

Engineered skeletal muscle tissue can be designed and optimized to serve as an *in vitro* model of both healthy and disease state skeletal muscle. Such *in vitro* models can be used to screen drug responses and address basic science questions that are difficult to address *in vivo*. *In vitro*, engineered muscle bundles can be used to examine the safety and efficacy of pharmaceuticals or allow for in-depth and noninvasive investigation into the basic function of skeletal muscle in a 3-dimensional environment. The drug discovery and testing process for treatment of skeletal muscle-associated diseases including sarcopenia, the age-related loss of muscle mass, type 2 diabetes, and neurodegenerative muscular diseases could benefit from an *in vitro* human tissue model[121]. For such applications, engineered muscle must mimic its *in vivo* counterpart both phenotypically and functionally.

1.1.4.1 Cell source considerations

Skeletal muscle tissue *in vivo* is composed of multinucleated, striated muscle fibers, or myofibers, which are in turn composed of organized contractile protein structures known as myofibrils. Satellite cells, located on the periphery of skeletal muscle fibers, are self-renewing Pax7 positive stem cells capable of asymmetric division, allowing them to produce myoblasts while simultaneously repopulating the satellite cell niche[122]. During the muscle repair process *in vivo*, myoblasts, the proliferative but fate-committed progeny of satellite cells[123], fuse with damaged myofibers. Several sources of myogenic cells are used to produce engineered skeletal muscle, including rodent cell lines, rodent and human primary cells, and induced pluripotent stem cells (iPSCs). These cell sources vary in their ability to accurately recapitulate the function of native human muscle tissue.

Cell lines

Cell lines that have been immortalized offer a nearly limitless cell source, and produce experimental results that are not affected by donor variability or cell senescence. While cell lines offer a stable, well-characterized, readily-available source of cells, they often behave differently than primary cells, impacting the function of the engineered skeletal muscle. Two cell lines commonly used to form engineered skeletal muscle are the C2C12 mouse myoblast line[124] and the L6 rat myoblast cell line[125]. Three-dimensional skeletal muscle constructs made without a hydrogel or polymer, called myooids, and derived from C2C12 cells, demonstrate significantly different force

production kinetics than myooids constructed with primary cells from adult mouse muscle[124]. Myooids made from the mouse cell line are less excitable and exhibit approximately 4 times lower specific force production than myooids made from primary adult cells, and they had a half relaxation time an order of magnitude higher than that seen in myooids made using primary adult cells[124]. Engineered skeletal muscle formed using C2C12 cells do not exhibit the tetanus force traces seen in normally-functioning skeletal muscle as a response to increased frequency of electrical stimulation, and peak force does not increase with increased frequency of stimulation[126]. These differences in force kinetics suggest dysfunction in calcium handling in engineered muscle formed from cell lines, specifically a slower decay of calcium transients. In human cultured myotubes, a slower decay of calcium transients is associated with functional immaturity and low abundance of calcium handling proteins when compared with adult muscle fibers[127]. In addition to differences in developmental phenotype, C2C12 cells differ in regulation of metabolism and growth rate when compared to primary cells[124]. For example, C2C12 cells grow more easily in culture than do primary cells, without the need for added growth factors, and have the potential for uncontrolled proliferation, unlike primary cells[128].

Primary cells

Primary cells are obtained directly from skeletal muscle tissue of the donor, and are not altered in a manner that immortalizes them. Satellite cells are isolated by physically freeing them from their niche within the structure of the muscle via

mechanical and enzymatic disruption of the surrounding extracellular matrix and muscle fibers[129]. Alternatively, explanted muscle tissue can be dissected, plated and cultured until an outgrowth of proliferative myogenic cells appears[130]. Using these approaches, there will likely be fibroblasts, red blood cells, adipocytes and cellular debris present[129]. Isolations can be enriched for satellite cells by using the pre-plate method, in which the cell suspension or explanted tissue is plated for a brief period of time to remove more quickly-adhering cell types such as fibroblasts before removing the cell solution to be plated on the intended culture substrate[131], or by cell sorting using flow cytometry to actively identify and retain cells with satellite cell-like morphologies[132,133] or specific combinations of cell markers[134,135].

The isolated cells can either be used immediately to form engineered skeletal muscle, or cultured and expanded in monolayer culture before being used for the engineered skeletal muscle. However, during *in vitro* culture satellite cells do not remain quiescent, instead entering into the cell cycle as proliferative muscle precursors[136]. Expansion of primary cells is limited, because as the cells reach their limit of population doublings, they become senescent and do not differentiate as efficiently. For example, primary cells obtained from two human skeletal muscle biopsies began losing their capacity for differentiation after seven population doublings[137]. Despite their relatively short lifetime in culture, primary cells are preferred over genetically abnormal

immortalized cell lines because they better retain a physiological phenotype, offering a more suitable model of *in vivo* function.

In native muscle tissue, satellite cells are the primary cell type responsible for muscle regeneration. They are normally quiescent and are identifiable both by their positioning close to myofibers, in a niche between the basal lamina and sarcolemma of the fiber, and expression of Pax7. Activation of satellite cells can be caused by injury, mechanical stretch, or secreted growth factors, and is marked by initiation of proliferation and the co-expression of Pax7 and MyoD[138]. Once the cells have been activated to a proliferative state they can either commit to a differentiated fate, downregulating Pax7 and upregulating myogenin (MyoG) expression until they undergo fusion to form $MyoG^+$ myotubes expressing differentiation markers such as myosin heavy chain, incorporate into an existing myotube, or continue to self-renew, eventually downregulating MyoD expression and repopulating the stem cell niche as $Pax7^+$ cells[138-140].

Despite the tendency of satellite cells to differentiate in culture, engineered three-dimensional skeletal muscle bundles fabricated using primary rat satellite cells that were adherently cultured *in vitro* for 36 hours after isolation actually retained a higher density of satellite cells in the mature engineered muscle than did engineered muscle fabricated using freshly isolated satellite cells[141]. Likely as a result of the adherent culture period, once in the engineered muscle, $MyoD^+$ and $MyoG^+$ cells that had been adherently

cultured, a population which includes recently fused myoblasts or myoblasts on the verge of fusion, differentiated more quickly to a mature MyoG$^+$ myofiber phenotype than their freshly isolated counterparts. These myofibers formed stem cell niches in which the remaining Pax7$^+$ satellite cell population was retained, reminiscent of similar niches found in muscle *in vivo*. Additionally, the capacity of the adherently cultured cells for more rapid differentiation results in higher contractile force production due to increased robustness of contractile elements[141]. Together, these results indicate that the use of adherently cultured cells may be preferable to freshly isolated satellite cells in engineered muscle.

During isolation of primary myogenic cells, fibroblasts are present in the isolated cell population. The number of fibroblasts is reduced by a brief pre-plating process, which takes advantage of the more rapid adhesion of fibroblasts than myoblasts to uncoated surfaces, and serves to decrease the final amount of fibroblasts present in the isolation[131]. However, a cell population that is composed of myogenic cells with some fibroblasts is desirable for the formation of engineered skeletal muscle. Attempts to form myooids using only C2C12 cells failed, as the cells never delaminated from the culture surface, instead forming a monolayer of differentiated and undifferentiated cells. Only once the C2C12 cells were cultured with a fibroblast cell line did myooids form, likely aided by the extracellular matrix produced by the fibroblasts.[124]

In addition, fibroblasts are necessary for the formation of a continuous basal lamina structure around differentiating myotubes. Fibroblasts deposit type IV collagen and laminin, two of the main components of the basal lamina structure[142]. *In vivo*, the basal lamina is important for its role in muscle structure and strength and as a crucial component of myogenesis and signaling[143]. In fibrin-based engineered skeletal muscle, fibroblasts contribute to the formation of a fibroblast-rich exterior, which resembles the connective tissue layer that surrounds muscles in native tissue[144]. Fibroblasts also play an important role in fibrin degradation and gel compaction over time[145], contributing to the passive forces present within the bundle structure.

Species of cell source

Commonly, the cell source for engineered skeletal muscle *in vitro* has been rodent cells, as they are simple to obtain and sufficient for first-pass, preliminary studies to detect overt toxicity. Rodent cells offer value as a way to optimize the engineered muscle fabrication process, but are not acceptable for translational studies. Human myoblasts are available commercially, and these cells behave comparably to freshly isolated primary cells[7]. However, if a source of tissue is available, cells can be isolated, expanded and frozen for future use. Importantly for regenerative purposes, it is possible to isolate a patient's own cells for use in the engineered muscle, although in the absence of iPS technology, the isolation would require an invasive procedure to obtain the tissue.

1.1.4.2 Scaffolding and extracellular matrix

Engineered skeletal muscle can be fabricated either in the absence or presence of a scaffold. Engineered muscle fabricated with no additional scaffolding is composed purely of cells and their own extracellular matrix. The myogenic cells grow to confluence, at which point they typically begin to fuse, and the resultant spontaneous contractions cause them to delaminate from the hydrophobic culture surface[146]. The cells in these scaffold-free constructs achieve the aligned structure necessary for proper muscle function by exerting passive tension on artificial tendons located on either end of the culture area[124,147]. This method, which is used to produce the myooids described earlier, relies solely on the extracellular matrix (ECM) produced by the myoblasts and fibroblasts to provide the structure of the muscle. Myogenic cells in culture secrete extracellular matrix proteins such as collagen[148,149], but fibroblasts are likely responsible for the bulk of the ECM proteins that provide the structural support in myooids[124]. However, many protocols for the formation of 3-dimensional engineered muscle use a scaffold, such as a hydrogel structure or a decellularized scaffold. A scaffold provides mechanical support and offers a three-dimensional environment for differentiation to occur, in contrast to the differentiation in monolayer culture required for formation of scaffold-free myooids. Additionally, a scaffold allows control over the dimensions and physical properties of the matrix in which the cells grow, offering a tunable engineered muscle system.

Fibrin, collagen, and Matrigel, a mixture of structural proteins secreted by mouse sarcoma cells, are purified natural biopolymers derived from tissues and used to create hydrogel-based engineered skeletal muscle. These biopolymers promote cellular growth in part because these components provide the cells with a matrix composition that mimics that of native ECM.

The extracellular matrix provided by Matrigel contains cell adhesion ligands[150] to which the differentiating myoblasts can attach[151], allowing the cells to differentiate in three dimensions within the matrix[152]. However, the composition of Matrigel is not clearly defined, leading to uncertainty about how variations in Matrigel lot impact engineered muscle function, and Matrigel contains xenogenic components that would be recognized by a human immune system as foreign, eliciting an unwanted immune response upon implantation and precluding use in humans.

In vitro, Matrigel is commonly combined with either collagen or fibrin in hydrogel scaffolds. In collagen-Matrigel gels, C2C12 myoblasts differentiated to form striated, multinucleated fibers with paxillin localizing to the ends of the fibers. This expression of paxillin, which is a protein specific to the myotendinous junction, indicates the possibility of an early stage junction forming between the myotubes and the cell-produced collagen I fibrils in the gel[153]. For engineered muscle to be used regeneratively, it will need to be able to form such connections in the native muscle. However,

engineered muscle made using collagen-Matrigel gels can only sustain small numbers of cells since they tend to compact quickly and rupture[152].

Alternatively, engineered skeletal muscle tissue has been prepared using fibrin-based gels, which form when thrombin cleaves fibrinogen, resulting in polymeric fibrin networks. These gels allow the cells to proliferate and self-organize, as well as produce their own extracellular matrix. Fibrin is highly bioactive; it contains the cell adhesion motif RGD, which promotes cell attachment, and the cleavage products produced during the transition from fibrinogen to fibrin act as mitogens, regulating proliferation of surrounding cells[154]. In smooth muscle and tendon engineered tissue systems, fibrin gels promote cell-ECM production to a greater extent than do collagen gels[155,156], perhaps due to the fact that fibrin binds growth factors such as fibroblast growth factor (FGF) and insulin growth factor (IGF), leading to increased protein synthesis[157]. Fibrin contains a heparin-binding domain that gives it this ability to bind growth factors and sequester them within the engineered construct[157]. IGF is known to promote skeletal muscle hypertrophy through stimulation of both proliferation and differentiation pathways; in fact, myoblast differentiation is stimulated in part by autocrine secretion of IGF, an effect that can be enhanced by introducing exogenous IGF[158]. FGF plays a role in increasing the number of proliferative satellite cells in rats, contributing to an enhanced injury response[159]. FGF-6 is specifically expressed in muscle and induces proliferation of cultured myoblasts while inhibiting differentiation, allowing for expansion of the

undifferentiated cell population[160]. In FGF-6 knockout mice, regenerative potential following injury was limited and damaged tissue exhibited fibrosis not seen in wild-type mice[161]. Although in a separate FGF-6 knockout model, regeneration following injury was not affected by the lack of FGF-6[162], injection of recombinant human FGF-6 into injured muscle of wild type mice accelerated the regenerative process[163]. FGF-2 is present in the basement membrane of adult muscle, and promotes satellite cell replication in murine models of muscular dystrophy[164].

As the cells mature, they remodel the fibrin matrix, eventually degrading much of the original fibrin and replacing it with their own ECM[165]. Unlike bundles formed using a collagen-Matrigel mixture, bundles formed using fibrin-based gels are capable of lasting for significant time periods in culture (up to at least 5 weeks) without deteriorating and rupturing[166]. This effect is likely due either to an improvement in mechanical strength due to the increased ECM produced in fibrin gels, or the higher compliance of fibrin fibers compared to collagen, allowing the matrix to better resist the force of spontaneous myofiber contractions[152].

1.1.4.3 Optimizing tissue-engineered skeletal muscle force production

In skeletal muscle, force production has been identified as a crucial functional characteristic of the muscle tissue *in vivo* that must be recapitulated *in vitro* for both regenerative and drug screening purposes.

Native muscle responds to a single electrical stimulus with a single contraction, producing a twitch force. When repeated electrical stimuli grow temporally closer together, the muscle engages in a sustained contraction, producing a tetanus force (Figure 5). In rats, maximum tetanic specific force (force normalized by cross-sectional area) *in vivo* reaches a magnitude of approximately 250 kN/m^2 [167,168], with a unitless tetanus to twitch ratio in adult rat skeletal muscle of 3.5-5[169,170]. Additionally, native muscle demonstrates a length-tension curve, with contractile forces increasing as the muscle is stretched until the muscle produces peak force when myosin and actin fibers optimally overlap. Stretching above the maximum level results in declining forces as the overlap of contractile elements begins to interfere with force production[169]. Engineered muscle is capable of recapitulating the force-length curve, as well as the production of twitch and tetanus forces matching adult muscle tetanus to twitch ratios[170,171], but falls short of the standard set by *in vivo* muscle when it comes to the magnitude of specific force (force/cross-sectional area) production. Prior to force optimization, most engineered muscle formed using rodent cells yields specific forces with a magnitude of approximately 1-8% of the magnitude produced by their native, adult muscle counterparts[124,166,172,173]. Due to the importance of high active force production for both regenerative and drug screening purposes, considerable effort has been invested in optimizing engineered muscle to produce improved forces. There are some circumstances inherent to the *in vivo* muscle environment, such as innervation and

vascularization, which impact the function of native muscle and remain largely elusive for *in vitro* culture, as discussed in a later section. However, the formulation and culture conditions of the engineered muscle can be altered to overcome some shortcomings of *in vitro* culture, leading to engineered muscle capable of producing higher, more physiologically relevant forces.

Optimizing formulation parameters

The absence of the native organization of muscle and the lack of maturity of muscle fibers *in vitro* are likely the major causes of the low forces seen in engineered skeletal muscle, as un-optimized engineered muscle is typically characterized by thin, incompletely matured fibers surrounded by excessive amounts of extracellular matrix and an acellular core[174]. By varying the matrix composition, and in turn the cell-matrix interactions, it is possible to enhance the maturation of the fibers within the engineered muscle and improve the function. Engineered skeletal muscle formed by suspending primary neonatal rat myoblasts in a fibrin gel produces approximately three-fold higher contractile forces than those formed using the same cell density in a collagen gel, suggesting that the interactions of the cells with specific matrix proteins may have a substantial impact on the force production of the muscle[166]. When the same investigators formed engineered muscle with increasing fibrinogen and increasing Matrigel concentrations, they saw increased protein:DNA ratios and increased myotube diameter, indicative of more robust fibers. These bundles with the largest myotube diameter also produced the highest active force. Fibrin hydrogel-based self-assembled rat engineered

skeletal muscle produced specific forces of 36.3 kN/m^2, which is a considerable improvement upon the forces achieved by fibrin-free self-assembled rat engineered skeletal muscle, which produced specific forces of 2.9 kN/m^2 [170].

The size of the engineered muscle influences its force production; though the specific force will not change, a thicker tissue will inherently produce larger absolute forces, which is ideal for regenerative purposes. However, in the absence of vascularization, the tissue thickness is constrained by the diffusion of nutrients and oxygen, so larger engineered muscle tissues produce a lower specific force because the center is either devoid of cells or contains necrotic cells[171,172]. The open pore structure of hydrogels is ideal for promoting diffusion, but even within such a structure, cells must be within 100-200 μm of the nutrient and oxygen source to remain viable[175]. A further limitation includes the relatively low solubility of oxygen in aqueous solutions such as culture media[176]. Decreasing the thickness of the engineered muscle can lessen the nutrient and oxygen gradients within the tissue[177], and decrease the relative volume of the acellular region, an ideal solution for the use of engineered muscle in the drug testing process. Other proposed methods for decreasing the acellular region while maintaining a clinically-relevant size of the tissue include mixing of the culture media[141], perfusion of media over the engineered tissue[178], or vascularization.

Effect of convection in culture media on skeletal muscle maturation

Typically, tissue engineered muscles are cultured under static conditions, with no fluid flow or bulk motion around the bundles. This can lead to a nutrient gradient

within the media, resulting in a lack of oxygen and nutrients directly surrounding and within the engineered muscle. In the absence of a vascular system to deliver oxygen and nutrients directly to the cells, other methods such as perfusion of the media[179] or media mixing can be used to overcome diffusion limitations and ensure that there is sufficient transport to the interior of engineered muscle. The introduction of dynamic culture conditions, in which muscle bundles are rocked during culture at 24 rocks per minute with a ± 30 degree tilt, aims to diminish the gradient within the bundle and culture media and allow for improved mass transport of oxygen and nutrients within the engineered muscle environment[141]. Static controls in this experiment showed only a thin layer of viable myofibers along the exterior of the muscle bundle, with a generally acellular core, indicative of cell migration towards a more nutrient-rich environment. Dynamic culture of the fibrin-based engineered muscle formed using rat myogenic cells increased the total cross-sectional area of the tissue occupied by viable myofibers from approximately 0.18 mm^2 in static controls to approximately 0.63 mm^2 [141]. In the same study, the diameter of myofibers in dynamically-cultured engineered muscle increased, and the muscles themselves produced 6-7 fold higher forces than those cultured in static conditions, indicating progress towards a more physiologically-relevant tissue structure.

Mechanical stimulation

In an attempt to produce engineered skeletal muscle that is highly aligned, mimicking the alignment of muscle fibers *in vivo*, some groups have applied unidirectional stretch to differentiating engineered muscle. In two-dimensional studies,

uniaxial strain induced directional differentiation of mouse myoblasts to form cross-striated fibers[180]. These externally-applied forces mimic those forces experienced by muscles *in vivo*, which affect protein synthesis[181] and muscle morphology in post-development muscle adaptations. When human skeletal muscle cells in a collagen-Matrigel construct were cyclically stretched over the course of differentiation, the resulting engineered muscle contained larger fibers with a mean diameter 12% greater than those of the un-stretched controls[174]. The stretch regimen used in these experiments began one week post-casting, and consisted of 3 stretch/relaxation cycles followed by about 28 minutes of static conditions, with stretches occurring at a 5% strain for 2 days, followed by 10% strain for 2 days, and 15% strain for 4 days. Although active force production was not measured in these experiments, the increase in both fiber diameter and fiber area indicates an improvement in the physiological structure of the engineered muscle that could translate to higher force production.

Electrical stimulation

Since native muscle is constantly receiving electrical signals from motor neurons, and upon denervation, skeletal muscle undergoes atrophy[182], electrical stimulation of engineered muscle more closely mimics the conditions seen by native muscle in *in vitro* cultures. When engineered skeletal muscles formed from fibrin gels containing C2C12 cells were chronically electrically stimulated (4x0.1ms pulses at 2.5V/mm delivered over the course of 400 ms with 3.6 s recovery for 7 days), the tetanus or twitch force was two times higher than unstimulated muscle, consistent with a more mature fiber

phenotype[183]. Electrical stimulation can also produce fiber type switching, which has important implications for the metabolic state of the engineered muscle[184].

1.1.4.4 Expanding the relevance of the tissue-engineered muscle model

To be fully representative of native muscle tissue, engineered muscle will need to incorporate the complex tissue interactions that are present in native muscle, including innervation and vascularization. These are well-established goals for any engineered tissue, but they have been difficult to achieve *in vitro*, in the absence of the complex environmental and signaling cues present *in vivo*.

Innervation

In vivo muscle forms neuromuscular junctions with motor neurons, at which they receive their electrical input from the neurons. Denervation of skeletal muscle results in changes in protein expression, leading to atrophy and decreases in force production, as well as fiber type switching resulting in metabolic changes in skeletal muscle[185,186]. When skeletal muscle is denervated, a group of myogenic factors involved in muscle development, including MyoD and myogenin, are up-regulated and accompanied by a significant decrease in myofiber cross-sectional area[187,188]. This upregulation of myogenin directly regulates the expression of atrophy-associated genes that have been connected with losses in muscle mass[189]. Electrical stimulation of engineered skeletal muscle may offer an alternative to innervation, but cannot completely recapitulate the *in vivo* environment. To more fully mimic the native environment of muscle, neuromuscular junctions have been formed *in vitro*, in both 2-D and 3-D culture systems. In 2-D,

functional neuromuscular junctions have been formed using a variety of cell species combinations, including more recently, human stem-cell derived motoneurons and human skeletal muscle cells: the ideal cell source for use as a drug screening platform. This neuromuscular junction model demonstrated striated skeletal muscle cells capable of firing action potentials in response to motoneuron stimulus, resulting in cell contraction[190].

Neuromuscular junction formation was achieved in fibrin-based tissue engineered muscle using rat motor neurons and myoblasts. These innervated engineered muscles demonstrated a high percentage of striated fibers, indicating increased fiber maturation, as well as an increase in active force production when compared with engineered muscle cultured using only myoblasts[191]. This result presents an opportunity for not only increasing the extent of biomimicry of skeletal muscle, but also expanding the functional aspects of skeletal muscle that can be examined *in vitro* to include the neuromuscular junction.

Vascularization

Vascularization offers advantages in terms of enabling the study of muscle-vasculature interactions, and also addresses the challenges of oxygen and nutrient diffusion limitations within tissue engineered muscle. Although fully vascularized engineered skeletal muscle has not yet been produced *in vitro*, there are some pre-implantation approaches that have achieved more rapid vascularization once the engineered muscle is implanted. One approach is to form engineered muscle using cells

that have been retrovirally transduced such that they produce the angiogenesis growth factor vascular endothelial growth factor (VEGF). Upon implantation, they promote capillary bed formation both internally as well as in nearby tissue[192]. In another pre-implantation approach, endothelial cells, fibroblasts, and myoblasts were co-cultured on a porous scaffold. The endothelial cells self-organized to form tubular networks which, after implantation, contained red blood cells, indicating that they had anastomosed with the *in vivo* vasculature[193]. However, functionally vascularized *in vitro* engineered skeletal muscle remains elusive.

1.1.4.5 Metabolism

The metabolic state of engineered skeletal muscle is a significant indicator of the suitability of engineered muscle as a replacement for or supplementation of *in vivo* drug studies. Recapitulating the metabolic milieu found *in vivo* is of the utmost importance when the engineered muscle is used to test the effects of pharmaceuticals, when changes in metabolism can indicate drug toxicity. Additionally, because skeletal muscle is a large contributor to the insulin-mediated glucose uptake response, the muscles must accurately simulate that process if they are to be used to screen drugs for Type 2 diabetes. Skeletal muscle accounts for 75% of glucose uptake post-insulin stimulation (for example, following a meal)[194]. Much of our knowledge about insulin-mediated uptake in skeletal muscle thus far has been obtained from *in vitro* experiments done with monolayer cultures, but there are indications that skeletal muscle cultured in a 2-D

system may not accurately represent intact skeletal muscle in the body. The increase in glucose uptake in response to insulin is typically diminished *in vitro* when compared to adult skeletal muscle *in vivo*. In humans, *in vivo* insulin-mediated glucose uptake rates are typically 6-8 fold higher than basal uptake rates[195,196] while *in vitro* insulin stimulation of cultured human myotubes typically only results in a 1.3-3 fold increase in uptake rates [197-202]. Because the conditions experienced by a cell cultured in monolayer is devoid of many of the tissue-specific interactions seen *in vivo*, such as mechanical cues, biochemical cues, and cell-cell contact[203], the three-dimensional environment offered by tissue engineered skeletal muscle may result in a more physiological metabolic state than that of monolayer cultures.

Glucose uptake and insulin response in vitro

Glucose enters skeletal muscle cells primarily via two glucose transporters, GLUT1 and GLUT4, which allow selective movement of glucose down its concentration gradient into the cell. GLUT1 is responsible for constitutive, basal glucose uptake in skeletal muscle, while GLUT4 is responsible for insulin-stimulated glucose uptake. However, the ratio of GLUT1 to GLUT4 expression increases when cells are taken from a 3D physiological environment and plated in a 2D culture system, causing a change in the metabolic behavior of cells cultured *in vitro*. *In vivo* rat muscle has a GLUT1/GLUT4 protein ratio value that varies from 0.1-0.6 [201,204], while rat constructs *in vitro* showed a GLUT1/GLUT4 protein ratio of 6.3:1[146]. *In vivo* human muscle was found to have a GLUT1:GLUT4 total cell mRNA expression ratio of 0.6:1[205], while total cell mRNA

expression levels in myotubes *in vitro* showed a ratio of 12:1[197]. The high GLUT1 content seen in cultured cells contributes to a high basal uptake rate that dilutes the insulin responsive glucose uptake by the relatively less abundant GLUT4 transporters.

This change in the GLUT1:GLUT4 ratio appears to be consistent with studies of denervated muscle. Protein expression analysis of transected muscles from mice reveals significantly decreased levels of GLUT4, while GLUT1 protein expression was significantly increased[206]. This study also found decreases in insulin responsiveness of the transected muscles at early time points, which is consistent with previous studies that found a decrease in insulin response following denervation of rat muscle with corresponding decreases in GLUT4 protein levels and increases in GLUT1 protein levels[185,186]. In addition, *ex vivo* muscle fibers cultured after removal from human muscle tissue show decreased insulin responses when compared with the insulin response seen in human muscle *in vivo*[196,207-211]. Thus, denervation of skeletal muscle cells may be one factor that skews the GLUT1:GLUT4 ratio *in vitro*, resulting in a decreased insulin response.

Culture conditions that expose skeletal muscle cells to supraphysiological levels of nutrients or hormones can also have an impact on the function of insulin-mediated glucose uptake. Human skeletal muscle myotubes cultured in hyperglycemic conditions (20 mM glucose) produce a 40% decrease in basal glucose uptake and complete absence of an insulin response[212]. In animal models, skeletal muscle GLUT4 protein levels are

depressed in hyperglycemic conditions[213]. In contrast, culturing control human cells in hyperglycemic conditions (10 and 20 mM) did not decrease insulin responsiveness in differentiated human myotubes, unless hyperglycemic conditions were combined with hyperinsulinemia[198].

Supraphysiological insulin levels stimulate proliferation and differentiation of myoblasts[214]. However, in hyperinsulinemia conditions (30 μM), differentiating human skeletal muscle myoblasts exhibited increased membrane-specific GLUT1 expression corresponding to a doubling of the basal glucose uptake rate, while also decreasing insulin-stimulated transport by 30-40%, yielding an undiscernible insulin response[198]. In the same study, cells grown in media containing only 22 pM insulin for both growth and differentiation periods showed a nearly 3-fold insulin-mediated increase in glucose uptake.

Glucose and fatty acids are both potential substrates for oxidative metabolism, and there is competition between the two as fuel sources in skeletal muscle. Studies on human leg skeletal muscle indicate that glucose oxidation accounts for 76% of oxygen consumption in hyperinsulinemic conditions, but upon addition of free fatty acids, that percentage drops to 53%, indicating a shift to fatty acid substrates[78]. In humans, high levels of free fatty acids in the plasma and increased intramuscular lipids are associated with insulin resistance, leading to decreased glucose disposal[215]. However, saturated and unsaturated fatty acids may have distinct effects on insulin-stimulated glucose disposal,

with saturated fatty acids such as palmitate primarily responsible for the reduction of the insulin response[216]. In contrast, unsaturated fatty acids such as oleate are capable of rescuing the insulin response following palmitate-induced insulin resistance[217]. Additionally, unsaturated fatty acids stimulate differentiation in L6 myotubes[218]. Typical skeletal muscle cell culture conditions are devoid of fatty acids, but the addition of physiological ratios of saturated and unsaturated fatty acids could serve a valuable role in re-creating the energy sources available to muscle *in vivo*.

Together, these results indicate that tissue engineered skeletal muscle culture conditions have the potential to exert a significant effect on both basal and insulin-stimulated uptake and must be optimized to allow for maximal differentiation potential while not shifting the metabolic pathways to a non-physiological state.

Fiber type switching

Mature skeletal muscle consists of four primary mature fiber types distinguished by the primary expressed form of myosin heavy chain; type 1 fibers, which are characterized by slow twitch kinetics and the presence of oxidative enzymes, and three forms of type 2 fibers characterized by fast twitch kinetics and the presence of more glycolytic enzymes. Fast twitch fibers express higher levels of GLUT1 and lower levels of GLUT4 than their slow twitch counterparts[55,219]. Interestingly, skeletal muscle cultured *in vitro* had a much higher percentage of fast twitch fibers, as identified by expression of fast twitch associated myosin heavy chain proteins, than the tissue from which it was isolated[220], and cultured myotubes typically express more immature embryonic and

perinatal myosin heavy chain isoforms[177]. If myotubes *in vitro* have a tendency to differentiate into fast twitch fibers, this may partially explain the lower expression levels of GLUT4 than their counterpart muscle *in vivo*.

Skeletal muscle fibers *in vivo* demonstrate some plasticity, with the capacity to switch fiber type in response to training, though the effect is subtle[64,221]. Fast to slow fiber type switching is more dramatic *in vitro*[221], and can be accomplished *in vitro* by electrical stimulation[184,222] and modification of culture conditions[223,224]. Engineered muscle formed with C2C12 cells and electrically stimulated at a frequency of 10 Hz and an active time of 60% responded in a duration-dependent manner to contraction durations of at least 6 seconds with a switch to slower adult MHC isoforms. A contraction duration of 0.6 seconds did not produce changes in expression of fast MHC isoforms, indicating that the duration of contraction is an important factor in the regulation of MHC protein expression. The fast-to-slow transition is additionally characterized by slower twitch kinetics and higher expression of GLUT4 and metabolic proteins associated with promoting a slow twitch fiber type[184]. In this case, inducing fiber type switching to produce cultures enriched with slow twitch fibers could elicit an insulin response more in line with that seen *in vivo*, due to increased GLUT4 expression.

1.2 Specific aims and hypotheses

The overall goals of this project were to characterize the factors affecting glucose uptake and insulin response by tissue-engineered skeletal muscle myobundles, to produce a more physiologically-relevant model of skeletal muscle by manipulating culture conditions, and to use the platform to model an inflammation-induced disease state. We hypothesized (1) that myobundles would exhibit relevant features of in vivo glucose uptake, and (2) that altering nutrient availability in the culture media would impact myobundle metabolism. We also hypothesized (3) that by incorporating either macrophages and/or pro-inflammatory cytokines with the healthy myobundles, an inflammation-mediated disease state could be induced that would recapitulate key aspects of in vivo inflammation-associated skeletal muscle dysfunction. To address these hypotheses, we undertook three specific aims.

Specific aim 1: Characterize the basal and insulin-mediated glucose uptake in tissue-engineered skeletal muscle myobundles. We identified a method for measuring glucose uptake using 2-deoxyglucose, a glucose analog, and tested the changes in myobundle glucose uptake in response to treatment with metformin. We then characterized the insulin sensitivity and responsiveness of the myobundles, and examined the effect of changes in culture conditions on insulin-stimulated glucose uptake. Finally, we examined the ability of the HDAC inhibitor 4-PBA to enhance myobundle function.

Specific aim 2: Use low amino acid and growth factor reduced conditions to promote a less glycolytic metabolism in myobundles. We tested the effect of a more physiologically-relevant set of culture conditions on myobundle metabolism, measuring the response in terms of basal glucose uptake, lactate production, glycolytic and oxidative metabolic activity, gene expression of glucose transporters, and contractile function.

Specific aim 3: Create a tissue-engineered human skeletal muscle model of inflammation. We induced inflammatory conditions during myobundle culture using the incorporation of human cord blood-derived macrophages and pro-inflammatory cytokine exposure. We tested the response of the myobundles to a pro-inflammatory environment by measuring contractile function, cytokine production, and glucose uptake.

2. Glucose Uptake and Insulin Response in Tissue-engineered Human Skeletal Muscle

2.1 Introduction

In vitro tissue-engineered skeletal muscle myobundles are a promising tool for studying drug efficacy and toxicity, as well as for elucidating mechanisms of disease states for targeted drug development[121]. Because the myobundles are formed from human cells, they are able to indicate harmful human-specific drug effects that may not be detected in animal platforms[7]. This saves not only the time and expense associated with clinical trials, but also prevents unnecessary harm to clinical trial participants. To this end, tissue-engineered muscle must be designed to functionally mimic its *in vivo* counterpart.

Most *in vitro* models of human skeletal muscle models of healthy and diseased states rely on two-dimensional culture of cells which lacks the structural three-dimensional aspect of tissues *in vivo*. Tissue engineered skeletal muscle improves upon this model by exhibiting unidirectional aligned fibers similar to those comprising muscle *in vivo*, and it has the capacity to undergo additional functional tests including measures of contractile function, oxygen consumption, metabolite production, and calcium handling[7,8,225,226]. Skeletal muscle is highly metabolically active and is responsible for 75% of post-prandial glucose uptake[194], so in addition to mimicking the structure and contractile function of native muscle, it is important that an *in vitro* model recapitulates key metabolic traits of healthy skeletal muscle. These traits include sensitivity to insulin

and the ability to respond to changes in energy availability with changes in nutrient uptake.

In this study, we identified and validated a method for measuring glucose uptake in myobundles, allowing us to measure changes in basal as well as insulin-stimulated 2-DG uptake. We examined the effect of the commonly-used hyperglycemia treatment metformin on the myobundle 2-DG uptake and contractile function and observed that the myobundle system was able to respond to the metformin-induced energy depletion with increased 2-DG uptake. Although the insulin response in myobundles is less robust than that of *in vivo* skeletal muscle, we found that insulin sensitivity of the myobundles was comparable to that of skeletal muscle *in vivo*. In order to create a more physiologically-relevant model, we manipulated various culture conditions including amino acid content and insulin concentration and examined the impact on 2-DG uptake in the myobundles. Finally, the insulin response and contractile function of the myobundles was improved via treatment with the general HDAC inhibitor 4-phenylbutyrate (4-PBA).

2.2 Materials and Methods

2.2.1 Isolation and monolayer culture of primary myoblasts and myotubes

Primary human myogenic cells were isolated from surgical waste samples under a Duke IRB-approved protocol. Briefly, muscle tissue was washed with Dulbecco's phosphate buffered saline (DPBS) (Sigma-Aldrich) containing 2X Antibiotic-Antimycotic

(ThermoFisher Scientific), then minced and digested using 0.05% Trypsin-EDTA (ThermoFisher Scientific). Minced tissue was pre-plated on an uncoated tissue culture flask for 2 hours before being transferred to a Matrigel (Corning)-coated flask for myogenic cell outgrowth. Tissue and cells were cultured during outgrowth in human growth media (hGM) consisting of low glucose (5.55 mM glucose) Dulbecco's Modified Eagle Medium (DMEM) with 1 mM sodium pyruvate (ThermoFisher Scientific) supplemented with 9% fetal bovine serum (FBS) (Hyclone), 0.25 μg/mL amphotericin B (ThermoFisher Scientific), 50 μg/mL gentamicin (ThermoFisher Scientific), 0.4 μg/mL dexamethasone (Sigma-Aldrich), 10 ng/mL EGF (Peprotech), and 50 μg/mL fetuin (Sigma-Aldrich).

For monolayer myotube culture, myoblasts were plated at a density of 20,000 cells/cm^2 in a 6-well plate coated with growth-factor reduced Matrigel (Corning). Myoblasts were cultured in hGM for 4 days, then switched to differentiation media for two weeks of differentiation prior to endpoint testing. Differentiation media, referred to as LAA media, consisted of a custom-formulated low amino acid base media (Appendix C) (ThermoFisher Scientific) containing 2% horse serum (Hyclone), 25 μg/mL gentamicin (ThermoFisher Scientific), 0.125 μg/mL amphotericin B (ThermoFisher Scientific), 100 μM L-carnitine (Sigma-Aldrich), 0.05% bovine serum albumin (BSA) (ThermoFisher Scientific), 5.55 mM D-glucose (ThermoFisher Scientific), 0.2 mM sodium pyruvate (ThermoFisher Scientific), 2 mM glutamine (ThermoFisher Scientific), 2 mg/mL

6-aminocaproic acid (ACA) (Sigma-Aldrich), 1.72 μM or 10 nM insulin, as specified (Sigma-Aldrich), 50 μM oleate (Sigma-Aldrich) and 50 μM palmitate (Sigma-Aldrich) in a 1:1 mixture.

2.2.2 Myobundle formation and culture

Myobundles were formed as previously described[7,8]. Briefly, a solution of Matrigel (Corning) (Baseline condition) and bovine fibrinogen (Sigma-Aldrich) in PBS was mixed with a myogenic cell solution containing 50 U/mL thrombin (Sigma Aldrich) and pipetted into the central channel of a PDMS mold surrounded by a nylon (Cerex Advanced Fabrics) frame. Each myobundle was formed with 50 μL of solution and 750,000 cells. The myobundles were allowed to gel for 30 minutes at 37°C before hGM supplemented with 1.5 mg/mL 6-aminocaproic acid (Sigma-Aldrich) (hGM + ACA) was added to the wells containing the molds. Myobundles were cultured in hGM + ACA for four days before being removed from the PDMS mold and switched to differentiation media. Unless otherwise specified, myobundles were differentiated for two weeks prior to endpoint testing. DMEM-based differentiation media consisted of low glucose DMEM containing 2% horse serum, 25 μg/mL gentamicin, 0.125 μg/mL amphotericin B, 100 μM L-carnitine, 2 mg/mL 6-aminocaproic acid (ACA), 1.72 μM insulin, 50 μM oleate (Sigma-Aldrich) and 50 μM palmitate (Sigma-Aldrich) in a 1:1 mixture. LAA-based differentiation media was formulated as described in the previous section.

2.2.3 Media-based glucose uptake assay

Myobundles were placed in a 12-well plate and washed with DPBS, then cultured for 18 hours in 2 mL per well of serum- and insulin-free differentiation media. After the 18 hour starvation period, the starvation media was removed and replaced with 1 mL per well of no glucose DMEM with 1 mM D-glucose + 2 mg/mL ACA + 1x antibiotic-antimycotic, with or without insulin. 10 μL samples of media were taken at 0, 1, 6 and 24 hours, then stored at -20°C.

To quantify the glucose concentration in the media samples, the Amplex Red Glucose/Glucose Oxidase Assay Kit (ThermoFisher Scientific) was used. Media samples were diluted to be within the range of the assay detection linear range, and fluorescence was measured using an excitation wavelength of 544 nm and an emission wavelength of 590 nm. Results could be presented either as the R_{max} of glucose consumption to account for concentration-driven changes in consumption rate or as total glucose consumed. To present the R_{max} value, the equation for Michaelis-Menten kinetics,

$$-\frac{dC}{dt} = \frac{R_{max}C}{K_m + C} \qquad \text{(Equation 1)}$$

can be integrated and linearized to the form $y = mx$, where $y = time$, $m = \frac{C_0}{R_{max}}$, and $x = \frac{K_m}{C_0} ln\frac{C}{C_0} + \frac{C}{C_0} - 1$. From the value for the slope and the initial glucose concentration, and assuming Km to be the value for R_{max} can be calculated. Alternatively, a simple rate of glucose consumption could be calculated based on the overall change in glucose concentration between two time points. Due to the nonlinear

nature of the kinetics of glucose uptake, this method would tend to underestimate the maximal rate.

2.2.4 2-deoxyglucose uptake quantification assay

Measurement of 2-DG uptake was done in myobundles using a modified version of the published protocol[227]. After optimization of the methods for use in myobundles, the following protocol was used; after differentiating for 2 weeks, unless otherwise specified, myotubes in monolayer and myobundles were cultured in serum- and insulin-free differentiation media for 18 hours prior to uptake. Myotubes and myobundles were washed in uptake buffer consisting of no glucose DMEM (ThermoFisher Scientific) with 0.1% (w/v) bovine serum albumin (Sigma-Aldrich) and 0.2 mM sodium pyruvate for 10 minutes. Myotubes and myobundles were then incubated in fresh uptake buffer for 30 minutes. Next, myotubes and myobundles (excluding negative control myobundles) were incubated for 20 minutes in uptake buffer with 5 mM 2-DG (Sigma-Aldrich). After uptake, myobundles were washed three times with ice-cold DPBS, then removed from the frames and lysed in 100 μl of 1X extraction buffer (Abcam) overnight at 4°C on a rocker. Myotubes were trypsinized and washed with DPBS via centrifugation and resuspension in ice-cold DPBS prior to lysis in the same manner as the myobundles. The next day, samples underwent a freeze/thaw cycle, were heated at 85°C for 40 minutes to remove endogenous NADP, and 50 μL of 200 mM triethanolamine (TEA) buffer (Sigma-Aldrich) was added to each sample. Samples were stored at -20°C until assayed. To

quantify the 2-DG6P in the lysed samples, the protocol was followed as put forth in the previous publication[227].

2.2.5 EC_{50} curve fitting

The 2-DG uptake of myobundles was measured in response to 7-9 different insulin concentrations in order to construct a curve showing the effect of insulin concentration on 2-DG uptake. All uptake rates were normalized to the basal uptake rate within each donor. Using Matlab's curve fitting tool, and the assumption that the effect of insulin on 2-DG uptake follows Michaelis Menten kinetics, the equation

$$f(x) = 1 + \frac{R_{max}x}{EC_{50}+x} \qquad \text{(Equation 2)}$$

where x represents insulin concentration and f(x) represents 2-DG uptake rate normalized to basal uptake rate was fitted to the data for each donor. To obtain the compiled R_{max} and EC_{50} values, the curve was fitted using all of the normalized 2-DG uptake rates from all donors.

2.2.6 Contractile function measurements

Myobundles were placed in a tissue bath kept at 37°C with one end of the myobundle pinned to a fixed PDMS platform and the other end pinned to a PDMS pad attached to a force transducer. Contractile force was measured in response to an electrical stimulus applied to the myobundle via two electrodes placed on either side of the bundle in the tissue bath. Myobundles were stretched to 115% of normal length prior to stimulation with one second of stimulation at 1 Hertz for a twitch contraction, one

second of stimulation at 20 Hertz for a tetanus contraction, and thirty seconds of stimulation at 20 Hertz to fatigue the muscle. Peak twitch and tetanus force, percent fatigue and twitch kinetics (time to peak twitch and half-relaxation time) were determined using a Matlab script. Peak twitch and tetanus were calculated as the difference between the highest measured force after stimulation and the baseline passive force prior to stimulation. Percent fatigue was calculated as $\frac{peak\ force - force\ after\ 30\ seconds\ of\ fatigue}{peak\ force - baseline\ force}\ x\ 100\%$. Time to peak twitch was calculated as the time between initiation of electrical stimulation and peak force. Half-relaxation time was calculated as the time between peak force and return to one-half of the difference between the peak force and the baseline force.

2.2.7 Electrical stimulation

For all post-exercise 2-DG uptake experiments, myobundles were differentiated in DMEM-based differentiation media with the addition of fatty acids and 1.72 μM insulin for 7 days prior to initiation of the exercise regime. During the second week of differentiation, trained myobundles were exposed to a cycle of 1 hour of 1 Hz, 10 Hz or 20 Hz stimulation followed by 7 hours of rest, as previously published[226]. Myobundles were cultured overnight prior to 2-DG uptake in serum- and insulin-free differentiation media. Post-exercise 2-DG uptake was performed immediately after a bout of 40 minutes of acute exercise during which myobundles were cultured in uptake buffer with or without insulin.

For the 2-DG uptake experiment during the initial stage of exercise, myobundles were differentiated in LAA-based differentiation media with the addition of fatty acids and 10 nM insulin for 7 days. Myobundles were electrically stimulated for 20 minutes at a frequency of 5 Hz while in uptake buffer containing 5 mM 2-DG.

2.2.8 Drug and inhibitor treatment

For experiments testing the effect of metformin, myobundles were treated with 400 μM metformin (Sigma-Aldrich) for 18 hours prior to the endpoint assays of 2-DG uptake and force testing. To determine the dose response to the Akt inhibitor CCT128930 (Selleck Chemicals), myobundles were treated for 1 hour prior to 2-DG uptake. The specific HDAC5 inhibitor LMK235 (Sigma-Aldrich) was added to myotubes at a concentration of 10 nM to myotubes for a variety of durations, as specified, during weeks 1 and 2 of differentiation. LMK235 was also added to myotubes at a concentration of 20 nM for an acute duration of 18 hours immediately prior to 2-DG uptake. The general HDAC inhibitor 4-phenylbutyric acid (4-PBA) (Sigma-Aldrich) was added to myotubes and myobundles at a concentration of 5 mM for 18 hours prior to 2-DG uptake.

2.2.9 qRT-PCR

Myobundles were flash frozen in liquid nitrogen prior to total RNA extraction using the Aurum Total RNA Mini Kit from BioRad. cDNA was produced using the iScript cDNA Synthesis Kit (BioRad). Genes of interest GLUT1, GLUT4, GLUT3, PGC-

1α, and housekeeping gene β-2 microglobulin were amplified and quantified using the iQ SYBR Green Supermix (BioRad) and CFX Connect Real-Time PCR Detection System (BioRad). Primer sequences are included in Table 1.

Table 1. Primer sequences used for qRT-PCR.

Primer	Forward primer	Reverse primer
β2M	5'-GGCTATCCAGCGTACTCCAAAG-3'	5'-CAACTTCAATGTCGGATGGATG-3'
GLUT1	5'-ATCATCGGTGTGTACTGCGG-3'	5'-GGTCATGGGTCACGTCAGCT-3'
GLUT4	5'-TTCCAACAGATAGGCTCCGAAG-3'	5'-AAGCACCGCAGAGAACACAG-3'
GLUT3	5'-ACTTTGACGGACAAGGGAAATG-3'	5'-ACCAGTGACAGCCAACAGG-3'
PGC-1α	5'-TGTGCAACTCTCTGGAACTG-3'	5'-TGAGGACTTGCTGAGTGGTG-3'

2.2.10 Normalization and statistical analysis

For experiments done with multiple donors, a global normalization process was used for each functional measure (twitch force, tetanus force, 2-DG uptake rate, etc.) to account for inherent differences between the functional output values of myobundles from each donor. A global average was determined, equivalent to the average of all raw output values from all conditions and all donors. Next, a donor-specific average was determined from all conditions within the experiment done using that donor. For each donor, a multiplier consisting of the ratio of the global average to the donor-specific average was propagated through the raw data. Finally, the normalized donor-specific averages for all donors for each condition were averaged to obtain the compiled average for that condition. This method preserves the relative differences in output between

conditions within donors while removing differences in background output between donors.

For experiments with multiple donors, the number of donors was used to determine S.E.M. and individual donor averages were used for statistical analysis. For experiments with only one donor, the number of myobundles per condition was used to determine S.E.M., and individual myobundle data were used for statistical analysis. Student's t-test was used for pairwise comparisons. For multiple comparisons an ANOVA was run, followed by Tukey HSD post-hoc testing for statistical significance. One symbol indicates $p < 0.05$, two symbols indicate $p < 0.01$, and three symbols indicate $p < 0.001$.

2.3 Results

2.3.1 Media-based glucose uptake assay

To measure glucose uptake in tissue engineered skeletal muscle myobundles, we investigated two approaches. The first approach was a media-based glucose uptake detection method for which media was sampled at several time points over the course of 24 hours to determine changes in the glucose concentration in the media as measured using the Amplex Red Glucose/Glucose Oxidase Assay kit. The media-based assay relies on taking media samples to measure changes in the bulk concentration of glucose over time (Figure 1A). Because glucose uptake rates are concentration-dependent, the most

accurate method of analyzing the rate is to calculate the R_{max}, which represents the maximal glucose uptake rate at saturation for that myobundle. The value for R_{max} for each sample can be determined by finding the slope of the line of best fit of the appropriately manipulated concentration data, as discussed in the materials and methods section (Figure 1B). When myobundles were kept in media containing the standard low glucose concentration of 5.55 mM over the course of sampling, the percent change in glucose concentration over 24 hours was about 45% (Figure 1C). In order to increase the sensitivity to better resolve changes in the glucose concentration of the media, the initial glucose concentration was lowered to 1 mM (Figure 1D). Although the media-based assay is non-destructive, it requires measurement over at least six hours to measure appreciable changes in glucose, making it poorly suited for measuring acute changes in glucose uptake.

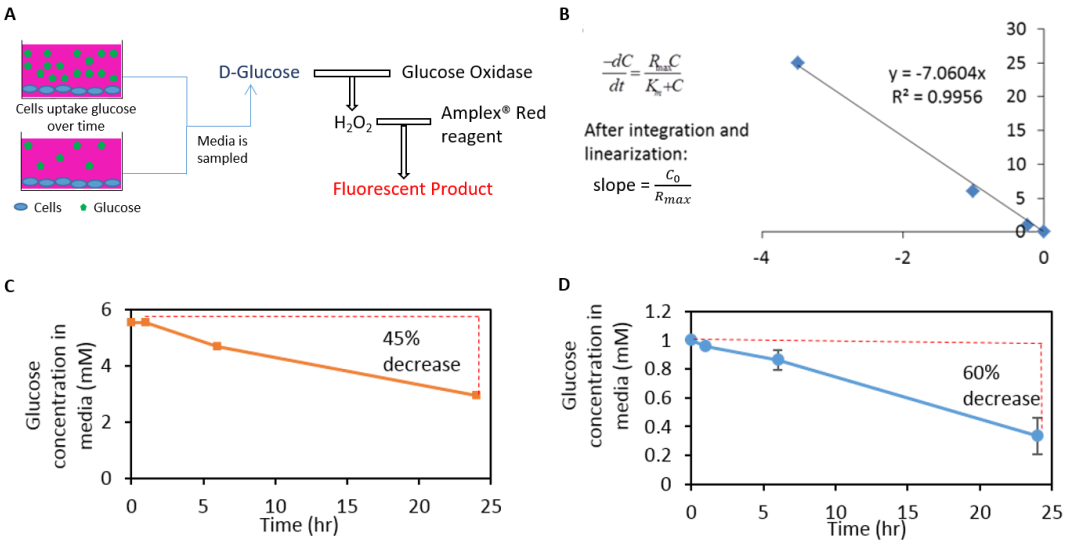

Figure 1. Media-based assay for measuring glucose uptake. A) The Amplex® assay relies on a coupled reaction in which the reaction of glucose oxidase with glucose in the media samples produces hydrogen peroxide, which reacts with the Amplex® Red reagent in the presence of HRP to produce the fluorescent product resorufin in a 1:1 stoichiometric ratio. B) Method of analyzing the rate of uptake with a changing concentration of glucose in the media, outputting the Rmax value. K_m is assumed to be 3 mM[228]. C) Glucose concentration in the media drops by 45% over the course of 24 hours with a starting concentration of 5.55 mM. D) Glucose concentration in the media drops by 60% over the course of 24 hours with a starting concentration of 1 mM.

2.3.2 2-deoxyglucose uptake assay

The second method of approximating glucose uptake makes use of the glucose analog 2-deoxyglucose, which is taken up into cells and phosphorylated, but is incapable of undergoing further metabolism. Due to the phosphorylation step, the 2-DG6P cannot be transported outside of the cell and accumulates within the cell until lysis. The lysed solution can be reacted as specified in the original protocol to produce a fluorescent product, which is quantified using a plate reader and a standard curve of 2-DG6P (Figure 2).

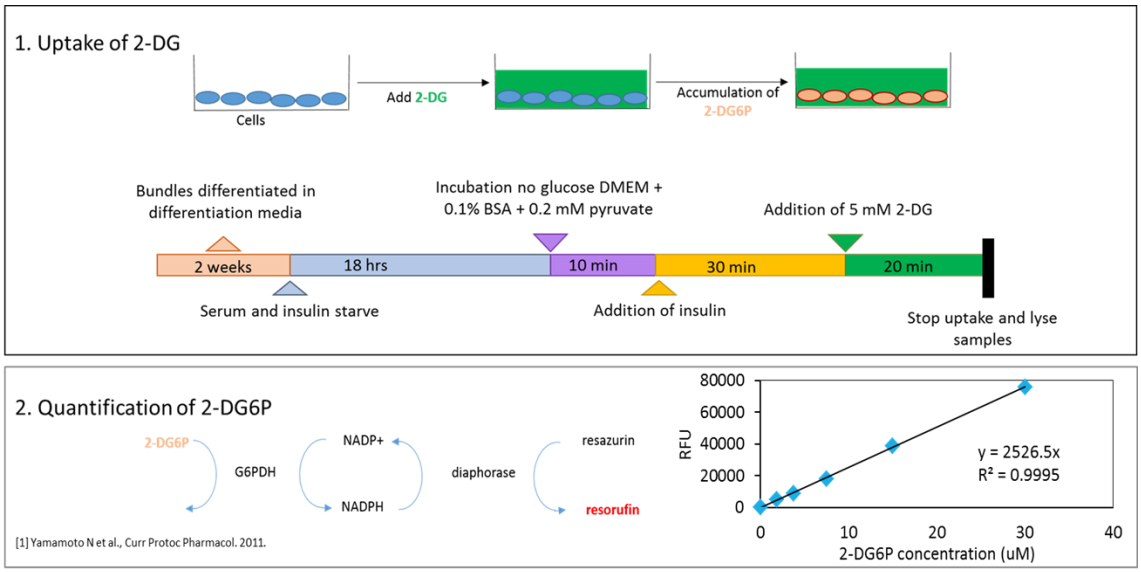

Figure 2. 2-deoxyglucose-based assay for measuring glucose uptake. Cells in monolayer culture or in myobundles are differentiate for two weeks, then serum and insulin starved for 18 hours prior to a 10 minute wash in glucose-free uptake buffer. Cells or myobundles are then cultured with or without insulin for 30 minutes, and 5 mM 2-DG is added for 20 minutes. After uptake, the cells or myobundles are washed with ice cold PBS and lysed overnight. The quantification assay[227] makes use of a coupled reaction to produce the fluorescent product resorufin.

The initial uptake protocol[227] was intended for use with cells grown in monolayer, and needed adaptation and validation for use with myobundles. Before performing the uptake experiment, the published protocol recommended that the cells be serum starved to enhance glucose uptake. To investigate whether the serum starvation step impacted myobundle function, myobundles were maintained in either normal differentiation media or in serum-free media for 18 hours prior to measuring contractile force. There were no significant differences in force production between the myobundles cultured in serum-containing and those in serum-free media (Figure 3A), indicating that the serum-starvation step does not impact contractile function. The

protocol suggested using a Krebs-Ringer-HEPES buffer during uptake, but we found an improved insulin response when using no glucose DMEM as the base for the uptake buffer (Figure 3B). The uptake of 2-DG was linear for up to 40 minutes, indicating that at a 2-DG bulk concentration of 5 mM, accumulation of the 2-DG6P within the myobundles did not inhibit further uptake over the duration of 20 minutes used for uptake experiments (Figure 3C). Further, though the original protocol recommended using 1 mM 2-DG, we found that using 5 mM 2-DG increased the rate of uptake in a manner proportional to the increase in concentration, suggesting that uptake was not saturated at these concentrations (Figure 3D). When myobundles were incubated with 2-DG in the presence of cytochalasin B, which inhibits carrier-mediated glucose transport, the apparent uptake rate from the quantification assay matched that of the bundle with no 2-DG added (Figure 3E). This indicated that, as expected, there was no background signal due to non-intracellular 2-DG, and myobundles without any 2-DG added are an appropriate negative control for the assay. The original protocol recommended lysis in NaOH, but this method produced a very low signal, so lysis was performed for 24 hours using RIPA buffer with phosphatase inhibitor, resulting in a much higher apparent 2-DG uptake rate and indicating better retrieval of 2-DG6P from the cells (Figure 3F). Use of extraction buffer further enhanced 2-DG6P retrieval (Figure 3G). When comparing uptake rates measured by the media-based versus the 2-DG assay, the 2-DG-based assay indicated a basal 2-DG uptake rate of approximately two-fold lower than the media-

based assay output (Figure 3H). This could be due to less than full retrieval of 2-DG6P from the myobundles or possible slight differences in the affinity of glucose transporters for 2-DG and glucose[229,230]. The ability to measure a snapshot of glucose uptake rates immediately following exercise or immediately following an acute treatment with an inhibitor was vital for future work. The fact that the 2-DG-based assay allowed us to capture acute changes in uptake rates, as well as its specificity for intracellular 2-DG were motivations for continuing further glucose uptake experiments using the 2-DG-based protocol.

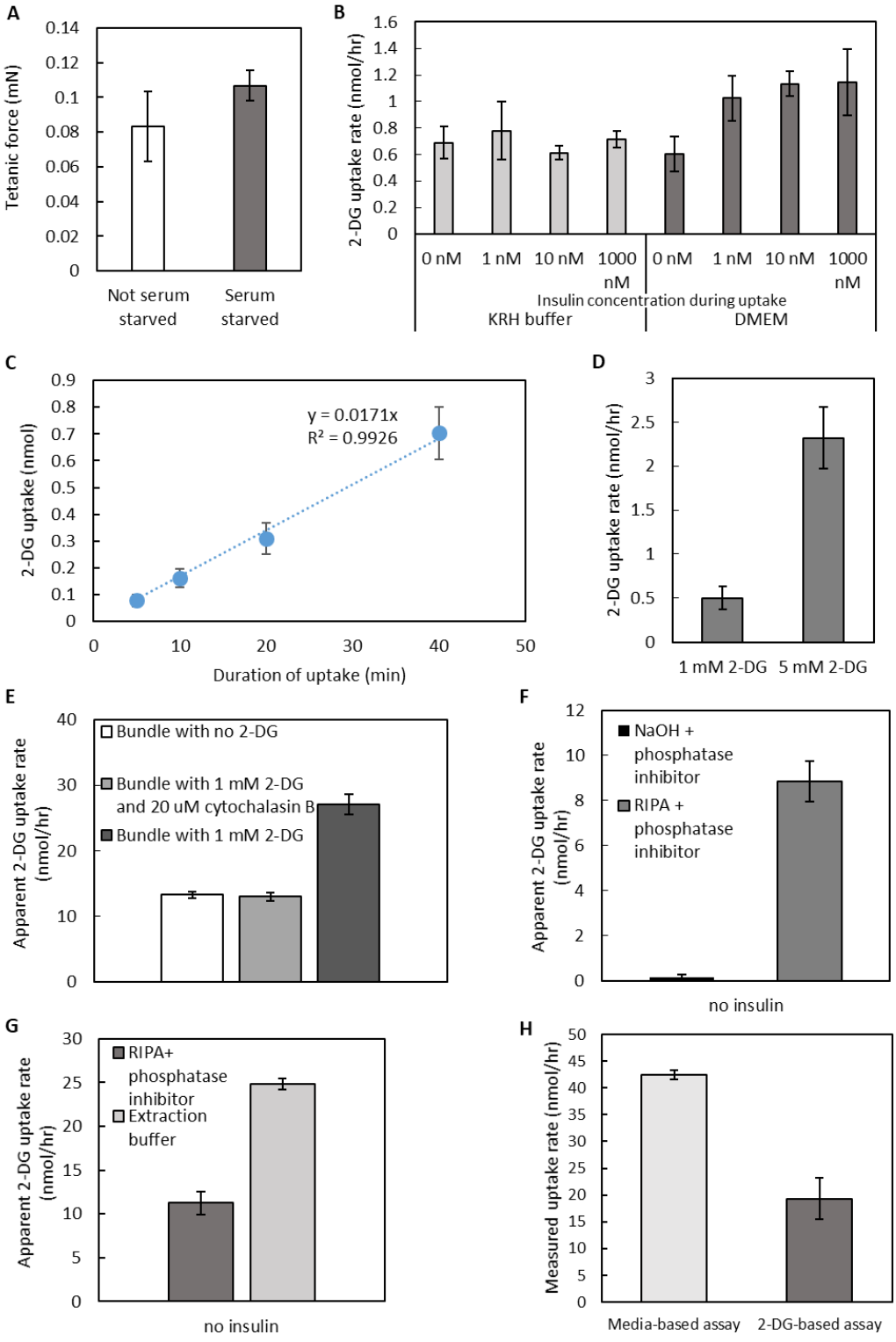
A
Tetanic force (mN)
0.14
0.12
0.1
0.08
0.06
0.04
0.02
0
Not serum starved
Serum starved
B
2-DG uptake rate (nmol/hr)
1.6
1.4
1.2
1
0.8
0.6
0.4
0.2
0
0 nM
1 nM
10 nM
1000 nM
0 nM
1 nM
10 nM
1000 nM
Insulin concentration during uptake
KRH buffer
DMEM
C
2-DG uptake (nmol)
y = 0.0171x
R² = 0.9926
0.9
0.8
0.7
0.6
0.5
0.4
0.3
0.2
0.1
0
0
10
20
30
40
50
Duration of uptake (min)
D
2-DG uptake rate (nmol/hr)
3
2.5
2
1.5
1
0.5
0
1 mM 2-DG
5 mM 2-DG
E
Apparent 2-DG uptake rate (nmol/hr)
40
30
20
10
0
Bundle with no 2-DG
Bundle with 1 mM 2-DG and 20 uM cytochalasin B
Bundle with 1 mM 2-DG
F
Apparent 2-DG uptake rate (nmol/hr)
12
10
8
6
4
2
0
NaOH + phosphatase inhibitor
RIPA + phosphatase inhibitor
no insulin
G
Apparent 2-DG uptake rate (nmol/hr)
30
25
20
15
10
5
0
RIPA+ phosphatase inhibitor
Extraction buffer
no insulin
H
Measured uptake rate (nmol/hr)
50
45
40
35
30
25
20
15
10
5
0
Media-based assay
2-DG-based assay

Figure 3. 2-DG uptake quantification assay optimization and validation. A) Tetanus contractile forces were measured in myobundles which were either serum-starved or maintained in serum-containing differentiation media. N=1 donor, n=3 myobundles per condition. B) 2-DG uptake rate in basal and insulin-stimulated conditions were quantified in myobundles that had undergone uptake in either a KRH-based or DMEM-based uptake buffer. N=1 donor, n=3 myobundles per condition. C) Total 2-DG uptake was quantified in myobundles that were incubated with 5 mM 2-DG and 10 nM insulin for 5-40 minutes to assess linearity of 2-DG uptake over time. N=3 donors, n=3 myobundles per time point per donor. D) To determine the effect of an increased concentration of 2-DG, myobundles were incubated with either 1 mM or 5 mM 2-DG. N=1 donor, n=3 myobundles per condition. E) Myobundles were incubated either without 2-DG, with 2-DG and 20 μM cytochalasin B, or with 2-DG alone during uptake. N=1 donor, n=3 myobundles per condition. F) After 2-DG uptake, myobundles were lysed in either NaOH + phosphatase inhibitor or RIPA lysis buffer + phosphatase inhibitor to determine the difference in 2-DG6P extraction using the two lysis methods. N=1 donor, n=3 myobundles per condition. G) After 2-DG uptake, myobundles were lysed in either RIPA lysis buffer + phosphatase inhibitor or extraction buffer (with phosphatase inhibitor already in solution) to determine the difference in 2-DG6P extraction using the two lysis methods. N=1 donor, n=3 myobundles per condition. H) A comparison of the media-based assay measured glucose uptake and 2-DG-based assay measured glucose uptake in similar conditions, both with 1 mM starting concentration of glucose or 2-DG. N=1 donor, n=3-5 myobundles per condition. Data in all panels presented as mean ± S.E.M.

2.3.3 Effect of lowering amino acid and insulin content

We examined 2-DG uptake and insulin response of the myobundles cultured with more physiologically-relevant amino acid levels and insulin availability. In myobundles cultured using the LAA-based differentiation media, there was a significant decrease in basal 2-DG uptake and a slight but non-significant increase in the insulin response (Figure 4A) compared to the myobundles in the DMEM-based media, without any changes in the protein content of the myobundles (Figure 4B). Manipulation of the insulin concentration during differentiation by removing insulin during the second week of differentiation appeared to slightly increase the fold-change in 2-DG uptake in

response to insulin by lowering the basal 2-DG uptake (Figure 4C) and maintained contractile function in the bundles (Figure 4D). Further reducing the week 1 insulin concentration to 10 nM and removing insulin during week 2 of differentiation also maintained force production, but removal of insulin entirely from differentiation significantly impaired tetanic contractile force (Figure 4D). These initial experiments to improve the physiological relevance of the differentiation conditions led to the use of LAA-based differentiation media with no insulin during the second week of differentiation for all subsequent experiments.

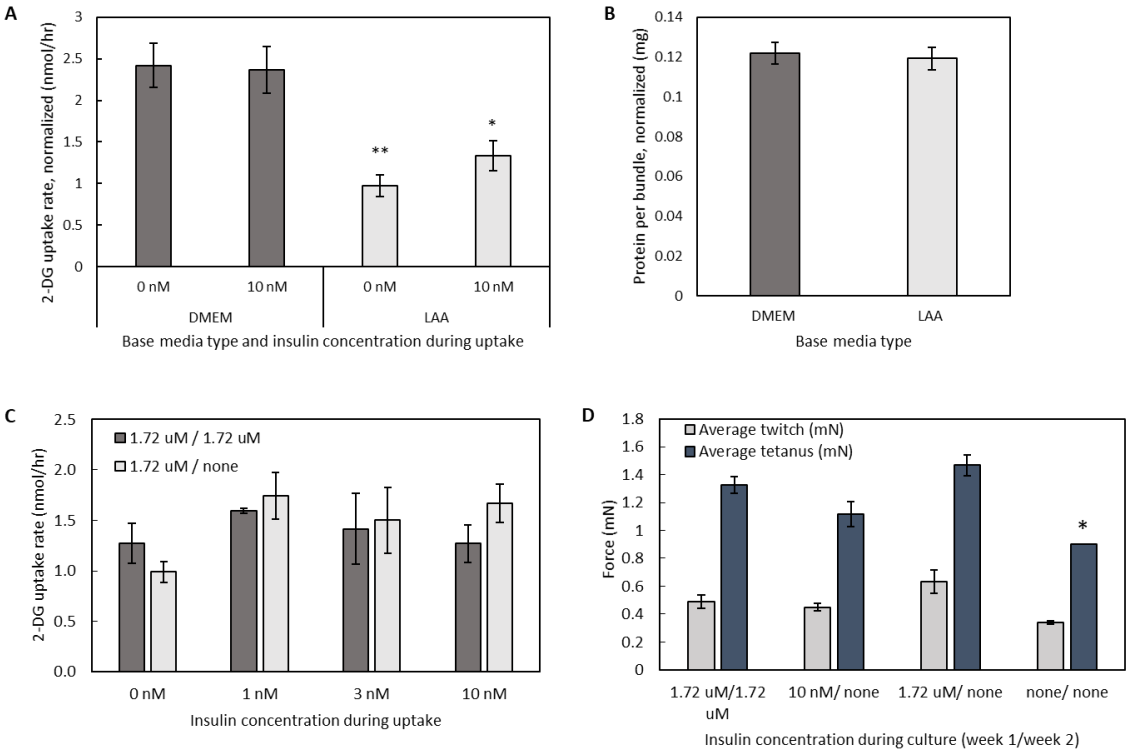

Figure 4. Effect of lowering amino acid and insulin content. A) Myobundles were differentiated in either DMEM-based or LAA-based differentiation media and 2-DG uptake was measured in basal and insulin stimulated states. N=4 donors, n=3-4

myobundles per condition per donor. * p <0.05, **p<0.01, *** p<0.001 when compared with the same insulin condition in the DMEM group. B) Myobundles cultured in either DMEM-based or LAA-based differentiation media were lysed and protein was measured using a BCA assay. N=2 donors, n=3 myobundles per condition per donor. C) Myobundles were cultured in differentiation media containing either 1.72 μM insulin for both weeks of differentiation (1.72 μM / 1.72 μM) or differentiation media containing 1.72 μM insulin for week 1 of differentiation and no insulin for week two of differentiation (1.72 μM / none) before measuring 2-DG uptake in the basal state and in response to several insulin concentrations. N=1 donor, n=3 myobundles per condition. D) Myobundles were cultured in differentiation media containing various levels of insulin; either 1.72 μM insulin for both weeks (1.72 μM / 1.72 μM), or low insulin the first week and no insulin the second week (10 nM / none), or 1.72 μM insulin the first week and no insulin the second week (1.72 μM / none), or no insulin for both weeks (none/ none) and contractile force production was measured. N=1 donor, n=3 myobundles per condition. * p<0.05 when compared with the same measurement in the 1.72 μM / 1.72 μM group. Data in all panels presented as mean ± S.E.M.

2.3.4 Effect of treatment with metformin on myotube and myobundle 2-DG uptake

To determine the suitability of the myobundle system as a model for detecting alterations in glucose metabolism in skeletal muscle, we treated both myotubes in monolayer culture and myobundles with metformin. Metformin is prescribed to promote increased glucose uptake in patients with type 2 diabetes, and is proposed to act via disruption of the function of complex I in the electron transport chain, leading to activation of the 5′ AMP-activated protein kinase (AMPK) pathway[231,232]. Both myotubes in 2-dimensional culture (Figure 5A) and the myobundles (Figure 5B) exhibited a statistically significant increase in glucose uptake in response to the metformin treatment. In the absence of insulin, metformin treatment increased the average 2-DG uptake rate of myotubes from 8.32 nmol/hr to 16.98 nmol/hr, a fold-change of 2.04. In

myotubes in the presence of insulin, metformin increased the average 2-DG uptake rate from 9.24 nmol/hr to 17.61 nmol/hr, a fold-change of 1.91. In myobundles in the absence of insulin, metformin treatment increased the average 2-DG uptake rate from 8.0 nmol/hr to 13.58 nmol/hr, a fold-change of 1.70. In the presence of insulin, metformin increased the average 2-DG uptake rate of myobundles from 9.57 nmol/hr to 16.86 nmol/hr, a fold-change of 1.76. Furthermore, we examined the impact of metformin treatment on contractile function and observed a 35% decrease in twitch force and a 29% decrease tetanus force production in the treated group (Figure 5C), matched by an increase in fatigue (Figure 5D) without changes in twitch kinetics (Figure 5E).

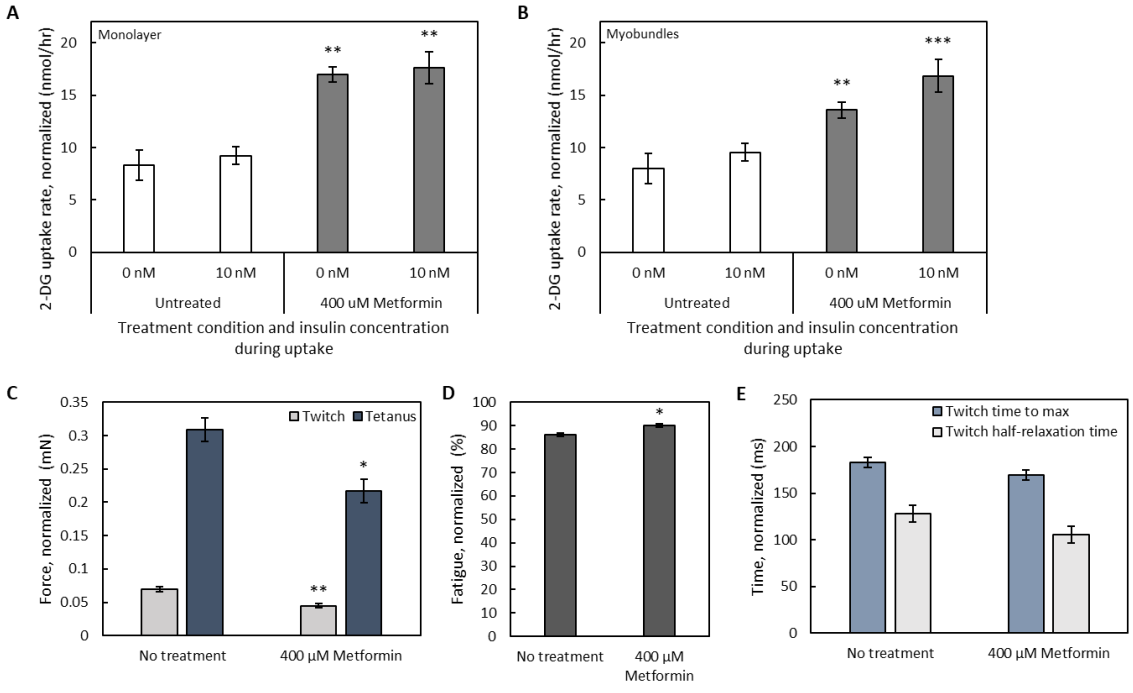

Figure 5. Effect of metformin treatment on myotubes in monolayer culture and myobundles. A) Myotubes were differentiated in a 6-well plate and treated with 400 µM metformin for 18 hours immediately prior to 2-DG uptake at the 2 week

differentiation time point. N=3 donors, n=3 wells per condition per donor. B) Myobundles were treated with 400 μM metformin for 18 hours immediately prior to 2-DG uptake at the 2 week differentiation time point. N=3 donors, n=3-4 myobundles per condition per donor. C-D) Myobundles were treated with 400 μM metformin for 18 hours immediately prior to measuring twitch and tetanus contractile force and percent fatigue at the 2 week differentiation time point. N=3 donors, n=3-4 myobundles per condition per donor. E) Analysis of time to maximum force and half-relaxation time of twitch contractions. N=3 donors, n=3-4 myobundles per condition per donor. * p <0.05, **p<0.01, *** p<0.001 when compared with the same insulin condition or contractile function measurement in the no treatment group. Data in all panels presented as mean ± S.E.M.

2.3.5 Characterization of myobundle insulin response

Next, we sought to establish the fold-change difference between insulin-stimulated and basal glucose uptake, as well as identify the concentration at which insulin stimulation is half-maximal (EC_{50}) in the myobundles. Curve fitting using the compiled results from insulin dose response experiments in four donors indicated an overall R_{max} value of 0.52 ± 0.007, which corresponds to a maximum 1.52-fold change in 2-DG uptake in the presence of insulin, and an EC_{50} of 0.268 ± 0.03 nM insulin (Figure 6A). Individual donor R_{max} values were 1.061 ± 0.03, 0.242 ± 0.016, and 1.433 ± 0.032, with EC_{50} values of 0.871 ± 0.13, 0.0005 ± 0.017 and 2.058 ± 0.23, respectively (Figure 6B). One donor yielded several insulin response values that were lower than the basal 2-DG uptake, which precluded the determination of the EC_{50} and R_{max} values for that donor. When taking into account only physiological concentrations of insulin, the maximum experimentally-determined fold-change of all donors compiled was 1.51 and occurred at an insulin concentration of 10 nM (Figure 6B). When including all of the insulin concentrations tested, there is a maximum experimental fold-change of 1.64, occurring at

1000 nM. This was heavily influenced by one donor, the S115 donor, which exhibited a large response to an insulin concentration of 1000 nM. The other donors all responded maximally to insulin concentrations of 10 nM or less.

A

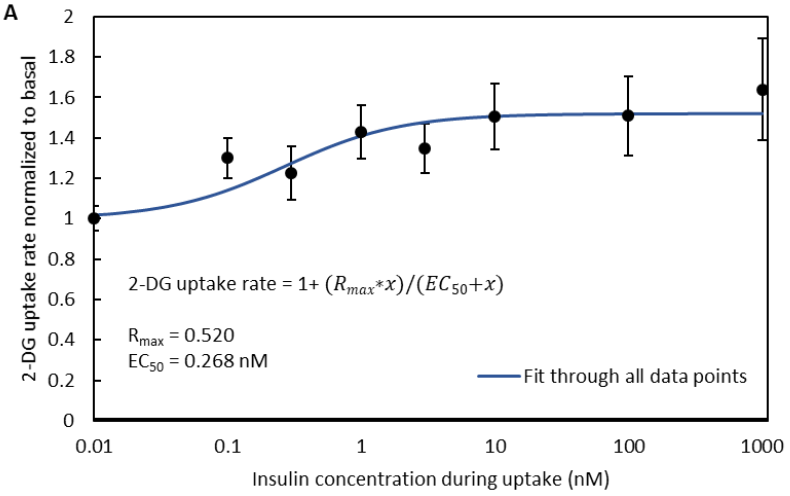

B

Donor	Maximum experimental fold-change in 2-DG uptake	Insulin concentration of maximum response (nM)	R_{max} parameter	EC50 parameter (nM)
S110	2.28	10	1.061 ± 0.03	0.871 ± 0.13
S111	1.20	0.05	N/A	N/A
S113	1.40	0.3	0.242 ± 0.016	0.005 ± 0.017
S115	1.95*; 3.39	1*; 1000	1.433 ± 0.032	2.058 ± 0.23
Compiled	1.51*; 1.64	10* ; 1000	0.520 ± 0.007	0.268 ± 0.03

Figure 6. Characterization of insulin sensitivity and dose response in myobundles. A) Basal and insulin-mediated 2-DG uptake were measured in myobundles at 2 weeks post-differentiation. The 2-DG uptake rates were normalized to the basal uptake rate for each donor. Using a curve fitting tool, the values for the R_{max} and EC_{50} parameters were determined. B) Individual donor experimental values for the maximum fold-change in 2-DG uptake with insulin stimulation and the insulin concentration at which that maximum fold-change occurred, as well as the individual donor R_{max} and EC_{50} values. For each donor, n=3-7 myobundles per insulin condition per donor. Data presented as mean ± S.E.M.

2.3.6 Effect of electrical stimulation on myobundle 2-DG uptake

Because exercise plays an important role in changes in glucose uptake and insulin sensitivity in skeletal muscle *in vivo*, we sought to understand how electrical stimulation models of exercise impacted 2-DG uptake by the myobundles. Initial experiments were carried out immediately after a bout of acute exercise in bundles that had either undergone training with a specific electrical stimulation regime (details in Materials and Methods) during the second week of differentiation or were untrained and had not undergone any electrical stimulation prior to the 40 minute acute bout of exercise after two weeks of differentiation. With a 1 Hertz electrical stimulation protocol, there was no observed change in either basal 2-DG uptake or insulin response measured immediately following acute exercise, nor were there significant differences between the trained and untrained groups (Figure 7A). Measuring the basal 2-DG uptake of rested bundles, meaning it had been two hours since the last bout of electrical stimulation, that were trained for one week using increasing frequencies of electrical stimulation resulted in a trend of increased basal glucose uptake with the 1 Hertz and 10 Hertz regimes, though the differences were not significant (Figure 7B).

Based on these results, we examined the impact of a more strenuous electrical stimulation regime using 10 Hertz frequency of stimulation to train all bundles during the second week of differentiation. Here we found that immediately following acute exercise at 10 Hertz for 40 minutes, the insulin response was diminished when

compared to bundles that had been rested (Figure 7C). However, myobundles that were cultured with lower or no insulin during week two of differentiation retained their response to insulin immediately following acute exercise (Figure 7C). These results are in accordance with earlier results (Figure 4A) that demonstrated improved acute insulin response in bundles with insulin removed from the culture media during the second week of differentiation. Overall, we observed higher basal 2-DG uptake in trained bundles than in untrained bundles in the rested state, but 2-DG uptake rates were not impacted immediately following acute exercise.

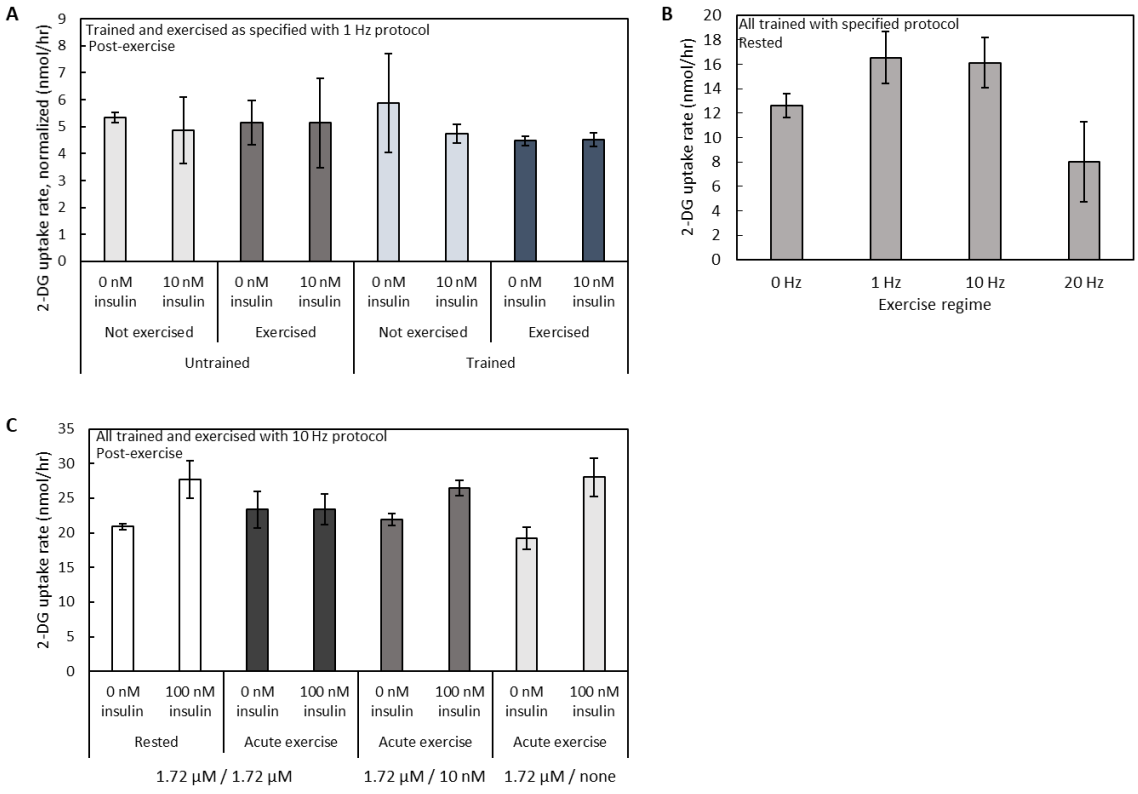

Figure 7. Effect of electrical stimulation on 2-DG uptake and insulin response. A) Myobundles were either untrained or trained using a 1 Hz electrical stimulation regime during week 2 of differentiation. Within these groups, myobundles either did

not undergo acute exercise (not exercised) or did undergo an acute exercise bout of 40 minutes during which myobundles were cultured either without insulin or with 10 nM insulin. 2-DG uptake was measured immediately following the acute exercise bout. N=2 donors, n=4 myobundles per condition per donor. B) Myobundles were either untrained or underwent training regimes of 1, 10, or 20 Hz during week 2 of differentiation. Myobundles were rested for at least two hours prior to 2-DG uptake to measure basal uptake rates in the absence of insulin. N=1 donor, n=4 myobundles per condition. C) All myobundles were trained using a 10 Hz electrical stimulation regime during week 2 of differentiation. Myobundles were differentiated using varying insulin conditions of either 1.72 μM for both weeks (1.72 μM / 1.72 μM), or 1.72 μM for the first week of differentiation and 10 nM for the second week (1.72 μM / 10 nM), or 1.72 μM for the first week and no insulin for the second week (1.72 μM / none). Within these groups, myobundles either did not undergo acute exercise or did undergo an acute exercise bout of 40 minutes during which myobundles were cultured either without insulin or with 10 nM insulin. 2-DG uptake was measured immediately following the acute exercise bout. N=1 donor, n=4 myobundles per condition per donor. All data presented as mean ± S.E.M.

2.3.7 Effect of altered ECM content on myobundle 2-DG uptake

In an effort to enhance the insulin response in the myobundles, we identified two variables that could be altered regarding the ECM used to form the myobundles. We hypothesized that the Matrigel, which contains growth factors such as IGF-1, could increase constitutive signaling through the insulin signaling pathway, which would impair the insulin response due to the presence of GLUT4 at the cell surface in the basal state. However, growth-factor reduced (GFR) Matrigel did not have a significant effect on insulin-mediated 2-DG uptake (Figure 8A). In contrast, there was a trend of increased insulin-mediated 2-DG uptake with increasing fibrinogen concentration (Figure 8B). This increase in the magnitude of insulin response was accompanied by a trend towards higher force production by bundles made with 25 mg/mL fibrinogen (Figure 8C).

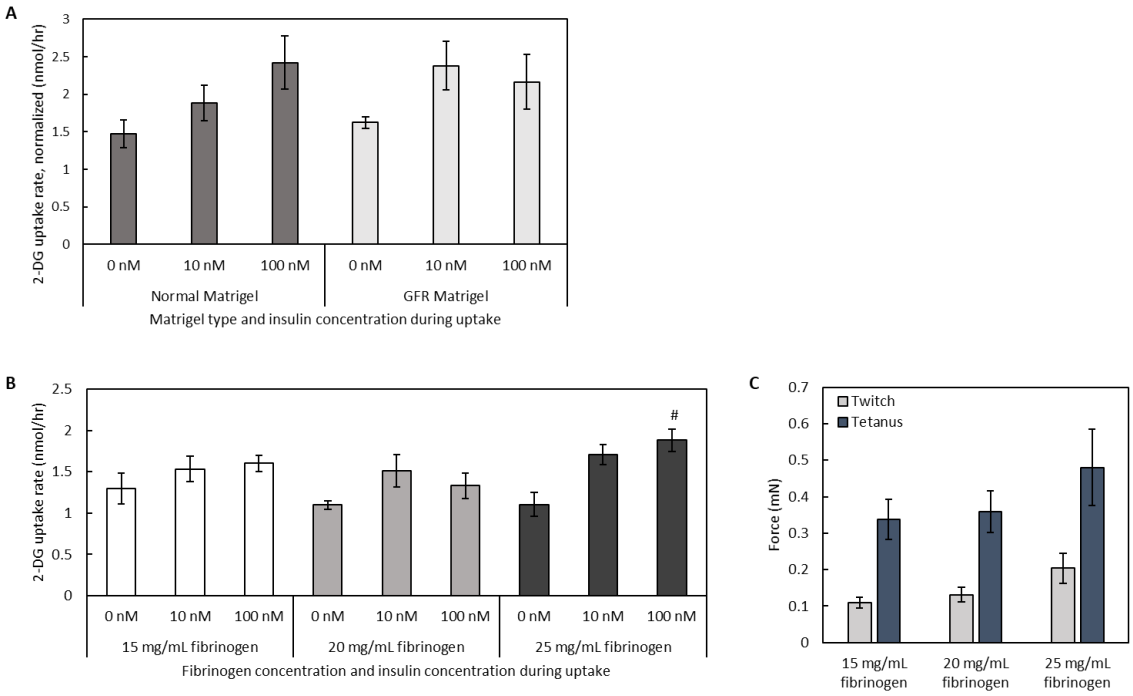

Figure 8. Effect of altering ECM components on myobundle function. A) Myobundles were formed using either normal Matrigel or growth-factor reduced Matrigel and basal and insulin-mediated 2-DG uptake was measured at the two weeks post-differentiation time point. N=3 donors, n=3-4 bundles per condition per donor. # $p<0.05$ when compared with the no insulin condition in the same group. B-C) Myobundles were formed using fibrinogen solutions of either 15 mg/mL, 20 mg/mL, or 25 mg/mL and B) basal and insulin-mediated 2-DG uptake and C) contractile force production was measured at the two-week post-differentiation time point. N=1 donor, 2 experiments, n=3 myobundles per condition per experiment. All data presented as mean ± S.E.M.

2.3.8 Effect of altered culture conditions on myobundle 2-DG uptake

We identified additional media-based factors that may impact myobundle insulin sensitivity and examined 2-DG uptake in myobundles cultured using alternative conditions. Because streptomycin has been associated with impaired function in tissue engineered muscle[233], we substituted gentamicin but found that this change did not

significantly affect 2-DG uptake or insulin response (Figure 9A). Dexamethasone is a glucocorticoid included in cell culture media to promote proliferation, but it has been implicated in the development of insulin resistance in humans[234]. When dexamethasone was removed from the growth media in which the myoblasts were expanded and the growth media that the myobundles were cultured in for the first 4 days post-fabrication, there was no significant improvement in insulin response (Figure 9B). The basal 2-DG uptake is lower in the group with no dexamethasone, but this is likely a result of decreased proliferation during the growth phase of the myobundles. L-glutamine concentrations higher than 500 μM caused mitochondrial uncoupling in human myotubes *in vitro*[235], but lowering the L-glutamine concentration to 300 μM in our differentiation media had no impact on 2-DG uptake or insulin response by the myobundles (Figure 9C). Skeletal muscle *in vivo* experiences cyclical availability of glucose and insulin associated with meals, which is a departure from the relatively constant and high levels of nutrients seen *in vitro*. To mimic fed and fasted states, we cultured myobundles primarily with 'fasting' media containing 1 mM glucose and no insulin and changed media to 'feeding' media containing 5.55 mM glucose and 10 nM insulin for one hour, twice per day. Control bundles experienced simultaneous media changes but were kept in the 'feeding' media at all times. Mimicking meals in this manner had no significant effect on the insulin response of the myobundles (Figure 9D).

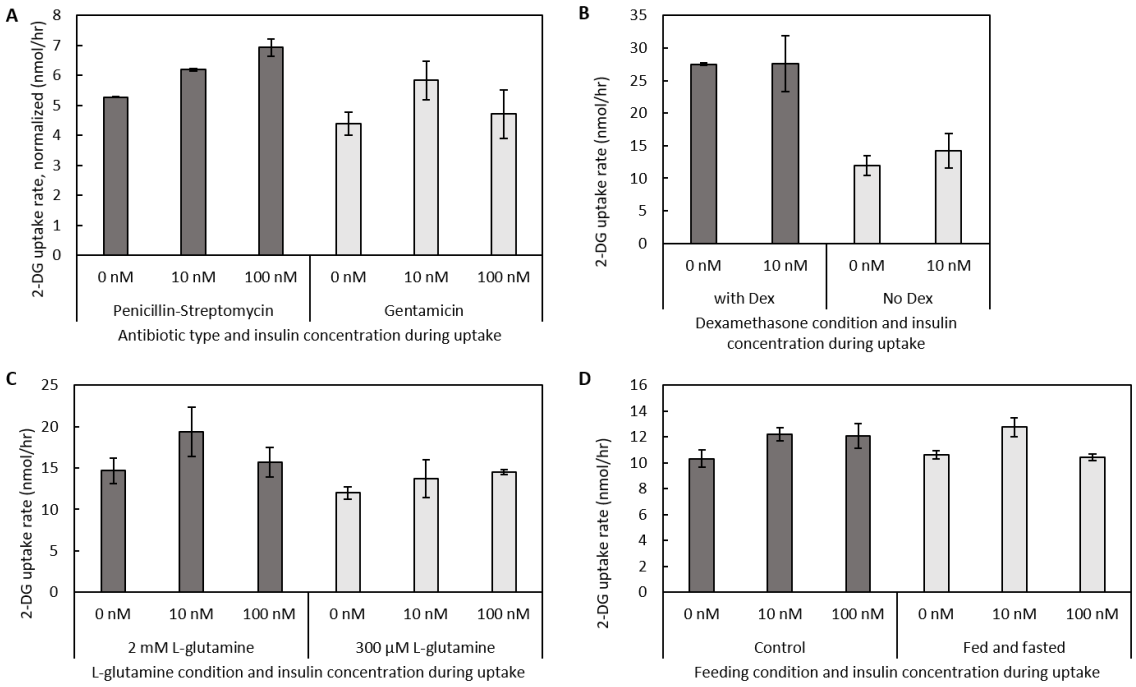

Figure 9. Effect of altering media components and culture conditions on basal and insulin-mediated 2-DG uptake. A) Myobundles were cultured in media containing either penicillin-streptomycin or gentamicin and basal and insulin-mediated 2-DG uptake was measured at the two weeks post-differentiation time point. N=2 donors, n=4 myobundles per condition per donor. B) Myoblasts were expanded in media with or without dexamethasone and myobundles were formed from either the with-dex or no-dex conditions. The myobundles were also cultured in growth media either with or without dexamethasone before differentiation for two weeks, at which point basal and insulin-mediated 2-DG uptake was measured. N=1 donor, n=3 myobundles per condition. C) Myobundles were differentiated in media containing either 2 mM L-glutamine or 300 µM L-glutamine and basal and insulin-mediated 2-DG uptake was measured at the two weeks post-differentiation time point. N=1 donor, n=3 myobundles per condition. D) During two weeks of differentiation, 'fed and fasted' myobundles were maintained primarily in 'fasting' media containing 1 mM glucose and no insulin, with media changed to 'feeding' media containing 5.55 mM glucose and 10 nM insulin for one hour, twice per day. Control bundles experienced simultaneous media changes but were kept in the 'feeding' media at all times. Basal and insulin-mediated 2-DG uptake was measured at two weeks post-differentiation. N=1 donor, n=3 myobundles per condition. All data presented as mean ± S.E.M.

2.3.9 Effect of Akt and HDAC inhibitors on myotube and myobundle 2-DG uptake and contractile function

Next, we turned to inhibitors of specific pathways or signaling cascades to probe the mechanisms responsible for the dampened insulin response *in vitro*. An Akt inhibitor would allow us to identify if the insulin signaling pathway was constitutively activated during the basal state due to myobundle or media components. Treatment with the Akt inhibitor CCT128930[236] for one hour immediately prior to endpoint testing at 2 weeks post-differentiation resulted in lower basal 2-DG uptake rates at a concentration of 40 μM, indicating some contribution of Akt signaling to the basal 2-DG uptake rate (Figure 10).

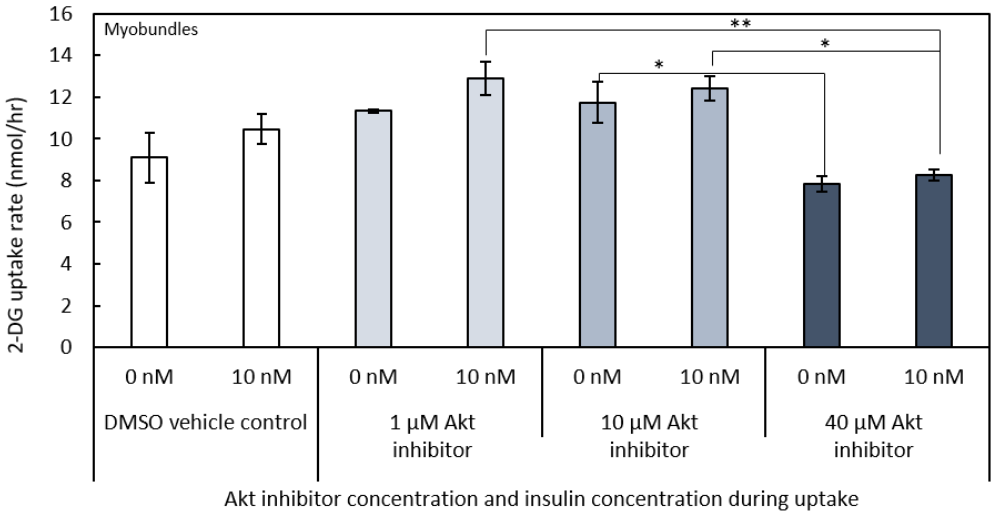

Figure 10. Effect of Akt inhibitor on basal and insulin-mediated 2-DG uptake by myobundles. Myobundles were treated with the Akt inhibitor CCT128930 at the indicated concentrations for 1 hour immediately prior to measuring 2-DG uptake. N=1 donor, n=3 myobundles per condition. * p<0.05, ** p<0.01 when compared to the indicated group. Data presented as mean ± S.E.M.

Histone deacetylase (HDAC) inhibitors prevent HDACs from condensing chromatin, and have been shown to regulate glucose uptake and insulin response in skeletal muscle[237]. LMK235 is an HDAC inhibitor that specifically targets HDAC5 with an IC_{50} of 4 nM. The IC_{50} for HDAC4 is 12 nM, with IC_{50} values for all other HDACs of 56 nM or higher[238]. To assess the impact of LMK235 treatment during early differentiation, myobundles were treated with 10 nM LMK235 during day 1 of differentiation (1 day duration), days 1-3 of differentiation (3 day duration), or days 1-6 of differentiation (6 day duration). There was no significant trend in 2-DG uptake or insulin response with these conditions, though it appeared that a longer-term 3 or 6-day duration of treatment during week 1 may impair insulin response (Figure 11A). To examine the effect of LMK235 when administered during week 2 of differentiation, it was added at a concentration of 10 nM during days 8 to 13 of differentiation (6 day duration). There was a significant increase in 2-DG uptake in the 100 nM insulin condition compared to basal 2-DG uptake in both the vehicle control group and the LMK 235 treatment group, but the LMK 235 resulted in a significant increase in the 100 nM insulin condition compared to the 100 nM insulin condition in the vehicle control group (Figure 11B). This indicates a positive effect of long-term week 2 LMK235 treatment on the insulin response in myotubes in 2D. However, when myotubes were treated with 20 nM LMK 235 for an acute time period, there was no significant impact on 2-DG uptake or insulin response (Figure 11C).

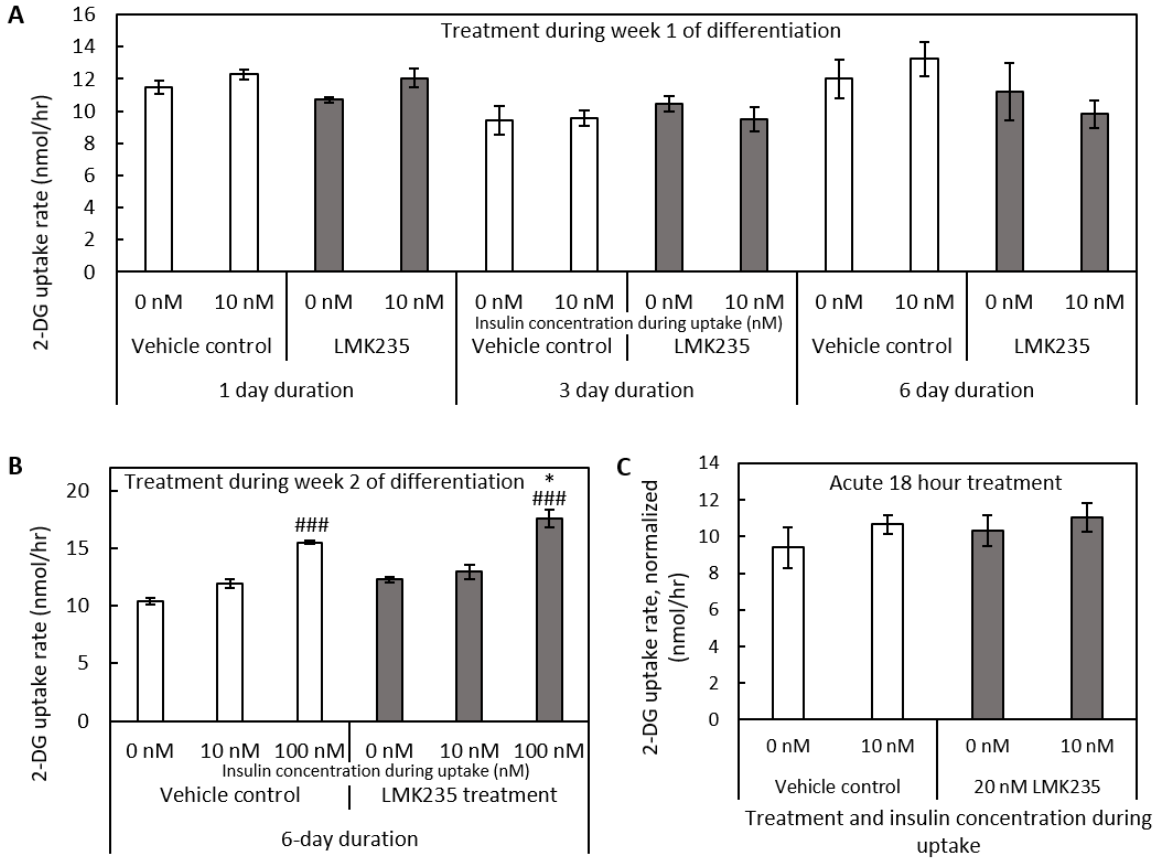

Figure 11. Effect of the specific HDAC4 and 5 inhibitor LMK235 on basal and insulin-mediated 2-DG uptake by myotubes. A) Myotubes in monolayer culture were treated with 10 nM LMK235 during the first week of differentiation. The 1-day duration corresponded to treatment during day 1 of differentiation, the 3-day duration corresponded to treatment during days 1-3 of differentiation, and the 6-day duration corresponded to treatment during days 1-6 of differentiation. Basal and insulin-mediated 2-DG uptake was measured at two weeks post-differentiation. N=1 donor, n=3 wells per condition. B) Myotubes in monolayer culture were treated with 10 nM LMK235 from days 8-13 of differentiation (6-day duration) and basal and insulin-mediated 2-DG uptake was measured at two weeks post-differentiation. N=1 donor, n=3 wells per condition. ### $p<0.001$ compared to the no insulin condition within the treatment group, *$p<0.05$ compared to the same insulin condition in the vehicle control treatment group. C) Myotubes were treated with 20 nM LMK235 for 18 hours immediately prior to measuring basal and insulin-stimulated 2-DG uptake at two weeks post-differentiation. N=3 donors, n=3 wells per condition per donor. All data presented as mean ± S.E.M.

We next examined the impact of a more general HDAC inhibitor, 4-phenylbutyrate (4-PBA). In myotubes in monolayer culture, 18 hours of 5 mM 4-PBA treatment resulted in an increase in insulin-stimulated 2-DG uptake, though the difference is not statistically significant (Figure 12A). In myobundles, the 4-PBA-treated group demonstrated significantly higher 2-DG uptake in the insulin-stimulated group than basal uptake, and increased the magnitude of insulin response from 1.2-fold to 1.4-fold (Figure 12B). 4-PBA treatment also enhanced twitch and tetanus force production (Figure 12C) and a significant 8.39 ± 0.7% decrease in fatigue following 30 seconds of electrical stimulation (Figure 12D), while also significantly lengthening the half-relaxation time of the myobundles during twitch contractions (Figure 12E). Analysis of gene expression of glucose transporters revealed decreased GLUT1 expression and increased GLUT4 expression by myobundles treated with 4-PBA (Figure 12F). These changes in glucose transporter expression were accompanied by a significant increase in expression of PGC-1α (Figure 12F).

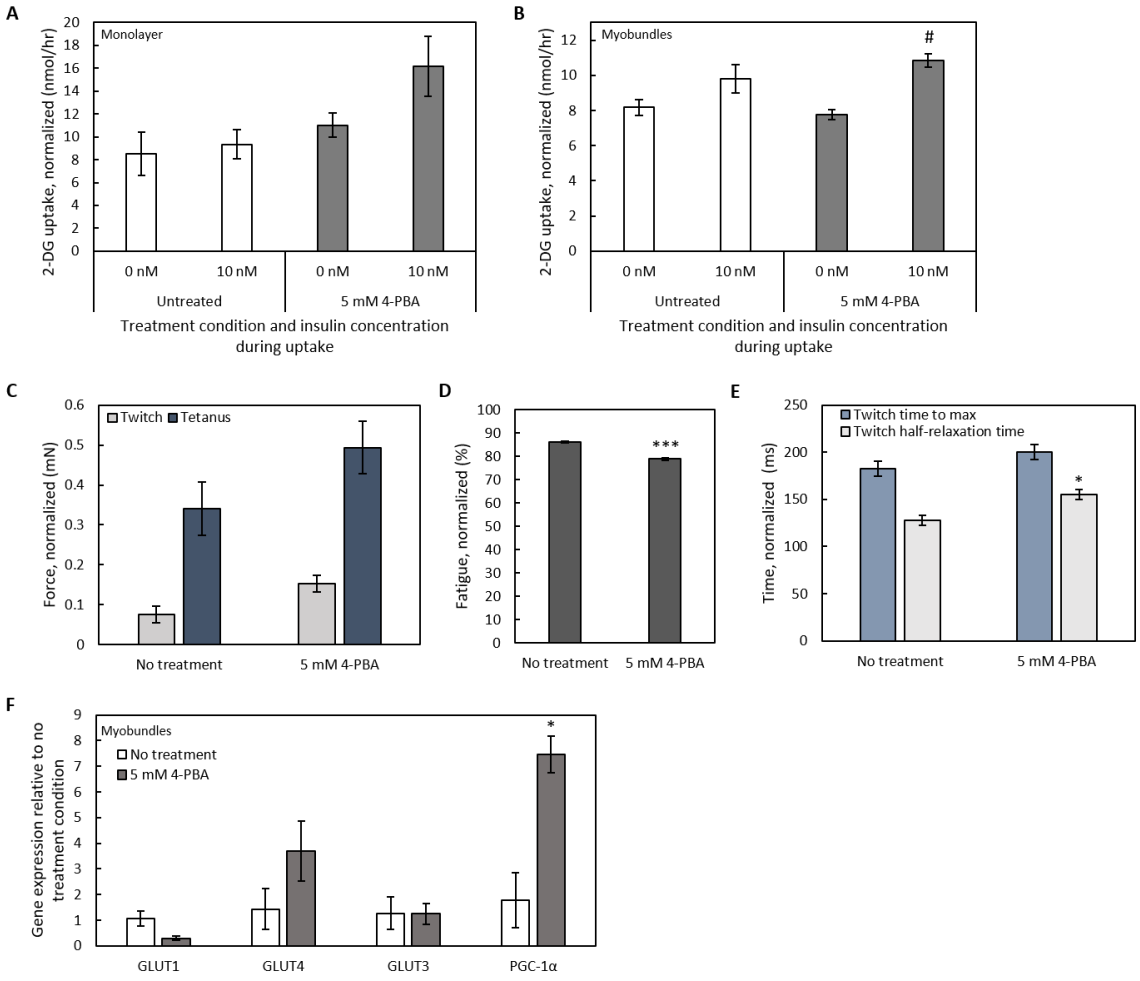

Figure 12. Effect of the general HDAC inhibitor 4-PBA on 2-DG uptake and contractile function. A) Myotubes were differentiated in a 6-well plate and treated with 5 mM 4-PBA for 18 hours immediately prior to 2-DG uptake at the 2 week differentiation time point. N=3 donors, n=3 wells per condition per donor. B) Myobundles were treated with 5 mM 4-PBA for 18 hours immediately prior to 2-DG uptake at the 2 week differentiation time point. N=3 donors, n=3-4 myobundles per condition per donor. C-E) Myobundles were treated with 5 mM 4-PBA for 18 hours immediately prior to measuring twitch and tetanus contractile force, percent fatigue, and twitch kinetics at the 2 week differentiation time point. N=3 donors, n=3-4 myobundles per condition per donor. F) Gene expression by myobundles treated with 5 mM 4-PBA for 18 hours. N=3 donors, n=3 myobundles per condition per donor. * p<0.05, **p<0.01, *** p<0.001 when compared with the same insulin condition or contractile function measurement in the no treatment group. # p<0.05 when compared

with the no insulin condition within the treatment group. Data in all panels presented as mean ± S.E.M.

2.4 Discussion

The goal of this work was to identify and optimize a method for measuring glucose uptake in tissue engineered skeletal muscle myobundles, to characterize the glucose uptake and insulin sensitivity of the myobundles and to test the ability of the system to respond appropriately to a drug challenge. We found that the insulin responsiveness of the myobundles is comparable to that of other *in vitro* skeletal muscle cultures, but myobundles retain the insulin sensitivity of *in vivo* muscle. Myobundles responded to metformin with a robust increase in 2-DG uptake, indicating the functionality of AMPK-mediated signaling pathways. Finally, we found that general HDAC inhibition improved the insulin response and contractile function of the myobundles.

We first identified two methods for measuring or approximating glucose uptake in the myobundles. The media-based Amplex assay is non-destructive and allows for repeated sampling from the same bundles over time, enabling those bundles to be used for other destructive endpoint assays. However, the ability to determine differences in glucose uptake over a short time frame is vital for pinpointing effects of acute drug treatments or immediate changes in glucose uptake subsequent to electrical stimulation. That the 2-DG assay detects only intracellular 2-DG by quantifying phosphorylated 2-DG (2-DG6P) specifically is an improvement over other glucose analog assays which

require negative controls to account for background signal due to un-internalized 2-DG. Additionally, the 2-DG assay is relatively inexpensive, requires no radioisotopic material, and needs only a fluorescent plate reader in terms of specialized equipment.

Before beginning full characterization of 2-DG uptake and insulin sensitivity in the myobundles, we identified two key changes to improve the physiological relevance of the culture conditions. The first was the use of a lower amino acid base media formulation, to better mimic the amino acid availability *in vivo* (see more in Chapter 2). The second was to lower the exposure of the myobundles to supraphysiological levels of insulin during differentiation by removing insulin during week 2 of differentiation. In the body, skeletal muscle cells are normally exposed to ≤10 nM insulin, so we hypothesized that supraphysiological levels of insulin could be oversaturating insulin signaling pathways in the basal state, which would account for the minimal insulin response typically seen *in vitro*. We found that while insulin removal during the second week of differentiation did have a slight effect on the insulin response by lowering the basal uptake, the effect was not significant. Lowering insulin availability during the first and second weeks of differentiation or removing it entirely during the second week had no negative impact on contractile force. Force production was only decreased when insulin was removed entirely during differentiation. These changes to the base media and insulin concentrations represented a step toward creating a more physiologically-

relevant system of nutrient availability, and so were maintained throughout the remaining experiments.

Metformin, the first-line form of medication for treating hyperglycemia in type 2 diabetes, is an AMPK activator which leads to increased glucose uptake in a manner independent of insulin signaling. We found that when the myobundles were treated with metformin, they responded with an approximate two-fold increase in basal 2-DG uptake rate. The effect in myobundles was consistent with the effect we observed in 2D cultures of myotubes and is comparable with other studies done using human myotubes in monolayer. One study found that after treatment of human myotubes with 800 μM metformin for 24 hours, 2-DG uptake was increased 1.4-2.2-fold over basal[201], while another found that treatment with 2 mM metformin for 16 hours resulted in an increase from 632.8 ± 50.4 to 1014 ± 79.3 pmol/mg/min, a fold-change of 1.6[239]. *In vivo*, metformin treatment caused a drop in blood glucose concentration of 1.2 mM, an approximate 1.25-fold decrease[240], and in type 2 diabetes subjects, long term treatment with metformin increased whole-body glucose disposal by 1.22-fold[241]. This response to a well-known drug affecting glucose metabolism in skeletal muscle validates the ability of the myobundle system to respond appropriately to a metabolic challenge, and the use of the 2-DG assay to detect that response. We additionally observed that metformin treatment significantly decreased myobundle force production and increased fatigue. Metformin activates AMPK by acting as an inhibitor of complex I, the mitochondrial respiratory

chain component, and there is some evidence that treatment with metformin reduces aerobic capacity during high intensity exercise[242], but does not affect aerobic capacity during moderate intensity exercise[243]. It is important to note that the concentration of metformin used in this study is far higher than the average therapeutic plasma concentration of 14.3 μM[244], so decreases in contractile function in the myobundles may predict skeletal muscle dysfunction associated with increased respiratory chain disruption at higher doses of metformin.

To characterize the sensitivity of the myobundles to insulin and to determine the magnitude of change in 2-DG uptake upon exposure to insulin, we measured 2-DG uptake at a variety of insulin concentrations in four donors. The magnitude of the response to physiological insulin concentrations was variable between donors, ranging from 1.2-fold to 2.28-fold, with a compiled response of 1.51-fold. These values are in line with what has typically been measured using *in vitro* human myotubes, with the magnitude of the insulin response ranging from 1.3-3-fold[197-200,202], but *in vivo*, the magnitude of change in glucose uptake in response to insulin ranges from 6-8-fold[195,196,207,245]. When the parameters for the Michaelis-Menten kinetics equation (Equation 2) were fitted to the compiled dose response data, the EC_{50} was 0.268 ± 0.03 nM. Others have reported EC_{50} values of 3.5 nM[202], 0.98 ± 0.12 nM[200], and 1.55 ± 0.52 nM[199] for human cultured myotubes isolated from non-diabetic subjects. The concentration at which insulin's effect is half-maximal *in vivo* is reported as 60 μU/mL[106],

which converts to 0.36 nM. Thus, although myobundles, like other *in vitro* cultures, lack the *in vivo* level of insulin responsiveness, they retain their intrinsic insulin sensitivity properties.

In humans, exercise results in increased glucose uptake via increased translocation of GLUT4 to the cell surface, as well as a short-term improvement in insulin sensitivity after the bout of exercise is over[246]. Electrical stimulation of skeletal muscle *in vitro* can be used to approximate the metabolic effects of exercise *in vivo*. Human *in vitro* cultures of skeletal muscle demonstrate increased glucose uptake in response to electrical stimulation, both in myotubes in monolayer[247-250] and in tissue engineered myobundles[226]. In studies which have examined the interaction of electrical stimulation with insulin stimulation in human myotubes, there have been mixed results. One study observed enhanced insulin response in electrically stimulated myotubes[249], while another found no additive effect of insulin stimulation and electrical stimulation on glucose uptake[248]. The electrical stimulation protocols were different between these two studies, with the first consisting of acute stimulation with 200 ms trains of 100 Hz at 30V delivered in 2 second intervals for 5 minutes during the 2-DG uptake period, and the second consisting of stimulation for 7.5 hours with single pulses of 2 ms at 1 Hertz and 11.5 V, immediately prior to the 2-DG uptake period. Thus, the different reported effects of electrical stimulation on insulin response may be a factor of the type of exercise being simulated. All reported protocols measured glucose or 2-DG uptake over a period

of at least one hour and up to 24 hours. In our studies, 2-DG uptake was measured over the course of only 20 minutes. We found no significant trends in the effect of acute exercise on basal 2-DG uptake or insulin response. It is possible that the effect of acute exercise on 2-DG uptake and insulin sensitivity is cyclical or delayed and requires longer measurement periods to capture the full effect. We did observe a trend of increased basal 2-DG uptake in myobundles that had been trained with 1 or 10 Hz stimulation regimes during the second week of differentiation, which is consistent with previously published results[226].

In an effort to identify components of the myobundle system which impacted glucose uptake and insulin responsiveness, we varied several factors involved in myobundle formation and culture. We found that forming myobundles with GFR Matrigel and higher fibrinogen concentrations tended to slightly improve the response to physiological insulin concentrations of 10 nM. The increased fibrinogen concentration additionally improved contractile force production. The GFR Matrigel contains lower concentrations of growth factors such as IGF-1, which could contribute to increased baseline signaling through insulin-response pathways. Substrate stiffness can impact myoblast differentiation[251], so the increased fibrinogen concentration may alter the ECM stiffness in a manner which promotes maturation. Additional alterations to culture conditions, including removal of streptomycin, removal of dexamethasone, lowering L-

glutamine concentrations, and altering glucose and insulin availability to mimic meals had no impact on the insulin response by the myobundles.

We next examined the impact of an Akt inhibitor on 2-DG uptake in myobundles. Akt is an essential component of the insulin-signaling pathway, and we would expect inhibition to prevent any increase in 2-DG uptake over basal uptake in the presence of insulin. We additionally hypothesized that there may be some constitutive signaling through the insulin pathway as a result of residual insulin from week 1 of differentiation or growth factors from the Matrigel or serum that could be contributing to increased 2-DG uptake in the basal state. Treatment with 10 μM Akt inhibitor abolishes the insulin response, and treatment with the higher concentration maintains this effect while also lowering the basal 2-DG uptake rate, suggesting a small activation of insulin signaling even during the basal state in the myobundles.

Because myotubes cultured *in vitro* tend to be immature, with low levels of mature myosin heavy chain isoforms and high levels of embryonic and neonatal myosin heavy chain isoforms[252], we examined the use of an HDAC inhibitor to promote maturation and an oxidative fiber phenotype in the myobundles. Class IIa HDACs include HDAC4, 5, 7, and 9 and are highly involved in the regulation of myogenesis via their interactions with the transcription factor MEF2[253]. During differentiation of myoblasts to myotubes, these HDACs are exported from the nucleus to the cytoplasm, and overexpression of HDAC4, 5, and 7 prevents myoblasts from differentiating *in*

vitro[254-256]. HDACs also play a role in metabolic regulation; HDAC4 is exported from the nucleus when skeletal muscle fibers are reprogrammed from glycolytic fiber types to more oxidative fiber types[257] and the general class IIa HDAC inhibitor Scriptaid has been shown to increase metabolic gene expression and oxidative metabolism in rats in a manner similar to exercise[258].

At the concentrations we used to treat the myobundles, LMK235 specifically inhibits HDAC4 and HDAC5. In our system, LMK235 had an effect on 2-DG uptake only when it was used long-term during the second week of differentiation, the time frame when increased MEF2 expression would likely be most useful for enhancing myotube differentiation. However, class IIa HDACs can act in redundant roles[253], so it is possible that there was a minimal effect of the specific HDAC inhibitor because other uninhibited HDACs were maintaining repressed MEF2 expression.

The general HDAC inhibitor 4-PBA[259] inhibits all class IIa HDACs, eliminating the ability of similar HDACs to override changes in phenotype by performing the functional role of the selectively inhibited HDACs. In C2C12 cells, 4-PBA increased insulin-stimulated glucose uptake and increased GLUT4 expression via suppressed HDAC5 repression of MEF2[260]. In our work, acute treatment with 4-PBA after two weeks of differentiation resulted in an improved insulin response in myobundles, as well as a trend toward increased force production, and a significant decrease in fatigue. Gene expression data from 4-PBA-treated myobundles indicated decreased GLUT1 and

increased GLUT4 expression compared to untreated controls. This shift in glucose transporter expression is potentially mediated by the observed increase in PGC-1α expression, as ectopic expression of PGC-1α has been shown to increase GLUT4 expression in myotubes[261]. Together, these results suggest promising improvements in metabolic and contractile function in myobundles treated with the general HDAC inhibitor. Future work could identify optimal timing and duration of treatment to encourage further myobundle maturation.

We had originally hypothesized that the three-dimensional structure of the myobundles would contribute to a more robust insulin response, but insulin responsiveness in our myobundles was comparable with reports in the literature from myotubes in monolayer culture, and we did not find differences in the insulin response between our 2-D cultures and our myobundles (Figure 13). We observed that sensitivity to insulin in the myobundles is comparable to that of *in vivo* skeletal muscle, indicating that poor insulin sensitivity is not the root of the dysfunction *in vitro*. It has been documented that the GLUT1:GLUT4 ratio is skewed in skeletal muscle cultures *in vitro*, and we have observed low expression of GLUT4 coupled with high expression of both GLUT1 and GLUT3 in the myobundles. Together, these findings support the hypothesis that the root cause of impaired insulin responsiveness *in vitro* is a lack of GLUT4 expression. In this study, we found the most success in improving the insulin response when treating myobundles with 4-PBA, which increased GLUT4 expression. Therefore,

enhancing the maturation of *in vitro* myotubes and manipulating glucose transporter expression offer promising avenues for improving insulin responsiveness *in vitro*.

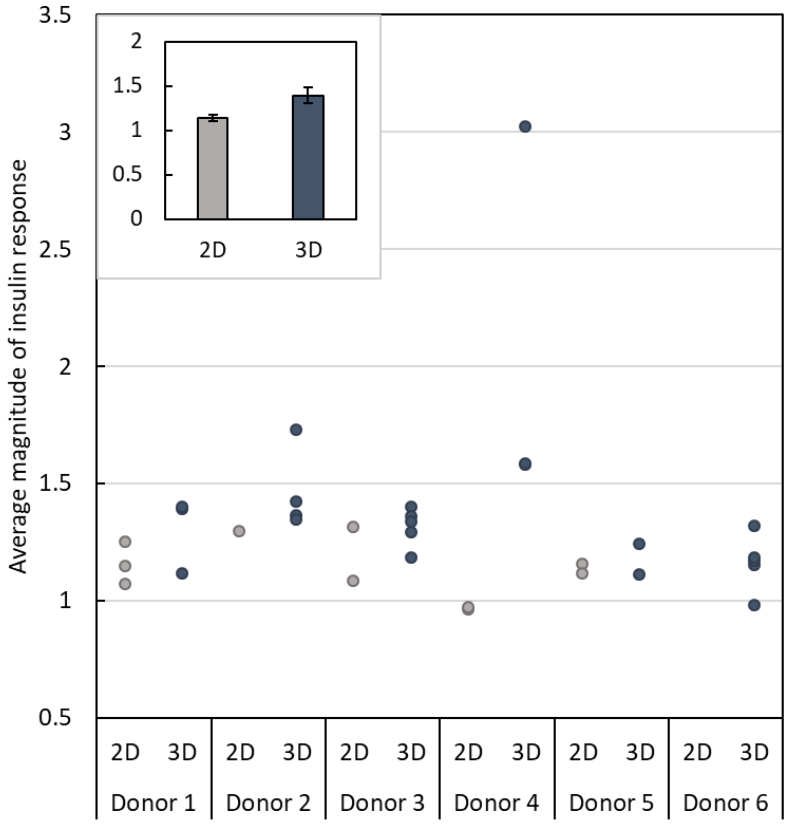

Figure 13. Compilation of insulin responsiveness in 2-D and 3-D. Data are compiled from experiments shown in this study. Each data point represents an average fold-change in the rate of 2-DG uptake in response to 10 nM insulin, where a value of 1 indicates no change in response to insulin. The inlayed graph depicts the average fold change from myotubes in 2-D culture and myobundles in 3-D culture. Data shown as mean ± S.E.M.

2.5 Conclusions

In conclusion, we have identified a method for measuring 2-DG uptake in myobundles and validated the ability of the myobundle system to respond appropriately to the metabolic pathway-targeting therapeutic metformin. We have

altered myobundle differentiation conditions to provide a more physiologically-relevant environment and characterized the insulin sensitivity of the myobundles, finding it to be similar to insulin sensitivity *in vivo*. Finally, we have demonstrated that treatment with a pan-HDAC inhibitor can improve the metabolic and contractile function of the myobundles. Taken together, we have demonstrated the utility of myobundles as an *in vitro* tissue-engineered human skeletal muscle model which is valuable for ascertaining both glucose-associated metabolic and contractile functional responses to manipulations of culture conditions and drug treatments.

2.6 Chapter acknowledgements

Electrical stimulation studies shown in Figure 7 were performed in collaboration with Lauran Madden. Anandita Ananthakumar performed the PCR shown in Figure 12. Tim Koves provided the custom low amino acid media formulation. This work was funded by the National Science Foundation Graduate Research Fellowship under Grant No. NSF DGE 1106401, NIH grant UH3TR000505 and the Common Fund for the Microphysiological Systems Initiative.

3. Low Amino Acid and Growth Factor Reduced Conditions Promote a Metabolic Shift in Tissue-engineered Human Skeletal Muscle

3.1 Introduction

Tissue engineered skeletal muscle is valuable as a tool to predict the responses of both healthy and diseased skeletal muscle tissue to drug treatment. Pre-clinical testing of drugs using *in vitro* human cell monolayers and animal models in some cases have been inadequate to identify issues with safety or efficacy of drugs in development. By providing a scaffold for skeletal muscle to grow in a three-dimensional environment, tissue engineered skeletal muscle more closely mimics the structure and function of skeletal muscle in the body. The amenability of the platform to functional tests makes it ideal for bridging the gap between *in vitro* monolayer studies and human clinical trials. Though several functional aspects of tissue engineered muscle have been validated, including force production, oxygen consumption and calcium handling[7,8], there has been relatively little focus on identifying how myobundle formulation and culture conditions can promote differentiation to a specific metabolic state.

In order to use myobundles as a test bed for the response of healthy skeletal muscle tissue to drug-induced toxicity, we must achieve a metabolic phenotype that mimics that of skeletal muscle in the body. However, primary human skeletal muscle cells isolated from tissue and cultured *in vitro* are typically highly glycolytic[262,263], a trend which is likely linked with the tendency of the cells to differentiate into fast twitch fibers

in vitro at a higher proportion than what is seen in the source muscle[220,264]. Additionally, skeletal muscle cultured *in vitro* has a significantly higher GLUT1:GLUT4 ratio than skeletal muscle *in vivo*, with reported expression ratios of 7-12:1 in myotubes *in vitro*[197,201] compared to 0.002:1 in human muscle *in vivo*[265]. This metabolic shift of skeletal muscle in culture may be induced by easy access to excess nutrients in cell culture media[262].

Standard cell culture media is optimized to promote cell growth and the levels of nutrients such as amino acids, fatty acids, glucose, and insulin present tend to be much higher than those present in plasma and interstitial fluid *in vivo*. Increased levels of amino acids, especially branched chain amino acids, are associated with the skeletal muscle metabolic defects seen in patients with type 2 diabetes, though it is unclear if the increased levels are causative or merely symptomatic[76,266]. In DMEM, which is typically used for the culture of skeletal muscle cells, levels of these amino acids are kept artificially high to promote cell growth, exposing the cells to concentrations of amino acids 2-8 times higher than normal plasma levels[267]. Additionally, most myogenic cells are maintained in culture in the absence of supplementary fatty acids or L-carnitine, eliminating one of the primary fuel sources of skeletal muscle and forcing cells to rely chiefly on glucose for energy[79].

Altering nutrient availability in the media influences glucose uptake and metabolic function of myotubes. When compared with normoglycemic controls (5.5 mM), high concentrations of glucose (20 mM) in the culture media of human myotubes

causes decreased fatty acid oxidation, likely as a result of reduced mitochondrial oxidative capacity[212]. Culture of primary human myotubes in hyperinsulinemic conditions results in increased basal glucose uptake and impairs the ability of cells to respond to an insulin stimulus with a further increase in glucose uptake[198].

The necessity for a tissue engineered skeletal muscle model that is not limited to a glycolytic metabolism is underlined by fiber type-specific differences in susceptibility to drug-induced toxicity and in chronic disease progression. For example, animal studies show that statin-induced toxicity is directed primarily at type II glycolytic fibers[268], while fibrates appear to induce toxicity primarily in type I oxidative fibers[269]. In humans, the development of chronic conditions such as obesity and insulin resistance is associated with a transition to increased glycolytic fibers[270,271]. Many drugs have been taken off the market due to unanticipated mitochondrial toxicity[15], which is more difficult to detect during *in vitro* preclinical studies if the cells are less reliant on oxidative metabolism due to high levels of glycolysis satisfying the energy demands[272].

Here, we demonstrate that culturing myobundles using physiologically-relevant low amino acid and growth factor reduced (LAAGFR) conditions results in a less glycolytic and more oxidative metabolism. These changes in metabolism are demonstrated by decreased glucose uptake and decreased lactate production, and are matched by a functional shift towards higher fatigue resistance, a trait associated with a more oxidative metabolism. In addition to paving the way for studies to be done using a

more oxidative skeletal muscle fiber phenotype, this finding offers the capacity to tune metabolism using only alterations of the nutrient availability in the culture media and myobundle ECM.

3.2 Materials and Methods

3.2.1 Primary human myogenic cell isolation and culture

Primary human myogenic cells were isolated from surgical waste samples under a Duke IRB-approved protocol. Briefly, muscle tissue was washed with Dulbecco's phosphate buffered saline (DPBS) (Sigma-Aldrich) containing 2X Antibiotic-Antimycotic (ThermoFisher Scientific), then minced and digested using 0.05% Trypsin-EDTA (ThermoFisher Scientific). Minced tissue was pre-plated on an uncoated tissue culture flask for 2 hours before being transferred to a Matrigel (Corning)-coated flask for myogenic cell outgrowth. Tissue and cells were cultured during outgrowth in human growth media (hGM) consisting of low glucose (5.55 mM glucose) Dulbecco's Modified Eagle Medium (DMEM) with 1 mM sodium pyruvate (ThermoFisher Scientific) supplemented with 9% fetal bovine serum (FBS) (Hyclone), 0.25 μg/mL amphotericin B (ThermoFisher Scientific), 50 μg/mL gentamicin (ThermoFisher Scientific), 0.4 μg/mL dexamethasone (Sigma-Aldrich), 10 ng/mL EGF (Peprotech), and 50 μg/mL fetuin (Sigma-Aldrich).

3.2.2 Formation and culture of myobundles

Myobundles were formed as previously described[7,8]. Briefly, a solution of either normal Matrigel (Corning) (Baseline condition) or growth-factor reduced Matrigel (Corning) (LAAGFR condition) and 20 mg/mL (Baseline condition) or 25 mg/mL (LAAGFR condition) bovine fibrinogen (Sigma-Aldrich) in PBS was mixed with a myogenic cell solution containing 50 U/mL thrombin (Sigma Aldrich) and pipetted into the central channel of a PDMS mold surrounded by a nylon (Cerex Advanced Fabrics) frame. Each myobundle was formed with 50 μL and 750,000 cells. The myobundles were allowed to gel for 30 minutes at 37°C before adding hGM supplemented with 1.5 mg/mL 6-aminocaproic acid (Sigma-Aldrich) (hGM + ACA) to the wells containing the molds. Myobundles were cultured in hGM + ACA for four days before being removed from the PDMS mold and switched to either Baseline or LAAGFR differentiation media. Complete LAAGFR and Baseline differentiation media formulations are shown in Appendix E. Myobundles were cultured in differentiation media for 1 week prior to endpoint testing, with media changes every other day.

3.2.3 Contractile force and kinetics measurement

Myobundles were placed in a tissue bath kept at 37°C with one end of the myobundle pinned to a fixed PDMS platform and the other end pinned to a PDMS pad attached to a force transducer. Contractile force was measured in response to an electrical stimulus applied to the myobundle via two electrodes placed on either side of

the bundle in the tissue bath. Myobundles were stretched to 115% of normal length prior to stimulation with one second of stimulation at 1 Hertz for a twitch contraction, one second of stimulation at 20 Hertz for a tetanus contraction, and thirty seconds of stimulation at 20 Hertz to fatigue the muscle. Peak twitch and tetanus force, percent fatigue, and twitch kinetics (time to peak twitch and half-relaxation time) were determined using a Matlab script. Peak twitch and tetanus were calculated as the difference between the highest measured force after stimulation and the baseline passive force prior to stimulation. Percent fatigue was calculated as $\frac{peak\ force - force\ after\ 30\ seconds\ of\ fatigue}{peak\ force - baseline\ force}\ x\ 100\%$. Time to peak twitch was calculated as the time between initiation of electrical stimulation and peak force. Half-relaxation time was calculated as the time between peak force and return to one-half of the difference between the peak force and the baseline force.

3.2.4 Quantification of 2-deoxyglucose (2-DG) uptake

Measurement of 2-DG uptake was done in myobundles using a modified version of the previously-published protocol[227]. After differentiating for 1 week, myobundles were cultured in serum- and insulin-free LAAGFR or Baseline media for 18 hours prior to uptake. Myobundles were washed in uptake buffer consisting of no glucose DMEM (ThermoFisher Scientific) with 0.1% (w/v) bovine serum albumin (Sigma-Aldrich) and 0.2 mM sodium pyruvate for 10 minutes. Myobundles were then incubated in fresh uptake buffer for 30 minutes. Next, myobundles (excluding negative control

myobundles) were incubated for 20 minutes in uptake buffer with 5 mM 2-DG (Sigma-Aldrich) in no glucose DMEM. After uptake, myobundles were washed three times with ice-cold PBS, then removed from the frames and lysed in 100 μl of 1X extraction buffer (Abcam) overnight at 4°C on a rocker. The next day, samples underwent a freeze/thaw cycle and were heated at 85°C for 40 minutes to remove endogenous NADP, and 50 μL of 200 mM triethanolamine (TEA) buffer (Sigma-Aldrich) was added to each sample. Samples were stored at -20°C until assayed. Phosphorylated 2-DG (2-DG6P) in the lysed samples was quantified as described previously[227].

3.2.5 Immunofluorescence staining of 3D myobundles

Myobundles were placed on a rocker for all incubation steps. Myobundles were fixed using 2% PFA overnight at 4°C, then rinsed three times with DPBS +/+ and incubated in blocking buffer overnight at 4°C. Myobundles were incubated with the primary antibody for sarcomeric alpha actinin (SAA) (Abcam) diluted 1:200 in blocking buffer for 24 hours at 4°C. After the primary antibody incubation, myobundles were rinsed three times with DPBS +/+ and incubated with goat anti-mouse secondary antibody at a dilution of 1:250 and Hoechst 33342 at a dilution of 1:1000 in blocking buffer. After secondary antibody incubation, myobundles were rinsed three more times with DPBS +/+ prior to imaging using a Zeiss LSM 510 inverted confocal microscope.

3.2.6 Nuclei quantification assay

Myobundles were removed from frames and lysed in a solution of 90% Buffer ATL (Qiagen) + 10% proteinase K (Qiagen) at 55°C for 3.5 hours. To quantify nuclei content, the lysed sample was diluted with Buffer ATL and combined at a 1:1 volume ratio in a 96-well plate with a solution of 2 μg/mL Hoechst 33258 dye (Sigma-Aldrich) in tris-buffered saline (Sigma-Aldrich), incubated for 15 minutes at room temperature, and fluorescence was measured using a plate reader with a 350 nm excitation and 460 nm emission filter. Fluorescence of samples was converted to number of nuclei using a standard curve formed using dilutions of a stock standard solution containing a lysed solution of a known quantity of myoblasts.

3.2.7 L-lactate quantification assay

Samples of media were collected after 24 hours of culture and deproteinated according to the L-Lactate Assay Kit (Cayman Chemicals). Samples were stored at -80°C until assayed. The L-Lactate concentration in the media was measured according to the manufacturer's instructions.

3.2.8 Seahorse XFe24 metabolic phenotype assay

Myobundles were miniaturized to fit in the Seahorse XF24 islet capture microplates and cultured in the same manner as the standard-sized myobundles. Miniaturized myobundles were made with 300,000 cells per myobundle and were 2 mm in length. At 1 week of differentiation, myobundles were washed with PBS followed by

a wash with assay media consisting of Seahorse XF DMEM (Agilent) supplemented with 1 mM sodium pyruvate (Agilent), 2 mM L-glutamine (Agilent), 10 mM glucose (Agilent), and 0.2% horse serum, and transferred to a Seahorse XF24 islet capture microplate containing fresh assay media. Empty frames were added to the plate to serve as blank controls. The islet plate was then incubated for one hour at 37°C in a non-CO_2 incubator. The instrument was calibrated and the cell plate was loaded. The instrument protocol was set to mix for 3 minutes, wait for 2 minutes, and measure for 3 minutes, looped five times. After completion of the Seahorse analysis, myobundles were removed from the islet plate and lysed for nuclei quantification. Background-corrected oxygen consumption rates (OCR) and extracellular acidification rates (ECAR) were obtained from the Wave desktop application from Agilent Technologies. OCR and ECAR values were normalized to myobundle nuclei content.

3.2.9 qRT-PCR

Myobundles were flash frozen in liquid nitrogen prior to total RNA extraction using the Aurum Total RNA Mini Kit from BioRad. cDNA was produced using the iScript cDNA Synthesis Kit (BioRad). Genes of interest GLUT1, GLUT4, GLUT3, PGC-1α, HIF-2α, MYH7 (type I myosin heavy chain (MHC)), MYH2 (type IIA MHC), MYH1 (type IIX MHC), MYH3 (embryonic MHC), and MYH8 (perinatal MHC) and housekeeping gene β-2 microglobulin were amplified and quantified using the iQ SYBR

Green Supermix (BioRad) and CFX Connect Real-Time PCR Detection System (BioRad). Primer sequences are included in Table 2.

Table 2. Primer sequences used for qRT-PCR.

Primer	Forward primer	Reverse primer
β2M	5'-GGCTATCCAGCGTACTCCAAAG-3'	5'-CAACTTCAATGTCGGATGGATG-3'
GLUT1	5'-ATCATCGGTGTGTACTGCGG-3'	5'-GGTCATGGGTCACGTCAGCT-3'
GLUT4	5'-TTCCAACAGATAGGCTCCGAAG-3'	5'-AAGCACCGCAGAGAACACAG-3'
GLUT3	5'-ACTTTGACGGACAAGGGAAATG-3'	5'-ACCAGTGACAGCCAACAGG-3'
PGC-1α	5'-TGTGCAACTCTCTGGAACTG-3'	5'-TGAGGACTTGCTGAGTGGTG-3'
HIF-2α	5'-GCCACCCAGTACCAGGACTACA-3'	5'-CCTCACAGTCATATCTGGTCAGTTCG-3'
Type I MHC	5'-GCCGAGTCCCAGGTCAACAAG-3'	5'-TGAGCAGATCAAGATGTGGCAAAG-3'
Type IIA MHC	5'-TTGCTGAGTCCCAGGTGAACA-3'	5'-TTTGTGCCTGTCTTCAGTCATTCC-3'
Type IIX MHC	5'-CTGAGGGTGAAGAGCAGGGAGGT-3'	5'-TTTTCACATTTTGTGCATTTCTTTGG-3'
Embryonic MHC	5'-GGAGCAGGACAGAAGATAT-3'	5'-CCCAGATTGAAACAAAGCA-3'
Perinatal MHC	5'-ATTTCCACCAAGAACCCA-3'	5'-AAAGGATTCTGCCTCTG-3'

3.2.10 Statistical analysis

Student's t-test was used for pairwise comparisons. For multiple comparisons an ANOVA was run, followed by Tukey HSD post-hoc testing for statistical significance. * indicates $p < 0.05$, ** indicates $p < 0.01$, and *** indicates $p < 0.001$ compared to the Baseline condition.

For the time course experiments, a global normalization was applied as described in the previous chapter.

3.3 Results

3.3.1 Effect of LAAGFR conditions on myobundle 2-DG uptake at two weeks post-differentiation and time course studies

Basal glucose uptake rates, which represent glucose uptake in the absence of insulin, were measured in four separate primary skeletal muscle donors using the glucose analog 2-DG. When tested at two weeks post-differentiation, myobundles formulated and cultured using LAAGFR conditions (Table 3) demonstrated significantly decreased basal glucose uptake rates when compared to myobundles formulated and cultured using baseline conditions (Figure 14).

Table 3. Baseline and LAAGFR culture conditions.

Variable	Baseline condition	LAAGFR condition
Basal media	DMEM	LAA
Insulin condition	1.72 µM	10 nM
Fibrinogen	20 mg/mL	25 mg/mL
Matrigel	Normal	Growth factor reduced
Media supplements	None	Fatty acids with L-carnitine

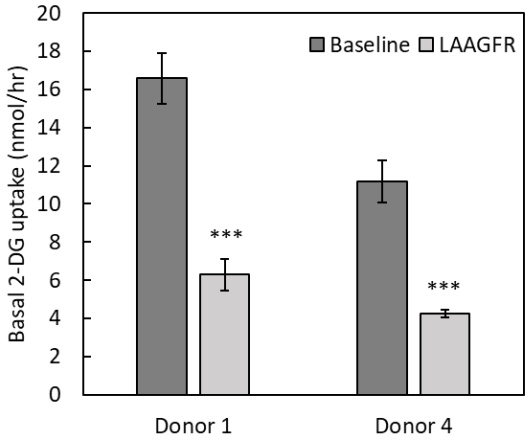

Figure 14. Basal 2-DG uptake in myobundles cultured in LAAGFR or Baseline conditions, tested at 2 weeks post-differentiation. The lower basal 2-DG uptake in LAAGFR-cultured myobundles is maintained at the later time point. Data shown as mean ± S.E.M, n=4 myobundles per condition, ***p<0.001.

Time course experiments of basal and insulin-stimulated 2-DG uptake and contractile force indicated a significant drop in myobundle basal 2-DG uptake (Figure 15A), significantly decreased contractile force production (Figure 15B), significantly increased fatigue (Figure 15C), no change in twitch kinetics (Figure 15D) and decreased integrity of sarcomeric structure (Figure 15E) in myobundles at two weeks post-differentiation. As a result of these findings, all future work was carried out using myobundles at one week post-differentiation.

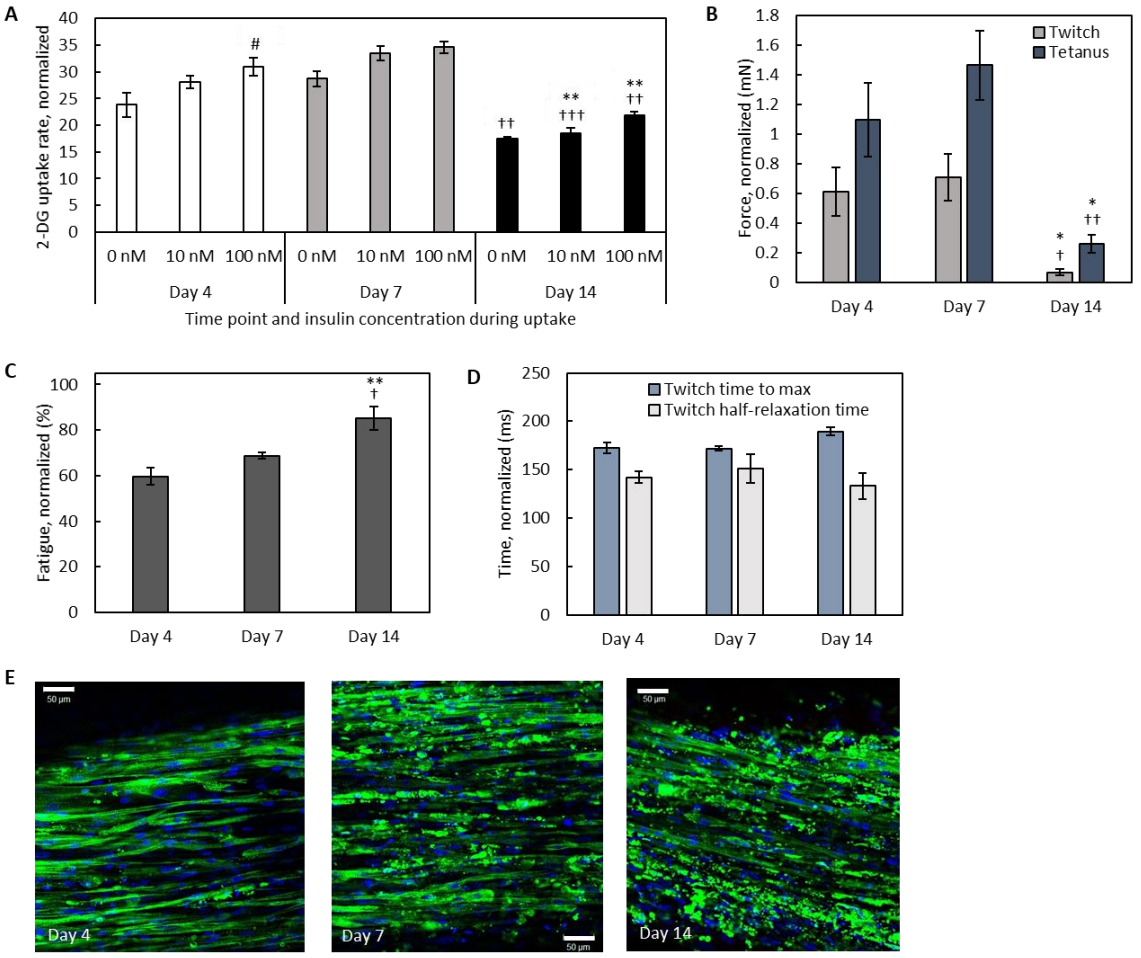

Figure 15. Time course of 2-DG uptake and contractile function of myobundles. Myobundles were tested at 4, 7, and 14 days post-differentiation. A) Basal and insulin-mediated 2-DG uptake of myobundles at each time point. N=3 donors, n=4 myobundles per condition per donor. B) Twitch and tetanus contractile force production at each time point. N=4 donors, n=4 myobundles per condition per donor. C) Percent of force depletion after fatigue at each time point. N=3 donors, n=4 myobundles per condition per donor. D) Twitch kinetics at each time point. N=3 donors, n=4 myobundles per condition per donor. E) Representative images of sarcomeric alpha actinin (green) expression and nuclei (blue) in myobundles at each time point. Scale bars represent 50 µm. *p<0.05, **p<0.01, ***p<0.01 indicates statistical significance when compared to same insulin concentration at the day 4 time point. † indicates statistical significance when compared to the same insulin concentration at the day 7 time point. # indicates statistical significance when compared to the 0 nM insulin concentration within the same time point. Data in all panels presented as mean ± S.E.M.

3.3.2 Effect of LAAGFR conditions on myobundle 2-DG uptake and cell quantity at one week post-differentiation

Because time course experiments indicated improved myobundle function at one week post-differentiation, we next examined the impact of LAAGFR conditions at one week post-differentiation. We again observed significantly decreased basal 2-DG uptake in the LAAGFR group (Figure 16A). When the number of nuclei was quantified in each bundle, there were no significant differences between the LAAGFR and the baseline conditions (Figure 16B), demonstrating that myoblast growth is maintained in LAAGFR conditions and the change in 2-DG uptake was not due to differences in cell quantity. Thus LAAGFR conditions impact basal glucose metabolism independent of cell quantity, pointing towards an intrinsic shift in myobundle metabolic phenotype.

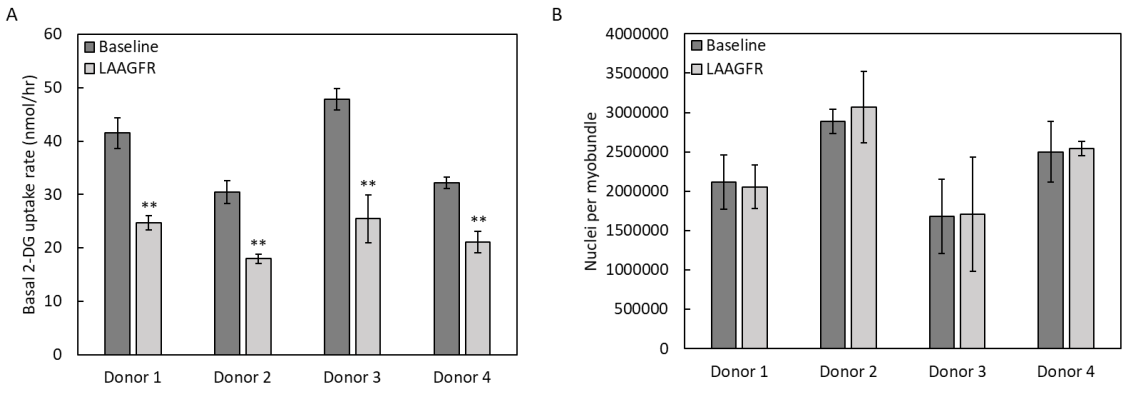

Figure 16. Myobundles cultured in LAAGFR conditions exhibit decreased basal glucose without differences in cellularity. A) 2-DG uptake in the absence of insulin stimulation by myobundles cultured in either Baseline or LAAGFR conditions for one week of differentiation. B) Nuclei quantification of myobundles cultured in either Baseline or LAAGFR conditions for one week of differentiation. For both panels, results from donors shown separately, data presented as mean ± S.E.M, n=4

myobundles per condition. Statistical significance determined using Student's t-test: *p<0.05, **p<0.01, ***p<0.001.

3.3.3 Analysis of individual variable effects

We examined the impact of the individual variables within the LAAGFR group of conditions (shown in Table 3) on basal 2-DG uptake in the myobundles through a series of direct comparisons in which only a single variable was altered and all other variables were held constant between the two groups. Of the five variables altered in the LAAGFR group, only the amino acid content of the base media had a significant effect on basal 2-DG uptake (Figure 17A). There were many additional experiments with variations of the LAAGFR and baseline conditions in which basal 2-DG uptake was measured, but which involved manipulation of more than one variable. Data from these experiments were compiled and a multivariable linear regression was performed to parse out the effects of individual variables. The linear relation between observed and predicted 2-DG uptake using this larger data set confirms the results of the direct comparison experiments, indicating that the only variable with a significant effect on basal glucose uptake is the base media (Figure 17B). To further test this idea, myobundles were cultured in either DMEM-, αMEM-, or LAA-based differentiation media and basal 2-DG uptake rates were determined. 2-DG uptake rates showed a downward trend associated with decreasing amino acid content of the base media (Figure 17C).

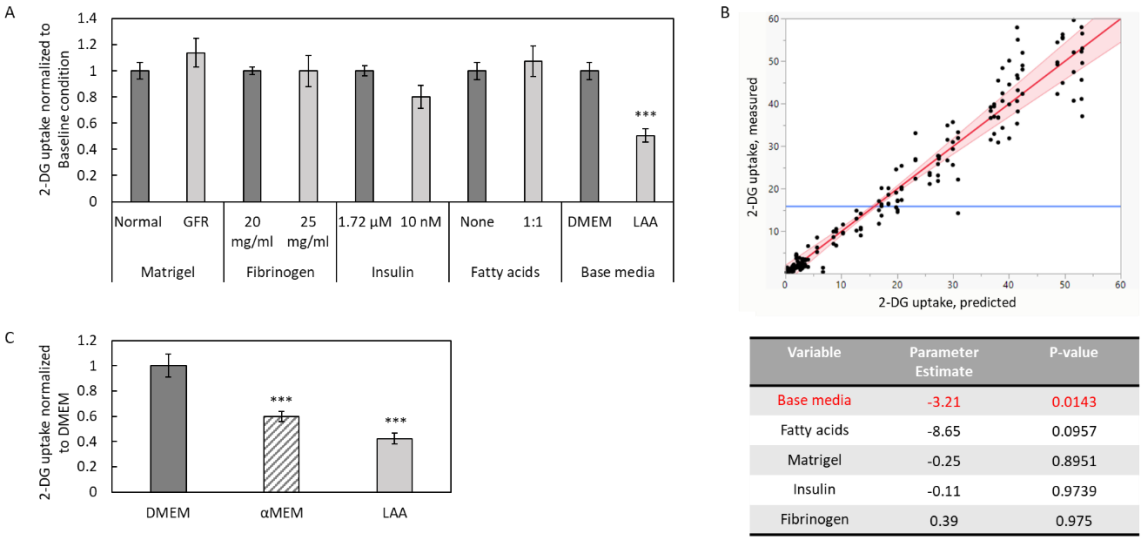

Variable	Parameter Estimate	P-value
Base media	-3.21	0.0143
Fatty acids	-8.65	0.0957
Matrigel	-0.25	0.8951
Insulin	-0.11	0.9739
Fibrinogen	0.39	0.975

Figure 17. Amino acid content of the base media is primarily responsible for lowered basal glucose uptake. A) Basal 2-DG uptake of the myobundles formulated and cultured using the LAAGFR-associated variable normalized to the basal uptake of myobundles formulated and cultured using the Baseline-associated variable. Normalized data compiled from 1-6 donors for each variable, n=3-4 myobundles per condition per donor. Data presented as mean ± S.E.M. Statistical significance determined using Student's t-test: ***p<0.001. B) A multivariable regression was performed on a large set of experimental results from 9 donors, and the resulting coefficients and p-values for each variable in the best fit is shown. C) Basal 2-DG uptake of myobundles cultured in differentiation media formulated with the same supplements but a different base media of DMEM, αMEM, or LAA. Results are compiled from three donors normalized to the basal 2-DG uptake in the DMEM condition. n=3-4 myobundles per condition per donor. Data presented as mean ± S.E.M. Statistical significance determined using one-way ANOVA followed by Tukey HSD post-hoc: ***p<0.001.

Upon comparison of the amino acid content of the base media types (Table 4), it is apparent that seven amino acids are incrementally changing between DMEM, αMEM and LAA; L-alanine, L-isoleucine, L-leucine, L-methionine, L-phenylalanine, L-proline, and L-tyrosine.

Table 4. Components of the base DMEM, αMEM, and LAA media compared with plasma amino acid reference values[273]. Italics and bold indicate components that are incrementally changing between base media types. Parentheses represent components that are not in the custom base media but are supplemented at the given concentration.

Components	DMEM mM	α-MEM mM	LAA mM	Plasma values mM
Amino Acids				
Glycine	0.4000	0.6667	0.2800	0.2554 ± 0.0659
L-Alanine		***0.2809***	***0.8800***	**0.3194 ± 0.0717**
L-Arginine hydrochloride	0.3981	0.6018	0.1050	0.0814 ± 0.0193
L-Asparagine-H2O		0.3333	0.2200	0.0484 ± 0.00929
L-Aspartic acid		0.2256	0.0100	0.00626 ± 0.00234
L-Cysteine hydrochloride-H2O		0.5682	0.0600	
L-Cystine 2HCl	0.2013	0.0990	0.1150	
L-Glutamic Acid		0.5102	0.1550	0.0462 ± 0.0214
L-Glutamine	4.0000	2.0000	(2.0000)	0.6579 ± 0.1062
L-Histidine hydrochloride-H2O	0.2000	0.2000	0.1950	0.0893 ± 0.0108
L-Isoleucine	***0.8015***	***0.4000***	***0.1700***	**0.0775 ± 0.0154**
L-Leucine	***0.8015***	***0.3969***	***0.2900***	**0.1501 ± 0.0277**
L-Lysine hydrochloride	0.7978	0.3989	0.4050	0.1974 ± 0.0307
L-Methionine	***0.2013***	***0.1007***	***0.0550***	**0.0254 ± 0.00505**
L-Phenylalanine	***0.4000***	***0.1939***	***0.1250***	**0.0600 ± 0.00775**
L-Proline		***0.3478***	***0.5950***	**0.1883 ± 0.0550**
L-Serine	0.4000	0.2381	0.2400	0.1151 ± 0.0250
L-Threonine	0.7983	0.4034	0.4050	0.1279 ± 0.0282
L-Tryptophan	0.0784	0.0490	0.1200	0.0630 ± 0.0107
L-Tyrosine disodium salt	***0.3985***	***0.1985***	***0.1350***	**0.0629 ± 0.0122**
L-Valine	0.8034	0.3932	0.5400	0.2436 ± 0.0452

3.3.4 Characterization of metabolic phenotype of myobundles cultured in LAAGFR and Baseline conditions

To examine whether the change in basal 2-DG uptake was associated with other alterations in metabolism, we collected media samples after 24 hours of culture with the

myobundles and measured the L-lactate concentration in the media. L-lactate is an indicator of aerobic glycolysis, in which lactate is produced as an end product of glycolysis in cells with a sufficient supply of oxygen[274,275]. A two-way ANOVA of the pooled data indicated a main effect of LAAGFR condition on L-lactate concentration, and L-lactate was statistically significantly lower in the LAAGFR group in two of the three donors tested (Figure 18A), suggesting decreased glycolysis in the LAAGFR group. When the 2-DG uptake rate is plotted against the production rate of lactate on a bundle-specific basis (Figure 19), there is a positive correlation between 2-DG uptake rates and L-lactate production rates, a trend which confirms that bundles taking up more 2-DG are also producing more L-lactate.

To further characterize the metabolic phenotype of the myobundles, they were miniaturized to the dimensions of a Seahorse XF islet capture cell plate, which has approximately the surface area of a well in a 96-well plate (Figure 20A). The miniaturized myobundles compact and exhibit fiber alignment as visible with a brightfield microscope (Figure 20B), and the effect of the LAAGFR conditions on basal glucose uptake was maintained (Figure 20C). The oxygen consumption rates (OCR), a surrogate measure for oxidative metabolism, and extracellular acidification rates (ECAR), a surrogate measure for glycolytic metabolism[276], were measured using the Seahorse XFe24. Myobundles from all three donors exhibited an increased OCR/ECAR ratio in the LAAGFR group, which suggests a shift away from glycolysis as an ATP

source (Figure 18B). In two donors, this ratio was altered by a decrease in overall glycolysis without a change in oxygen consumption, while in the other donor the ratio was altered by an increase in the oxygen consumption and a slight decrease in glycolysis (Figure 18C).

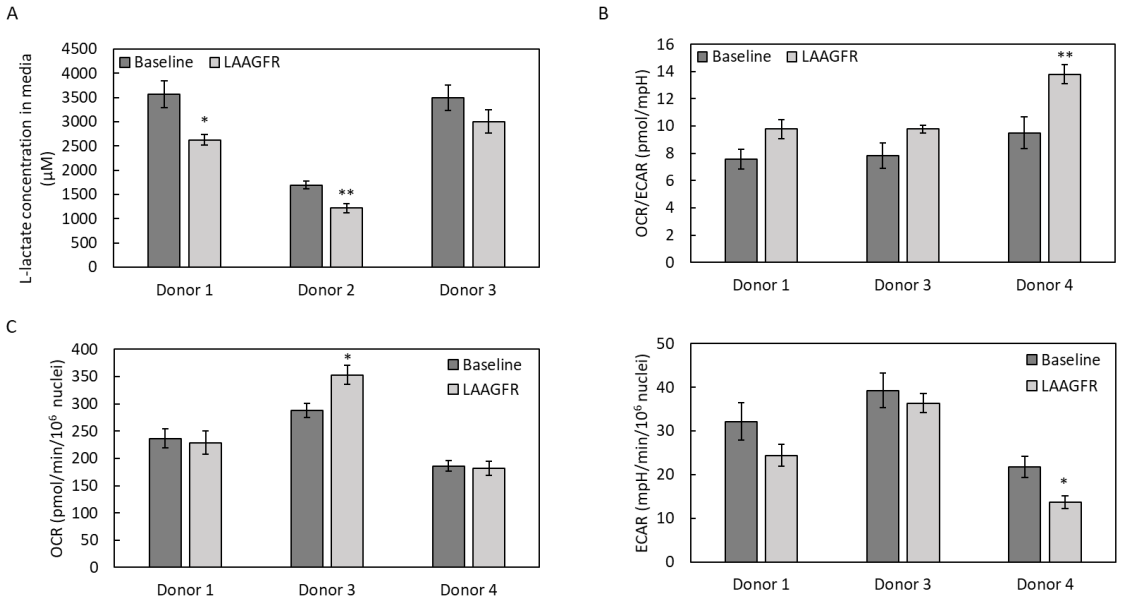

Figure 18. Myobundles cultured in LAAGFR conditions exhibit shift toward decreased glycolysis. A) L-lactate concentration in the media, produced by the myobundles over a 24 hour period. n=5 myobundles per condition per donor. Data presented as mean ± S.E.M. Statistical significance determined using Student's t-test: *p<0.05, **p<0.01. B) The ratio of oxygen consumption rate (OCR)/ extracellular acidification rate (ECAR), indicating the ratio of oxidative phosphorylation to glycolysis in the myobundles. Ratios were obtained for each individual myobundle, n=4-14 myobundles per condition per donor. Data presented as mean ± S.E.M. Statistical significance determined using Student's t-test: **p<0.01. C) OCR and ECAR values for myobundles cultured in baseline and LAAGFR conditions. n=4-14 myobundles per condition per donor. Data presented as mean ± S.E.M. Statistical significance determined using Student's t-test: *p<0.05.

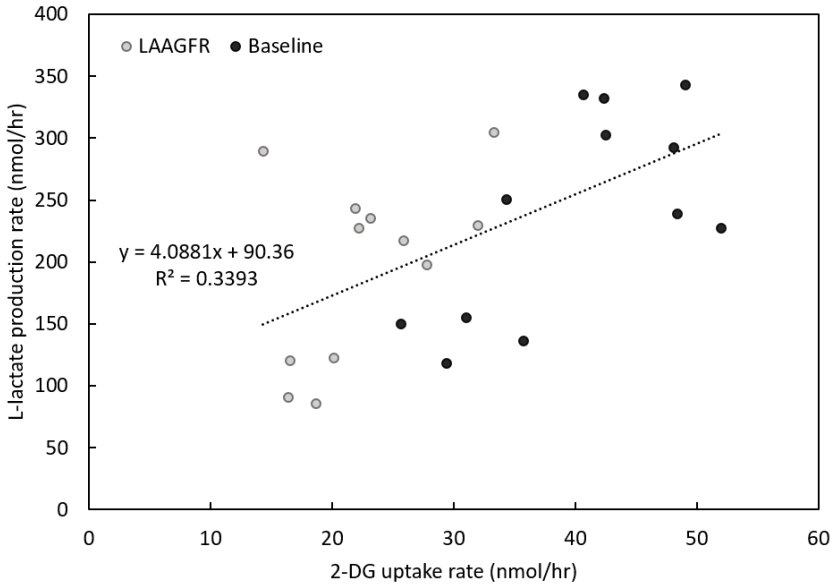

Figure 19. Positive correlation of 2-DG uptake rates and L-lactate production. 2-DG uptake rates and L-lactate concentrations were obtained for individual myobundles, with each point representing a single myobundle. A line of best fit was applied to all points.

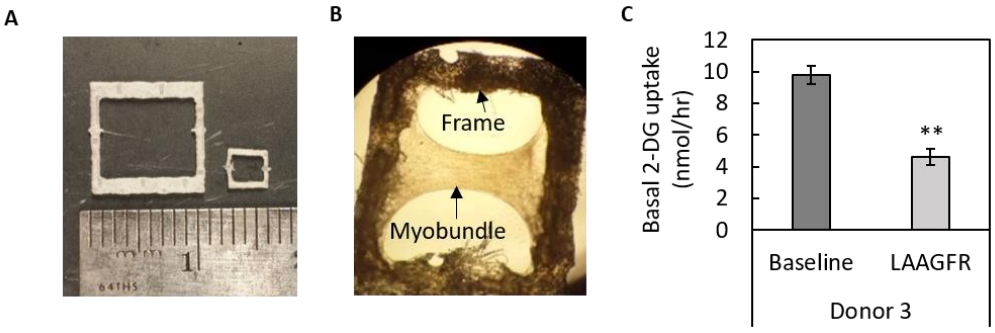

Figure 20. Miniaturized myobundles used for Seahorse testing. A) Frame for standard sized myobundles next to the frame for the miniaturized myobundles. B) A brightfield image of a miniaturized myobundle indicates myobundle compaction and fiber alignment. Taken at 4x magnification. C) Basal 2-DG uptake in miniaturized myobundles indicates significantly lower basal 2-DG uptake in the LAAGFR group. Data shown as mean ± S.E.M, n=3 myobundles per condition.

3.3.5 Gene expression of myobundles cultured in LAAGFR and Baseline conditions

We next examined several genes of interest associated with glucose transport and metabolic regulation and measured expression changes in these genes using qRT-PCR. We observed a trend of decreased GLUT1 and GLUT4 expression in myobundles cultured in LAAGFR conditions, while GLUT3 expression remained unaffected (Figure 21A). Expression of PGC-1α, a master regulator of oxidative metabolism, was unchanged in two donors and significantly low for myobundles from one donor cultured in LAAGFR conditions, while expression of its downstream target, HIF-2α was unchanged in the LAAGFR condition (Figure 21B). Interestingly, GLUT3, which is present in fetal skeletal muscle[277] but is not characteristically found in significant amounts in adult skeletal muscle *in vivo* except in association with nerves or regenerating fibers[265,277-280], is expressed at only slightly lower levels than GLUT1 in our myobundles, and it is important to note that overall expression levels of GLUT1 and GLUT3 were substantially higher than expression of GLUT4 (Figure 21C). When the relative abundance of each of the glucose transporter genes in the Baseline and LAAGFR conditions is plotted against the 2-DG uptake (Figure 21D) there is a positive correlation between changes in 2-DG uptake and GLUT1 levels, but not with GLUT3 or GLUT4. Taken together, these results indicate that changes in GLUT1 and GLUT4 expression may be occurring apart from regulation by PGC-1α, or may be temporally separated

from changes in PGC-1α expression, and that the change in gene expression of GLUT1 is the primary effector of the decreased glucose uptake in the LAAGFR condition.

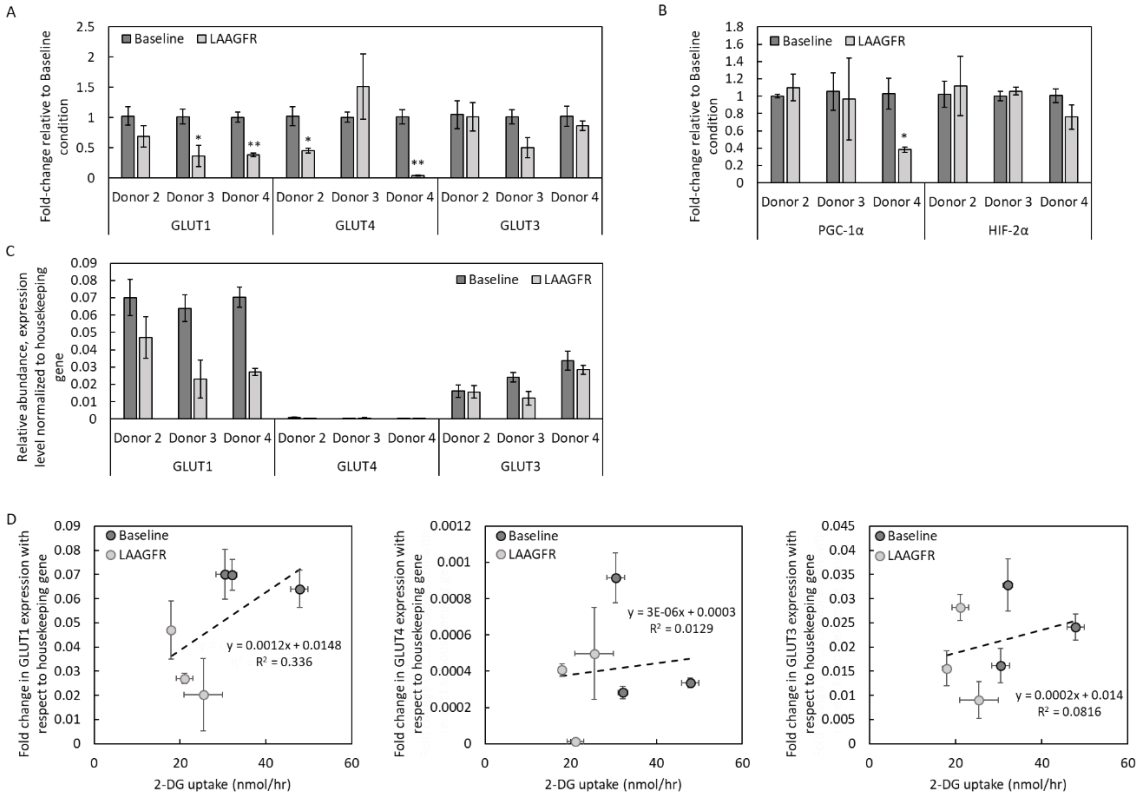

Figure 21. LAAGFR formulation and culture conditions are linked to decreased glucose transporter expression. A) Gene expression of glucose transporters GLUT1, GLUT4, and GLUT3 in myobundles. B) Gene expression of metabolic regulator PGC-1α and downstream gene HIF-2α in myobundles. C) Gene expression level of glucose transporters normalized to the housekeeping gene indicates relative abundance of expression for each of the transporters. D) Relative abundance of glucose transporters plotted against 2-DG uptake for the three donors, shown with a line of best fit for all data points. For all panels, n=3-4 myobundles per condition per donor. Data presented as mean ± S.E.M. Statistical significance determined using Student's t-test: *p<0.05, **p<0.01.

To determine if the metabolic reprogramming seen with the LAAGFR condition is associated with alterations in myosin heavy chain expression, we examined gene

expression of several myosin heavy chain isoforms (Figure 22). We did not observe consistent trends of enrichment for isoforms associated with oxidative or glycolytic metabolic phenotypes in the two culture conditions (Figure 22A). There does appear to be a trend of higher adult MHC isoform expression and lower immature MHC isoform expression in the LAAGFR condition, perhaps indicating increased maturation. Relative to the housekeeping gene, myobundles express substantial amounts of the mature MHC isoforms as well as the embryonic MHC isoform, with very little perinatal MHC (Figure 22B).

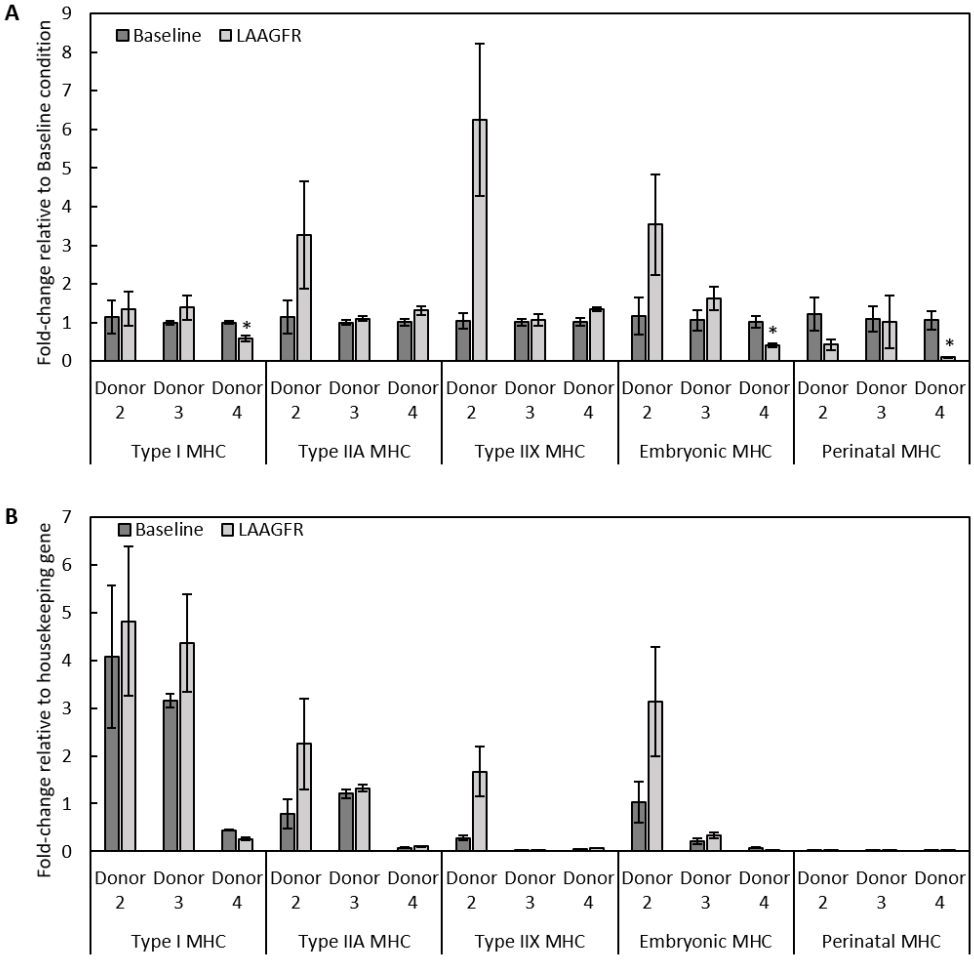

Figure 22. Gene expression of myosin heavy chain isoforms. A) Gene expression of myosin heavy chain isoforms, fold-change relative to the Baseline group. B) Gene expression of myosin heavy chain isoforms, fold-change relative to the housekeeping gene to show relative abundance. For all panels, n=3 myobundles per condition per donor. Data presented as mean ± S.E.M. Statistical significance determined using Student's t-test: *p<0.05 indicates statistical significance compared to the Baseline condition.

3.3.6 Contractile function of myobundles cultured in LAAGFR and Baseline conditions

To assess whether the changes in glucose metabolism in the LAAGFR condition are associated with a change in contractile function, we examined tetanic contractile

force production, fatigue resistance, and twitch kinetics of myobundles. A tetanic contraction was induced in each bundle and there were no consistent trends or significant differences between the LAAGFR and baseline groups, indicating the retention of myobundle function in LAAGFR conditions (Figure 23A). Of note, Donor 2 produced higher contractile force in the LAAGFR conditions and also expressed higher levels of myosin heavy chain associated with fast twitch fibers, which are associated with greater force production[36]. Twitch kinetics were quantified, where time to peak is the time it takes the myobundle to reach peak twitch force and half relaxation time is the time it takes the myobundles to relax to half of the magnitude of the peak force. There were no significant differences between the two groups when twitch kinetics were quantified, although there was a trend of slightly longer half relaxation times in the LAAGFR group (Figure 23B). Myobundles were fatigued by exposure to a 20 Hz electrical stimulation for 30 seconds and force production was recorded. Percent fatigue is significantly lower in the LAAGFR group (Figure 23C), indicating the ability of myobundles in the LAAGFR group to resist fatigue more effectively than those in the Baseline group. The representative fatigue traces demonstrate the differences between the two groups in the ability of the myobundles to produce force after being fatigued (Figure 23D).

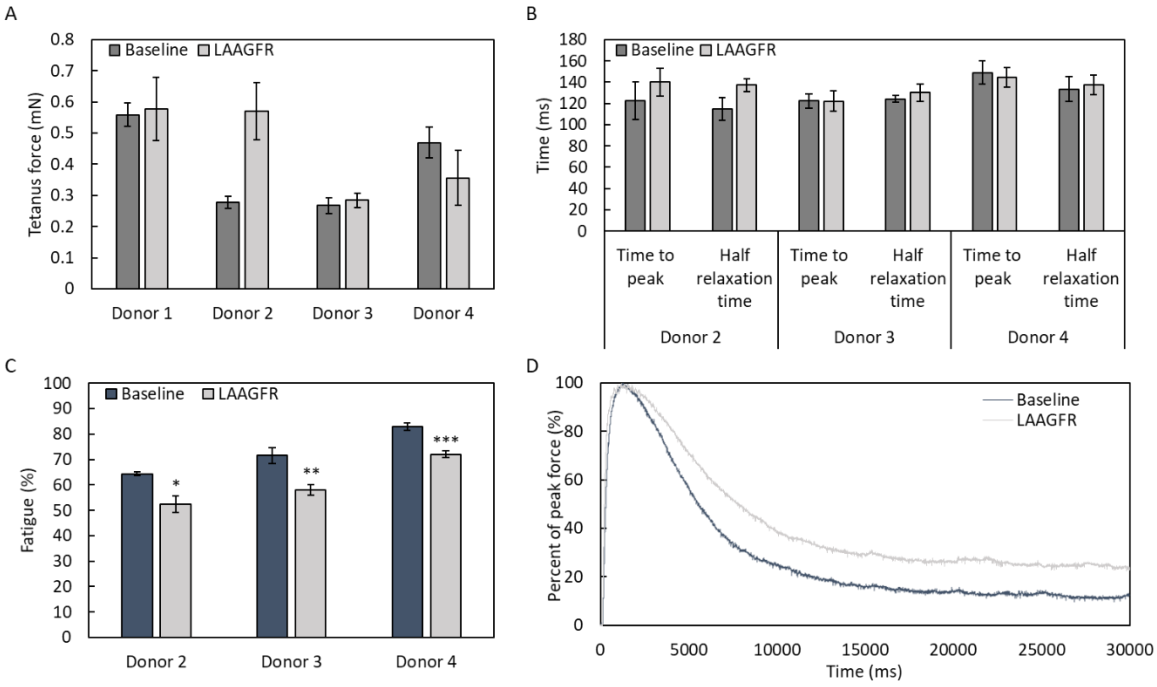

Figure 23. Myobundles cultured in LAAGFR conditions exhibit functional changes in fatigue resistance, without an impact on tetanic force production or twitch kinetics. A) Force production by myobundles exposed to a 20 Hz electrical stimulation to produce tetanic contraction. n=4 myobundles per condition per donor. Data presented as mean ± S.E.M. B) Twitch kinetics of myobundles, including the time to peak and the half-relaxation time of the myobundles, measured from the force traces produced by myobundles following a single stimulation resulting in a twitch contraction. n=5 myobundles per condition per donor. Data presented as mean ± S.E.M. C) Percent fatigue of myobundles, where a lower percent indicates improved fatigue resistance. n=5 myobundles per condition per donor. Data presented as mean ± S.E.M. Statistical significance determined using Student's t-test: *p<0.05, **p<0.01, ***p<0.001. D) Representative force traces of myobundles being fatigued by a 20 Hz electrical stimulation over the course of 30 seconds.

3.4 Discussion

In vitro skeletal muscle models are promising tools to investigate mechanisms of disease progression, or for use as a drug development and testing platform. Chronic diseases such as inflammation and insulin resistance are associated with metabolic

dysfunction and glycolytic fiber types in skeletal muscle. A number of studies have found that primary myoblasts and myotubes retain certain phenotypic aspects of the source muscle[200,281-283], making them a valuable resource for modeling such diseases. However, cultured human skeletal muscle inherently differs metabolically from skeletal muscle *in vivo* in that it exhibits greater expression of GLUT1 than GLUT4 and an increased reliance on glycolysis. In light of this, our work is significant for three reasons; first, these observations highlight the importance of beginning with a healthy skeletal muscle model that accurately portrays the metabolic function of muscle *in vivo* in order to observe functional changes occurring in a diseased state and second, there is already muscle dysfunction in normal *in vitro* culture conditions that mimics chronic disease states, which can make *in vitro* cultures less suitable models of healthy tissue. Third, manipulation of nutrient conditions may be a viable strategy to more closely mimic *in vivo* skeletal muscle metabolism.

In this study we showed that by culturing tissue engineered skeletal muscle myobundles in low amino acid and growth factor reduced conditions that better recapitulate the nutrient availability of skeletal muscle *in vivo*, myobundle metabolism was remodeled away from high levels of basal glucose uptake typically seen in skeletal muscle *in vitro* cultures. This is an intrinsic metabolic shift, as cellularity and tetanic force production is retained in LAAGFR conditions. Further, the lowered basal glucose uptake was associated with a decrease in L-lactate production by the myobundles and

an increased OCR/ECAR ratio, indicating that decreased glucose uptake is coupled with a shift away from glycolysis. Gene expression analysis indicates that the effect on glucose uptake and glycolysis is likely mediated by decreased glucose transporter expression, primarily decreased GLUT1 expression. Finally, we show that these changes in metabolic state elicit corresponding changes in myobundle function, promoting increased fatigue resistance.

In the body, there is a dynamic environment of protein synthesis and degradation. In an environment conducive to protein synthesis, such as during rest following exercise, essential amino acids act to stimulate anabolic pathways, promoting muscle protein synthesis[284]. The mTORC1 pathway is involved in this metabolic regulation in response to growth factor and amino acid sensing. mTORC1 is activated by the presence of growth factors and amino acids[285] and constitutive activation of mTORC1 results in increased fiber size, increased numbers of glycolytic fast twitch fibers, and increased aerobic glycolysis in rat skeletal muscle[286]. The branched chain amino acids leucine, isoleucine and valine, which are known to activate mTORC1[285,287], are all present at lower concentrations in the LAAGFR base media than in the Baseline base media (DMEM). Specifically, leucine is present in DMEM at a concentration of 801.5 μM, while in the LAA base media it is at a concentration of 290 μM. For comparison, leucine concentrations in human plasma range from 130-300 μM in the fasted and fed states, respectively[285,288,289]. Typical baseline *in vitro* culture conditions may

result in tonic activation of mTORC1, and limited amino acid and growth factor availability could impact metabolism via decreased activation of this pathway. Though outside the scope of these studies, the assessment of mTORC1 and its downstream targets[290] may shed light on the observed phenotypes.

LAAGFR conditions may be comparable to caloric restriction, which is associated with metabolic reprogramming to a state of increased fatty acid oxidation in mice[47] and increased mitochondrial biogenesis in human skeletal muscle independent of changes in fiber type enrichment[291,292]. Skeletal muscle satellite cells from mice on a calorie-restricted diet exhibit increased oxygen consumption and decreased lactate production[293].

While manipulations of culture conditions successfully decreased GLUT1 expression and shifted the metabolic phenotype of tissue engineered skeletal muscle toward oxidative metabolism, the issue of low GLUT4 expression and dampened insulin responsiveness in *in vitro* culture remains a hurdle for the field. One possible explanation for these obstacles may lie in the lack of innervation of the myobundles, as neuronal stimulation is highly involved in determining fiber type *in vivo*[36]. Another possible explanation is immaturity of cultured myotubes, which express neonatal and fetal isoforms of myosin heavy chain at high levels[294]. During development, immature muscle expresses substantially higher amounts of GLUT1, and as the muscle matures, GLUT1 levels decrease while GLUT4 levels increase until GLUT4 is expressed at substantially higher levels than GLUT1, creating a more insulin-responsive tissue[277].

While there is substantial expression of adult myosin heavy chain isoforms in the myobundles, the expression of embryonic MHC coupled with the high expression levels of GLUT1 and the regenerating skeletal muscle-associated GLUT3 suggest that they remain somewhat immature. Future work could involve direct perturbation of the mTORC1 pathway to induce changes in skeletal muscle metabolism and examine whether the insulin response is improved via a more targeted method.

3.5 Conclusions

Low amino acid and growth factor-reduced conditions for the formation and culture of myobundles resulted in a tissue that expressed lower levels of the GLUT1 transporter and was less reliant on glycolysis for energy production. Functionally, the myobundles cultured in LAAGFR conditions produced contractile force comparable to that of myobundles cultured in baseline conditions, but were more fatigue resistant. Taken together, this study links nutrient availability to glucose metabolism and contractile function in myobundles, and reveals the benefit of manipulating culture conditions to produce a more physiologically-relevant tissue-engineered skeletal muscle model.

3.6 Chapter acknowledgements

The studies shown in this chapter were done in collaboration with Anandita Ananthakumar, who performed the PCR shown in Figure 22. Xu Zhang facilitated the design of the small molds and frames used for the myobundles tested in the Seahorse.

Tim Koves provided the custom low amino acid media formulation. We would like to thank the Meyer lab for use of their Seahorse equipment. This work was funded by the National Science Foundation Graduate Research Fellowship under Grant No. NSF DGE 1106401, NIH grant UG3TR0002142 and the Common Fund for the Microphysiological Systems Initiative.

4. A Tissue-engineered Human Skeletal Muscle Model of Inflammation

4.1 Introduction

Chronic inflammation in obesity is one of a cluster of risk factors known as metabolic syndrome that predict an increased likelihood of the development of coronary artery disease and type 2 diabetes[295,296]. Due to its large mass and substantial metabolic activity, skeletal muscle plays an important role in the pathogenesis of inflammation-mediated disease[98,297]. Inflammation-associated skeletal muscle contractile dysfunction includes increased muscle weakness, fatigability, and atrophy[298,299]. Chronic inflammation is also associated with changes in skeletal muscle metabolism, characterized by shifts in fiber type from oxidative to glycolytic and the development of insulin resistance[270,271]. The role of inflammation in disease progression is not always well-understood due in part to the complexity of the *in vivo* environment, which has many confounding factors. In contrast, *in vitro* models offer the ability to tightly control certain parameters while perturbing others, enabling fine-tuned approaches to achieving mechanistic insights into disease pathology and validation of the safety and efficacy of potential therapeutics.

Tissue-engineered skeletal muscle offers several advantages over traditional 2-dimensional skeletal muscle cultures, including a three-dimensional environment that allows for cell-cell and cell-ECM interactions which are not present in monolayer culture. Additionally, because tissue-engineered skeletal muscle makes use of passive

tension to produce aligned myofibers, contractile force production is one key functional measure. Other measures of tissue-engineered skeletal muscle function include detection of calcium handling, oxygen consumption and glucose metabolism[7,8,225,226]. The increased physiological relevance of a three-dimensional environment and the ability to analyze multiple functional benchmarks make tissue engineered myobundles a promising platform for studying the mechanistic effects of inflammation on skeletal muscle for the development of targeted therapeutics. These attributes also enhance the potential of the model for studying the efficacy of therapeutics in the context of a pro-inflammatory skeletal muscle environment.

In this study, we investigated the creation of a human skeletal muscle model of inflammation using both macrophage-dependent and macrophage-independent methods. In the myobundles, macrophages exert little influence on the inflammatory state of the myobundles, and the skeletal muscle fibers themselves engage in the robust secretion of a wide array of cytokines after exposure to pro-inflammatory cytokines. Lipopolysaccharide (LPS) and interferon gamma (IFNγ) are commonly used to polarize macrophages to the pro-inflammatory M1 phenotype[300]. However, LPS is a component of the bacterial wall and is not typically implicated in chronic inflammation. Therefore, we developed a sterile inflammation model using the pro-inflammatory cytokines GM-CSF, IFNγ, and TNFα, which play central roles in mediating inflammatory responses in skeletal muscle[299]. Myobundles treated with these pro-inflammatory cytokines exhibit

contractile dysfunction, increased cytokine production, and altered glucose metabolism. Metformin is a type 2 diabetes therapeutic that treats hyperglycemia by stimulating increased glucose uptake. In pro-inflammatory cytokine-treated myobundles, metformin promotes increased 2-DG uptake, validating the model's suitability to mimic inflammatory-based dysfunction while also retaining the capacity to respond to relevant therapeutics.

4.2 Materials and Methods

4.2.1 Isolation of primary cord blood-derived monocytes and differentiation to monocyte-derived macrophages (MDM)

Primary human monocytes were isolated from human umbilical cord blood under a Duke IRB-approved protocol. Briefly, blood was diluted 1:1 with Hank's buffered saline solution (HBSS) (ThermoFisher Scientific) and layered onto an equal volume of Histopaque-1077 (Sigma-Aldrich). After centrifugation, the buffy coat layer was collected and centrifuged to pellet cells. Cell lysis buffer (BD Pharmingen) was added to lyse contaminating red blood cells. CD14+ monocytes were isolated using CD14 MicroBeads (Miltenyi Biotec) and a magnetic assisted cell sorting (MACS) system (Miltenyi Biotec). Purified monocytes were plated at a density of $1.5x10^5$ cells/cm^2 on uncoated tissue-culture treated petri dishes and were cultured in MDM culture media consisting of RPMI 1640 (ThermoFisher Scientific) supplemented with 10% heat-inactivated fetal bovine serum (FBS) (Hyclone) and 10 ng/mL granulocyte-macrophage colony-stimulating factor (GM-CSF) (PeproTech). For comparisons of macrophage

colony-stimulating factor (M-CSF) (PeproTech) and GM-CSF, 50 ng/mL of M-CSF was added to MDM culture media for the M-CSF condition in the place of GM-CSF. Monocytes were differentiated to MDMs in MDM culture media for at least six days prior to use.

4.2.2 Polarization of MDMs in 2D culture

For all 2D studies, MDMs were incubated with 10 mM EDTA and scraped to remove them from the culture surface, then re-plated onto Matrigel (Corning) – coated 6-well plates at a density of $6x10^4$ cells/cm^2. For 2D studies comparing M-CSF and GM-CSF-derived MDMs, re-plated MDMs were maintained in RPMI 1640 supplemented with 10% FBS and either 50 ng/mL M-CSF or 10 ng/mL GM-CSF beginning immediately following isolation for up to 7 days, with media changes every 3 days. Cells were scraped and prepared for flow at the specified time point post- re-plating. For 2D polarization studies using lipopolysaccharide (LPS) (Sigma-Aldrich) and interferon gamma (IFNγ) (PeproTech), MDMs were maintained in MDM culture media for 24 hours after re-plating, then treated for 48 hours (media refreshed after 24 hours) with 100 ng/mL LPS and 20 ng/mL IFNγ, with or without 10 ng/mL GM-CSF. After polarization for 48 hours, cells were either fixed for staining or scraped and prepared for flow cytometry. For 2D polarization studies using 'sterile' inflammatory cytokines, MDMs were maintained in MDM culture media for four days after re-plating, then treated for 48 hours (media refreshed after 24 hours) with the specified concentrations

and combinations of tumor necrosis factor (TNFα) (Sigma-Aldrich) and interferon gamma (IFNγ) (PeproTech).

4.2.3 Flow cytometry

MDMs were incubated with 10 mM EDTA (Sigma-Aldrich) and scraped to remove them from the culture surface, then fixed in 4% paraformaldehyde (Alfa Aesar). Cells from each condition were either left un-stained to act as negative controls, or stained with PE anti-human CD80 antibody (Biolegend), APC anti-human CD68 (Biolegend), or FITC anti-human CD163 (Biolegend). All antibodies were incubated with cells for 30 minutes at 4°C using a dilution factor of 1:20 in FACS buffer consisting of DPBS with 0.5% bovine serum albumin (BSA)(Sigma-Aldrich) and 2 mM EDTA. Cells were rinsed with DPBS and resuspended in 500 μL of FACS buffer. Cells were analyzed immediately after staining using a FACSCanto IIs analyzer (BD). Results were analyzed using FlowJo software. Within each experiment, one gate for each antibody was used to determine the percent positive cells for all treatment conditions to prevent any effect of gating bias.

4.2.4 Immunofluorescence in 2D cultures and 3D myobundles

MDMs cultured in 2D were fixed for 20 minutes at room temperature in 4% PFA, then rinsed three times with DPBS with calcium and magnesium (DPBS +/+). Cells were incubated for 1 hour at 37°C in blocking solution consisting of DPBS +/+ with 10% goat serum (Hyclone), 3% BSA, and 0.2% Triton-X (Sigma-Aldrich). Next, cells were

incubated overnight at 4°C with an antibody for CD80 (Biolegend), using a dilution of 1:100 in blocking solution. Cells were rinsed and incubated for 1 hour at room temperature with goat anti-mouse and goat anti-rabbit secondary antibodies (ThermoFisher Scientific) at a dilution of 1:250 in blocking buffer and Hoechst 33342 (ThermoFisher Scientific) at a dilution of 1:1000. Cells were rinsed three more times with DPBS +/+ prior to imaging. CD80 expression was quantified using ImageJ to analyze cell-specific integrated fluorescent density and normalizing to the number of nuclei.

Myobundles were placed on a rocker for all incubation steps. Myobundles were fixed using 2% PFA overnight at 4°C, then rinsed three times with DPBS +/+ and incubated in blocking buffer overnight at 4°C. Myobundles were incubated with the primary antibody for sarcomeric alpha actinin (SAA) (Abcam) diluted 1:200 in blocking buffer for 24 hours at 4°C. After the primary antibody incubation, myobundles were rinsed three times with DPBS +/+ and incubated with goat anti-mouse secondary antibody at a dilution of 1:250 and Hoechst 33342 at a dilution of 1:1000 in blocking buffer. After secondary antibody incubation, myobundles were rinsed three more times with DPBS +/+ prior to imaging using a Zeiss LSM 510 inverted confocal microscope.

4.2.5 Isolation and culture of primary myoblasts

Primary human myogenic cells were isolated from surgical waste samples under a Duke IRB-approved protocol. Briefly, muscle tissue was washed with Dulbecco's phosphate buffered saline (DPBS) (Sigma-Aldrich) containing 2X Antibiotic-Antimycotic

(ThermoFisher Scientific), then minced and digested using 0.05% Trypsin-EDTA (ThermoFisher Scientific). Minced tissue was pre-plated on an uncoated tissue culture flask for 2 hours before being transferred to a Matrigel (Corning)-coated flask for myogenic cell outgrowth. Tissue and cells were cultured during outgrowth in human growth media (hGM) consisting of low glucose (5.55 mM glucose) Dulbecco's Modified Eagle Medium (LG DMEM) with 1 mM sodium pyruvate (ThermoFisher Scientific) supplemented with 9% fetal bovine serum (FBS) (Hyclone), 0.25 μg/mL amphotericin B (ThermoFisher Scientific), 50 μg/mL gentamicin (ThermoFisher Scientific), 0.4 μg/mL dexamethasone (Sigma-Aldrich), 10 ng/mL EGF (Peprotech), and 50 μg/mL fetuin (Sigma-Aldrich).

4.2.6 Myobundle formation and culture

Myobundles were formed as previously described[7,8]. Briefly, a solution of Matrigel (Corning) (Baseline condition) and bovine fibrinogen (Sigma-Aldrich) in PBS was mixed with the cell solution containing 50 U/mL thrombin (Sigma Aldrich) and pipetted into the central channel of a PDMS mold surrounded by a nylon (Cerex Advanced Fabrics) frame. Each myobundle without MDMs was formed with 50 μL of solution and 750,000 cells. For myobundles with MDMs, MDMs were rinsed three times with DPBS without calcium and magnesium (DPBS -/-), then incubated in 10 mM EDTA for 15 minutes at 37°C, after which MDMs were gently dislodged by rinsing the surface with the 10 mM EDTA solution. MDMs were then added to the myoblast cell solution as

a specified percentage of the number of myogenic cells. For example, an MDM bundle with 5% MDM would contain 37,500 MDMs and 750,000 myogenic cells. The myobundles were allowed to gel for 30 minutes at 37°C before hGM supplemented with 1.5 mg/mL 6-aminocaproic acid (Sigma-Aldrich) (hGM + ACA) was added to the wells containing the molds. Myobundles were cultured in hGM + ACA for four days before being removed from the PDMS mold and switched to differentiation media. Myobundles were differentiated for 7-10 days prior to endpoint testing in differentiation media consisting of LG DMEM supplemented with 25 μg/mL gentamicin, 0.125 μg/mL amphotericin B, 2 mg/mL 6-aminocaproic acid (ACA), and 1X N-2 supplement (ThermoFisher Scientific). All myobundles in experiments with MDMs included were cultured in hGM + ACA and differentiation media supplemented with 10 ng/mL GM-CSF. Media was changed every other day.

Myobundles which were cytokine-treated were cultured with cytokines for 72 hours prior to endpoint testing. Cytokine concentrations used were, unless otherwise specified, 10 ng/mL GM-CSF, 100 ng/mL LPS, 20 ng/mL IFNγ, and 40 ng/mL TNFα.

4.2.7 Contractile function measurements

Myobundles were placed in a tissue bath kept at 37°C with one end of the myobundle pinned to a fixed PDMS platform and the other end pinned to a PDMS pad attached to a force transducer. Contractile force was measured in response to an electrical stimulus applied to the myobundle via two electrodes placed on either side of

the bundle in the tissue bath. Myobundles were stretched to 115% of normal length prior to stimulation with one second of stimulation at 1 Hertz for a twitch contraction, one second of stimulation at 20 Hertz for a tetanus contraction, and thirty seconds of stimulation at 20 Hertz to fatigue the muscle. Peak twitch and tetanus force, percent fatigue and twitch kinetics (time to peak twitch and half-relaxation time) were determined using a Matlab script. Peak twitch and tetanus were calculated as the difference between the highest measured force after stimulation and the baseline passive force prior to stimulation. Percent fatigue was calculated as $\frac{peak\ force - force\ after\ 30\ seconds\ of\ fatigue}{peak\ force - baseline\ force}\ x\ 100\%$. Time to peak twitch was calculated as the time between initiation of electrical stimulation and peak force. Half-relaxation time was calculated as the time between peak force and return to one-half of the difference between the peak force and the baseline force.

4.2.8 Cytokine arrays

Media samples were collected from myobundles immediately prior to initiating cytokine treatment and 48 hours after initiating cytokine treatment. Each sample was taken after media had been incubating with the myobundles for 48 hours. Media samples were stored at -80°C until assayed for cytokines. Cytokine concentrations in the media were quantified using a ProcartaPlex immunoassay (ThermoFisher Scientific).

4.2.9 2-deoxyglucose uptake quantification assay

Measurement of 2-DG uptake was done in myobundles using a modified version of the published protocol[227]. After optimization of the methods for use in myobundles, the following protocol was used; after differentiating for 2 weeks, unless otherwise specified, myotubes in monolayer and myobundles were cultured in serum- and insulin-free differentiation media for 18 hours prior to uptake. Myotubes and myobundles were washed in uptake buffer consisting of no glucose DMEM (ThermoFisher Scientific) with 0.1% (w/v) bovine serum albumin (Sigma-Aldrich) and 0.2 mM sodium pyruvate for 10 minutes. Myotubes and myobundles were then incubated in fresh uptake buffer for 30 minutes. Next, myotubes and myobundles (excluding negative control myobundles) were incubated for 20 minutes in uptake buffer with 5 mM 2-DG (Sigma-Aldrich). After uptake, myobundles were washed three times with ice-cold DPBS, then removed from the frames and lysed in 100 µl of 1X extraction buffer (Abcam) overnight at 4°C on a rocker. Myotubes were trypsinized and washed with DPBS via centrifugation and resuspension in ice-cold DPBS prior to lysis in the same manner as the myobundles. The next day, samples underwent a freeze/thaw cycle, were heated at 85°C for 40 minutes to remove endogenous NADP, and 50 µL of 200 mM triethanolamine (TEA) buffer (Sigma-Aldrich) was added to each sample. Samples were stored at -20°C until assayed. To quantify the 2-DG6P in the lysed samples, the protocol was followed as put forth in the previous publication[227].

4.2.10 Statistical analysis

Statistical significance determined using one or two-factor ANOVA, where appropriate, followed by Tukey HSD post-hoc testing. One symbol indicates $p<0.05$, two symbols indicate $p<0.01$, three symbols indicate $p<0.001$. All data shown as mean ± S.E.M.

4.3 Results

4.3.1 Optimization of differentiation conditions for monocyte-derived macrophages

In 2D culture, monocytes were differentiated to monocyte-derived macrophages (MDMs) beginning immediately following isolation in the presence of either 50 ng/mL M-CSF or 10 ng/mL GM-CSF to determine which process would produce MDMs that would best recapitulate a pro-inflammatory environment. Studies have shown that differentiation with M-CSF results in macrophages with an M2-like phenotype, while GM-CSF results in a more pro-inflammatory M1-like phenotype, both before and after polarization[301-303]. In these studies, CD68 represents the general macrophage marker, CD80 represents M1-like macrophage marker, and CD163 represents the M2 macrophage marker. At 6 days of differentiation, MDMs differentiated using M-CSF and GM-CSF had comparable CD68+ and CD80+ populations, but GM-CSF resulted in MDMs with a smaller CD163+ population, indicating that the GM-CSF-derived MDMs were less M2-like (Table 5). Re-plating the MDMs enhanced the M1-like phenotype in the GM-CSF-derived MDMs, with increased CD80+ cells and decreased CD163+ cells,

but after a further six days in culture the CD80 and CD163 expression had returned to that of MDMs prior to re-plating.

Table 5. Flow cytometry analysis of time course of macrophage marker expression by MDMs derived using M-CSF and GM-CSF. Marker expression was measured at day 6 of differentiation, day 1 post re-plate (day 7 of differentiation), and day 7 post re-plate (day 14 of differentiation). Data shown from one donor.

	CD68+ (%)			CD80+ (%)			CD163+ (%)		
	Day 6	Day 1 post-re-plate	Day 7 post-re-plate	Day 6	Day 1 post-re-plate	Day 7 post-re-plate	Day 6	Day 1 post-re-plate	Day 7 post-re-plate
M-CSF	93.6	77.0	73.3	7.06	0.71	9.38	94.4	83.1	72.7
GM-CSF	89.8	82.0	69.9	5.70	11.70	6.87	48.9	33.3	46.4

Next, MDMs were cultured beginning immediately after isolation until 20 days post-isolation in media containing GM-CSF, with media refreshed every 3 days, to determine if there were changes in phenotype with extended time in culture. We found comparable positive expression of CD68, CD80, and CD163 in the MDMs at 20 days post-isolation (Table 6) as we did in MDMs at 6 days post-isolation (Table 5) indicating little impact of long-term culture on the phenotype of GM-CSF-derived MDMs. The effect of an increased GM-CSF concentration on differentiation was examined, and we found little effect of the increased concentration (Table 6).

Table 6. Flow cytometry analysis of macrophage marker expression by MDMs differentiated using 10 and 50 ng/mL GM-CSF. Marker expression was measured at day 20 of differentiation. Data shown from one donor.

20 days post-isolation	CD68+ (%)	CD80+ (%)	CD163+ (%)
10 ng/mL GM-CSF	86.9	3.57	36.1
50 ng/mL GM-CSF	96.2	2.58	27.2

At 20 days post-isolation, the difference in phenotype between the adherent population and the non-adherent population was probed using flow cytometry. The adherent MDMs had a slightly higher CD80+ population and much lower CD163+ population than the non-adherent MDMs, indicating a more M1-like phenotype in the adherent cells (Table 7).

Table 7. Flow cytometry analysis of macrophage marker expression by adherent and non-adherent MDMs. Marker expression was measured at day 20 of differentiation. Data shown from one donor.

20 days post-isolation	CD68+ (%)	CD80+ (%)	CD163+ (%)
Adherent population	89.9	5.11	28.7
Non-adherent population	95.8	3.84	67.1

On the basis of these results, further experiments were carried out using MDMs differentiated using 10 ng/mL GM-CSF, and only the adherent population was utilized.

4.3.2 Polarization of MDMs to a pro-inflammatory state using LPS and IFNγ

To determine the ability of MDMs to be polarized to a pro-inflammatory phenotype, MDMs were differentiated for 12 days, then re-plated and allowed to adhere for 24 hours before being treated with 100 ng/mL LPS and 20 ng/mL IFNγ, with or without 10 ng/mL GM-CSF, for another 48 hours. The addition of LPS and IFNγ substantially increased pro-inflammatory marker CD80 expression as measured by both flow cytometry (Table 8) and immunofluorescence (Figure 24), indicating successful polarization to a pro-inflammatory phenotype. These experiments further confirm the use of GM-CSF during culture to promote a more M1-like phenotype, as CD80 expression as determined by flow cytometry (Table 8) and immunofluorescence (Figure 24) was higher in the un-polarized MDMs cultured with GM-CSF than in un-polarized MDMs cultured without GM-CSF for the 48 hours prior to endpoint testing. While GM-CSF does not appear to further contribute to CD80 expression in the polarized condition, it does reduce the M2 marker CD163 expression (Table 8). With this in mind, subsequent experiments utilized GM-CSF during polarization.

Table 8. Flow cytometry analysis of macrophage marker expression by un-polarized MDMs and MDMs polarized using LPS and IFNγ. MDMs were differentiated using GM-CSF prior to polarization with 100 ng/mL LPS and 20 ng/mL IFNγ with or without 10 ng/mL GM-CSF for 48 hours, at which time cells were prepared for flow. Data shown from one donor.

GM-CSF	LPS + IFNγ	CD68+ (%)		CD80+ (%)		CD163+ (%)	
		Donor 1	Donor 2	Donor 1	Donor 2	Donor 1	Donor 2
-	-	89.3		7.98		96.1	
+	-	92.9	82.3	11.5	18.5	84.1	83.0
-	+	88.6	70.7	85.8	68.9	92.8	67.7
+	+	95.5		84.6		82.9	

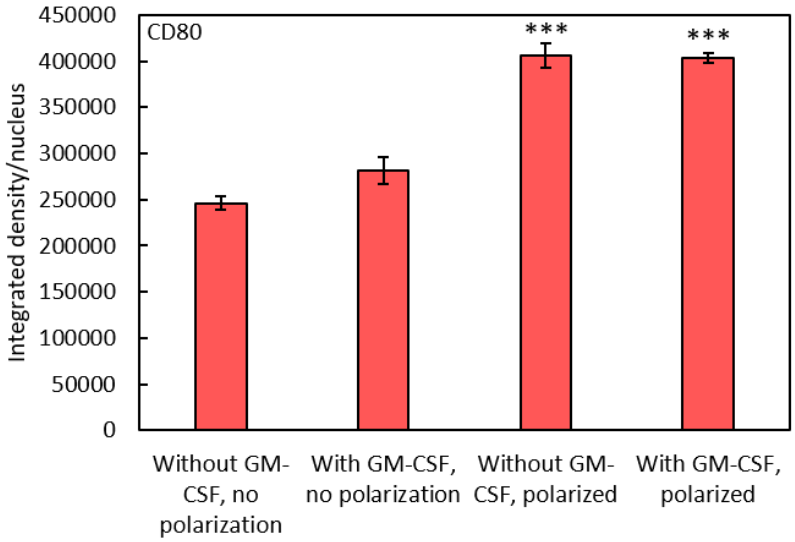

Figure 24. Expression of the M1 marker CD80 after polarization with LPS and IFNγ. MDMs were re-plated and allowed to adhere for 24 hours before being treated for 48 hours with 100 ng/mL LPS and 20 ng/mL IFNγ with or without 10 ng/mL GM-CSF. CD80 expression was quantified using image analysis of immunostained MDMs. N=1 donor, n=10 images per condition. ***p<0.001 denotes significance compared to corresponding GM-CSF condition without polarization. Data shown as mean ± S.E.M.

4.3.3 Polarization of MDMs to a pro-inflammatory state using TNFα and IFNγ

In chronic inflammation, LPS is not a relevant pro-inflammatory substance, because most chronic inflammation occurs in a sterile environment, in the absence of bacterial infection. To mimic sterile inflammation, we polarized MDMs with TNFα and IFNγ. MDMs were re-plated, then cultured for four days before a 48-hour treatment with varying concentrations and combinations of TNFα and IFNγ. The combination of 10 ng/mL TNFα and 20 ng/mL IFNγ produced the most substantial shift to a pro-inflammatory phenotype (Table 9). Although the shift was not as drastic as that elicited via treatment with LPS and IFNγ, we demonstrate that it is possible to shift MDMs to a pro-inflammatory phenotype using only sterile inflammatory cytokines.

Table 9. Flow cytometry analysis of macrophage marker expression by MDMs polarized using TNFα and/or IFNγ. MDMs were differentiated using GM-CSF prior to polarization with the specified concentrations and combinations of cytokines for 48 hours, at which time cells were prepared for flow. Data shown from one donor.

Polarization condition	CD68+ (%)	CD80+ (%)	CD163+ (%)
GM-CSF only	41.6	9.99	26.4
2 ng/ml TNFα	61.8	18.0	48.9
10 ng/ml TNFα	75.4	9.13	62.1
40 ng/ml TNFα	64.3	7.61	71.7
20 ng/ml IFNγ	48.6	14.7	75.0
2 ng/ml TNFα + 20 ng/ml IFNγ	73.5	10.8	42.8
10 ng/ml TNFα + 20 ng/ml IFNγ	77.5	25.9	53.3
40 ng/ml TNFα + 20 ng/ml IFNγ	85.1	13.9	64.4

4.3.4 Impact of un-polarized MDMs on myobundle function

We first examined the incorporation of increasing quantities of MDMs into myobundles, to determine whether un-polarized MDMs would impact myobundle function. Myobundles were formed with 1-15% MDMs and contractile force was measured. MDMs tended to increase force production, with a significant increase in tetanus force at 15% MDMs (Figure 25A). There were no significant changes in the twitch kinetics with MDMs (Figure 25B).

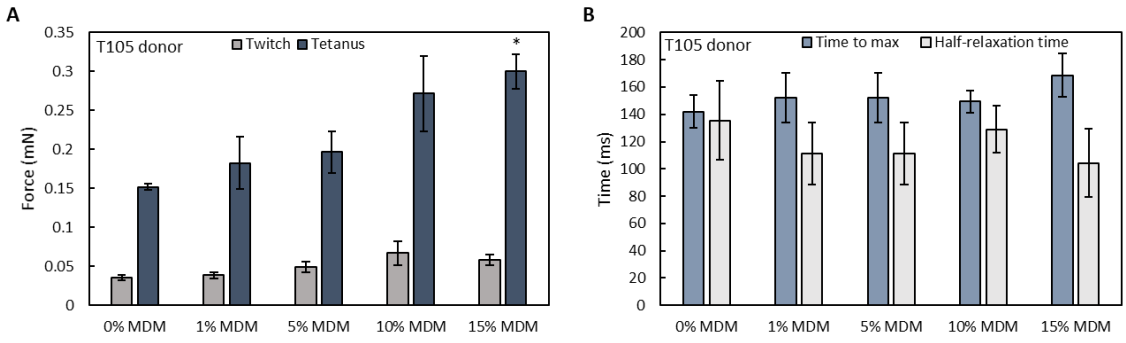

Figure 25. Impact of non-polarized MDMs on contractile function of myobundles. MDM myobundles containing 1, 5, 10, or 15 percent MDMs were tested for A) twitch and tetanus contractile force production and B) twitch kinetics. For both panels, myobundles formed using the T105 skeletal muscle donor, n=4 myobundles per condition. *p<0.05 denotes significance compared to 0% MDM control. Data shown as mean ± S.E.M.

4.3.5 Polarization of MDM myobundles with LPS and IFNγ at one week post-differentiation

To examine the effect of polarizing MDMs while incorporated in myobundles, we treated myobundles containing 0, 5, and 10% MDMs with 100 ng/mL LPS and 20 ng/mL IFNγ for 72 hours from day 4 to day 7 of myobundle differentiation, at which

point endpoint testing was carried out. Contractile force production of myobundles formed using the skeletal muscle donor T103 was impacted by polarization cytokines, without an additional effect of macrophages, although forces did trend downward with increased MDM percentages (Figure 26A). Polarization cytokines did not significantly affect contractile force of myobundles made with the T104 skeletal muscle donor, and there was no effect of macrophages (Figure 26B). Despite decreased contractile force, T103 myobundles treated with LPS and IFNγ without MDMs demonstrated significantly lower fatigue (Figure 26C), while fatigability of T104 myobundles treated with LPS and IFNγ was not significantly impacted (Figure 26D). In the T103 donor experiment, polarization cytokines significantly decreased the time to maximum twitch force in myobundles without MDMs (Figure 26E), while in the T104 donor experiment there was no significant effect of polarization cytokines on twitch kinetics (Figure 26F).

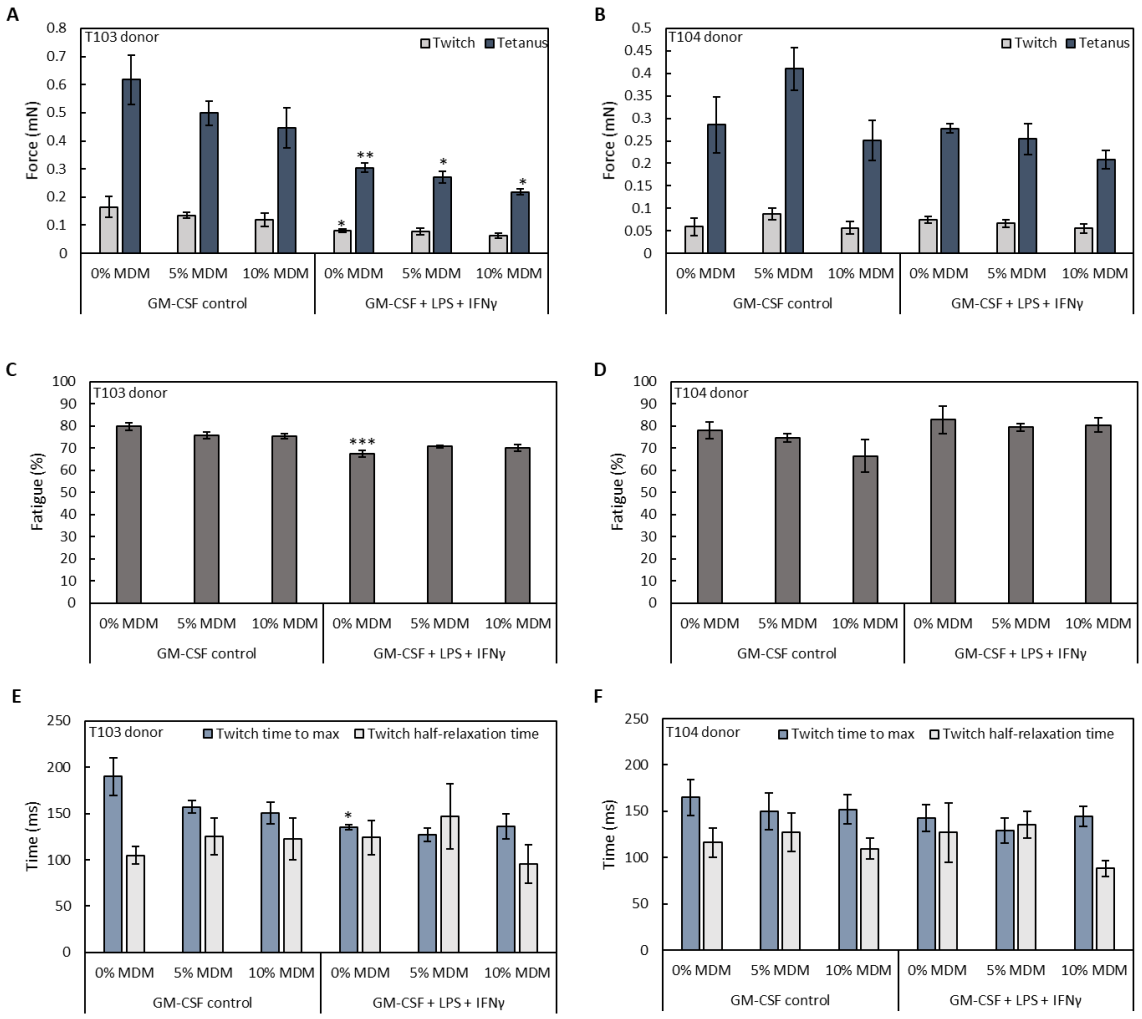

Figure 26. Impact of polarization with LPS and IFNγ on contractile function of MDM myobundles tested at 7 days post-differentiation. Myobundles containing 0, 5, or 10 percent MDMs were either kept in control media containing 10 ng/mL GM-CSF or polarized for 72 hours with 10 ng/mL GM-CSF + 100 ng/mL LPS + 20 ng/mL IFNγ and tested at one week post-differentiation for A-B) twitch and tetanus contractile force production, C-D) percent force depletion after fatigue, and E-F) twitch kinetics. For panels A, C, and E, myobundles formed using T103 skeletal muscle donor, n=5 myobundles per condition. For panels B, D, and F, myobundles formed using T104 skeletal muscle donor, n=4 myobundles per condition. *p<0.05, **p<0.01, ***p<0.001 denotes significance compared to the same MDM percentage in the GM-CSF control group. Data shown as mean ± S.E.M.

To determine the impact of polarization cytokines on expression of other cytokines, as well as to pinpoint the contribution of MDMs to the pro-inflammatory environment, media samples were collected from the same myobundles used for Figure 3 before (Day 4) and after (Day 6) addition of polarization cytokines. Some cytokines were produced by polarized MDM-containing myobundles at significantly higher levels than polarized myobundles without MDMs. These included TNFα, IL-12p70, and IL-23 (Figure 27A-C). Additionally, some cytokines were produced by un-polarized MDM-containing myobundles at significantly higher levels than un-polarized myobundles without MDMs, indicating production of these cytokines by MDMs at baseline. These included IL-7, IL-10, and IL-1α (Figure 27D-F). Of the cytokines measured, IL-1β, IL-15, IL-6, M-CSF, VEGF-A, and OSM were produced as statistically significantly higher levels after polarization of myobundles, but there was no effect of macrophages on production of these cytokines (Figure 27G-L). This indicates that the myobundles themselves are capable of producing a number of cytokines in response to a pro-inflammatory challenge.

Of note, the T103 donor, which exhibited significantly lower forces in response to LPS and IFNγ treatment, exhibited overall lower concentrations of many cytokines with the exception of IL-12p70 and IFNγ, the latter of which was present at a concentration of 53 ng/mL, an approximately 5-fold higher concentration than in the T104 donor. As IFNγ was added to the media at a concentration of 20 ng/mL, this excess production of

IFNγ could explain why LPS and IFNγ had an effect on contractile force with the T103 donor and not with the T104 donor. It is important to note that MDMs were also obtained from different donors for these experiments. It appears that the MDMs used for the T104 experiment produced more cytokines in the un-polarized state, namely IL-7, IL-10, and IL-1α, than did those used for the T103 experiment (Figure 27D-F). This donor to donor variability in MDMs is an important consideration when evaluating the use of MDMs in an inflammation model.

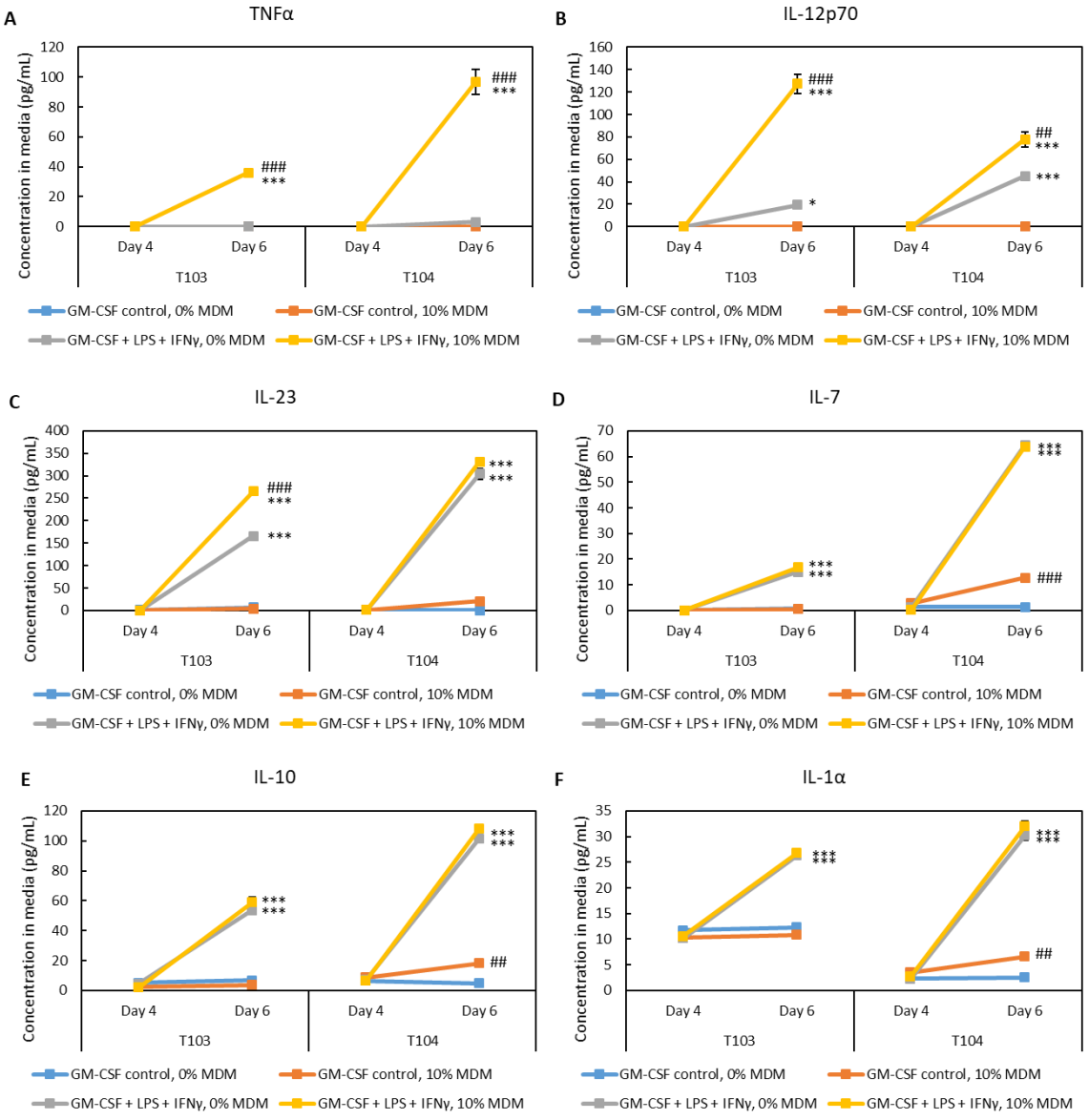
A
TNFα
Concentration in media (pg/mL)
120
100
80
60
40
20
0
###
***
###
***
Day 4
Day 6
Day 4
Day 6
T103
T104
GM-CSF control, 0% MDM
GM-CSF control, 10% MDM
GM-CSF + LPS + IFNγ, 0% MDM
GM-CSF + LPS + IFNγ, 10% MDM
B
IL-12p70
Concentration in media (pg/mL)
160
140
120
100
80
60
40
20
0
###
***
*
##
***
***
Day 4
Day 6
Day 4
Day 6
T103
T104
GM-CSF control, 0% MDM
GM-CSF control, 10% MDM
GM-CSF + LPS + IFNγ, 0% MDM
GM-CSF + LPS + IFNγ, 10% MDM
C
IL-23
Concentration in media (pg/mL)
400
350
300
250
200
150
100
50
0
###
***
***
***
***
Day 4
Day 6
Day 4
Day 6
T103
T104
GM-CSF control, 0% MDM
GM-CSF control, 10% MDM
GM-CSF + LPS + IFNγ, 0% MDM
GM-CSF + LPS + IFNγ, 10% MDM
D
IL-7
Concentration in media (pg/mL)
70
60
50
40
30
20
10
0
***
***
***
***
###
Day 4
Day 6
Day 4
Day 6
T103
T104
GM-CSF control, 0% MDM
GM-CSF control, 10% MDM
GM-CSF + LPS + IFNγ, 0% MDM
GM-CSF + LPS + IFNγ, 10% MDM
E
IL-10
Concentration in media (pg/mL)
120
100
80
60
40
20
0
***
***
***
***
##
Day 4
Day 6
Day 4
Day 6
T103
T104
GM-CSF control, 0% MDM
GM-CSF control, 10% MDM
GM-CSF + LPS + IFNγ, 0% MDM
GM-CSF + LPS + IFNγ, 10% MDM
F
IL-1α
Concentration in media (pg/mL)
35
30
25
20
15
10
5
0
***
***
***
***
##
Day 4
Day 6
Day 4
Day 6
T103
T104
GM-CSF control, 0% MDM
GM-CSF control, 10% MDM
GM-CSF + LPS + IFNγ, 0% MDM
GM-CSF + LPS + IFNγ, 10% MDM

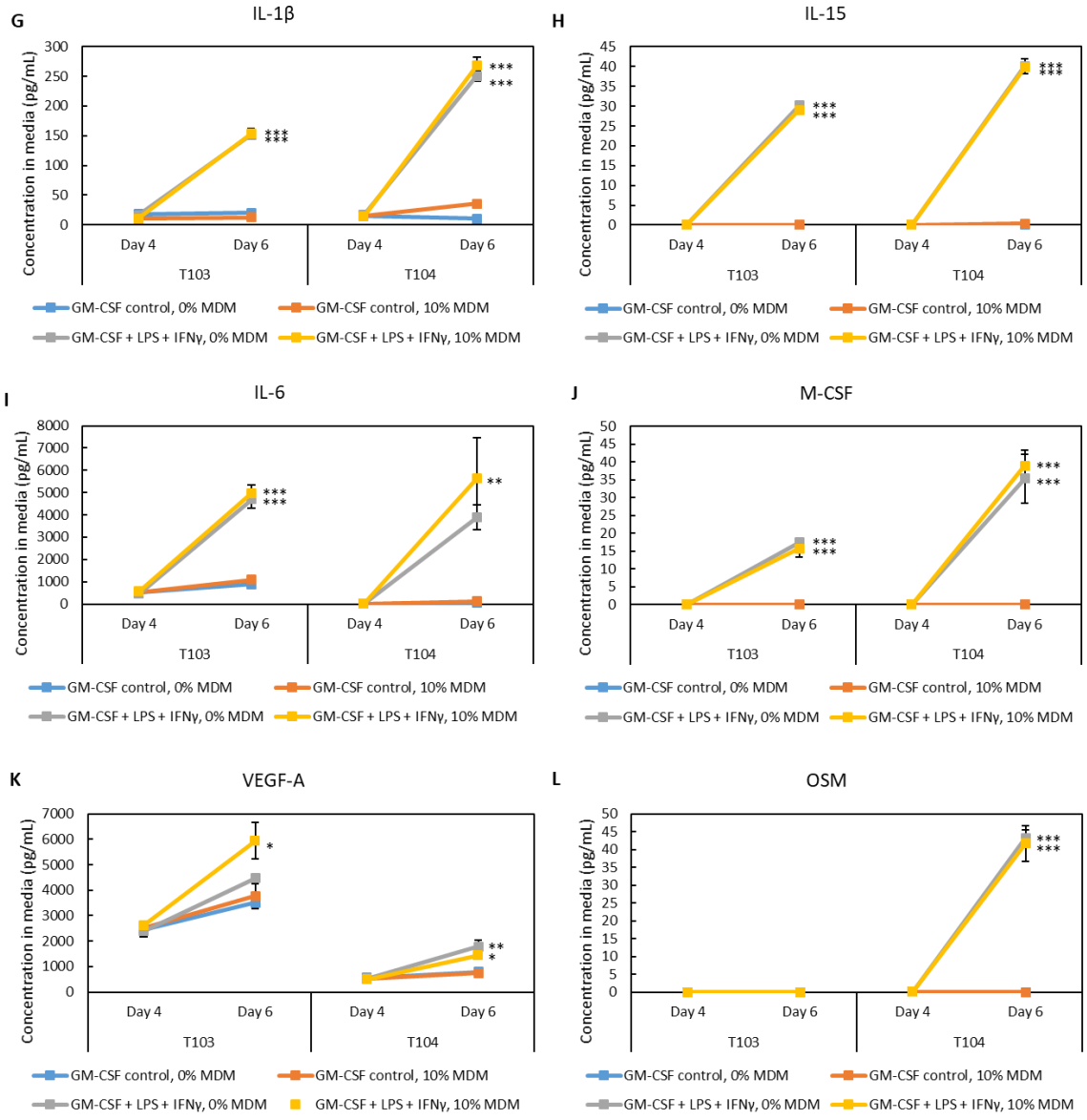

Figure 27. Cytokine concentrations in the media of MDM myobundles. Media was sampled from myobundles containing 0 or 10% MDMs maintained in GM-CSF control media or polarized with 10 ng/mL GM-CSF + 100 ng/mL LPS + 20 ng/mL IFNγ. Samples were obtained immediately prior to polarization (Day 4) and following 48 hours of polarization (Day 6). Cytokines measured were A) TNFα, B) IL-12p70, C) IL-23, D) IL-7, E) IL-10, F) IL-1α, G) IL-1β, H) IL-15, I) IL-6, J) M-CSF, K) VEGF-A, L) OSM,. Each panel contains results from MDM myobundles made using either the T103 or T104 skeletal muscle donor, n=4 myobundles per condition per donor. *p<0.05, **p<0.01, ***p<0.001 denotes significance compared to the same MDM

percentage in the GM-CSF control group. # denotes significance compared to 0% MDM condition in the same cytokine treatment group. Data shown as mean ± S.E.M.

4.3.6 Polarization of MDM myobundles with LPS, IFNγ, and TNFα at ten days post-differentiation

To ensure we were modeling inflammatory effects on differentiated myofibers rather than on myogenesis, we tested the effect of treating MDM myobundles with LPS and IFNγ at a later time point of ten days post-differentiation, when myobundles would be more mature at the point of initiating pro-inflammatory cytokine treatment. To potentially enhance the impact of polarized MDMs on myobundle function and because MDMs themselves produce TNFα, we also examined the effect of adding TNFα to the polarization cytokines and used 15% MDMs when forming the MDM myobundles. We examined the impact of treatment with 100 ng/mL LPS + 20 ng/mL IFNγ and 100 ng/mL LPS + 20 ng/mL IFNγ + 40 ng/mL TNFα on contractile force production in two experiments. In the experiment with the T103 skeletal muscle donor, MDMs increased force in the un-polarized state, but MDM myobundles treated with 100 ng/mL LPS + 20 ng/mL IFNγ exhibited significantly decreased tetanic force when compared to myobundles without MDMs in the same treatment condition, indicating a significant impact of polarized MDMs on myobundle function (Figure 28A). While the positive impact on contractile force of un-polarized MDMs was also observed in a second experiment with the T109 skeletal muscle donor, there was a significant decline in contractile force regardless of the presence of MDMs in both polarization conditions (Figure 28B). In both experiments, the addition of TNFα appeared to further decrease

contractile force, but the effect is not statistically significant. MDMs appeared to contribute to increased fatigability of the myobundles when in the polarized state, but not in the un-polarized state (Figure 28C, D). There was no significant effect of polarization or MDMs on twitch kinetics (Figure 28E, F).

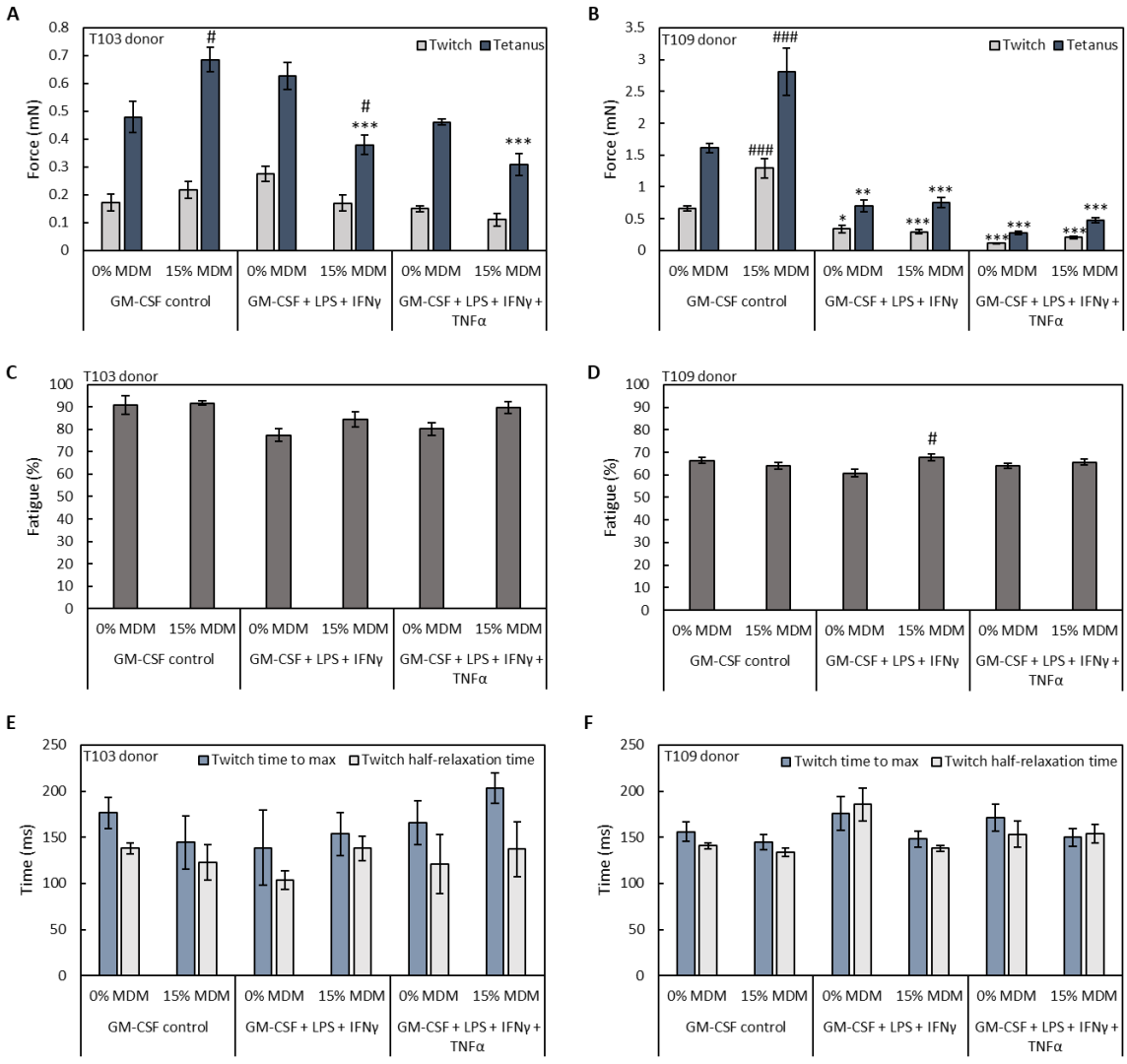

Figure 28. Impact of polarization with LPS and IFNγ and TNFα on contractile function of MDM myobundles tested at 10 days post-differentiation. Myobundles containing 0 or 15 percent MDMs were either kept in control media containing 10

ng/mL GM-CSF or polarized for 72 hours with 10 ng/mL GM-CSF + 100 ng/mL LPS + 20 ng/mL IFNγ or 10 ng/mL GM-CSF + 100 ng/mL LPS + 20 ng/mL IFNγ + 40 ng/mL TNFα and tested at 10 days post-differentiation for A-B) twitch and tetanus contractile force production, C-D) percent force depletion after fatigue, and E-F) twitch kinetics. For panels A, C, and E, myobundles formed using T103 skeletal muscle donor, n=3-5 myobundles per condition. For panels B, D, and F, myobundles formed using T109 skeletal muscle donor, n=5 myobundles per condition. *p<0.05, **p<0.01, ***p<0.001 denotes significance compared to the same MDM percentage in the GM-CSF control group. # denotes significance compared to 0% MDM condition in the same cytokine treatment group. Data shown as mean ± S.E.M.

4.3.7 Polarization of MDM myobundles with TNFα and IFNγ to model sterile inflammation

We next treated myobundles with or without MDMs with 40 ng/mL TNFα and 20 or 100 ng/mL IFNγ to model sterile inflammation. We found that treatment with the inflammatory cytokines tended to decrease contractile force, but this was not a statistically significant effect (Figure 29A). MDMs appeared to exert a protective effect against the decrease in force and fatigue resistance caused by inflammatory cytokines (Figure 29B). We observed no trends in twitch kinetics (Figure 29C). Immunostaining of the myobundles for SAA revealed that while striations are observed in all treatment conditions, there is sarcomeric degradation with cytokine treatment (Figure 29E-I). In the myobundles without MDMs, 40 ng/mL TNFα and 20 ng/mL IFNγ contributed to the appearance of thinner fibers with increased disruption of SAA architecture (Figure 29E), a phenotype that appears exacerbated in the 40 ng/mL TNFα and 100 ng/mL IFNγ treatment group (Figure 29F). Interestingly, in myobundles with MDMs, the thickness of the myofibers and lack of SAA deterioration observed in the un-polarized condition (Figure 29G) is maintained in the 40 ng/mL TNFα and 20 ng/mL IFNγ treatment group

(Figure 29H), and the integrity of the myofibers in the 40 ng/mL TNFα and 100 ng/mL IFNγ treatment group (Figure 29I) is noticeably improved when compared to the myobundle without MDMs in the same treatment group (Figure 29F). These observations support the idea that MDMs may have served a protective role against pro-inflammatory conditions in this experiment, as suggested by the contractile force and fatigue results.

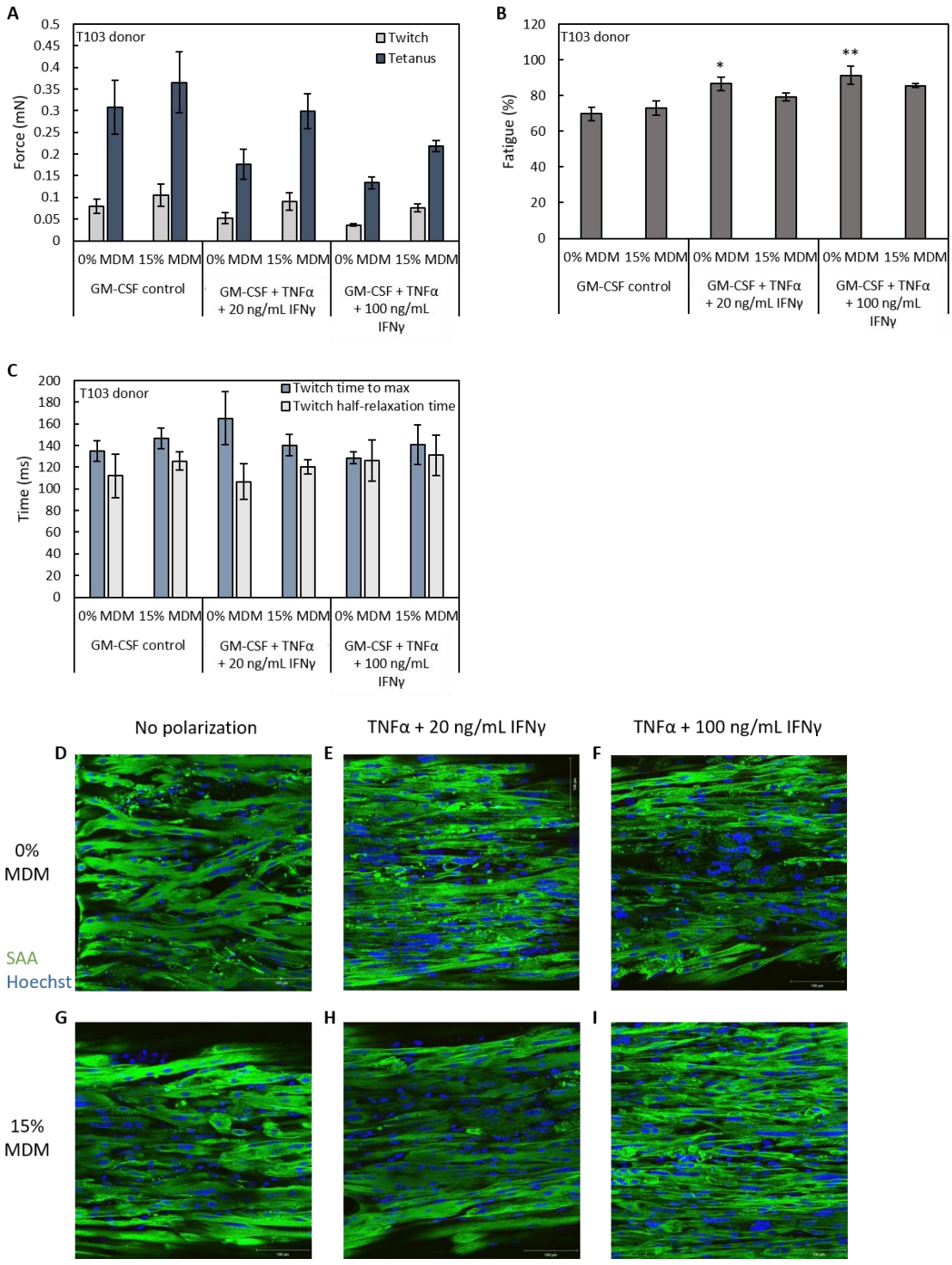

Figure 29. Impact of polarization with IFNγ and TNFα on contractile function and sarcomeric structure of MDM myobundles tested at 10 days post-differentiation.

Myobundles containing 0 or 15 percent MDMs were either kept in control media containing 10 ng/mL GM-CSF or polarized for 72 hours with 10 ng/mL GM-CSF + 40 ng/mL TNFα + 20 ng/mL IFNγ or 10 ng/mL GM-CSF + 40 ng/mL TNFα + 100 ng/mL IFNγ and tested at 10 days post-differentiation for A) twitch and tetanus contractile force production, B) percent force depletion after fatigue, and C) twitch kinetics. Myobundles from each condition were fixed and stained for sarcomeric alpha actinin (green) and nuclei (blue). Representative images are from myobundles cultured in the D) 0% MDM, GM-CSF control condition, E) 0% MDM, TNFα + 20 ng/mL IFNγ condition, F) 0% MDM, TNFα + 100 ng/mL IFNγ condition, G) 15% MDM, GM-CSF control condition, H) 15% MDM, TNFα + 20 ng/mL IFNγ condition, and I) 15% MDM, TNFα + 100 ng/mL IFNγ condition. Scale bars represent 100 μm. For all panels, myobundles formed using T103 skeletal muscle donor. For panels A-C, n=5 myobundles per condition. *p<0.05, **p<0.01, ***p<0.001 denotes significance compared to the same MDM percentage in the GM-CSF control group. Data shown as mean ± S.E.M.

4.3.8 Inflammatory cytokine treatment of myobundles without MDMs using GM-CSF, TNFα, and IFNγ to model sterile inflammation

To characterize the effect of inflammatory cytokine treatment on myobundles without MDMs, myobundles were treated with either 10 ng/mL GM-CSF + 20 ng/mL IFNγ or 10 ng/mL GM-CSF + 20 ng/mL IFNγ + 40 ng/mL TNFα for 72 hours, from day 7 to day 10 post-differentiation of the myobundles, followed immediately by endpoint testing. In two of the three skeletal muscle donors, treatment with GM-CSF + IFNγ alone or in combination with TNFα significantly reduced contractile force production (Figure 30A-C). In all donors, the addition of TNFα tended to further reduce force when compared to treatment with GM-CSF + IFNγ alone, but the effect was not statistically significant. Myobundles formed using the T109 donor exhibited significantly decreased fatigue after treatment with GM-CSF + IFNγ + TNFα when compared with untreated control myobundles, but the effect was not significant in the remaining two donors

(Figure 30D-F). Finally, there were no significant trends in twitch kinetics, with the exception of a significantly decreased half-relaxation time in the T111 donor treated with GM-CSF + IFNγ + TNFα, which likely indicates dysfunction associated with the low contractile force in that condition (Figure 30G-I). Myobundles immunostained for SAA depict effects of inflammatory cytokine treatment on myofiber morphology and sarcomeric structure (Figure 30J-O). As with the MDM myobundles, treatment with GM-CSF + IFNγ + TNFα appears to result in thinner myofibers, with some myofibers showing signs of balling up or losing the integrity of the sarcomeric structure, as indicated by white arrows (Figure 30L,O).

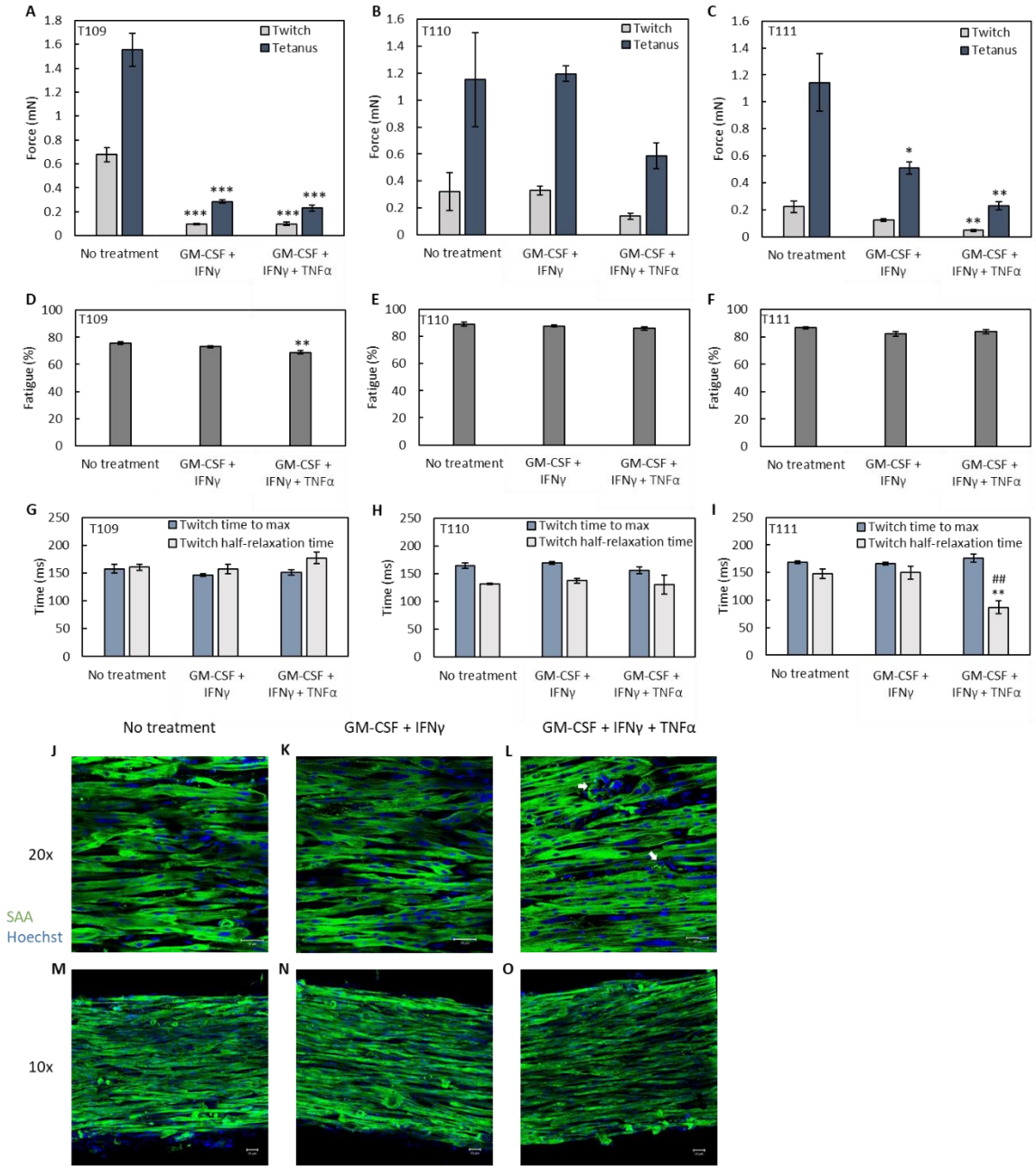

Figure 30. Impact of treatment with GM-CSF and IFNγ and TNFα on contractile function and sarcomeric structure of myobundles without MDMs tested at 10 days post-differentiation. Myobundles without MDMs were treated for 72 hours with either 10 ng/mL GM-CSF + 20 ng/mL IFNγ or 10 ng/mL GM-CSF + 20 ng/mL IFNγ + 40 ng/mL TNFα and tested at 10 days post-differentiation for A-C) twitch and tetanus contractile force production, D-F) percent force depletion after fatigue, and G-I)

twitch kinetics. Myobundles from each condition were fixed and stained for sarcomeric alpha actinin (green) and nuclei (blue). Representative images are from myobundles cultured in the J) no treatment control condition, taken at 20x magnification, K) 10 ng/mL GM-CSF + 20 ng/mL IFNγ condition, taken at 20x magnification, L) 10 ng/mL GM-CSF + 20 ng/mL IFNγ + 40 ng/mL TNFα condition, taken at 20x magnification, M) no treatment control condition, taken at 10x magnification, N) 10 ng/mL GM-CSF + 20 ng/mL IFNγ condition, taken at 10x magnification, and O) 10 ng/mL GM-CSF + 20 ng/mL IFNγ + 40 ng/mL TNFα condition, taken at 10x magnification. Scale bars represent 50 μm. For panels A, D, and G, myobundles formed using T109 skeletal muscle donor. For panels B, E, H, and J-O, myobundles formed using the T110 donor. For panels C, F, and I, myobundles formed using the T111 donor. For panels A-I, n=4 myobundles per condition. *p<0.05, **p<0.01, ***p<0.001 denotes significance compared to the no treatment control. # denotes significance compared to the GM-CSF + IFNγ treatment group. Data shown as mean ± S.E.M.

Next, we examined the ability of the sterile inflammatory cytokines to stimulate further cytokine production by myobundles. We observed that in the GM-CSF + IFNγ + TNFα group, production of all cytokines measured, with the exception of VEGF-A, was upregulated (Figure 31). The effect of GM-CSF + IFNγ on cytokine production was less pronounced than in the presence of TNFα, indicating a significant role for TNFα in the stimulation of myobundle cytokine production. In terms of individual skeletal muscle donors, the T109 donor exhibited the largest reduction in contractile force in response to the GM-CSF + IFNγ, but did not produce notably different levels of cytokines in that condition than the T111 donor. The T110 donor, which exhibited the least change in contractile force in response to treatment with GM-CSF + IFNγ ± TNFα, consistently produced lower concentrations of cytokines than the other two donors, including the potent pro-inflammatory cytokines IL-1α and IL-1β, as well as IL-12p70, IL-15, IL-23,

and IL-7. This suggests a relationship between the levels of cytokines produced and changes in contractile force in response to inflammatory cytokine treatment.

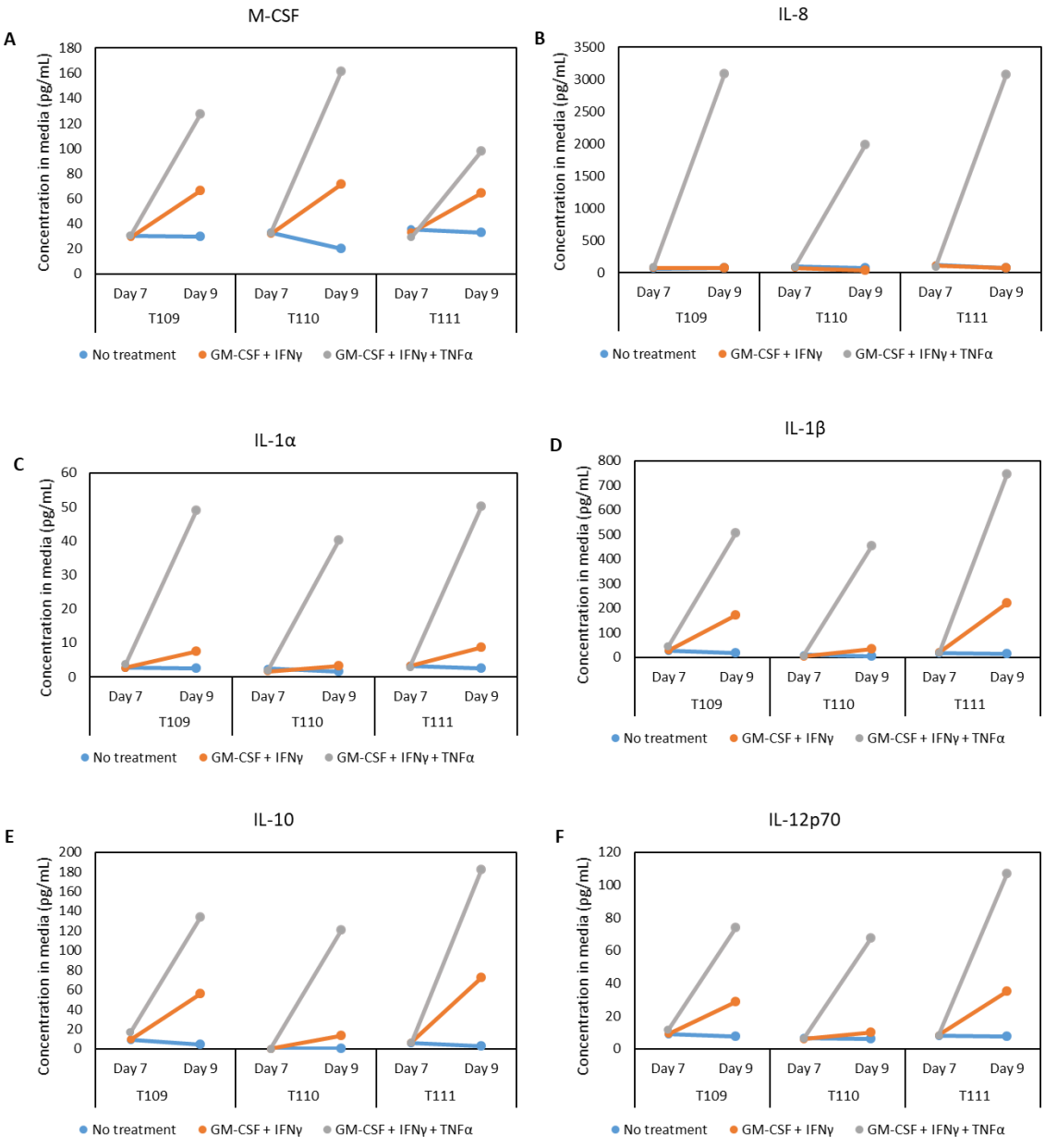

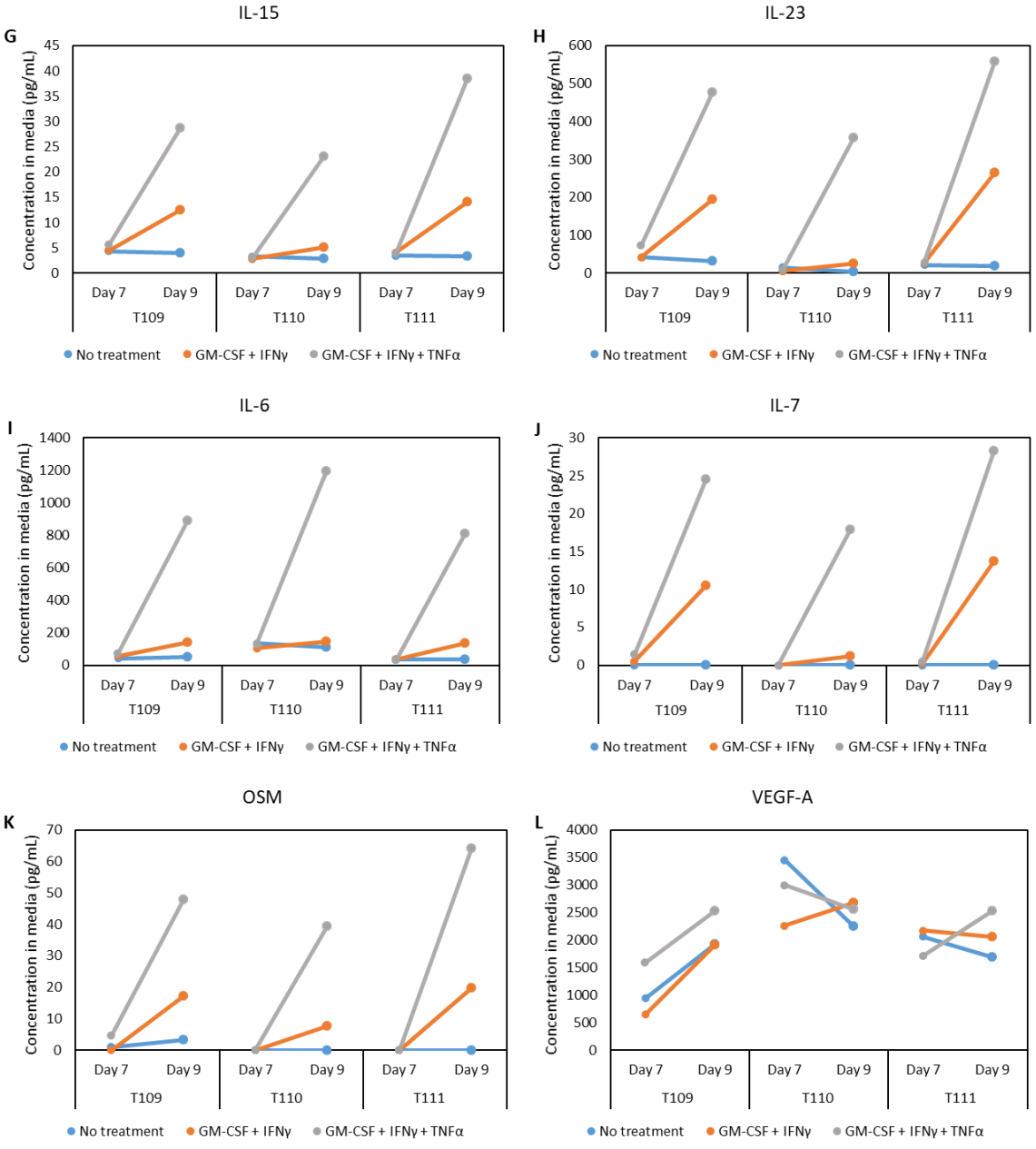

Figure 31. Cytokine concentrations in the media of myobundles treated with GM-CSF, IFNγ, and TNFα. Media was sampled from myobundles cultured in the absence of cytokines or treated with 10 ng/mL GM-CSF + 20 ng/mL IFNγ or 10 ng/mL GM-CSF + 20 ng/mL IFNγ + 40 ng/mL TNFα. Samples were obtained immediately prior to polarization (Day 7) and following 48 hours of polarization (Day 9). Cytokines measured were A) M-CSF, B) IL-8, C) IL-1α, D) IL-1β, E) IL-10, F) IL-12p70, G) IL-15, H) IL-23, I) IL-6, J) IL-7, K) OSM, and L) VEGF-A. Each panel contains results from

myobundles made using the T109, T110, and T111 skeletal muscle donors, n=2 myobundles per condition per donor. Data shown as mean.

Table 10. Compiled cytokine response by pro-inflammatory cytokine-treated myobundles without MDMs. Table contains cytokine concentrations at the time point after cytokine treatment, as shown in Figure 27 and Figure 31, averaged between donors. N=2-3 donors. Data presented as mean ± S.E.M.

Cytokine (pg/mL)	No treatment	GM-CSF	GM-CSF + IFNγ	GM-CSF + IFNγ + LPS	GM-CSF + IFNγ + TNFα
GM-CSF	35.09 ± 8.97	4055.42 ± 442.83	15286.33 ± 2817.81	5290.31 ± 604.65	16852.18 ± 2282.71
IFNγ	4.62 ± 2.7	100.65 ± 45.21	9353.09 ± 1183.1	30029.03 ± 20862.79	9362.17 ± 1095.23
IL-1α	2.2 ± 0.35	7.43 ± 4.87	6.38 ± 1.65	28.26 ± 1.97	46.4 ± 3.1
IL-1β	12.11 ± 3.36	15.33 ± 4.93	142.08 ± 56.5	200.89 ± 49.72	568.31 ± 90.26
IL-10	2.33 ± 1.22	5.87 ± 0.97	47.26 ± 17.75	77.67 ± 23.95	145.42 ± 18.56
IL-12p70	7.06 ± 0.48	0 ± 0	24.55 ± 7.47	32.21 ± 12.9	82.78 ± 12.19
IL-15	3.39 ± 0.32	0 ± 0	10.59 ± 2.78	35.1 ± 4.97	30.08 ± 4.47
IL-23	18.37 ± 8.13	3.18 ± 3.18	160.96 ± 70.96	235.11 ± 68.97	463.91 ± 58.3
IL-6	65.34 ± 22.68	458.19 ± 417.83	141.38 ± 2.88	4289.89 ± 407.14	964.94 ± 116.78
IL-7	0 ± 0	0.99 ± 0.27	8.47 ± 3.75	39.73 ± 24.75	23.53 ± 3.03
IL-8	76.3 ± 2.08	1436.65 ± 1159.32	61.1 ± 14.82	23227.14 ± 20264.25	2712.06 ± 364.7
M-CSF	27.56 ± 3.77	0 ± 0	67.43 ± 2.07	26.37 ± 8.91	128.75 ± 18.38
OSM	1.1 ± 1.1	0 ± 0	14.76 ± 3.7	21.6 ± 21.6	50.51 ± 7.28
TNFα	0 ± 0	0 ± 0	28.77 ± 1.36	1.59 ± 1.59	5774.71 ± 590.3
VEGF-A	1953.67 ± 161.13	2143.83 ± 1358.64	2215.49 ± 236.35	3127.36 ± 1335.15	2542.62 ± 10.1

The average cytokine concentrations in the media after treatment with the various pro-inflammatory cytokine combinations were compiled for all myobundles without MDMs (Table 10). As seen in Figure 31, the addition of TNFα stimulated a large increase in cytokine production over GM-CSF + IFNγ alone, but it is also apparent that

many cytokines were produced in greater quantities after treatment with TNFα + GM-CSF + IFNγ than with LPS + GM-CSF + IFNγ. These include IL-1α, IL-1β, IL-10, IL-12p70, IL-23, GM-CSF, and M-CSF (Table 10).

Finally, because inflammation is associated with glucose metabolism dysregulation, we examined the effect of sterile inflammatory cytokine treatment on basal and insulin-stimulated 2-DG uptake in myobundles. All three donors exhibited a significant increase in basal 2-DG uptake after treatment with GM-CSF + IFNγ + TNFα (Figure 32A-C). The T109 and T111 donors, which both exhibited significant decreases in contractile force in response to the GM-CSF + IFNγ treatment, also responded to this treatment with a significant increase in basal 2-DG uptake. Thus, it is evident that treatment with inflammatory cytokines increases the basal 2-DG uptake rate in myobundles.

Insulin-mediated 2-DG uptake was measured to assess the impact of cytokine treatment on insulin responsiveness. Treatment with GM-CSF + IFNγ + TNFα appeared to reduce the average magnitude of insulin response of all three donors, most strikingly in the T110 donor, as calculated by the ratio of the insulin-mediated 2-DG uptake to the basal 2-DG uptake (Table 11).

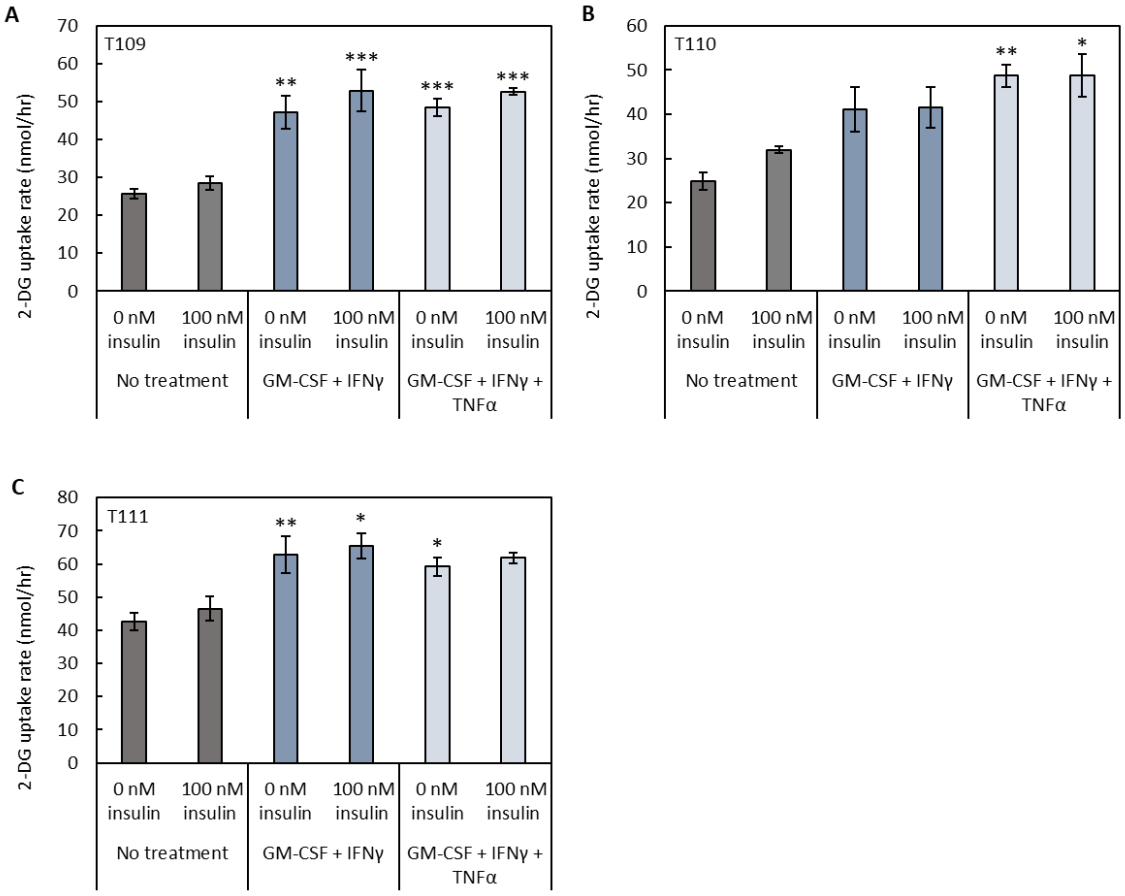

Figure 32. Effect of inflammatory cytokine treatment on 2-DG uptake by myobundles. Myobundles without MDMs were treated for 72 hours prior to endpoint testing at 10 days post-differentiation with either 10 ng/mL GM-CSF + 20 ng/mL IFNγ or 10 ng/mL GM-CSF + 20 ng/mL IFNγ + 40 ng/mL TNFα. Basal and insulin-stimulated 2-DG uptake were measured in myobundles formed using A) the T109 skeletal muscle donor, B) the T110 skeletal muscle donor, or C) the T111 skeletal muscle donor. For all panels, n=4 myobundles per condition. *p<0.05, **p<0.01, ***p<0.001 denotes significance compared to the no treatment control. Data shown as mean ± S.E.M.

Table 11. Effect of inflammatory cytokine treatment on myobundle insulin responsiveness. Insulin responsiveness is the ratio of the insulin-mediated 2-DG uptake rate to the basal 2-DG uptake rate, calculated from the data shown in Figure 32.

Insulin response	No treatment	GM-CSF + IFNγ	GM-CSF + IFNγ + TNFα
T109 donor	1.11 ± 0.09	1.12 ± 0.15	1.08 ± 0.05
T110 donor	1.28 ± 0.11	1.01 ± 0.17	1.0 ± 0.11
T111 donor	1.10 ± 0.11	1.04 ± 0.11	1.05 ± 0.06

4.3.9 Treatment of inflammatory cytokine-treated myobundles with metformin

To probe the effect of the type 2 diabetes therapeutic metformin on inflammatory cytokine-treated myobundles, healthy or cytokine-treated myobundles were treated with 400 μM metformin for 18 hours prior to endpoint testing at ten days post-differentiation. As expected, myobundles that had been treated with 10 ng/mL GM-CSF + 20 ng/mL IFNγ + 40 ng/mL TNFα for 72 hours prior to force testing exhibited significantly impaired contractile force production when compared with healthy, untreated myobundles (Figure 33A-C). Metformin treatment did not impact force production of healthy myobundles for two of the three donors, and notably, did not impact force production of inflammatory cytokine-treated myobundles (Figure 33A-C). Inflammatory cytokine-treated myobundles tended to exhibit increased fatigue, as did myobundles treated with metformin (Figure 33D-F). The combination of metformin and inflammation resulted in significantly decreased half-relaxation time when compared

with healthy controls, metformin treatment alone, or inflammation alone in one donor (Figure 33G).

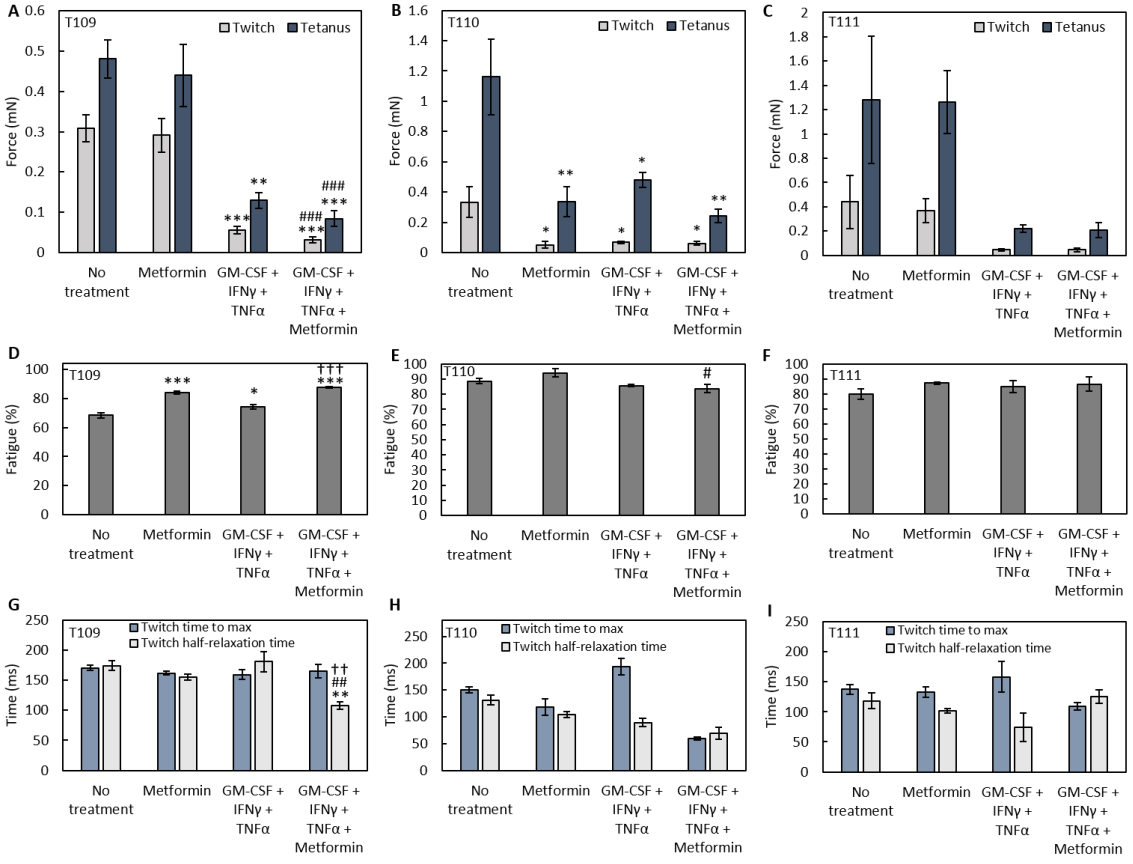

Figure 33. Effect of metformin treatment on contractile function of inflamed myobundles. Myobundles without MDMs were either left untreated or treated with metformin only, GM-CSF + IFNγ + TNFα only, or with a combination of GM-CSF + IFNγ + TNFα and metformin. Cytokine-treated myobundles were cultured with 10 ng/mL GM-CSF + 20 ng/mL IFNγ + 40 ng/mL TNFα for 72 hours prior to endpoint testing at 10 days post-differentiation, and metformin-treated myobundles were treated with 400 μM metformin for 18 hours prior to endpoint testing. Myobundles were tested for A-C) twitch and tetanus contractile force production, D-F) percent force depletion after fatigue, and G-I) twitch kinetics. For panels A, D, and G, myobundles formed using the T109 skeletal muscle donor. For panels B, E, and H, myobundles formed using the T110 skeletal muscle donor. For panels C, F, and I, myobundles formed using the T111 skeletal muscle donor. For all panels, n=4

myobundles per condition. ***p<0.001, **p<0.01, *p<0.05 denotes significance compared to the comparable insulin condition in the no treatment group, # denotes significance compared to the metformin only group, † denotes significance compared to the cytokine treatment only group. Data shown as mean ± S.E.M.

Basal (Figure 34A-C) and insulin-stimulated (Figure 34A, C) 2-DG uptake was measured in healthy myobundles, healthy myobundles treated with metformin, cytokine-treated myobundles, and cytokine-treated myobundles treated with metformin. In all three donors, metformin treatment of healthy myobundles significantly increased basal 2-DG uptake (Figure 34A-C). In accordance with previous results, cytokine-treated myobundles also exhibited increased 2-DG uptake, significantly so in the T109 donor which was treated with GM-CSF and IFNγ and TNFα (Figure 34C). Treatment with metformin stimulated a further statistically significant increase in 2-DG uptake in inflammatory cytokine-treated myobundles from all three donors.

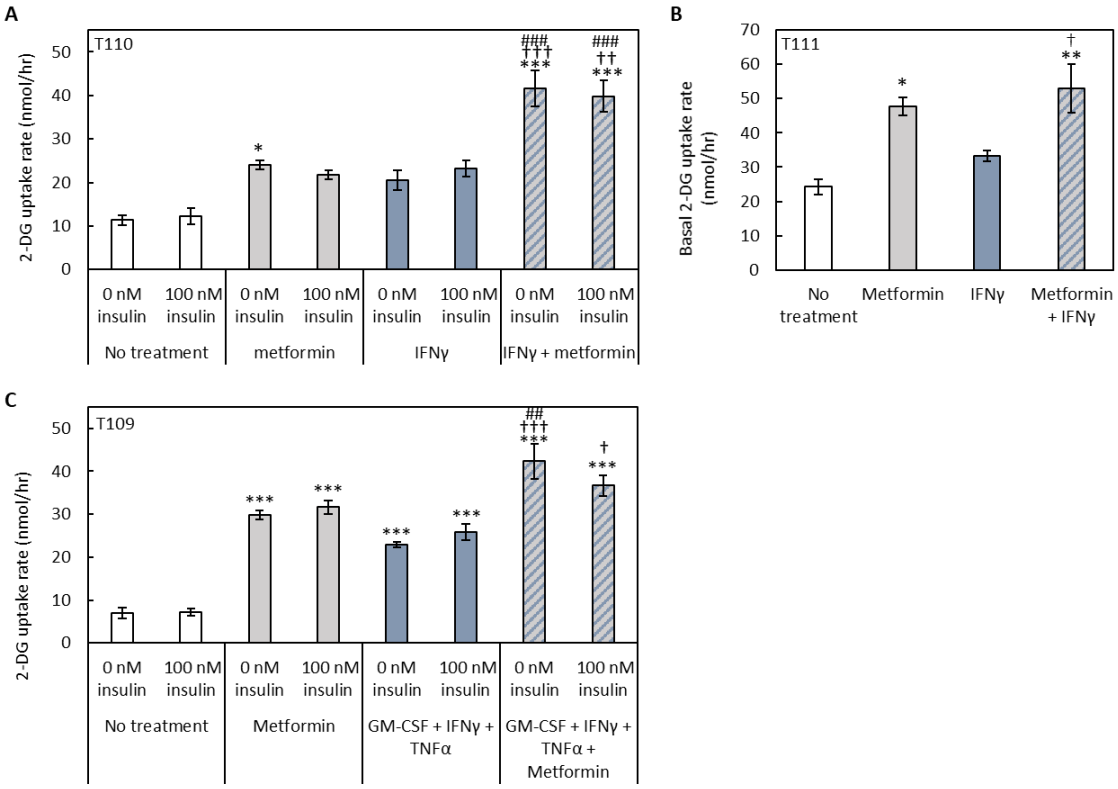

Figure 34. Effect of metformin on 2-DG uptake by inflamed myobundles. Myobundles without MDMs were either left untreated or treated with metformin only, inflammatory cytokines only, or with a combination of inflammatory cytokines and metformin. Cytokine-treated myobundles were cultured with 20 ng/mL IFNγ or 10 ng/mL GM-CSF + 20 ng/mL IFNγ + 40 ng/mL TNFα, as specified, for 72 hours prior to endpoint testing at 10 days post-differentiation, and metformin-treated myobundles were treated with 400 μM metformin for 18 hours prior to endpoint testing. A) Basal and insulin-stimulated 2-DG uptake by myobundles treated with metformin only, IFNγ only, or a combination of the two. Myobundles formed using the T110 donor, n=4 myobundles per condition. B) Basal 2-DG uptake by myobundles treated with metformin only, IFNγ only, or a combination of the two. Myobundles formed using the T111 donor, n=3 myobundles per condition. C) Basal and insulin-stimulated 2-DG uptake by myobundles treated with metformin only, GM-CSF + IFNγ + TNFα only, or a combination of cytokine and metformin. Myobundles formed using the T109 donor, n=4 myobundles per condition. ***p<0.001, **p<0.01, *p<0.05 denotes significance compared to the comparable insulin condition in the no treatment group, # denotes significance compared to the metformin only group, † denotes significance compared to the cytokine treatment only group. Data shown as mean ± S.E.M.

4.4 Discussion

The objective of this work was to create an *in vitro* human cell based three-dimensional model of skeletal muscle inflammation capable of providing a platform for improved insights into the consequences of and therapeutic options for inflammation in skeletal muscle. We incorporated human monocyte-derived macrophages into the myobundle system and found that although polarized MDMs contributed to significantly increased TNFα, IL-12p70, and IL-23 concentrations, the myobundle itself responded to polarization cytokines with a significant increase in a wide array of cytokines, and the MDMs did not impact the myobundle contractile function in the polarized state. Pro-inflammatory cytokine treatment of the myobundles alone elicited contractile dysfunction, cytokine production, and altered glucose metabolism.

To create a tissue-engineered skeletal muscle model of inflammation, we first investigated the incorporation of monocyte-derived macrophages into the system. Macrophages are involved in the acute inflammation associated with injury repair and myofiber regeneration, but they also play an important role in chronic inflammation associated with disease. During acute injury response in skeletal muscle, pro-inflammatory macrophages are recruited to the site of injury, where they undergo a switch to an anti-inflammatory phenotype and begin to assist with fiber regeneration[85]. In the chronic low-grade inflammatory state associated with obesity and insulin resistance, pro-inflammatory macrophage infiltration into adipose tissue is well-

documented[92,304]. The role of skeletal muscle in perpetuating systemic inflammation has been less well-characterized, but in obese individuals there is also evidence of increased macrophage presence in skeletal muscle[100,305].

In order to incorporate monocyte-derived macrophages into the myobundle system, we first identified ideal differentiation conditions to produce MDMs most suited to a pro-inflammatory role. We found that the use of GM-CSF during differentiation decreased expression of the M2 marker CD163, positioning the MDMs in a less M2-like phenotype. This is in agreement with studies that demonstrate differentiation with M-CSF results in macrophages with an M2-like phenotype, while GM-CSF results in a more pro-inflammatory M1-like phenotype, both before and after polarization[301-303]. The GM-CSF-derived MDMs exhibited a robust increase in CD80 expression in response to classical pro-inflammatory polarization cytokines LPS and IFNγ. While less commonly used than LPS, TNFα has been used in conjunction with IFNγ to polarize macrophages to an M1 phenotype *in vitro*[306]. We found that polarization with TNFα and IFNγ to mimic sterile inflammation did increase CD80 expression, but the response was not as robust as with LPS.

Upon combining MDMs with myobundles, we discovered that macrophages contributed to increased contractile force production in the un-polarized state in multiple experiments, and even had a protective effect against pro-inflammatory treatments in two experiments. In the un-activated state, macrophages have been shown

to enhance the proliferation and survival of satellite cells[307,308] as well as promote differentiation and fusion[85]. MDM myobundles that were tested at 10 days post-differentiation demonstrated a greater effect of macrophages in the un-polarized state than did those tested at 7 days post-differentiation, suggesting that macrophages may promote force most effectively during later stages of myofiber differentiation. The protective impact of macrophages on contractile force production following treatment with inflammatory cytokines that we occasionally observed may be due to the macrophages switching to an anti-inflammatory phenotype and promoting myofiber regeneration after pro-inflammatory cytokine exposure[85]. Interestingly, in one donor, MDMs contributed to a significant increase in the concentrations of IL-7, IL-10, and IL-1α in the un-polarized state between day 4 and day 6. The production of IL-10, an anti-inflammatory cytokine[309], in conjunction with pro-inflammatory cytokines, points to an M2b-like macrophage phenotype[310], which is involved in dampening inflammation responses[311]. This supports the idea that the MDMs could be engaging in anti-inflammatory processes while in the myobundles.

M1 macrophages produce high levels of IL-12, IL-23, IL-1β, and TNFα[309,312]. Because of this, we hypothesized that polarized myobundles with MDMs incorporated would exhibit lower forces than those without MDMs. However, in polarized myobundles, MDMs resulted in decreased contractile force in only one of five experiments. Measuring the cytokine release from myobundles exposed to LPS and

IFNγ revealed that while MDMs did indeed contribute significantly to the production of TNFα, IL-12p70, and IL-23 in the polarized state, the myobundles themselves are capable of secreting pro-inflammatory cytokines including IL-1β, IL-1α, and IL-6 in response to pro-inflammatory stimuli. IL-6 production was especially robust, which is in line with its classification as a myokine due to the known ability of skeletal muscle to produce substantial levels of IL-6, especially after exercise[313]. Studies have shown that skeletal muscle is capable of producing hundreds of peptides in addition to IL-6, including IL-4, IL-5, IL-7, and IL-15[102]. While the majority of these studies have been in the context of exercise-induced cytokine production, cultured skeletal muscle cells have also been shown to release IL-6 and IL-1 in response to TNFα and LPS treatment[314,315] and to express IL-1α and IL-6 constitutively and IL-1β and TNFα in response to IFNγ and TNFα treatment[316]. Overall, this powerful response by the myobundles likely explains the lack of effect of MDMs on contractile force production following MDM myobundle polarization, because the cytokines secreted by the myobundles themselves are overwhelming the macrophage-specific response.

The varied results of polarization of myobundles containing MDMs indicate that donor to donor variability in MDM phenotype has a significant role in macrophage-specific responses to polarization cytokines, and MDMs should not be assumed to have identical pre-polarization phenotypes or even comparable polarization potential. Additionally, while polarized macrophages do produce a number of specific cytokines,

treatment of myobundles with pro-inflammatory factors alone is sufficient to initiate a cascade of cytokine secretion within the myobundle itself that is associated with contractile dysfunction. With these findings in mind, we moved forward with characterization of the inflammation model using cytokine treatment alone to mimic the presence of pro-inflammatory macrophages. In a mouse model of obesity, macrophages have been shown to switch to an M1 phenotype, at which point they produce IFNγ and TNFα [317,318]. To better mimic the cytokine profile in an obesity-associated state of inflammation, we incorporated TNFα into the cytokine treatment instead of LPS.

Skeletal muscle atrophy is a well-documented characteristic of inflammatory diseases, including obesity-associated inflammation[117,299,319]. We found that treatment of myobundles with GM-CSF and IFNγ and TNFα induced a significant decrease in twitch and tetanus contractile force production. Studies have shown that IFNγ at a concentration of 5 ng/mL can inhibit myogenin expression in myoblasts[320], thereby disrupting myofiber formation[321]. However, this is not the likely mechanism by which inflammatory cytokines impacted myobundle force, as the cytokines were not added until 7 days post-differentiation, at which point the myobundles already exhibit substantial myofiber formation. TNFα has been shown to directly contribute to skeletal muscle atrophy *in vitro* via increased protein degradation[322]. Here, we show that cytokine-treated myobundles exhibited sarcomeric degradation and decreased fiber

diameter, which, along with the impaired force production, indicate inflammation-mediated atrophy.

In general obesity and metabolic syndrome, pro-inflammatory cytokines IL-4, IL-5, IL-6, IL-8, IL-10, IL-12, IL-13, GM-CSF, IFNγ, and TNFα are present at elevated serum levels than in non-obese individuals[93-97]. IL-1β is an additional pro-inflammatory cytokine that has been identified as a central player in the progression of type 2 diabetes[323]. Of these cytokines, we added GM-CSF, IFNγ, and TNFα exogenously and measured IL-6, IL-8, IL-10, IL-12, and IL-1β, all of which were elevated in the cytokine-treated myobundles. Thus, the cytokine profile of GM-CSF, IFNγ, and TNFα-treated myobundles mimics that of obesity-associated inflammation *in vivo*. These results also support the idea that although adipose tissue has been the primary focus of pro-inflammatory cytokine production in obesity[324], endogenous cytokine secretion in skeletal muscle may play a significant role in the propagation of inflammatory signals.

Inflammation is implicated in changes in the regulation of glucose metabolism in skeletal muscle. In the context of obesity, inflammation and the development of insulin resistance are closely related[325,326], and in obese individuals there is a shift from oxidative to glycolytic muscle fiber types[270,271]. This shift to a more glycolytic metabolic phenotype in muscle is also present in the inflammation-associated diseases chronic obstructive pulmonary disorder (COPD)[327,328] and rheumatoid arthritis (RA)[329]. Studies have found that treatment of myotubes *in vitro* with both IFNγ (using L6 myotubes) and TNFα

(using C2C12 and human myotubes) stimulate increased glucose uptake and increased GLUT1 expression[328,330,331]. We found that inflammatory cytokine-treated myobundles exhibited a significantly increased rate of 2-DG uptake which denotes increased glucose usage and could be indicative of a more glycolytic phenotype. With further investigation, this model could contribute to elucidating the role of inflammation in the obesity-induced shift to glycolytic metabolism in skeletal muscle.

Finally, we treated inflammatory cytokine-treated myobundles with metformin and found that its effects on contractile function and 2-DG uptake of healthy myobundles were maintained in the inflamed state. Of note, there is evidence that metformin has anti-inflammatory properties in addition to its primary anti-hyperglycemic function[332]. We did not observe recovery of contractile function in inflamed myobundles treated with metformin, which supports the hypothesis that metformin's anti-inflammatory properties may be primarily due to an ability to influence macrophage polarization toward an M2 phenotype[333,334] rather than a direct effect on skeletal muscle. These results are in agreement with findings that metformin does not protect C2C12 cells from IFNγ and TNFα-induced atrophy[335]. To our knowledge, this is the first time that the effects of metformin in the context of skeletal muscle inflammation have been tested in an *in vitro* human model.

There are some limitations of the model. Because tissue-engineered skeletal muscle is only viable in culture for a limited time, it is challenging to truly recapitulate a

chronic inflammatory state. As it is, this model may be a better representation of acute high-grade inflammation, similar to drug-induced myopathies, than a model of low-level chronic inflammation. However, acute inflammation may still predict responses in chronic inflammation[336]. Future work could involve lowering cytokine concentrations and extending the duration of exposure to achieve a more chronic inflammatory state.

4.5 Conclusions

Here, we show a tissue-engineered human skeletal muscle model of inflammation that recapitulates several key aspects of obesity-related inflammation *in vivo*. Specifically, the inflammatory cytokine-treated myobundles demonstrate impaired contractile force production indicative of atrophy, increased levels of pro-inflammatory cytokine secretion, and significantly greater basal glucose usage accompanied by a shift towards decreased insulin responsiveness. Robust cytokine secretion by the myobundles in response to a pro-inflammatory challenge indicates a potentially central role of endogenous cytokine production in inflammatory disease-related skeletal muscle dysfunction. This human tissue-based model exhibits inflammation-associated dysfunction but remains capable of a functional response to the diabetes therapeutic metformin, indicating its suitability for testing drug efficacy.

4.6 Chapter acknowledgements

The studies shown in this chapter were done in collaboration with Catherine Oliver, who performed the experiments done using the T103 donor shown in Figure 26,

Figure 27, and Figure 28, and contributed to data shown in Table 5 and Table 8. These studies were also done in collaboration with Anandita Ananthakumar, who performed the experiments done using the T110 and T111 donors shown in Figure 33. We would like to thank Varun Prasad for skeletal muscle and cord blood isolations. This work was funded by the NIH under grant number UG3TR0002142 and the Common Fund for the Microphysiological Systems Initiative.

5. Conclusions

5.1 Key findings

In aim 1, we found that tissue-engineered myobundles exhibit insulin sensitivity similar to that of *in vivo* skeletal muscle, but insulin responsiveness is substantially lower, in accordance with other *in vitro* studies. Additionally, treatment with the diabetes therapeutic metformin stimulated a robust increase in basal glucose uptake, indicating the ability of myobundles to respond appropriately to a well-characterized drug. Finally, treatment with the HDAC inhibitor 4-PBA enhanced myobundle contractile function and insulin responsiveness, indicating that improved myobundle maturation could improve function. In aim 2, we showed that altering myobundle culture conditions to provide more physiologic nutrient availability was sufficient to metabolically reprogram the myobundles to a less glycolytic state as evidenced by changes in glucose uptake, lactate production, surrogate markers for oxidative and glycolytic metabolism, and fatigue resistance. In aim 3, we exposed myobundles to pro-inflammatory cytokines and found that the inflamed myobundles recapitulated key aspects of inflammation-mediated *in vivo* skeletal muscle dysfunction, including impaired contractile force production, increased secretion of an array of pro-inflammatory cytokines, and increased basal glucose uptake. We determined that metformin does not rescue the contractile dysfunction caused by cytokine exposure, but is able to elicit a robust increase in glucose uptake in the inflamed myobundles. Overall,

this work validates the suitability of a tissue-engineered skeletal muscle model for detecting metabolic perturbations mediated by drug treatment, nutrient availability, and inflammatory conditions.

5.2 Dissertation summary

Engineered muscle offers a promising approach for developing a human *in vitro* model of healthy and diseased muscle for drug development and testing, providing a platform that better models the three-dimensional structure of native skeletal muscle than does monolayer culture and which is useful for drug toxicity testing, using functional measures such as force production, oxygen consumption, calcium handling, and metabolite production to monitor the tissue's health. In order to study the mechanisms of induction and progression of metabolic diseases or to identify promising drug targets for such diseases and evaluate their safety and efficacy, the metabolic function of the engineered muscle must also be characterized. To this end, in chapter 2 we validated the use of a non-radioactive 2-deoxyglucose-based assay to approximate glucose uptake in a tissue engineered skeletal muscle myobundle system, and found that treatment of myobundles with 400 μM metformin increased basal 2-DG uptake 1.7-fold. Additionally, treatment with metformin caused a significant drop in twitch and tetanus contractile force and decreased fatigue resistance, indicating possible toxicity at this concentration due to metformin's mechanism of action as a complex I disruptor. In the myobundle system, insulin is capable of stimulating a 50% increase in 2-DG uptake

with a compiled EC_{50} of 0.268 ± 0.03 nM. Treatment with the HDAC inhibitor 4-phenylbutyrate (4-PBA) increased the magnitude of insulin response from a 1.2-fold to a 1.4-fold increase over basal 2-DG uptake. This increase in the insulin response corresponded with increased fatigue resistance and increased twitch half-relaxation time. Taken together, this study demonstrates recapitulation of *in vivo* insulin sensitivity by tissue engineered skeletal muscle and validates the model's functionality in exhibiting drug-mediated perturbations in contractile function and glucose metabolism.

In order to examine the effects of disease progression or drug treatment on skeletal muscle metabolism, *in vitro* models of healthy skeletal muscle must accurately reflect the metabolism of native muscle. However, skeletal muscle cultured *in vitro* is exposed to artificially high levels of nutrients meant to promote cell growth, and it exhibits altered metabolism, with a higher basal glucose uptake rate and dampened insulin response associated with skewed levels of GLUT1 and GLUT4 glucose transporters. To address this dysfunction, in chapter 3 we used a human three-dimensional engineered skeletal muscle tissue and identified formation and culture conditions that promote a more physiologically-relevant environment of nutrient availability using a lower amino acid and growth factor (LAAGFR) content, as well as accessibility to fatty acids. LAAGFR conditions decreased basal 2-deoxyglucose (2-DG) uptake, which appears to be primarily mediated through decreased GLUT1 expression, while maintaining myobundle cellularity and contractile function. The decrease in basal

2-DG uptake is accompanied by decreased L-lactate production, and an increased ratio of oxygen consumption to extracellular acidification, indicating a departure from reliance on glycolysis in the LAAGFR conditions. Additionally, LAAGFR conditions promote a contractile phenotype that includes increased fatigue resistance. These findings represent a promising approach to improve the physiological relevance of tissue engineered skeletal muscle by regulating nutrient availability.

Inflammation is closely linked with skeletal muscle dysfunction in obesity and type 2 diabetes. An *in vitro* model of skeletal muscle inflammation can provide a platform to obtain mechanistic insights into the role of inflammation in disease pathogenesis and to test the efficacy of potential therapeutics. To create a skeletal muscle model of inflammation *in vitro*, in chapter 4 we first demonstrated the capacity of monocyte-derived macrophages (MDMs) to be polarized to a pro-inflammatory phenotype, then incorporated the MDMs into tissue-engineered skeletal muscle myobundles. Upon polarization of MDM myobundles with LPS and IFNγ, the MDMs minimally impacted contractile function and cytokine secretion. Myobundles alone were capable of responding to LPS and IFNγ treatment with a marked increase in cytokine production. Upon exposing myobundles without MDMs to the sterile inflammatory cytokines GM-CSF, IFNγ, and TNFα, they recapitulated several aspects of chronic inflammation *in vivo*, including impaired contractile force production, increased production of the cytokines IL-8, IL-1α, IL-1β, IL-10, IL-12, and IL-6, and increased

glucose usage coupled with impaired insulin responsiveness. GM-CSF and IFNγ treatment alone elicited these responses as well, but the addition of TNFα further exacerbated the contractile dysfunction and the cytokine production. The cytokine-treated myobundles responded to metformin treatment with a significant increase in basal 2-DG uptake, indicating their suitability for examining therapeutic efficacy. Thus, human tissue-engineered myobundles treated with the pro-inflammatory cytokines GM-CSF, IFNγ, and TNFα can serve as an *in vitro* model of inflamed skeletal muscle.

5.3 Future directions

In chapter 2, it was observed that metformin treatment impaired contractile force production. Further work could be done using lower metformin concentrations nearer to the expected therapeutic plasma concentrations to determine if this impaired force production is an artifact of a high metformin concentration, or if contractile dysfunction with metformin occurs at lower concentrations as well. Studies are currently underway to examine the effect of the HDAC inhibitor treatment on MHC isoforms and glucose transporter expression, but further experiments could be carried out to determine if the HDAC inhibitor applied at a different point during differentiation, such as during early fusion, followed by removal of the inhibitor, could induce sustained improvements in myobundle function.

In chapter 3, we determined that LAAGFR conditions promoted a more oxidative metabolic phenotype with increased fatigue resistance. Because similar effects

are seen in the skeletal muscle of calorie-restricted individuals, it would be useful to examine whether mitochondrial biogenesis is central to the effect of LAAGFR conditions in the myobundles, as it is relevant in calorie restriction. Because LAAGFR conditions promote a more oxidative metabolism, it is possible that mitochondrial toxicity will be more pronounced in those conditions due to increased reliance on oxidative metabolism for energy production. Future studies could examine the functional response of myobundles cultured in LAAGFR or baseline conditions to a drug with known mitochondrial toxicity such as rotenone to determine if there are any differences in sensitivity. The use of physiologically-relevant culture conditions may allow for more accurate predictions of drug toxicity.

Future work for chapter 4 could include measuring the gene expression of MHC isoforms in healthy and inflamed myobundles to determine if there is a shift in fiber type enrichment mimicking the switch to type II fibers seen in *in vivo* chronic inflammation. Further measures of glycolytic metabolism such as those used in chapter 3 could be obtained from the inflammation model to confirm the connection between increased glucose uptake and increased glycolytic reliance. Additionally, cytokine-treated myobundles could be treated with an anti-inflammatory salicylate such as aspirin, which inhibits NF-κB signaling[337], or with an anti-oxidant to attenuate potential cytokine-induced oxidative stress. Finally, the inflammation model as laid out here is comparable to inflammation in the context of high nutrient availability. As calorie

restriction has been linked to the mitigation of sarcopenia[338], future studies could examine the effect of inflammatory cytokine exposure on myobundles cultured in LAAGFR conditions to determine if this state of amino acid and growth factor restriction could attenuate inflammatory dysfunction. These additional studies would contribute to the body of knowledge about the mechanisms linking inflammation and fuel availability to skeletal muscle dysfunction.

Appendix A: Protocol for myogenic cell isolation from surgical waste sample

Before isolation:

Prepare matrigel-coated flasks (5 or 6 T-175 flasks for large isolation)

1. Prepare sterile PBS + anti/anti (2X)
2. Aliquot 30 mL of the sterile PBS+AA into a 50 mL falcon tube and place in the refrigerator to be chilled before sample pickup.
3. When ready, place the falcon tube with the ice-cold PBS+AA into a Styrofoam box filled with ice and into a normal cardboard box.
4. Go to the operating room to pick up the sample.
5. Upon return, wash the sample 3x with PBS+AA – aspirate off excess and add more to the muscle, let it sit for 5 minutes per wash.
6. In a plastic petri dish, mince the tissue.
    a. Anything white or black should be removed.
    b. Pull the fibers apart - more of a pulling motion than a chopping motion. If it doesn't pull apart easily, it is probably not muscle tissue.
7. With the scale tared at the weight of the petri dish, weigh the tissue
8. Split the tissue into groups of 0.5-1g each
9. Transfer the tissue in groups of 0.5 g -1 g to individual falcon tubes containing PBS + AA to wash.

    a. Wash the minced tissue 3-5x – each time, aspirate off excess fluid (and any floating fat) and then forcefully resuspend, then allow the tissue to settle to the bottom of the tube before repeating.

10. Have pre-warmed 0.05% trypsin ready, put 20 mL of trypsin into each tube containing tissue– put in the water bath and shake periodically for 30 min.
11. Deactivate with the same amount of hSkM media (warmed)
12. Allow the tissue to settle and aspirate off trypsin mixture
13. Resuspend in 20 mL media per flask
14. Plate the muscle on uncoated flasks, keeping the muscle tissue in the tip of the pipette while transferring.
15. After two hours, transfer the muscle tissue and media to a matrigel coated flask.
16. Don't move for 2 days
17. Change media
    a. Try to leave as much tissue in the flask as possible. Tilt the flask, allow the tissue to settle in a corner and use a serological pipet to remove the media (as opposed to aspirating it). This will prevent accidental aspiration of the tissue.
18. Don't move for another 3 days
19. Change media

20. At this point, you will change media every other day until outgrowth cells are confluent enough that they need to be passaged.
    a. Cells will grow in patches. Try to allow as many cells as possible to grow out without allowing them to start differentiating before passaging.
21. When cells are ready to passage, coat enough flasks with Matrigel to passage 1:2 (from one flask into two).
    a. Be sure to wash flasks several times with PBS, especially if there is a large amount of tissue, to thoroughly remove residual media.
    b. Trypsinize cells with 0.05% trypsin.
    c. At this stage, any remaining tissue should be left behind in the old flask. Try to remove the cell solution without removing tissue.
22. After cells have been passaged, continue to change media every other day. Once again, try to allow the cells to proliferate as much as possible without beginning to differentiate. This can be a tricky balance. We tend to err on the side of greater confluence at the cost of some differentiation.
23. Once cells are fully confluent, freeze them down. When these cells are thawed, they will be P2. Freeze cells down in a freezing media containing 90% growth media and 10% DMSO, at 1-2 million cells per mL.

Sample timeline for <u>large</u> tissue sample:

Isolated: Day 0

Fed: Day 2, Day 5 (cell outgrowth observed approx. Day 3)

Passaged: Day 7 (from 5 flasks into 10 flasks)

Fed: Day 9, Day 11

Frozen: Day 13/14

Appendix B: Protocol for standard size myobundle formation

Materials list:

- PDMS: Sylgard 184 Silicone Elastomer Kit, Dow Corning
- Pins : Minutien Pins, Fisher Scientific, NC9681411
- Frames material: PBN II 4.0 fabric from Cerex Advanced Fabrics, Inc.
- Pluronic solution: Pluronic F-127, Sigma-Aldrich, P2443. Create 0.2% stock by dissolving 2 g of Pluronic powder in 1 L of water. Sterile filter. Store at 4 C.
- Matrigel: Corning, 354234 – 10 mL. Aliquot and store at -20 C.
- Fibrinogen: Fibrinogen from bovine plasma, Sigma-Aldrich, F8630. Store at -20 C. Fibrinogen solution must be made fresh each time.
- Thrombin: Sigma Aldrich, T7513 – 50 UN. Thrombin should be resuspended in 0.1% BSA + PBS at a concentration of 50 U/mL. Aliquot and store at -20 C.

Making PDMS molds from Teflon masters

- Place Teflon masters in a petri dish
- Mix PDMS at a ratio of 10 parts base elastomer : 1 part curing agent
- Stir the mixture with a pipette tip
- Place mixture in desiccator to remove air bubbles (about 30 min)
- Pour PDMS mixture over Teflon masters
- Remove any air bubbles that may have formed while pouring the PDMS, either using pipette tip or by placing in desiccator again

- Place in oven to cure
- Break petri dish to remove the PDMS block
- Carefully remove the Teflon masters
- Cut around the outside of the mold area using a razor blade to create a small square containing the bundle reservoir area. It is important to retain the flat area surrounding the bundle reservoir, as this is where the frame will be pinned.

Early Prep

Sterilizing molds

- After removing bundles from the molds, place molds in a bottle containing 70% ethanol.
- Sonicate molds for 45 minutes in ethanol
- Wash with PBS overnight
- Autoclave molds for 20 minutes on gravity cycle in sealable autoclave pouches (typically 12 molds per pouch)

Sterilizing frames

- Put pins in frames
    - Place pin through a corner of the frame
- Soak in ethanol for at least 1 hour, remove ethanol
- UV overnight

Day-of or day-before prep

Coat molds with 0.2% pluronic solution

- Place molds into 12-well plate using sterile forceps
- Add 200 µL of 0.2% pluronic solution to each mold, being sure that the entire indented area is filled with the solution
- Incubate at room temp for at least 30 minutes
- Aspirate off pluronics solution.
- Add sterile water to the molds and let sit for 30 minutes.
- Aspirate off water and ensure that molds are dry.

Pin frames in molds

- Ensure that frames are dry.
- Pin the frames into the molds using sterile forceps.

The above prep can all be done before the day you plan to make bundles.

Day-of prep

Place Matrigel in the fridge to thaw. Each aliquot should be sufficient for 12 bundles.

Place thrombin in the fridge to thaw. Each aliquot should be sufficient for 12 bundles.

Make a solution of 20 mg/mL fibrinogen

- Weigh anywhere from 15-30 mg fibrinogen, depending on how many bundles you will be making.

- Take note of the mass of fibrinogen, bring the tube into the hood, and resuspend with the correct amount of warmed muscle growth media to produce a 20 mg/mL solution.
- The tube may need to be placed in the water bath to help the fibrinogen go into solution.
- After the fibrinogen has gone into solution, sterile filter the fibrinogen into a 15 mL falcon tube or sterile microcentrifuge tube using a syringe and syringe filter.
- Keep the filtered fibrinogen solution on ice.

Passaging prep

- Warm up muscle growth media in water bath - enough for neutralizing trypsin and plating if you will be plating your excess cells.
- Warm 0.025% trypsin to room temp (8 mL per T175)

Have on ice

- Filtered fibrinogen (see above)
- Matrigel for bundles
- Thrombin
- Muscle growth media (usually about 3 mL is fine)

Making bundles

1. Passage cells as you normally would – wash with PBS, add 0.025% trypsin for about 3 minutes, check detachment under microscope, neutralize with equal volume growth media.
2. Count cells.
3. Refer to the bundle reagents spreadsheet to determine the number of cells you will need.
4. Divide the cells based on the number of bundles you feel comfortable making at a time. I have found that 4 bundles is a good number. So if you want to make 16 bundles total, prepare 4 tubes of cell solution that each contain enough cells for 4 bundles (3.3 M cells).
5. If planning on replating, place extra cells in incubator in the falcon tube.
6. Centrifuge cells intended for bundles at 1000 rpm for 5 min.
7. After centrifuging, quickly aspirate excess media and resuspend the pellet in the appropriate amount of cold growth media (according to the bundle reagents spreadsheet). Transfer to 600 µL microcentrifuge tube and place on ice.
8. Prepare second set of tubes containing the appropriate volumes of fibrinogen, matrigel, and growth media.
9. For each pair of tubes:
    a. First, add thrombin to the tube containing the cell solution.

These next steps must be performed quickly – this is when the gel will start to form as thrombin cleaves fibrinogen when the contents of the two tubes are mixed.

b. Next, add the entire contents of the cell solution / thrombin tube to the corresponding tube containing the matrigel/growth media/fibrinogen. Keep the tube on ice.

c. Pipette up and down about 10 times to mix.

d. Add 50 µL of the bundle solution to each mold, pipetting the majority of the volume into the center of the mold, and using the remaining solution to bring the middle volume into contact with the sides of the frames. You should aim for a dogbone shape of bundle solution.

10. When you have finished making the bundles, place them in the incubator for 25-30 minutes. Check that gelation has occurred.
11. After the 25-30 minute incubation, add 3 mL of warm growth media + ACA to each well.

    Don't forget to spin down and replate your extra cells.

Bundle feeding

- Days 1-3 : feed bundles daily with growth media + ACA media
- Day 4: Remove bundles and frames from the molds and switch to differentiation media + ACA. Continue to feed bundles every other day.

Removing bundles from molds

- Prepare differentiation media and add 2 mL to each well in a 12-well plate, filling the same number of wells as bundles you have.
- Using two sets of sterile forceps, use one set to grip the pin and pull the pin, along with the frame with attached bundle out of the mold, which you will hold down with the other set of forceps. Then remove the pin from the frame and place the pin to the side for later disposal in the biohazard sharps bin.
- Transfer the bundle to the new 12-well plate containing differentiation media.
- When finished, place the empty molds into a bottle containing 70% ethanol to begin the sterilization process.

Appendix C: Custom low amino acid base media formulation

Table 12. Custom low amino acid (LAA) base media formulation compared to DMEM and α-MEM. Parentheses represent components that are not in the custom base media but are supplemented at the given concentration.

Components	DMEM mM	α-MEM mM	LAA mM
Amino Acids			
Glycine	0.4000	0.6667	0.2800
L-Alanine		0.2809	0.8800
L-Arginine hydrochloride	0.3981	0.6018	0.1050
L-Asparagine-H2O		0.3333	0.2200
L-Aspartic acid		0.2256	0.0100
L-Cysteine hydrochloride-H2O		0.5682	0.0600
L-Cystine 2HCl	0.2013	0.0990	0.1150
L-Glutamic Acid		0.5102	0.1550
L-Glutamine	4.0000	2.0000	(2.0000)
L-Histidine hydrochloride-H2O	0.2000	0.2000	0.1950
L-Isoleucine	0.8015	0.4000	0.1700
L-Leucine	0.8015	0.3969	0.2900
L-Lysine hydrochloride	0.7978	0.3989	0.4050
L-Methionine	0.2013	0.1007	0.0550
L-Phenylalanine	0.4000	0.1939	0.1250
L-Proline		0.3478	0.5950
L-Serine	0.4000	0.2381	0.2400
L-Threonine	0.7983	0.4034	0.4050
L-Tryptophan	0.0784	0.0490	0.1200
L-Tyrosine disodium salt	0.3985	0.1985	0.1350
L-Valine	0.8034	0.3932	0.5400
Vitamins			
Ascorbic Acid		0.2841	
Biotin		0.0004	0.0004
Choline chloride	0.0286	0.0071	0.0071
D-Calcium pantothenate	0.0084	0.0021	0.0021
Folic Acid	0.0091	0.0023	0.0023
Niacinamide	0.0328	0.0082	0.0082
Pyridoxal hydrochloride	0.0196	0.0049	0.0049

Riboflavin	0.0011	0.0003	0.0003
Thiamine hydrochloride	0.0119	0.0030	0.0030
Vitamin B12		0.0010	0.0010
i-Inositol	0.0400	0.0111	0.0111
Inorganic Salts			
Calcium Chloride (CaCl2) (anhyd.)	1.8018	1.8018	1.8000
Magnesium Sulfate (MgSO4) (anhyd.)	0.8139	0.8139	0.8140
Potassium Chloride (KCl)	5.3333	5.3333	5.3300
Sodium Bicarbonate (NaHCO3)	44.0476	26.1905	(26.900)
Sodium Chloride (NaCl)	110.344	117.2414	117.2400
Sodium Phosphate monobasic (NaH2PO4-H2O)	0.9058	1.0145	1.0100
Other Components			
D-Glucose (Dextrose)	5.5556	5.5556	(5.5556)
Lipoic Acid		0.0010	
Phenol Red	0.0399	0.0266	
Sodium Pyruvate	1.0000	1.0000	(0.2000)

Appendix D: Protocol for preparing custom low amino acid base media formulation

LAA powder media – 8.3 g/L

Sodium bicarbonate (Sigma 55761) – 2.2 g/L

Distilled water (Gibco 15230) – 1 L

➔ pH to 7.2

➔ Sterile filter into 2 500 mL bottles

Reconstituting powder:

1. Put clean stir bar into 1 L of distilled water (Gibco)
2. Weigh out 2.2 g of sodium bicarbonate.
    a. Dump into water, wash the weigh boat with 1000 µL pipette
3. Get LAA powder from small fridge (lower righthand drawer)
4. Weigh out 8.3 g
    a. Dump into water, wash weigh boat
5. Shake bottle to mix
6. Set bottle on stir plate, turn on stirring to level 2 or 3. Make sure heat is off!!

pH to 7.2

7. To calibrate pH probe:
    a. Wash the probe with DI water, using a weigh boat to catch the water
    b. Put probe into the pink pH 4 solution
    c. Hit Calibrate

d. Hit Read

    i. Wait until the machine says it's stable

e. Wash probe with DI water

f. Put into pH 7 solution

g. Hit Read

h. When stable, done calibrating.

8. To pH the media:

    a. Make sure the media is fully mixed (let it mix for about 20 minutes) prior to pHing it.

    b. Put the probe in the media, press Read

        i. Will usually stabilize around 7.4-7.5 after a few minutes in the media.

    c. Add HCl to a pH of 7.2

        i. Approximately 1 mL takes it from 7.5 to 7.3, then approx. an additional 150 µL to 7.2

    d. Wash probe with water

    e. Put probe back in the electrode buffer solution.

9. Sterile filter the media and place in refrigerator.

Appendix E: LAAGFR and Baseline complete media formulations

Table 13. LAAGFR and Baseline complete media formulations

For LAAGFR:
Low amino acid differentiation media:
Low amino acid base media (custom, ThermoFisher Scientific)
2% horse serum (Hyclone)
25 µg/mL gentamicin (ThermoFisher Scientific)
0.125 µg/mL amphotericin B (ThermoFisher Scientific)
100 µM L-carnitine (Sigma-Aldrich)
0.05% BSA (ThermoFisher Scientific)
5.55 mM D-glucose (ThermoFisher Scientific)
0.2 mM sodium pyruvate (ThermoFisher Scientific)
2 mM glutamine (ThermoFisher Scientific)
2 mg/mL ACA (Sigma-Aldrich)
To the LAA media with supplements, add:
10 nM insulin (Sigma-Aldrich)
50 µM each of oleate and palmitate (Sigma-Aldrich)
For Baseline:
Baseline standard media
DMEM base media
2% horse serum
25 µg/mL gentamicin
0.125 µg/mL amphotericin B
2 mg/mL ACA
1.72 µM insulin

Appendix F: Protocol for 2-deoxyglucose uptake quantification assay

Modified version of the protocol described in Basic Protocol 3:

Yamamoto, N. *et al.* Measurement of glucose uptake in cultured cells. *Curr Protoc Pharmacol* **Chapter 12**, Unit 12 14 11-22, doi:10.1002/0471141755.ph1214s55 (2011).

Materials needed:

Material name	**Vendor**	**Catalog number**
DMEM, no glucose	ThermoFisher Scientific	11966025
Bovine Serum Albumin (BSA)	Sigma Aldrich	A9418
Sodium pyruvate (100 mM)	ThermoFisher Scientific	11360070
Insulin solution, human	Sigma Aldrich	I9278
2-deoxy-D-glucose	Sigma Aldrich	D6134
5X Extraction buffer	Abcam	ab193970
200 mM TEA buffer	Sigma Aldrich	T0449

Stocks of 500 mM 2-DG can be prepared by dissolving 2-DG in no glucose DMEM and storing at -20C.

Plan to perform 2-DG uptake experiment on day 7 after switching myobundles to differentiation media.

1. Switch bundle media to differentiation media without serum and without insulin for 18 hours prior to the start of uptake experiment. Bundles should be in 24-well plate for uptake.
    a. Plan to use at least 4 bundles per insulin condition and 3 bundles as negative controls for each treatment group.

Day-of uptake

2. Prepare uptake buffer: no glucose DMEM + 0.1% BSA + 0.2 mM sodium pyruvate.
3. Prepare insulin stimulation solutions: First make a solution of 1000 nM insulin in uptake buffer. Use this to prepare solutions of lower insulin concentration (100 nM, 10 nM) in uptake buffer for the insulin-stimulated condition.
4. Prepare 2-DG solutions: Add the appropriate amount of stock 500 mM 2-DG to each insulin concentration (including the 0 nM condition) to form a final concentration of 5 mM 2-DG.

Uptake protocol

1. Remove starvation media from myobundles. Add 1000 μL of uptake buffer to each well. Incubate in incubator on rocker for 10 minutes.
2. Remove uptake buffer wash from all wells except negative control wells. These remain in the uptake buffer for the duration of the experiment.
3. Add 1000 μL of uptake buffer with the appropriate insulin concentration.

4. Incubate in incubator on rocker for 30 minutes.
5. Remove insulin stimulation media from all non- negative control wells and add 1000 μL of the appropriate insulin concentration + 5 mM 2-DG.
6. Incubate with 2DG for 20 minutes.
7. Wash bundles 3 times with ice-cold PBS to remove exogenous 2DG.
8. Prepare 1X Abcam extraction buffer, diluting in water. Aliquot 100 μL per tube into 0.6 mL microcentrifuge tubes. Prepare one tube for each bundle.
9. Use forceps to remove bundle from the well, place onto a kimwipe to remove excess liquid, cut the bundle from the frame and transfer to a microcentrifuge tube containing lysis buffer.
10. Allow bundles to lyse overnight at 4C on a rocker.
11. The next day, place samples in -80C freezer until frozen.
12. Heat samples at 85C for 40 minutes.
13. Add 50 μL of 200 mM TEA to each sample.
14. Store samples in the -20C until ready to assay. It is best to assay within 1 week of sample collection.

See protocol for 2-DG detection assay below.

2DG detection assay

Modified version of the protocol described in Basic Protocol 3:

Yamamoto, N. *et al.* Measurement of glucose uptake in cultured cells. *Curr Protoc Pharmacol* **Chapter 12**, Unit 12 14 11-22, doi:10.1002/0471141755.ph1214s55 (2011).

Preparation of reagents

Reagent Name	Vendor	Catalog number	Stock concentration	Aliquot volume	Storage
TEA buffer	Sigma Aldrich	T0449	200 mM	NA	4C
7.5% BSA solution	ThermoFisher Scientific	15260037	0.4% in sterile water	500 μL	-20C
2-DG	Sigma Aldrich	D6134	500 mM in no glucose DMEM	110 μL	-20C
NADP	Sigma Aldrich	N0505	10 mM in sterile water	100 μL	-20C
Diaphorase	Sigma Aldrich	D5540	2 units/ 50 μL in 50 mM TEA buffer	50 μL	-20C*
Resazurin	Sigma Aldrich	R7017	2 mM in 50 mM TEA buffer	NA	4C*
DG6P	Santa Cruz Biotechnology	sc-220734	300 μM in 50 mM TEA buffer	100 μL	-20C
G6PDH	Sigma Aldrich	G8404		NA	4C

*protect from light

Note: Aliquots contain enough volume to prepare assay buffer for 50 wells of a 96-well plate.

Suggested starting quantities for reagents:

	Mass/ amount	**Volume of solvent**	**Solvent**	**Volume of aliquot**	**#aliquots**
0.4% BSA	800 µL 7.5% BSA	14.2 mL	Distilled water	500 µL	14
500 mM 2-DG	184.6 mg	2.25 mL	no glucose DMEM + 0.1% BSA*	100 µL	20
10 mM NADP	100 mg	13.07 mL	Distilled water	100 µL	130
Diaphorase	100 units	2.5 mL	50 mM TEA buffer	50 µL	50
2 mM Resazurin sodium salt	5 mg	10 mL	50 mM TEA buffer		none

TEA buffers:

- Prepare 200 mM TEA with 200 mM KCl. Dissolve 0.7455 g KCl in 50 mL of 200 mM TEA buffer stock.
    - Alternatively, purchase pre-made TEA buffer (Sigma, T0449)
- Prepare 50 mM TEA by diluting 200 mM TEA buffer with sterile distilled water. (10 mL 200 mM TEA buffer + 30 mL water)

Making DG6P standards:

- To make a 3 mM stock, add 12.52 mL of 50 mM TEA buffer to 10 mg DG6P. Make 11 aliquots of 1 mL of 3 mM stock.
- From 3 mM aliquot, make 300 µM stock aliquots by combining 50 µL of 3 mM stock with 450 µL of 50 mM TEA buffer. Make 250 µL aliquots.

- For each assay, thaw one 300 μM stock aliquot.

2-DG quantification assay protocol

1. Prepare DG6P standard curve:

Concentration (μM)	**volume 300 μM stock**	**volume 30 μM solution (μL)**	**volume 50 mM TEA buffer (μL)**
300	100		
30	50		450
15		50	50
7.5		25	75
3.75		12.5	87.5
1.875		6.25	93.75
0		0	100

2. Prepare assay buffer. For enough assay buffer for 50 wells in a 96-well plate, combine the following volume of reagents. Scale as needed for number of samples. Protect the assay buffer from light.
    a. 6.8 mL DI water
    b. 2.5 mL 200 mM TEA buffer + 200 mM KCl
    c. 500 μL 0.4% BSA
    d. 50 μL diaphorase (2 units)
    e. 100 μL 10 mM NADP
    f. 25 μL 2 mM resazurin
    g. 50 μL G6PDH
3. Allow samples to thaw.

4. Add 20 μL of standards to a black 96-well plate, in duplicate.
5. Add 20 μL of each sample to the well plate, in duplicate.
6. Add 200 μL of assay buffer to each well containing standards and sample.
7. Cover in foil, incubate in incubator at 37C for 1 hour.
8. Use a plate reader capable of fluorometric detection with excitation filters in the 530-570 nm range and an emission filter in the range of 590-620 nm.
    a. We use ex = 544 nm, em = 590 nm.
9. Subtract the average value of the negative control bundles from the sample readings. Use the slope of the standard curve to determine the concentration of 2DG6P in each sample. Total uptake can be calculated by multiplying the concentration of 2DG6P in the sample by the total volume of the lysed bundle (150 μL). Rate is calculated as nmol/hr.

Appendix G: Protocol for immunostaining myobundles

- Fix bundles overnight at 4C in 2% PFA
- Wash in PBS++ 3x for 5 minutes each.
- Making blocking buffer
    - Need 250 µL per bundle half for permeabilization/blocking, and 175 µL per bundle half x primary, secondary antibodies = 600 µL blocking per bundle half. 6 bundles halves
- Blocking buffer:
    - 10% goat serum
    - 3% BSA
    - 0.2% Triton (using 2% Triton stock)
    - Remainder PBS++
    - Vortex to mix to dissolve all BSA, before adding Triton (if vortex after adding Triton, it will foam up)
        - Filter
- Permeabilize and block bundles in 250 µL 0.2% Triton-X + 10% goat serum + 3% BSA on rocker **overnight at 4C**.
- Remove blocking solution,
- Dilute primary antibodies in the blocking solution, add 175 µL per bundle half, incubate on rocker at **4C for 24 hours**.

    - SAA (1:200)

- Wash with PBS++ 3x for 5 minutes each.
- Dilute secondary antibody 1:250 in blocking solution, Hoechst 1:1000 incubate on rocker at **4C overnight**
- Wash with PBS++ 3x for 5 minutes each.

Appendix H: Protocol for nuclei quantification of myobundles

For quantification of DNA/cellularity

** Hoechst is light sensitive and should be protected from light **

A.) Preparation of stock Hoechst dye

- Purchase 100 mg Hoechst 33258 from Sigma, cat # H1398
- http://www.lifetechnologies.com/order/catalog/product/H1398 $63.25 in Jan 2014
- Dilute 100 mg Hoechst into 50 mL water (DI or tissue culture grade) for 2 mg/ml stock solution. Vortex thoroughly until dissolved,
- Aliquot ~1.5 ml of stock Hoechst into 2 ml tubes and freeze. Thawed aliquots stable at 4°C for ~ 6 months.

B.) Preparation of TBS assay buffer, using one of the following two methods.

- Combine 50 ml of 10x TBS with 450 ml water. Add 0.146 g of EDTA and mix on stirring plate until dissolved. May take about 1 hour. *Assay buffer is 20 mM Tris, 136 mM NaCl, 1 mM EDTA, pH 7.4*
- Combine 5 mL of 10x TBS with 45 mL of DI water (Gibco). Add 100 μL of 0.5 M EDTA solution (03690 SIGMA-ALDRICH).

C.) To make standards, spin down 10 million myoblasts, resuspend in 1 mL PBS and transfer to a microcentrifuge tube. Spin down again and resuspend in 1 mL of ATL +

proteinase K. (900 µL ATL and 100 µL proteinase K) for a standard stock solution of 1 million cells / 100 µL of working lysis buffer. Lyse at 56°C, 3-4 hours.

- Vortex solution to resuspend pellet, as it may be too viscous to pipet up and down.
- Standards can be stored at room temperature after heated lysis.

D.) Lysis of myobundles

- Wash bundle 3x 5 minutes in PBS.
- Cut bundle in half, then remove the halves from the frame using a scalpel and forceps. (For the small bundles for 96-well plate, place entire bundle + frame in the lysis solution.)
- Lyse each bundle half in 100 µL of working ATL buffer + proteinase K lysis solution to lyse sample at 56° C, 3-4 hours until bundle half is completely dissolved.
    - Prepare ATL buffer + proteinase K by combining 90 µL buffer ATL + 10 µL proteinase K (Qiagen), scaled up for number of bundles

<u>Day of running assay</u>

E.) Preparation of working Hoechst solutions

- Prepare a 1:1,000 dilution of Hoescht in the TBS assay buffer. Working concentration of Hoechst is 2 µg/ml (can be adjusted if needed).
    - Make enough for 90 µL x (number of standards + number of samples) x number of replicates for each standard/sample (usually 2)

F.) DNA measurement

Standards: Starting with 1M cells/100 µL stock solution:

- Make 0 standard: Combine 10 µL of proteinase K with 190 µL ATL buffer in a tube. This matches the 2-fold diluted lysis solution used for the samples.
- *Note: If running without other standards, you must still include the 0 standard for background subtraction
- For each standard: Makes 200 µL of standard total, enough for 2 duplicates of 90 µL with error.

Number of nuclei added to plate in 90 uL	**Volume ATL buffer**	**Volume 1M nuclei /100 µL stock**
28,125	193.76 µL	6.24 µL
56,250	187.52 µL	12.48 µL
112,500	175.04 µL	24.96 µL
281,250	137.6 µL	62.4 µL
500,000	88.89 µL	111.11 µL

Samples: Make a 2-fold dilution of each sample

- Add 100 µL of ATL buffer to each sample.

Adding to plate:

- Add 85 µL of standards/ samples per well, in duplicate to a black 96-well plate
- Add 85 µL of working Hoechst solution to each well containing standards/sample
- Incubate at room temperature for 15 minutes before going to plate reader
- Measure fluorescence with plate reader. Excitation peak is ~ 350 nm and emission peak ~ 460 nm. On Yuan lab plate reader, use Umbelliferone protocol (1s).

Data Analysis:

Number of nuclei in each well for standards are:

28,125 nuclei

56,250 nuclei

112,500 nuclei

281,250 nuclei

500,000 nuclei

- Make a standard curve using these values and the corresponding measured fluorescent intensities.
- Subtract the value for the 0 standard (ATL with proteinase K diluted 2-fold) from each *sample*.

- Use the slope of the standard curve to determine the number of nuclei in each sample well. Average the values from duplicates for each bundle half.
- For a two-fold dilution of samples, the total number of nuclei in the bundle half can be found by multiplying this number by (200/85) = 2.35.
- The total number of nuclei in a bundle can be found by adding the values for the two bundle halves.

Appendix I: Protocol for preparing myobundles for 96-well plate

Small bundles for Seahorse assay fabrication notes

- Coating molds – Use 20 µL of pluronics solution and proceed as normally – 30 minutes incubation followed by 30 minute incubation with 20 µL water.
- Coat molds in a 24-well plate for bundle fabrication. Culture using 1 mL of media in the 24 well plate during growth phase – hGM+ACA. Transition to 48-well plate with 500 µL media volume during differentiation.

Making bundles

- Each bundle will be 7.5 µL and contain 300,000 cells.
- Note: Use all the hGM allotted for vial 2 and vial 1 in vial 1 to resuspend the cells:

Number of Bundles	4				
Vial 1			**Vial 2**		
Cells	1.30	M	hGM	0	µL
hGM	18	µL	20/25 mg/ml Fibrinogen GFR/norm	6.6	µL
Thrombin	1.3	µL	Matrigel	6.6	µL

- After formation, allow bundles to gel for only 15 minutes instead of 30 minutes. Add 1 mL of hGM+ACA to each well.
- Differentiate in 500 µL differentiation media, change media every other day.

Appendix J: Protocol for Seahorse measurements using myobundles for 96-well plate

Prepared by Megan Kondash with help from Dora Kohnke, Tim Koves, adapted from Agilent literature

Materials needed

Seahorse XFe24 Islet Capture FluxPak (Agilent, 103518-100)

- Includes six sensor cartridges for Seahorse XFe24 machine, six islet capture cell culture plates, and a 500 ml bottle of XF calibrant
- Note that the sensor cartridges cannot be purchased separately and must be purchased as part of a Flux Pak

Seahorse XF DMEM Medium, pH 7.4 (Agilent, 103575-100)

200 mM L-Glutamine solution (Agilent, 103579-100)

100 mM Sodium Pyruvate solution (Agilent, 103578-100)

1.0 M Glucose solution (Agilent, 103577-100)

Day before assay: Hydrate the sensors

1. Open the Agilent Seahorse XFe24 Flux Assay Kit and remove the contents.
2. Place the Sensor Cartridge next to the Utility Plate
3. Fill each well of the Utility Plate with 1 mL of XF Calibrant
4. Place the Hydro Booster on top of the Utility Plate.

5. Lower the Sensor Cartridge through the openings on the Hydro Booster plate, into the Utility Plate, submerging the sensors in XF Calibrant.
6. Verify the XF Calibrant level is high enough to keep the sensors submerged.
7. Place in a non-CO2 37C incubator overnight. To prevent evaporation of the XF Calibrant, the incubator should be humidified.
8. The next day, remove the Hydro Booster from between the Sensor Cartridge and Utility Plate, also remove the Sensor Cartridge lid.
9. Load compounds into the ports as required. Place into the XFe24 analyzer for calibration.

WARNING: Remember to remove the Hydro Booster and Cartridge Lid prior to placing the Sensor Cartridge and Utility Plate in the XFe24 Analyzer.

<u>Day before assay: Prepare assay media</u>

Need 500 uL per well when not using it for drug resuspension: make 20 mL of complete assay media

Seahorse DMEM with 1 mM pyruvate, 2 mM glutamine, 10 mM glucose, and 0.2% horse serum (all but the horse serum are recommended by Agilent for the XF cell energy phenotype test, horse serum recommended by Tim Koves)

To 20 mL of XF DMEM, add

- 200 µL of 100 mM sodium pyruvate stock solution

- 200 µL of 200 mM glutamine stock solution
- 200 µL of 1 M glucose stock solution
- 40 µL of horse serum

Day of assay, immediately before using Seahorse:

Place bundles in islet capture plate (takes approx. 1 hr)

1. In cell culture hood, add 500 µL of assay media to each well in the islet capture plate.
2. To four of the wells, add frames with no bundles to serve as the blank wells.
3. Use sterile forceps to transfer bundles to remaining wells.
4. Pre-wet islet screens in a small petri dish containing assay media to avoid formation of air bubbles. Position the screens so that the ring is facing up.
5. Place the islet screens in the wells, including blank wells, using forceps with blunt tips.

Sample plate layout:

Blank	LAAGFR B1	LAAGFR B2	LAAGFR B3	LAAGFR B4	LAAGFR B5
LAAGFR B6	LAAGFR B7	LAAGFR B8	Blank	LAAGFR B9	LAAGFR B10
Baseline B1	Baseline B2	Blank	Baseline B3	Baseline B4	Baseline B5
Baseline B6	Baseline B7	Baseline B8	Baseline B9	Baseline B10	Blank

Running the assay:

Place the islet culture plate in the non-CO2 incubator for 1 hour prior to running the assay.

While the cell plate is incubating

Set up the Seahorse protocol

- Ensure heater is on, at 37C and XFe analyzer is connected to the computer
- Click Templates, select Blank template or a Agilent Seahorse Default template
    - Add, remove, modify group definitions to label the plate
        - Can add info for the injection strategy, pretreatment, cell type, assay media
            - Set pretreatment only: LAAGFR and Baseline
        - Under groups, click Add Group, and assign appropriate group definitions
    - Set up the plate map
        - Click the group on the Groups list on the left
        - Click the well on the plate map to assign that well to the selected group. You can select an area by dragging the cursor.
- Under Instrument protocol tab, set up protocol
    - 1 – Calibrate probes
    - 2- Equilibrate
    - 3- Loops 4 times
        - Mix for 3 minutes
        - Wait for 2 minutes

        - Measure for 3 minutes
- Assay summary general information is saved in the assay results file
- After customizing assay template, click Start Run to begin XFe assay.
    - Select a location to save the assay template file. The assay results file will be saved in the same location following assay completion.
    - After selecting a save location, the tray door on the analyzer will open. Place the Sensor Cartridge (hydrated) along with the Utility Plate onto the tray. Ensure the Cartridge fits properly on the Utility plate, the lid is removed from the Cartridge, and the direction of the Cartridge is in the proper orientation. When facing the machine with the tray pointing towards you, should be able to read the numbers/letters on the plate.
    - After loading, press I'm Ready to initiate calibration.
        - Time to complete calibration is about 10-20 minutes
    - After completing calibration, click Open Tray to eject the utility plate and load the cell plate. Ensure the lid is removed from the cell plate before loading.
    - Click Load cell plate to begin equilibration. Once equilibration has finished, the assay will begin acquiring the first Baseline measurement.

- After completing the Instrument Protocol, the assay will finish and display an Unload Sensor Cartridge message prompt. To eject the Sensor Cartridge and Cell Plate from the Analyzer, press Eject.
- The assay result file will automatically save to the location specified prior to starting the assay and can be opened immediately following the assay using the on-screen prompt.

After assay:

Remove bundles from the cell plate and lyse in ATL buffer + proteinase K for nuclei quantification assay to normalize results.

Appendix K: Protocol for preparing myobundles for cryosectioning

Preparing bundles for cryosectioning – fixing bundles

1. Wash bundles in PBS ++
2. Fix bundles overnight in 2% PFA on rocker at 4C
3. Wash bundles 3x with PBS ++
4. Store bundles in refrigerator until you are ready to flash freeze

Preparing bundles for cryosectioning – flash freezing in O.C.T.

1. Cut off the frames so that only a little bit remains on each end of the bundle.
2. Next, cut the bundles in half, so that you have to halves, each with a piece of frame on the end.
    a. Place bundle on the top of a petri dish (using this as a cutting board)
    b. Line a scalpel up at the halfway point of the bundle, and pressing hard, rock the scalpel forward to make a clean cut through the bundle.
    c. Place bundle halves back in their wells.
    d. Repeat for each bundle.
3. Add the O.C.T. to the cryomold, slowly. If there are air bubbles, try to pop them with a needle. If there are too many, get a new cryomold and start over.
    a. Prepare enough cryomolds for 3-6 bundles per mold for cross-sections and 1-2 bundles per mold for longitudinal sections.

b. Note: If the O.C.T. is left in the cryomold for too long, it will begin to get very viscous.

4. Choose the shorter half of the bundle for cross-sections, and the longer half for longitudinal sections.
5. For cross-sections
    a. Blot both sides of the bundle half on a kimwipe to remove excess moisture
    b. Place the bundle halves in the mold with the frame at the surface.
6. For longitudinal sections
    a. Blot both sides of the bundle half on a kimwipe to remove excess moisture
    b. Place the bundle half in the mold with the frame on the left-hand side
7. Allow bundles to sit in O.C.T. for 20-30 minutes so that excess moisture can evaporate.
    a. Final adjustments to the bundle positioning will be made immediately prior to freezing.
8. In the meantime, get liquid nitrogen in a liquid nitrogen carrier.
    a. Fashion a small "boat" of aluminum foil to place in the liquid nitrogen, submerge just enough so that there is a small layer of liquid nitrogen at the bottom of the boat.

9. Final adjustments
    a. Cross sectional: Make sure all bundles are vertical, with the edge of the bundle pushed down against the bottom of the mold.
    b. Longitudinal: Make sure bundle is parallel to the sides of the mold, and pushed down against the bottom of the mold.
    c. Check for and remove any air bubbles.
10. Once the final adjustments have been made for each individual mold, use long forceps to place it in the aluminum foil boat. Wait until sizzling sound stops, and place mold into a freezer box, store at -20C while the remaining molds are being frozen.
11. Molds should be stored at -80C if not sectioning within the next couple of days.
12. Before sectioning, move molds into the -20C freezer for at least 1 hour.

Appendix L: Protocol for isolation of CD14+ monocytes from umbilical cord blood

Protocol for Primary Monocyte Isolation (CD14+) and Macrophage (M1)

Differentiation

Ellen Weburg, Catherine Oliver, Varun Prasad, Megan Kondash

Updated: 08/10/2018

Materials:

Cord Blood Isolation

1. 50 ml or more of whole blood (anti-coagulated, fresh not frozen)
2. Histopaque 1077 (Sigma 10771-500ML)
3. Hank's Buffered Salt Solution (HBSS) w/o $CaCl_2$, $MgCl_2$, & $MgSO_4$ (Gibco 14175-095)
4. 50-ml Falcon Tubes
5. DPBS -/- (Sigma D8637-500ML)
6. BD pharmingen lysis buffer (BD 555899)
7. Cell culture water (Sigma W3500-500ML)

MACS Separation

1. CD14+ Beads (Miltenyi Biotec 130-050-201)
2. LS Column (Miltenyi Biotec 130-042-401)
3. MidiMACS Separator (Miltenyi Biotec 130-042-302)
4. MidiMACS MultiStand (Miltenyi Biotec 130-042-303)

5. DPBS -/- (Sigma D8637-500ML)

Plating and Detachment of Cells

1. 36.3 cm^2 Petri dishes (Genesee 25-201)
2. RPMI Media 1640 w/ L-Glutamine (Gibco 11875-093) + 10% H.I. FBS
3. 10 mM EDTA
4. GM-CSF (Peprotech 300-03)

Protocol

Part 1: Cord Blood Isolation

1. Remove Histopaque and Lysis Buffer from the fridge and allow them to equilibrate to room temperature.
2. Dilute blood in a 1:1 ratio with HBSS
3. Layer Blood-HBSS mixture slowly on top of equal volume of Histopaque. Use 25
4. Centrifuge the four falcon tubes of the Blood-HBSS-Histopaque mixture for 30 minutes at 740 g. (low brake, setting 1)
    a. You can make the MACS Buffer during this time. See Part 2.
5. Aspirate off platelet-rich plasma layer.
6. Collect buffy coat with 10 ml pipette. From one 50 ml falcon tube, you should be able to remove 10 ml of buffy coat (MNC) mixture. It is fine to collect some plasma as well as some of the red cells near the buff coat as long as you do not disturb the main red pellet.

7. Dilute buffy coat 1:3 with PBS (or basal media). About 12 ml buffy coat, 36 ml PBS.
8. Spin cells down at 300g for 10 min.
9. Prepare 1X solution of lysis buffer by diluting 10X stock 1:9 with sterile water and equilibrate to room temperature. Need 2 mL/pellet. *Note: can be made up to 30 days in advance and stored at 4°C*
10. Remove supernatant and add 2 mL lysis buffer to each pellet (*Best way is to re-suspend one pellet in 2 mL buffer, and then for 4 other pellets add 1 mL and mix vigorously, then transfer to the original conical. Rinse 4 conicals with an additional 1 mL buffer each and combine). Incubate pellets at room temperature for 15 minutes, inverting to mix at 5 and 10 minutes.
11. Dilute the buffer/cell mixture in PBS so the total volume reaches 50 mL. Spin at 300gx10min.
12. Check the pellet to see if most of the red is gone. The pellet should be mostly white, and any RBCs should be on the outside edges of the pellet. If you do see any RBC, repeat step 10 adding 10 mL lysis buffer to each conical (don't repeat merging of pellets).
13. After lysis is complete, bring total volume of each conical up to 50 mL with PBS. Re-spin for 10 min at 300g.

Part 2: Magnetic Assisted Cell Sorting (MACS)

1. Make MACS buffer during the 30 min spin. You can save MACS buffer you don't use at 4 degrees stably for weeks.
    a. 0.5% BSA, sterile filtered. 2mM EDTA in PBS.
    b. For 50mL MACS buffer, measure out 0.25g BSA, add in 200μL 0.5M EDTA.
    c. You may need to heat up the BSA to dissolve. Chill the MACS buffer on ice afterwards.
2. After the last PBS wash, spin the PBMC with some MACS buffer at 300g for 10 min. I usually do 10mL – 15mL, but it mainly depends on how much buffer you have left. You want to save plenty for the actual MACS process. Dilute the cells 1:50 and count while spinning. I can get anywhere from hundred million to billions of cells every isolation (3-4 bags of ~100mL cord blood).
3. For every 10 million cells, label with 20μL MACS buffer and 3.3μL CD14 magnetic beads. Create a labeling solution for all cells while spinning.
4. Aspirate the MACS buffer. Flush the pellet with labeling solution. Incubate on shaker for 15min on ice.
5. Add 10 mL MACS buffer to dilute labeling solution. Spin at 300g for 10 min, aspirate supernatant.
6. Set up MACS stand, magnet, and take a clean column. Pull the plunger out of the syringe and carefully place it back in the plastic sleeve. Mount the column on the

magnet and wet with ~500μL MACS buffer until it runs through all the beads. You'll see the liquid moving down. Always monitor the column. Don't let it run dry!

7. Dilute your labeled cells in MACS buffer. I would do ~3-4mL for 4 bags. But this number always varies depending on how well your lysis is, how many cells you have etc. You can start with 3 mL and see if that works (if buffer drips consistently).
    a. Use 1 ml for 1 unit of blood
8. Run the cells through the column. **Collect the negative fraction and run them through again.**
    a. I usually notice that each column can last for about 1-1.5 bags of blood (what you started off with), assuming that you run through the negative fraction again. Remember to change columns!
9. After you run the cells through twice, wash with ~500μL MACS buffer 3 times. Remove the column from the magnet, add 1mL of PBS and flush out the monocytes you isolated from the column using the plunger. Put these on ice as you set up your next column and run again.
10. Collect all your positive fractions, spin to remove PBS. Count while spinning.
    a. I usually expect ~10-20% of the PBMC to be CD14+. Compare your current cell count with what you started off with.

i. From one unit of blood (if 100 ml), you can obtain around 300 million PBMCs and around 60 million CD14+

Part 3: Plating Cells

1. Separate the resuspended solution into 2 parts: plating and freezing down.
    a. Split the solution based on how many plates you want (about 5 million cells per plate).
2. Spin each solution at 300g for 10 minutes.
3. Re-suspend the cell pellet for plating in culture media (RPMI 1640 + 10% heat inactivated FBS + 10 ng/ml GM-CSF) at a density of 5 million cells per ml.
4. Fill a 36.3 cm^2 petri dish with 4 ml of media.
5. Add 1.1 ml of resuspended cell solution to each plate. You want a density of approximately 150,000 cells per cm^2, resulting in about 5.4-5.5 million cells per plate.

Part 4 (if necessary): Freezing Down CD14+

1. Create a sterile solution of 90% FBS and 10% DMSO.
    a. Sterile filter the FBS first and then add to DMSO.
2. Resuspend the cell pellet for freezing down at a density of approximately 8 million cells/ml.
3. Fill cryovials with 1 ml of solution.
4. Place in a Mr. Frosty in the -80 freezer.

5. Transfer the cells to liquid nitrogen the next day.

Part 5: Differentiation to Monocyte-Derived Macrophages (MDMs)

2. Five days after isolation, change the media.
    a. Prepare culture media (RPMI 1640 + 10% heat inactivated FBS + 10 ng/ml GM-CSF). Prepare enough for 5 ml per dish (if using 36.3 cm^2 dishes).
    b. Remove spent media from the dish and place in a conical tube kept on ice.
    c. Add 4 ml of fresh media to the dish and replace in the incubator.
    d. Spin down the spent media at 300g for 10 minutes.
    e. Aspirate the supernatant and resuspend the cell pellet in fresh media (1 ml per dish).
    f. Add 1 ml of cell solution to each dish by pipetting dropwise in a zigzag fashion over the surface of the dish to obtain even cell distribution.
3. Continue to maintain MDMs by changing the media every three days.
    a. MDMs should be fully mature and ready to use by around day 7 post-isolation, and maintain their phenotype in culture until around day 11 post-isolation.

Part 6: Detach MDMs for use in 2D studies or Myobundles

1. Prepare a stock of ice-cold 10 mM EDTA.
2. Remove spent media from dishes and save in a conical tube kept on ice.

3. Wash each dish 3x with PBS -/-.
4. Add 3 ml of 10 mM EDTA to each dish.
5. Allow to incubate at 37C in the incubator for approximately 15 minutes.
6. Using a P1000, pipette the EDTA up and down, washing the surface of the petri dish to remove cells that are still adherent. This method is not as efficient as scraping at removing the MDMs, but is less harsh.
    a. Collect cell solution in a conical separate from the conical with the spent media. Depending on your application, you may want to combine the adhered cell population with the non-adhered cell population in the spent media, or to keep them separate. For MDM myobundle experiments we have been using the adherent population only.
7. For 2D plating
    a. Plate MDMs at a density of 600,000 cells/well in a Matrigel-coated 6-well plate.
8. For 3D myobundles
    a. Add appropriate volume of MDM cell solution directly to the tubes containing the skeletal muscle cells, then spin down and proceed with bundle-making.

Appendix M: Protocol for staining macrophages for flow cytometry

Antibodies:

Antibody name	Vendor, catalog number	Stock concentration	Recommended dilution
PE anti-human CD80 (488 ex.)	Biolegend, 305207	200 μg/mL	5 μL/ 1 million cells in 100 uL volume
APC anti-human CD68 (633 ex.)	Biolegend, 333809	25 μg/mL	5 μL/ 1 million cells in 100 uL volume
Anti-human CD163 – FITC (ex 494 em 520)	Bio rad, MCA1853F	1 mg/mL	Use 10 μL of 1/10-1/50 dilution to label 1 million cells in 100 μL (overall dilution 1:100-1:500, final concentration 2-10 μg/mL)

1. Make FACS buffer:
    a. PBS -/-
    b. 0.5% BSA
    c. 2 mM EDTA
    d. Filter
2. Divide each sample into 4 equal volumes for the following groups:
    a. Negative control (cells only, no antibody)
    b. CD68 staining
    c. CD163 staining
    d. CD80 staining
3. Spin down each group at 300xg, 10 minutes.

4. Aspirate supernatant, resuspend each sample in 100 μl FACS buffer.
5. Add 5 μl of the appropriate antibody to each sample.
6. Incubate at 4C (in the dark) for 30 minutes.
7. Add 10 ml of PBS -/- to dilute antibody.
8. Spin down at 300xg, 10 minutes. Remove supernatant.
9. Resuspend in 500 μl of FACS buffer, transfer to tube for FACS.
10. Keep samples protected from light.

References

1 Kondash, M. E., Davis, B.N.J., Truskey, G.A. in *Engineering 3D Tissue Test Systems* (ed D. Dreau and T. Burg K.J.L. Burg) Ch. 18, 321-250 (CRC Press, 2017).

2 Paul, S. M. *et al.* How to improve R&D productivity: the pharmaceutical industry's grand challenge. *Nat Rev Drug Discov* **9**, 203-214, doi:10.1038/nrd3078 (2010).

3 Hay, M., Thomas, D. W., Craighead, J. L., Economides, C. & Rosenthal, J. Clinical development success rates for investigational drugs. *Nat Biotechnol* **32**, 40-51, doi:10.1038/nbt.2786 (2014).

4 Low, L. A. & Tagle, D. A. Microphysiological Systems ("Organs-on-Chips") for Drug Efficacy and Toxicity Testing. *Clin Transl Sci* **10**, 237-239, doi:10.1111/cts.12444 (2017).

5 Truskey, G. A. Human Microphysiological Systems and Organoids as in Vitro Models for Toxicological Studies. *Front Public Health* **6**, 185, doi:10.3389/fpubh.2018.00185 (2018).

6 Ewart, L. *et al.* Application of Microphysiological Systems to Enhance Safety Assessment in Drug Discovery. *Annu Rev Pharmacol Toxicol* **58**, 65-82, doi:10.1146/annurev-pharmtox-010617-052722 (2018).

7 Madden, L., Juhas, M., Kraus, W. E., Truskey, G. A. & Bursac, N. Bioengineered human myobundles mimic clinical responses of skeletal muscle to drugs. *Elife* **4**, e04885, doi:10.7554/eLife.04885 (2015).

8 Davis, B. N. *et al.* Human, Tissue-Engineered, Skeletal Muscle Myobundles to Measure Oxygen Uptake and Assess Mitochondrial Toxicity. *Tissue Eng Part C Methods* **23**, 189-199, doi:10.1089/ten.tec.2016.0264 (2017).

9 Fernandez, C. E. *et al.* Human Vascular Microphysiological System for in vitro Drug Screening. *Sci Rep* **6**, 21579, doi:10.1038/srep21579 (2016).

10 Vernetti, L. A. *et al.* A human liver microphysiology platform for investigating physiology, drug safety, and disease models. *Exp Biol Med (Maywood)* **241**, 101-114, doi:10.1177/1535370215592121 (2016).

11 Weber, E. J. *et al.* Development of a microphysiological model of human kidney proximal tubule function. *Kidney Int* **90**, 627-637, doi:10.1016/j.kint.2016.06.011 (2016).

12 Schwartz, M. P. *et al.* Human pluripotent stem cell-derived neural constructs for predicting neural toxicity. *Proc Natl Acad Sci U S A* **112**, 12516-12521, doi:10.1073/pnas.1516645112 (2015).

13 Seok, J. *et al.* Genomic responses in mouse models poorly mimic human inflammatory diseases. *Proc Natl Acad Sci U S A* **110**, 3507-3512, doi:10.1073/pnas.1222878110 (2013).

14 Mestas, J. & Hughes, C. C. Of mice and not men: differences between mouse and human immunology. *J Immunol* **172**, 2731-2738 (2004).

15 Dykens, J. A. & Will, Y. The significance of mitochondrial toxicity testing in drug development. *Drug Discov Today* **12**, 777-785, doi:10.1016/j.drudis.2007.07.013 (2007).

16 Furberg, C. D. & Pitt, B. Withdrawal of cerivastatin from the world market. *Current controlled trials in cardiovascular medicine* **2**, 205-207 (2001).

17 Manzoni, M. & Rollini, M. Biosynthesis and biotechnological production of statins by filamentous fungi and application of these cholesterol-lowering drugs. *Applied microbiology and biotechnology* **58**, 555-564, doi:10.1007/s00253-002-0932-9 (2002).

18 von Keutz, E. & Schluter, G. Preclinical safety evaluation of cerivastatin, a novel HMG-CoA reductase inhibitor. *The American journal of cardiology* **82**, 11J-17J (1998).

19 Backman, J. T., Kyrklund, C., Neuvonen, M. & Neuvonen, P. J. Gemfibrozil greatly increases plasma concentrations of cerivastatin. *Clinical pharmacology and therapeutics* **72**, 685-691, doi:10.1067/mcp.2002.128469 (2002).

20 Staffa, J. A., Chang, J. & Green, L. Cerivastatin and reports of fatal rhabdomyolysis. *The New England journal of medicine* **346**, 539-540, doi:10.1056/NEJM200202143460720 (2002).

21 Atchison, L., Zhang, H., Cao, K. & Truskey, G. A. A Tissue Engineered Blood Vessel Model of Hutchinson-Gilford Progeria Syndrome Using Human iPSC-derived Smooth Muscle Cells. *Sci Rep* **7**, 8168, doi:10.1038/s41598-017-08632-4 (2017).

22 Birey, F. *et al.* Assembly of functionally integrated human forebrain spheroids. *Nature* **545**, 54-59, doi:10.1038/nature22330 (2017).

23 Janssen, I., Heymsfield, S. B., Wang, Z. M. & Ross, R. Skeletal muscle mass and distribution in 468 men and women aged 18-88 yr. *J Appl Physiol (1985)* **89**, 81-88, doi:10.1152/jappl.2000.89.1.81 (2000).

24 Latroche, C. *et al.* Skeletal Muscle Microvasculature: A Highly Dynamic Lifeline. *Physiology (Bethesda)* **30**, 417-427, doi:10.1152/physiol.00026.2015 (2015).

25 Cromie, M. J., Sanchez, G. N., Schnitzer, M. J. & Delp, S. L. Sarcomere lengths in human extensor carpi radialis brevis measured by microendoscopy. *Muscle Nerve* **48**, 286-292, doi:10.1002/mus.23760 (2013).

26 Huxley, H. & Hanson, J. Changes in the cross-striations of muscle during contraction and stretch and their structural interpretation. *Nature* **173**, 973-976 (1954).

27 Huxley, A. F. Muscle structure and theories of contraction. *Prog Biophys Biophys Chem* **7**, 255-318 (1957).

28 Spudich, J. A. The myosin swinging cross-bridge model. *Nat Rev Mol Cell Biol* **2**, 387-392, doi:10.1038/35073086 (2001).

29 Gordon, A. M., Huxley, A. F. & Julian, F. J. The variation in isometric tension with sarcomere length in vertebrate muscle fibres. *J Physiol* **184**, 170-192 (1966).

30 Bigland-Ritchie, B., Jones, D. A. & Woods, J. J. Excitation frequency and muscle fatigue: electrical responses during human voluntary and stimulated contractions. *Exp Neurol* **64**, 414-427 (1979).

31 Allen, D. G., Lamb, G. D. & Westerblad, H. Skeletal muscle fatigue: cellular mechanisms. *Physiol Rev* **88**, 287-332, doi:10.1152/physrev.00015.2007 (2008).

32 Westerblad, H., Lee, J. A., Lannergren, J. & Allen, D. G. Cellular mechanisms of fatigue in skeletal muscle. *Am J Physiol* **261**, C195-209, doi:10.1152/ajpcell.1991.261.2.C195 (1991).

33 Karatzaferi, C., de Haan, A., Ferguson, R. A., van Mechelen, W. & Sargeant, A. J. Phosphocreatine and ATP content in human single muscle fibres before and after maximum dynamic exercise. *Pflugers Arch* **442**, 467-474 (2001).

34 Clanton, T. L., Zuo, L. & Klawitter, P. Oxidants and skeletal muscle function: physiologic and pathophysiologic implications. *Proc Soc Exp Biol Med* **222**, 253-262 (1999).

35 Bottinelli, R., Betto, R., Schiaffino, S. & Reggiani, C. Maximum shortening velocity and coexistence of myosin heavy chain isoforms in single skinned fast fibres of rat skeletal muscle. *J Muscle Res Cell Motil* **15**, 413-419 (1994).

36 Schiaffino, S. & Reggiani, C. Fiber types in mammalian skeletal muscles. *Physiol Rev* **91**, 1447-1531, doi:10.1152/physrev.00031.2010 (2011).

37 Smerdu, V., Karsch-Mizrachi, I., Campione, M., Leinwand, L. & Schiaffino, S. Type IIx myosin heavy chain transcripts are expressed in type IIb fibers of human skeletal muscle. *Am J Physiol* **267**, C1723-1728, doi:10.1152/ajpcell.1994.267.6.C1723 (1994).

38 Rossi, A. C., Mammucari, C., Argentini, C., Reggiani, C. & Schiaffino, S. Two novel/ancient myosins in mammalian skeletal muscles: MYH14/7b and MYH15 are expressed in extraocular muscles and muscle spindles. *J Physiol* **588**, 353-364, doi:10.1113/jphysiol.2009.181008 (2010).

39 Han, Y. S., Geiger, P. C., Cody, M. J., Macken, R. L. & Sieck, G. C. ATP consumption rate per cross bridge depends on myosin heavy chain isoform. *J Appl Physiol (1985)* **94**, 2188-2196, doi:10.1152/japplphysiol.00618.2002 (2003).

40 He, Z. H., Bottinelli, R., Pellegrino, M. A., Ferenczi, M. A. & Reggiani, C. ATP consumption and efficiency of human single muscle fibers with different myosin isoform composition. *Biophys J* **79**, 945-961, doi:10.1016/S0006-3495(00)76349-1 (2000).

41 Hughes, S. M., Chi, M. M., Lowry, O. H. & Gundersen, K. Myogenin induces a shift of enzyme activity from glycolytic to oxidative metabolism in muscles of transgenic mice. *J Cell Biol* **145**, 633-642 (1999).

42 Prakash, Y. S., Miller, S. M., Huang, M. & Sieck, G. C. Morphology of diaphragm neuromuscular junctions on different fibre types. *J Neurocytol* **25**, 88-100 (1996).

43 Vollestad, N. K., Vaage, O. & Hermansen, L. Muscle glycogen depletion patterns in type I and subgroups of type II fibres during prolonged severe exercise in man. *Acta physiologica Scandinavica* **122**, 433-441, doi:10.1111/j.1748-1716.1984.tb07531.x (1984).

44 Tarnopolsky, M. A. *et al.* Influence of endurance exercise training and sex on intramyocellular lipid and mitochondrial ultrastructure, substrate use, and mitochondrial enzyme activity. *Am J Physiol Regul Integr Comp Physiol* **292**, R1271-1278, doi:10.1152/ajpregu.00472.2006 (2007).

45 Egan, B. & Zierath, J. R. Exercise metabolism and the molecular regulation of skeletal muscle adaptation. *Cell Metab* **17**, 162-184, doi:10.1016/j.cmet.2012.12.012 (2013).

46 Gollnick, P. D. *et al.* Effect of training on enzyme activity and fiber composition of human skeletal muscle. *J Appl Physiol* **34**, 107-111, doi:10.1152/jappl.1973.34.1.107 (1973).

47 Anderson, R. M. & Weindruch, R. Metabolic reprogramming, caloric restriction and aging. *Trends Endocrinol Metab* **21**, 134-141, doi:10.1016/j.tem.2009.11.005 (2010).

48 Talbot, J. & Maves, L. Skeletal muscle fiber type: using insights from muscle developmental biology to dissect targets for susceptibility and resistance to muscle disease. *Wiley Interdiscip Rev Dev Biol* **5**, 518-534, doi:10.1002/wdev.230 (2016).

49 Schiaffino, S., Rossi, A. C., Smerdu, V., Leinwand, L. A. & Reggiani, C. Developmental myosins: expression patterns and functional significance. *Skeletal muscle* **5**, 22, doi:10.1186/s13395-015-0046-6 (2015).

50 Barbet, J. P., Thornell, L. E. & Butler-Browne, G. S. Immunocytochemical characterisation of two generations of fibers during the development of the human quadriceps muscle. *Mech Dev* **35**, 3-11 (1991).

51 Cho, M., Webster, S. G. & Blau, H. M. Evidence for myoblast-extrinsic regulation of slow myosin heavy chain expression during muscle fiber formation in embryonic development. *J Cell Biol* **121**, 795-810 (1993).

52 Draeger, A., Weeds, A. G. & Fitzsimons, R. B. Primary, secondary and tertiary myotubes in developing skeletal muscle: a new approach to the analysis of human myogenesis. *J Neurol Sci* **81**, 19-43 (1987).

53 Sartore, S., Gorza, L. & Schiaffino, S. Fetal myosin heavy chains in regenerating muscle. *Nature* **298**, 294-296 (1982).

54 Richter, E. A. & Hargreaves, M. Exercise, GLUT4, and skeletal muscle glucose uptake. *Physiol Rev* **93**, 993-1017, doi:10.1152/physrev.00038.2012 (2013).

55 Daugaard, J. R. *et al.* Fiber type-specific expression of GLUT4 in human skeletal muscle: influence of exercise training. *Diabetes* **49**, 1092-1095 (2000).

56 Taniguchi, C. M., Emanuelli, B. & Kahn, C. R. Critical nodes in signalling pathways: insights into insulin action. *Nat Rev Mol Cell Biol* **7**, 85-96, doi:10.1038/nrm1837 (2006).

57 Middelbeek, R. J. *et al.* Insulin stimulation regulates AS160 and TBC1D1 phosphorylation sites in human skeletal muscle. *Nutr Diabetes* **3**, e74, doi:10.1038/nutd.2013.13 (2013).

58 Schultze, S. M., Hemmings, B. A., Niessen, M. & Tschopp, O. PI3K/AKT, MAPK and AMPK signalling: protein kinases in glucose homeostasis. *Expert Rev Mol Med* **14**, e1, doi:10.1017/S1462399411002109 (2012).

59 Kennedy, J. W. *et al.* Acute exercise induces GLUT4 translocation in skeletal muscle of normal human subjects and subjects with type 2 diabetes. *Diabetes* **48**, 1192-1197 (1999).

60 Ahlborg, G., Felig, P., Hagenfeldt, L., Hendler, R. & Wahren, J. Substrate turnover during prolonged exercise in man. Splanchnic and leg metabolism of glucose, free fatty acids, and amino acids. *J Clin Invest* **53**, 1080-1090, doi:10.1172/JCI107645 (1974).

61 Lemieux, K., Han, X. X., Dombrowski, L., Bonen, A. & Marette, A. The transferrin receptor defines two distinct contraction-responsive GLUT4 vesicle populations in skeletal muscle. *Diabetes* **49**, 183-189 (2000).

62 Coderre, L., Kandror, K. V., Vallega, G. & Pilch, P. F. Identification and characterization of an exercise-sensitive pool of glucose transporters in skeletal muscle. *J Biol Chem* **270**, 27584-27588 (1995).

63 Harridge, S. D. R. Plasticity of human skeletal muscle: gene expression to in vivo function. *Exp Physiol* **92**, 783-797, doi:10.1113/expphysiol.2006.036525 (2007).

64 Scott, W., Stevens, J. & Binder-Macleod, S. A. Human skeletal muscle fiber type classifications. *Phys Ther* **81**, 1810-1816 (2001).

65 Coggan, A. R., Kohrt, W. M., Spina, R. J., Bier, D. M. & Holloszy, J. O. Endurance training decreases plasma glucose turnover and oxidation during moderate-intensity exercise in men. *J Appl Physiol (1985)* **68**, 990-996, doi:10.1152/jappl.1990.68.3.990 (1990).

66 McGarrah, R. W., Slentz, C. A. & Kraus, W. E. The Effect of Vigorous- Versus Moderate-Intensity Aerobic Exercise on Insulin Action. *Curr Cardiol Rep* **18**, 117, doi:10.1007/s11886-016-0797-7 (2016).

67 Jensen, J., Rustad, P. I., Kolnes, A. J. & Lai, Y. C. The role of skeletal muscle glycogen breakdown for regulation of insulin sensitivity by exercise. *Front Physiol* **2**, 112, doi:10.3389/fphys.2011.00112 (2011).

68 Baker, J. S., McCormick, M. C. & Robergs, R. A. Interaction among Skeletal Muscle Metabolic Energy Systems during Intense Exercise. *J Nutr Metab* **2010**, 905612, doi:10.1155/2010/905612 (2010).

69 Morales-Alamo, D. *et al*. Skeletal Muscle Pyruvate Dehydrogenase Phosphorylation and Lactate Accumulation During Sprint Exercise in Normoxia and Severe Acute Hypoxia: Effects of Antioxidants. *Front Physiol* **9**, 188, doi:10.3389/fphys.2018.00188 (2018).

70 Scott, C. Misconceptions about Aerobic and Anaerobic Energy Expenditure. *J Int Soc Sports Nutr* **2**, 32-37, doi:10.1186/1550-2783-2-2-32 (2005).

71 van Loon, L. J., Greenhaff, P. L., Constantin-Teodosiu, D., Saris, W. H. & Wagenmakers, A. J. The effects of increasing exercise intensity on muscle fuel utilisation in humans. *J Physiol* **536**, 295-304 (2001).

72 Romijn, J. A. *et al.* Regulation of endogenous fat and carbohydrate metabolism in relation to exercise intensity and duration. *Am J Physiol* **265**, E380-391, doi:10.1152/ajpendo.1993.265.3.E380 (1993).

73 Wagenmakers, A. J. *et al.* Carbohydrate supplementation, glycogen depletion, and amino acid metabolism during exercise. *Am J Physiol* **260**, E883-890, doi:10.1152/ajpendo.1991.260.6.E883 (1991).

74 Brosnan, J. T. & Brosnan, M. E. Branched-chain amino acids: enzyme and substrate regulation. *J Nutr* **136**, 207S-211S, doi:10.1093/jn/136.1.207S (2006).

75 Wagenmakers, A. J. Muscle amino acid metabolism at rest and during exercise: role in human physiology and metabolism. *Exerc Sport Sci Rev* **26**, 287-314 (1998).

76 Lerin, C. *et al.* Defects in muscle branched-chain amino acid oxidation contribute to impaired lipid metabolism. *Mol Metab* **5**, 926-936, doi:10.1016/j.molmet.2016.08.001 (2016).

77 Kelley, D. E., Goodpaster, B., Wing, R. R. & Simoneau, J. A. Skeletal muscle fatty acid metabolism in association with insulin resistance, obesity, and weight loss. *Am J Physiol* **277**, E1130-1141, doi:10.1152/ajpendo.1999.277.6.E1130 (1999).

78 Kelley, D. E., Mokan, M., Simoneau, J. A. & Mandarino, L. J. Interaction between glucose and free fatty acid metabolism in human skeletal muscle. *J Clin Invest* **92**, 91-98, doi:10.1172/JCI116603 (1993).

79 Koves, T. R. *et al.* Mitochondrial overload and incomplete fatty acid oxidation contribute to skeletal muscle insulin resistance. *Cell Metab* **7**, 45-56, doi:10.1016/j.cmet.2007.10.013 (2008).

80 Goodpaster, B. H. & Sparks, L. M. Metabolic Flexibility in Health and Disease. *Cell Metab* **25**, 1027-1036, doi:10.1016/j.cmet.2017.04.015 (2017).

81 Zammit, P. S. *et al.* Muscle satellite cells adopt divergent fates: a mechanism for self-renewal? *J Cell Biol* **166**, 347-357, doi:10.1083/jcb.200312007 (2004).

82 Olguin, H. C. & Olwin, B. B. Pax-7 up-regulation inhibits myogenesis and cell cycle progression in satellite cells: a potential mechanism for self-renewal. *Dev Biol* **275**, 375-388, doi:10.1016/j.ydbio.2004.08.015 (2004).

83 Tidball, J. G., Berchenko, E. & Frenette, J. Macrophage invasion does not contribute to muscle membrane injury during inflammation. *J Leukoc Biol* **65**, 492-498 (1999).

84 Tidball, J. G. & Villalta, S. A. Regulatory interactions between muscle and the immune system during muscle regeneration. *Am J Physiol Regul Integr Comp Physiol* **298**, R1173-1187, doi:10.1152/ajpregu.00735.2009 (2010).

85 Arnold, L. *et al.* Inflammatory monocytes recruited after skeletal muscle injury switch into antiinflammatory macrophages to support myogenesis. *J Exp Med* **204**, 1057-1069, doi:10.1084/jem.20070075 (2007).

86 Segawa, M. *et al.* Suppression of macrophage functions impairs skeletal muscle regeneration with severe fibrosis. *Exp Cell Res* **314**, 3232-3244, doi:10.1016/j.yexcr.2008.08.008 (2008).

87 Chen, S. E., Jin, B. & Li, Y. P. TNF-alpha regulates myogenesis and muscle regeneration by activating p38 MAPK. *Am J Physiol Cell Physiol* **292**, C1660-1671, doi:10.1152/ajpcell.00486.2006 (2007).

88 Troy, A. *et al.* Coordination of satellite cell activation and self-renewal by Par-complex-dependent asymmetric activation of p38alpha/beta MAPK. *Cell Stem Cell* **11**, 541-553, doi:10.1016/j.stem.2012.05.025 (2012).

89 Cheng, M., Nguyen, M. H., Fantuzzi, G. & Koh, T. J. Endogenous interferon-gamma is required for efficient skeletal muscle regeneration. *Am J Physiol Cell Physiol* **294**, C1183-1191, doi:10.1152/ajpcell.00568.2007 (2008).

90 Wang, X. *et al.* Effects of interleukin-6, leukemia inhibitory factor, and ciliary neurotrophic factor on the proliferation and differentiation of adult human myoblasts. *Cell Mol Neurobiol* **28**, 113-124, doi:10.1007/s10571-007-9247-9 (2008).

91 Saltiel, A. R. & Olefsky, J. M. Inflammatory mechanisms linking obesity and metabolic disease. *J Clin Invest* **127**, 1-4, doi:10.1172/JCI92035 (2017).

92 Weisberg, S. P. *et al.* Obesity is associated with macrophage accumulation in adipose tissue. *J Clin Invest* **112**, 1796-1808, doi:10.1172/JCI19246 (2003).

93 Dandona, P. *et al.* Tumor necrosis factor-alpha in sera of obese patients: fall with weight loss. *J Clin Endocrinol Metab* **83**, 2907-2910, doi:10.1210/jcem.83.8.5026 (1998).

94 Arvidsson, E. *et al.* Effects of different hypocaloric diets on protein secretion from adipose tissue of obese women. *Diabetes* **53**, 1966-1971 (2004).

95 Schmidt, F. M. *et al.* Inflammatory cytokines in general and central obesity and modulating effects of physical activity. *PLoS One* **10**, e0121971, doi:10.1371/journal.pone.0121971 (2015).

96 Hotamisligil, G. S., Shargill, N. S. & Spiegelman, B. M. Adipose expression of tumor necrosis factor-alpha: direct role in obesity-linked insulin resistance. *Science* **259**, 87-91 (1993).

97 Surendar, J., Mohan, V., Rao, M. M., Babu, S. & Aravindhan, V. Increased levels of both Th1 and Th2 cytokines in subjects with metabolic syndrome (CURES-103). *Diabetes Technol Ther* **13**, 477-482, doi:10.1089/dia.2010.0178 (2011).

98 Wu, H. & Ballantyne, C. M. Skeletal muscle inflammation and insulin resistance in obesity. *J Clin Invest* **127**, 43-54, doi:10.1172/JCI88880 (2017).

99 Khan, I. M. *et al.* Intermuscular and perimuscular fat expansion in obesity correlates with skeletal muscle T cell and macrophage infiltration and insulin resistance. *Int J Obes (Lond)* **39**, 1607-1618, doi:10.1038/ijo.2015.104 (2015).

100 Fink, L. N. *et al.* Pro-inflammatory macrophages increase in skeletal muscle of high fat-fed mice and correlate with metabolic risk markers in humans. *Obesity (Silver Spring)* **22**, 747-757, doi:10.1002/oby.20615 (2014).

101 Hartwig, S. *et al.* Secretome profiling of primary human skeletal muscle cells. *Biochim Biophys Acta* **1844**, 1011-1017, doi:10.1016/j.bbapap.2013.08.004 (2014).

102 Pedersen, B. K. & Febbraio, M. A. Muscles, exercise and obesity: skeletal muscle as a secretory organ. *Nat Rev Endocrinol* **8**, 457-465, doi:10.1038/nrendo.2012.49 (2012).

103 Carey, A. L. *et al.* Interleukin-6 increases insulin-stimulated glucose disposal in humans and glucose uptake and fatty acid oxidation in vitro via AMP-activated protein kinase. *Diabetes* **55**, 2688-2697, doi:10.2337/db05-1404 (2006).

104 Lee, Y. S. *et al.* Inflammation is necessary for long-term but not short-term high-fat diet-induced insulin resistance. *Diabetes* **60**, 2474-2483, doi:10.2337/db11-0194 (2011).

105 Ciaraldi, T. P., Ryan, A. J., Mudaliar, S. R. & Henry, R. R. Altered Myokine Secretion Is an Intrinsic Property of Skeletal Muscle in Type 2 Diabetes. *PLoS One* **11**, e0158209, doi:10.1371/journal.pone.0158209 (2016).

106 Abdul-Ghani, M. A. & DeFronzo, R. A. Pathogenesis of insulin resistance in skeletal muscle. *J Biomed Biotechnol* **2010**, 476279, doi:10.1155/2010/476279 (2010).

107 Gaster, M., Staehr, P., Beck-Nielsen, H., Schroder, H. D. & Handberg, A. GLUT4 is reduced in slow muscle fibers of type 2 diabetic patients: is insulin resistance in type 2 diabetes a slow, type 1 fiber disease? *Diabetes* **50**, 1324-1329 (2001).

108 Lillioja, S. *et al.* Skeletal muscle capillary density and fiber type are possible determinants of in vivo insulin resistance in man. *J Clin Invest* **80**, 415-424, doi:10.1172/JCI113088 (1987).

109 Meng, Z. X. *et al.* Baf60c drives glycolytic metabolism in the muscle and improves systemic glucose homeostasis through Deptor-mediated Akt activation. *Nat Med* **19**, 640-645, doi:10.1038/nm.3144 (2013).

110 Lecker, S. H. *et al.* Multiple types of skeletal muscle atrophy involve a common program of changes in gene expression. *FASEB J* **18**, 39-51, doi:10.1096/fj.03-0610com (2004).

111 Mammucari, C. *et al.* FoxO3 controls autophagy in skeletal muscle in vivo. *Cell Metab* **6**, 458-471, doi:10.1016/j.cmet.2007.11.001 (2007).

112 Zhao, J. *et al.* FoxO3 coordinately activates protein degradation by the autophagic/lysosomal and proteasomal pathways in atrophying muscle cells. *Cell Metab* **6**, 472-483, doi:10.1016/j.cmet.2007.11.004 (2007).

113 Schiaffino, S. & Mammucari, C. Regulation of skeletal muscle growth by the IGF1-Akt/PKB pathway: insights from genetic models. *Skeletal muscle* **1**, 4, doi:10.1186/2044-5040-1-4 (2011).

114 Morissette, M. R., Cook, S. A., Buranasombati, C., Rosenberg, M. A. & Rosenzweig, A. Myostatin inhibits IGF-I-induced myotube hypertrophy through Akt. *Am J Physiol Cell Physiol* **297**, C1124-1132, doi:10.1152/ajpcell.00043.2009 (2009).

115 Roubenoff, R. The "cytokine for gerontologists" has some company. *The journals of gerontology. Series A, Biological sciences and medical sciences* **69**, 163-164, doi:10.1093/gerona/glt184 (2014).

116 Schrager, M. A. *et al.* Sarcopenic obesity and inflammation in the InCHIANTI study. *J Appl Physiol (1985)* **102**, 919-925, doi:10.1152/japplphysiol.00627.2006 (2007).

117 Stenholm, S. *et al.* Sarcopenic obesity: definition, cause and consequences. *Curr Opin Clin Nutr Metab Care* **11**, 693-700, doi:10.1097/MCO.0b013e328312c37d (2008).

118 Lexell, J., Taylor, C. C. & Sjostrom, M. What is the cause of the ageing atrophy? Total number, size and proportion of different fiber types studied in whole

vastus lateralis muscle from 15- to 83-year-old men. *J Neurol Sci* **84**, 275-294 (1988).

119 Larsson, L., Li, X. & Frontera, W. R. Effects of aging on shortening velocity and myosin isoform composition in single human skeletal muscle cells. *Am J Physiol* **272**, C638-649, doi:10.1152/ajpcell.1997.272.2.C638 (1997).

120 Reid, M. B. & Moylan, J. S. Beyond atrophy: redox mechanisms of muscle dysfunction in chronic inflammatory disease. *J Physiol* **589**, 2171-2179, doi:10.1113/jphysiol.2010.203356 (2011).

121 Truskey, G. A. *et al.* Design considerations for an integrated microphysiological muscle tissue for drug and tissue toxicity testing. *Stem cell research & therapy* **4 Suppl 1**, S10, doi:10.1186/scrt371 (2013).

122 Brack, A. S. & Rando, T. A. Tissue-specific stem cells: lessons from the skeletal muscle satellite cell. *Cell Stem Cell* **10**, 504-514, doi:10.1016/j.stem.2012.04.001 (2012).

123 Campion, D. R. The muscle satellite cell: a review. *International review of cytology* **87**, 225-251 (1984).

124 Dennis, R. G., Kosnik, P. E., 2nd, Gilbert, M. E. & Faulkner, J. A. Excitability and contractility of skeletal muscle engineered from primary cultures and cell lines. *Am J Physiol Cell Physiol* **280**, C288-295 (2001).

125 Chen, S., Nakamoto, T., Kawazoe, N. & Chen, G. Engineering multi-layered skeletal muscle tissue by using 3D microgrooved collagen scaffolds. *Biomaterials* **73**, 23-31, doi:10.1016/j.biomaterials.2015.09.010 (2015).

126 Rhim, C., Cheng, C. S., Kraus, W. E. & Truskey, G. A. Effect of microRNA modulation on bioartificial muscle function. *Tissue Eng Part A* **16**, 3589-3597, doi:10.1089/ten.TEA.2009.0601 (2010).

127 Olsson, K. *et al.* Intracellular Ca(2+)-handling differs markedly between intact human muscle fibers and myotubes. *Skeletal muscle* **5**, 26, doi:10.1186/s13395-015-0050-x (2015).

128 Rando, T. A. & Blau, H. M. Primary mouse myoblast purification, characterization, and transplantation for cell-mediated gene therapy. *J Cell Biol* **125**, 1275-1287 (1994).

129 Danoviz, M. E. & Yablonka-Reuveni, Z. Skeletal muscle satellite cells: background and methods for isolation and analysis in a primary culture system. *Methods in molecular biology* **798**, 21-52, doi:10.1007/978-1-61779-343-1_2 (2012).

130 Merrick, D., Chen, H. C., Larner, D. & Smith, J. Adult and embryonic skeletal muscle microexplant culture and isolation of skeletal muscle stem cells. *Journal of visualized experiments : JoVE*, doi:10.3791/2051 (2010).

131 Richler, C. & Yaffe, D. The in vitro cultivation and differentiation capacities of myogenic cell lines. *Dev Biol* **23**, 1-22 (1970).

132 Yablonka-Reuveni, Z. Discrimination of myogenic and nonmyogenic cells from embryonic skeletal muscle by 90 degrees light scattering. *Cytometry* **9**, 121-125, doi:10.1002/cyto.990090204 (1988).

133 Baroffio, A. *et al.* Purification of human muscle satellite cells by flow cytometry. *Muscle Nerve* **16**, 498-505, doi:10.1002/mus.880160511 (1993).

134 Liu, L., Cheung, T. H., Charville, G. W. & Rando, T. A. Isolation of skeletal muscle stem cells by fluorescence-activated cell sorting. *Nature protocols* **10**, 1612-1624, doi:10.1038/nprot.2015.110 (2015).

135 Pasut, A., Oleynik, P. & Rudnicki, M. A. Isolation of muscle stem cells by fluorescence activated cell sorting cytometry. *Methods in molecular biology* **798**, 53-64, doi:10.1007/978-1-61779-343-1_3 (2012).

136 Montarras, D. *et al.* Direct isolation of satellite cells for skeletal muscle regeneration. *Science* **309**, 2064-2067, doi:10.1126/science.1114758 (2005).

137 Owens, J., Moreira, K. & Bain, G. Characterization of primary human skeletal muscle cells from multiple commercial sources. *In vitro cellular & developmental biology. Animal* **49**, 695-705, doi:10.1007/s11626-013-9655-8 (2013).

138 Le Grand, F. & Rudnicki, M. A. Skeletal muscle satellite cells and adult myogenesis. *Current opinion in cell biology* **19**, 628-633, doi:10.1016/j.ceb.2007.09.012 (2007).

139 Fishman, J. M. *et al.* Skeletal muscle tissue engineering: which cell to use? *Tissue engineering. Part B, Reviews* **19**, 503-515, doi:10.1089/ten.TEB.2013.0120 (2013).

140 Edom, F., Mouly, V., Barbet, J. P., Fiszman, M. Y. & Butler-Browne, G. S. Clones of human satellite cells can express in vitro both fast and slow myosin heavy chains. *Dev Biol* **164**, 219-229, doi:10.1006/dbio.1994.1193 (1994).

141 Juhas, M. & Bursac, N. Roles of adherent myogenic cells and dynamic culture in engineered muscle function and maintenance of satellite cells. *Biomaterials* **35**, 9438-9446, doi:10.1016/j.biomaterials.2014.07.035 (2014).

142 Kuhl, U. *et al.* Role of muscle fibroblasts in the deposition of type-IV collagen in the basal lamina of myotubes. *Differentiation; research in biological diversity* **28**, 164-172 (1984).

143 Sanes, J. R. The basement membrane/basal lamina of skeletal muscle. *J Biol Chem* **278**, 12601-12604, doi:10.1074/jbc.R200027200 (2003).

144 Juhas, M., Engelmayr, G. C., Jr., Fontanella, A. N., Palmer, G. M. & Bursac, N. Biomimetic engineered muscle with capacity for vascular integration and functional maturation in vivo. *Proc Natl Acad Sci U S A* **111**, 5508-5513, doi:10.1073/pnas.1402723111 (2014).

145 De Jesus, A. M. & Sander, E. A. Observing and quantifying fibroblast-mediated fibrin gel compaction. *Journal of visualized experiments : JoVE*, e50918, doi:10.3791/50918 (2014).

146 Baker, E. L., Dennis, R. G. & Larkin, L. M. Glucose transporter content and glucose uptake in skeletal muscle constructs engineered in vitro. *In vitro cellular & developmental biology. Animal* **39**, 434-439, doi:10.1290/1543-706X(2003)039<0434:GTCAGU>2.0.CO;2 (2003).

147 Strohman, R. C. *et al.* Myogenesis and histogenesis of skeletal muscle on flexible membranes in vitro. *In vitro cellular & developmental biology : journal of the Tissue Culture Association* **26**, 201-208 (1990).

148 Gillies, A. R. & Lieber, R. L. Structure and function of the skeletal muscle extracellular matrix. *Muscle Nerve* **44**, 318-331, doi:10.1002/mus.22094 (2011).

149 Beach, R. L., Rao, J. S. & Festoff, B. W. Extracellular-matrix synthesis by skeletal muscle in culture. Major secreted collagenous proteins of clonal myoblasts. *Biochem J* **225**, 619-627 (1985).

150 Meng, Y. *et al.* Characterization of integrin engagement during defined human embryonic stem cell culture. *FASEB J* **24**, 1056-1065, doi:10.1096/fj.08-126821 (2010).

151 Swasdison, S. & Mayne, R. Formation of highly organized skeletal muscle fibers in vitro. Comparison with muscle development in vivo. *J Cell Sci* **102 (Pt 3)**, 643-652 (1992).

152 Bian, W. & Bursac, N. Engineered skeletal muscle tissue networks with controllable architecture. *Biomaterials* **30**, 1401-1412, doi:10.1016/j.biomaterials.2008.11.015 (2009).

153 Rhim, C. *et al.* Morphology and ultrastructure of differentiating three-dimensional mammalian skeletal muscle in a collagen gel. *Muscle Nerve* **36**, 71-80, doi:10.1002/mus.20788 (2007).

154 Herrick, S., Blanc-Brude, O., Gray, A. & Laurent, G. Fibrinogen. *The international journal of biochemistry & cell biology* **31**, 741-746 (1999).

155 Grassl, E. D., Oegema, T. R. & Tranquillo, R. T. Fibrin as an alternative biopolymer to type-I collagen for the fabrication of a media equivalent. *Journal of biomedical materials research* **60**, 607-612 (2002).

156 Breidenbach, A. P. *et al.* Fibrin gels exhibit improved biological, structural, and mechanical properties compared with collagen gels in cell-based tendon tissue-engineered constructs. *Tissue Eng Part A* **21**, 438-450, doi:10.1089/ten.TEA.2013.0768 (2015).

157 Martino, M. M., Briquez, P. S., Ranga, A., Lutolf, M. P. & Hubbell, J. A. Heparin-binding domain of fibrin(ogen) binds growth factors and promotes tissue repair when incorporated within a synthetic matrix. *Proc Natl Acad Sci U S A* **110**, 4563-4568, doi:10.1073/pnas.1221602110 (2013).

158 Florini, J. R., Ewton, D. Z. & Coolican, S. A. Growth hormone and the insulin-like growth factor system in myogenesis. *Endocrine reviews* **17**, 481-517, doi:10.1210/edrv-17-5-481 (1996).

159 Yablonka-Reuveni, Z., Seger, R. & Rivera, A. J. Fibroblast growth factor promotes recruitment of skeletal muscle satellite cells in young and old rats. *The journal of histochemistry and cytochemistry : official journal of the Histochemistry Society* **47**, 23-42 (1999).

160 Bentzinger, C. F., von Maltzahn, J. & Rudnicki, M. A. Extrinsic regulation of satellite cell specification. *Stem cell research & therapy* **1**, 27, doi:10.1186/scrt27 (2010).

161 Floss, T., Arnold, H. H. & Braun, T. A role for FGF-6 in skeletal muscle regeneration. *Genes & development* **11**, 2040-2051 (1997).

162 Fiore, F., Sebille, A. & Birnbaum, D. Skeletal muscle regeneration is not impaired in Fgf6 -/- mutant mice. *Biochemical and biophysical research communications* **272**, 138-143, doi:10.1006/bbrc.2000.2703 (2000).

163 Armand, A. S. *et al.* Injection of FGF6 accelerates regeneration of the soleus muscle in adult mice. *Biochim Biophys Acta* **1642**, 97-105 (2003).

164 Lefaucheur, J. P. & Sebille, A. Basic fibroblast growth factor promotes in vivo muscle regeneration in murine muscular dystrophy. *Neuroscience letters* **202**, 121-124 (1995).

165 Lam, M. T., Huang, Y. C., Birla, R. K. & Takayama, S. Microfeature guided skeletal muscle tissue engineering for highly organized 3-dimensional free-standing constructs. *Biomaterials* **30**, 1150-1155, doi:10.1016/j.biomaterials.2008.11.014 (2009).

166 Hinds, S., Bian, W., Dennis, R. G. & Bursac, N. The role of extracellular matrix composition in structure and function of bioengineered skeletal muscle. *Biomaterials* **32**, 3575-3583, doi:10.1016/j.biomaterials.2011.01.062 (2011).

167 Mendias, C. L., Marcin, J. E., Calerdon, D. R. & Faulkner, J. A. Contractile properties of EDL and soleus muscles of myostatin-deficient mice. *J Appl Physiol (1985)* **101**, 898-905, doi:10.1152/japplphysiol.00126.2006 (2006).

168 Urbanchek, M. G., Picken, E. B., Kalliainen, L. K. & Kuzon, W. M., Jr. Specific force deficit in skeletal muscles of old rats is partially explained by the existence of denervated muscle fibers. *The journals of gerontology. Series A, Biological sciences and medical sciences* **56**, B191-197 (2001).

169 Close, R. I. Dynamic properties of mammalian skeletal muscles. *Physiol Rev* **52**, 129-197 (1972).

170 Huang, Y. C., Dennis, R. G., Larkin, L. & Baar, K. Rapid formation of functional muscle in vitro using fibrin gels. *J Appl Physiol (1985)* **98**, 706-713, doi:10.1152/japplphysiol.00273.2004 (2005).

171 Dennis, R. G. & Kosnik, P. E., 2nd. Excitability and isometric contractile properties of mammalian skeletal muscle constructs engineered in vitro. *In vitro cellular & developmental biology. Animal* **36**, 327-335, doi:10.1290/1071-2690(2000)036<0327:EAICPO>2.0.CO;2 (2000).

172 Liao, H. & Zhou, G. Q. Development and progress of engineering of skeletal muscle tissue. *Tissue engineering. Part B, Reviews* **15**, 319-331, doi:10.1089/ten.teb.2009.0092 (2009).

173 Yamamoto, Y. *et al.* Functional evaluation of artificial skeletal muscle tissue constructs fabricated by a magnetic force-based tissue engineering technique. *Tissue Eng Part A* **17**, 107-114, doi:10.1089/ten.TEA.2010.0312 (2011).

174 Powell, C. A., Smiley, B. L., Mills, J. & Vandenburgh, H. H. Mechanical stimulation improves tissue-engineered human skeletal muscle. *Am J Physiol Cell Physiol* **283**, C1557-1565, doi:10.1152/ajpcell.00595.2001 (2002).

175 Lovett, M., Lee, K., Edwards, A. & Kaplan, D. L. Vascularization strategies for tissue engineering. *Tissue engineering. Part B, Reviews* **15**, 353-370, doi:10.1089/ten.TEB.2009.0085 (2009).

176 Allen, C. B., Schneider, B. K. & White, C. W. Limitations to oxygen diffusion and equilibration in in vitro cell exposure systems in hyperoxia and hypoxia. *American journal of physiology. Lung cellular and molecular physiology* **281**, L1021-1027 (2001).

177 Cheng, C. S., Davis, B. N., Madden, L., Bursac, N. & Truskey, G. A. Physiology and metabolism of tissue-engineered skeletal muscle. *Exp Biol Med (Maywood)* **239**, 1203-1214, doi:10.1177/1535370214538589 (2014).

178 Chromiak, J. A., Shansky, J., Perrone, C. & Vandenburgh, H. H. Bioreactor perfusion system for the long-term maintenance of tissue-engineered skeletal muscle organoids. *In vitro cellular & developmental biology. Animal* **34**, 694-703, doi:10.1007/s11626-998-0065-2 (1998).

179 Salehi-Nik, N. *et al.* Engineering parameters in bioreactor's design: a critical aspect in tissue engineering. *BioMed research international* **2013**, 762132, doi:10.1155/2013/762132 (2013).

180 Pennisi, C. P., Olesen, C. G., de Zee, M., Rasmussen, J. & Zachar, V. Uniaxial cyclic strain drives assembly and differentiation of skeletal myocytes. *Tissue Eng Part A* **17**, 2543-2550, doi:10.1089/ten.TEA.2011.0089 (2011).

181 Goldspink, D. F. *et al.* Muscle growth in response to mechanical stimuli. *Am J Physiol* **268**, E288-297 (1995).

182 Wilson, S. J. & Harris, A. J. Formation of myotubes in aneural rat muscles. *Dev Biol* **156**, 509-518, doi:10.1006/dbio.1993.1097 (1993).

183 Donnelly, K. *et al.* A novel bioreactor for stimulating skeletal muscle in vitro. *Tissue Eng Part C Methods* **16**, 711-718, doi:10.1089/ten.TEC.2009.0125 (2010).

184 Khodabukus, A., Baehr, L. M., Bodine, S. C. & Baar, K. Role of contraction duration in inducing fast-to-slow contractile and metabolic protein and functional changes in engineered muscle. *J Cell Physiol* **230**, 2489-2497, doi:10.1002/jcp.24985 (2015).

185 Block, N. E., Menick, D. R., Robinson, K. A. & Buse, M. G. Effect of denervation on the expression of two glucose transporter isoforms in rat hindlimb muscle. *J Clin Invest* **88**, 1546-1552, doi:10.1172/JCI115465 (1991).

186 Coderre, L. *et al.* Alteration in the expression of GLUT-1 and GLUT-4 protein and messenger RNA levels in denervated rat muscles. *Endocrinology* **131**, 1821-1825, doi:10.1210/endo.131.4.1396328 (1992).

187 Voytik, S. L., Przyborski, M., Badylak, S. F. & Konieczny, S. F. Differential expression of muscle regulatory factor genes in normal and denervated adult rat hindlimb muscles. *Developmental dynamics : an official publication of the American Association of Anatomists* **198**, 214-224, doi:10.1002/aja.1001980307 (1993).

188 Chen, L. *et al.* The study of myogenin expression in denervated human skeletal muscles. *The Journal of international medical research* **39**, 378-387 (2011).

189 Macpherson, P. C., Wang, X. & Goldman, D. Myogenin regulates denervation-dependent muscle atrophy in mouse soleus muscle. *Journal of cellular biochemistry* **112**, 2149-2159, doi:10.1002/jcb.23136 (2011).

190 Guo, X. F., Gonzalez, M., Stancescu, M., Vandenburgh, H. H. & Hickman, J. J. Neuromuscular junction formation between human stem cell-derived motoneurons and human skeletal muscle in a defined system. *Biomaterials* **32**, 9602-9611, doi:10.1016/j.biomaterials.2011.09.014 (2011).

191 Martin, N. R. *et al.* Neuromuscular Junction Formation in Tissue-Engineered Skeletal Muscle Augments Contractile Function and Improves Cytoskeletal Organization. *Tissue Eng Part A* **21**, 2595-2604, doi:10.1089/ten.TEA.2015.0146 (2015).

192 Lu, Y. *et al.* Recombinant vascular endothelial growth factor secreted from tissue-engineered bioartificial muscles promotes localized angiogenesis. *Circulation* **104**, 594-599 (2001).

193 Levenberg, S. *et al.* Engineering vascularized skeletal muscle tissue. *Nat Biotechnol* **23**, 879-884, doi:10.1038/nbt1109 (2005).

194 Baron, A. D., Brechtel, G., Wallace, P. & Edelman, S. V. Rates and tissue sites of non-insulin- and insulin-mediated glucose uptake in humans. *Am J Physiol* **255**, E769-774, doi:10.1152/ajpendo.1988.255.6.E769 (1988).

195 Bonadonna, R. C. *et al.* Obesity and insulin resistance in humans: a dose-response study. *Metabolism* **39**, 452-459 (1990).

196 DeFronzo, R. A. *et al.* The effect of insulin on the disposal of intravenous glucose. Results from indirect calorimetry and hepatic and femoral venous catheterization. *Diabetes* **30**, 1000-1007 (1981).

197 Al-Khalili, L. *et al.* Insulin action in cultured human skeletal muscle cells during differentiation: assessment of cell surface GLUT4 and GLUT1 content. *Cell Mol Life Sci* **60**, 991-998, doi:10.1007/s00018-003-3001-3 (2003).

198 Ciaraldi, T. P., Abrams, L., Nikoulina, S., Mudaliar, S. & Henry, R. R. Glucose transport in cultured human skeletal muscle cells. Regulation by insulin and glucose in nondiabetic and non-insulin-dependent diabetes mellitus subjects. *J Clin Invest* **96**, 2820-2827, doi:10.1172/JCI118352 (1995).

199 Ciaraldi, T. P. *et al.* Effects of the rapid-acting insulin analog glulisine on cultured human skeletal muscle cells: comparisons with insulin and insulin-like growth factor I. *J Clin Endocrinol Metab* **90**, 5551-5558, doi:10.1210/jc.2005-1007 (2005).

200 Henry, R. R., Abrams, L., Nikoulina, S. & Ciaraldi, T. P. Insulin action and glucose metabolism in nondiabetic control and NIDDM subjects. Comparison using human skeletal muscle cell cultures. *Diabetes* **44**, 936-946 (1995).

201 Sarabia, V., Lam, L., Burdett, E., Leiter, L. A. & Klip, A. Glucose transport in human skeletal muscle cells in culture. Stimulation by insulin and metformin. *J Clin Invest* **90**, 1386-1395, doi:10.1172/JCI116005 (1992).

202 Sarabia, V., Ramlal, T. & Klip, A. Glucose uptake in human and animal muscle cells in culture. *Biochem Cell Biol* **68**, 536-542 (1990).

203 Pampaloni, F., Reynaud, E. G. & Stelzer, E. H. The third dimension bridges the gap between cell culture and live tissue. *Nat Rev Mol Cell Biol* **8**, 839-845, doi:10.1038/nrm2236 (2007).

204 Kraegen, E. W. *et al.* Glucose transporters and in vivo glucose uptake in skeletal and cardiac muscle: fasting, insulin stimulation and immunoisolation studies of GLUT1 and GLUT4. *Biochem J* **295 (Pt 1)**, 287-293 (1993).

205 Stuart, C. A., Wen, G., Gustafson, W. C. & Thompson, E. A. Comparison of GLUT1, GLUT3, and GLUT4 mRNA and the subcellular distribution of their

proteins in normal human muscle. *Metabolism* **49**, 1604-1609, doi:10.1053/meta.2000.18559 (2000).

206 Callahan, Z. J. *et al.* Compensatory responses of the insulin signaling pathway restore muscle glucose uptake following long-term denervation. *Physiological reports* **3**, doi:10.14814/phy2.12359 (2015).

207 Bonadonna, R. C. *et al.* Transmembrane glucose transport in skeletal muscle of patients with non-insulin-dependent diabetes. *J Clin Invest* **92**, 486-494, doi:10.1172/JCI116592 (1993).

208 Andreasson, K., Galuska, D., Thorne, A., Sonnenfeld, T. & Wallberg-Henriksson, H. Decreased insulin-stimulated 3-0-methylglucose transport in in vitro incubated muscle strips from type II diabetic subjects. *Acta physiologica Scandinavica* **142**, 255-260, doi:10.1111/j.1748-1716.1991.tb09154.x (1991).

209 Dohm, G. L. *et al.* An in vitro human muscle preparation suitable for metabolic studies. Decreased insulin stimulation of glucose transport in muscle from morbidly obese and diabetic subjects. *J Clin Invest* **82**, 486-494, doi:10.1172/JCI113622 (1988).

210 Zierath, J. R. *et al.* Effects of glycaemia on glucose transport in isolated skeletal muscle from patients with NIDDM: in vitro reversal of muscular insulin resistance. *Diabetologia* **37**, 270-277 (1994).

211 Zierath, J. R. *et al.* Insulin action on glucose transport and plasma membrane GLUT4 content in skeletal muscle from patients with NIDDM. *Diabetologia* **39**, 1180-1189 (1996).

212 Aas, V. *et al.* Chronic hyperglycemia reduces substrate oxidation and impairs metabolic switching of human myotubes. *Biochim Biophys Acta* **1812**, 94-105, doi:10.1016/j.bbadis.2010.09.014 (2011).

213 Klip, A., Tsakiridis, T., Marette, A. & Ortiz, P. A. Regulation of expression of glucose transporters by glucose: a review of studies in vivo and in cell cultures. *FASEB J* **8**, 43-53 (1994).

214 Ewton, D. Z., Roof, S. L., Magri, K. A., McWade, F. J. & Florini, J. R. IGF-II is more active than IGF-I in stimulating L6A1 myogenesis: greater mitogenic actions of IGF-I delay differentiation. *J Cell Physiol* **161**, 277-284, doi:10.1002/jcp.1041610212 (1994).

215 Schwenk, R. W., Holloway, G. P., Luiken, J. J., Bonen, A. & Glatz, J. F. Fatty acid transport across the cell membrane: regulation by fatty acid transporters. *Prostaglandins, leukotrienes, and essential fatty acids* **82**, 149-154, doi:10.1016/j.plefa.2010.02.029 (2010).

216 Dimopoulos, N., Watson, M., Sakamoto, K. & Hundal, H. S. Differential effects of palmitate and palmitoleate on insulin action and glucose utilization in rat L6 skeletal muscle cells. *Biochem J* **399**, 473-481, doi:10.1042/BJ20060244 (2006).

217 Coll, T. *et al.* Oleate reverses palmitate-induced insulin resistance and inflammation in skeletal muscle cells. *J Biol Chem* **283**, 11107-11116, doi:10.1074/jbc.M708700200 (2008).

218 Hurley, M. S., Flux, C., Salter, A. M. & Brameld, J. M. Effects of fatty acids on skeletal muscle cell differentiation in vitro. *Br J Nutr* **95**, 623-630 (2006).

219 Gaster, M., Poulsen, P., Handberg, A., Schroder, H. D. & Beck-Nielsen, H. Direct evidence of fiber type-dependent GLUT-4 expression in human skeletal muscle. *Am J Physiol Endocrinol Metab* **278**, E910-916 (2000).

220 Gaster, M., Kristensen, S. R., Beck-Nielsen, H. & Schroder, H. D. A cellular model system of differentiated human myotubes. *APMIS* **109**, 735-744 (2001).

221 Booth, F. W. & Thomason, D. B. Molecular and cellular adaptation of muscle in response to exercise: perspectives of various models. *Physiol Rev* **71**, 541-585 (1991).

222 Kubis, H. P., Scheibe, R. J., Meissner, J. D., Hornung, G. & Gros, G. Fast-to-slow transformation and nuclear import/export kinetics of the transcription factor NFATc1 during electrostimulation of rabbit muscle cells in culture. *J Physiol* **541**, 835-847 (2002).

223 Kubis, H. P., Haller, E. A., Wetzel, P. & Gros, G. Adult fast myosin pattern and Ca2+-induced slow myosin pattern in primary skeletal muscle culture. *Proc Natl Acad Sci U S A* **94**, 4205-4210 (1997).

224 Hanke, N. *et al.* Metabolic transformation of rabbit skeletal muscle cells in primary culture in response to low glucose. *Biochim Biophys Acta* **1783**, 813-825, doi:10.1016/j.bbamcr.2007.12.012 (2008).

225 Cheng, C. S., Ran, L., Bursac, N., Kraus, W. E. & Truskey, G. A. Cell Density and Joint microRNA-133a and microRNA-696 Inhibition Enhance Differentiation and Contractile Function of Engineered Human Skeletal Muscle Tissues. *Tissue Eng Part A* **22**, 573-583, doi:10.1089/ten.TEA.2015.0359 (2016).

226 Khodabukus, A. *et al.* Electrical stimulation increases hypertrophy and metabolic flux in tissue-engineered human skeletal muscle. *Biomaterials*, doi:10.1016/j.biomaterials.2018.08.058 (2018).

227 Yamamoto, N. *et al.* Measurement of glucose uptake in cultured cells. *Curr Protoc Pharmacol* **Chapter 12**, Unit 12 14 11-22, doi:10.1002/0471141755.ph1214s55 (2011).

228 Uldry, M., Ibberson, M., Hosokawa, M. & Thorens, B. GLUT2 is a high affinity glucosamine transporter. *FEBS Lett* **524**, 199-203 (2002).

229 Augustin, R. The protein family of glucose transport facilitators: It's not only about glucose after all. *IUBMB Life* **62**, 315-333, doi:10.1002/iub.315 (2010).

230 Taghikhani, M., Lavi, L. W., Woost, P. G. & Griffin, C. C. Kinetics of D-glucose and 2-deoxy-D-glucose transport by Rhodotorula glutinis. *Biochim Biophys Acta* **803**, 278-283 (1984).

231 Owen, M. R., Doran, E. & Halestrap, A. P. Evidence that metformin exerts its anti-diabetic effects through inhibition of complex 1 of the mitochondrial respiratory chain. *Biochem J* **348 Pt 3**, 607-614 (2000).

232 El-Mir, M. Y. *et al.* Dimethylbiguanide inhibits cell respiration via an indirect effect targeted on the respiratory chain complex I. *J Biol Chem* **275**, 223-228 (2000).

233 Khodabukus, A. & Baar, K. Factors That Affect Tissue-Engineered Skeletal Muscle Function and Physiology. *Cells Tissues Organs* **202**, 159-168, doi:10.1159/000446067 (2016).

234 Geer, E. B., Islam, J. & Buettner, C. Mechanisms of glucocorticoid-induced insulin resistance: focus on adipose tissue function and lipid metabolism. *Endocrinol Metab Clin North Am* **43**, 75-102, doi:10.1016/j.ecl.2013.10.005 (2014).

235 Krajcova, A. *et al.* Normalizing glutamine concentration causes mitochondrial uncoupling in an in vitro model of human skeletal muscle. *JPEN J Parenter Enteral Nutr* **39**, 180-189, doi:10.1177/0148607113513801 (2015).

236 Yap, T. A. *et al.* Preclinical pharmacology, antitumor activity, and development of pharmacodynamic markers for the novel, potent AKT inhibitor CCT128930. *Mol Cancer Ther* **10**, 360-371, doi:10.1158/1535-7163.MCT-10-0760 (2011).

237 Raichur, S. *et al.* Histone deacetylase 5 regulates glucose uptake and insulin action in muscle cells. *J Mol Endocrinol* **49**, 203-211, doi:10.1530/JME-12-0095 (2012).

238 Marek, L. *et al.* Histone deacetylase (HDAC) inhibitors with a novel connecting unit linker region reveal a selectivity profile for HDAC4 and HDAC5 with improved activity against chemoresistant cancer cells. *J Med Chem* **56**, 427-436, doi:10.1021/jm301254q (2013).

239 Brown, A. E., Dibnah, B., Fisher, E., Newton, J. L. & Walker, M. Pharmacological activation of AMPK and glucose uptake in cultured human skeletal muscle cells from patients with ME/CFS. *Biosci Rep* **38**, doi:10.1042/BSR20180242 (2018).

240 Popov, D. V. *et al.* AMPK does not play a requisite role in regulation of PPARGC1A gene expression via the alternative promoter in endurance-trained human skeletal muscle. *Exp Physiol* **102**, 366-375, doi:10.1113/EP086074 (2017).

241 Kim, Y. B. *et al.* Troglitazone but not metformin restores insulin-stimulated phosphoinositide 3-kinase activity and increases p110beta protein levels in skeletal muscle of type 2 diabetic subjects. *Diabetes* **51**, 443-448 (2002).

242 Braun, B. *et al.* Impact of metformin on peak aerobic capacity. *Appl Physiol Nutr Metab* **33**, 61-67, doi:10.1139/H07-144 (2008).

243 Das, S. *et al.* Effect of metformin on exercise capacity: A meta-analysis. *Diabetes Res Clin Pract* **144**, 270-278, doi:10.1016/j.diabres.2018.08.022 (2018).

244 Hess, C., Unger, M., Madea, B., Stratmann, B. & Tschoepe, D. Range of therapeutic metformin concentrations in clinical blood samples and comparison to a forensic case with death due to lactic acidosis. *Forensic Sci Int* **286**, 106-112, doi:10.1016/j.forsciint.2018.03.003 (2018).

245 Yki-Jarvinen, H., Young, A. A., Lamkin, C. & Foley, J. E. Kinetics of glucose disposal in whole body and across the forearm in man. *J Clin Invest* **79**, 1713-1719, doi:10.1172/JCI113011 (1987).

246 Richter, E. A., Mikines, K. J., Galbo, H. & Kiens, B. Effect of exercise on insulin action in human skeletal muscle. *J Appl Physiol (1985)* **66**, 876-885, doi:10.1152/jappl.1989.66.2.876 (1989).

247 Nikolic, N. *et al.* Electrical pulse stimulation of cultured human skeletal muscle cells as an in vitro model of exercise. *PLoS One* **7**, e33203, doi:10.1371/journal.pone.0033203 (2012).

248 Aas, V., Torbla, S., Andersen, M. H., Jensen, J. & Rustan, A. C. Electrical stimulation improves insulin responses in a human skeletal muscle cell model of hyperglycemia. *Ann N Y Acad Sci* **967**, 506-515 (2002).

249 Lambernd, S. *et al.* Contractile activity of human skeletal muscle cells prevents insulin resistance by inhibiting pro-inflammatory signalling pathways. *Diabetologia* **55**, 1128-1139, doi:10.1007/s00125-012-2454-z (2012).

250 Feng, Y. Z. *et al.* Myotubes from lean and severely obese subjects with and without type 2 diabetes respond differently to an in vitro model of exercise. *Am J Physiol Cell Physiol* **308**, C548-556, doi:10.1152/ajpcell.00314.2014 (2015).

251 Romanazzo, S. *et al.* Substrate stiffness affects skeletal myoblast differentiation in vitro. *Sci Technol Adv Mater* **13**, 064211, doi:10.1088/1468-6996/13/6/064211 (2012).

252 Gholobova, D. *et al.* Human tissue-engineered skeletal muscle: a novel 3D in vitro model for drug disposition and toxicity after intramuscular injection. *Sci Rep* **8**, 12206, doi:10.1038/s41598-018-30123-3 (2018).

253 Martin, M., Kettmann, R. & Dequiedt, F. Class IIa histone deacetylases: regulating the regulators. *Oncogene* **26**, 5450-5467, doi:10.1038/sj.onc.1210613 (2007).

254 Dressel, U. *et al.* A dynamic role for HDAC7 in MEF2-mediated muscle differentiation. *J Biol Chem* **276**, 17007-17013, doi:10.1074/jbc.M101508200 (2001).

255 McKinsey, T. A., Zhang, C. L., Lu, J. & Olson, E. N. Signal-dependent nuclear export of a histone deacetylase regulates muscle differentiation. *Nature* **408**, 106-111, doi:10.1038/35040593 (2000).

256 Lu, J., McKinsey, T. A., Zhang, C. L. & Olson, E. N. Regulation of skeletal myogenesis by association of the MEF2 transcription factor with class II histone deacetylases. *Mol Cell* **6**, 233-244 (2000).

257 Cohen, T. J. *et al.* HDAC4 regulates muscle fiber type-specific gene expression programs. *Mol Cells* **38**, 343-348, doi:10.14348/molcells.2015.2278 (2015).

258 Gaur, V. *et al.* Disruption of the Class IIa HDAC Corepressor Complex Increases Energy Expenditure and Lipid Oxidation. *Cell Rep* **16**, 2802-2810, doi:10.1016/j.celrep.2016.08.005 (2016).

259 Koutsounas, I., Giaginis, C. & Theocharis, S. Histone deacetylase inhibitors and pancreatic cancer: are there any promising clinical trials? *World J Gastroenterol* **19**, 1173-1181, doi:10.3748/wjg.v19.i8.1173 (2013).

260 Hu, H. *et al.* 4-Phenylbutyric acid increases GLUT4 gene expression through suppression of HDAC5 but not endoplasmic reticulum stress. *Cell Physiol Biochem* **33**, 1899-1910, doi:10.1159/000362967 (2014).

261 Michael, L. F. *et al.* Restoration of insulin-sensitive glucose transporter (GLUT4) gene expression in muscle cells by the transcriptional coactivator PGC-1. *Proc Natl Acad Sci U S A* **98**, 3820-3825, doi:10.1073/pnas.061035098 (2001).

262 Aas, V. *et al.* Are cultured human myotubes far from home? *Cell Tissue Res* **354**, 671-682, doi:10.1007/s00441-013-1655-1 (2013).

263 Zuurveld, J. G., Oosterhof, A., Veerkamp, J. H. & van Moerkerk, H. T. Oxidative metabolism of cultured human skeletal muscle cells in comparison with biopsy material. *Biochim Biophys Acta* **844**, 1-8 (1985).

264 Ghosh, S. & Dhoot, G. K. Evidence for distinct fast and slow myogenic cell lineages in human foetal skeletal muscle. *J Muscle Res Cell Motil* **19**, 431-441 (1998).

265 Stuart, C. A. *et al.* Hexose transporter mRNAs for GLUT4, GLUT5, and GLUT12 predominate in human muscle. *Am J Physiol-Endoc M* **291**, E1067-E1073, doi:10.1152/ajpendo.00250.2006 (2006).

266 Yoon, M. S. The Emerging Role of Branched-Chain Amino Acids in Insulin Resistance and Metabolism. *Nutrients* **8**, doi:10.3390/nu8070405 (2016).

267 Armstrong, M. D. & Stave, U. A study of plasma free amino acid levels. II. Normal values for children and adults. *Metabolism* **22**, 561-569 (1973).

268 Westwood, F. R., Scott, R. C., Marsden, A. M., Bigley, A. & Randall, K. Rosuvastatin: characterization of induced myopathy in the rat. *Toxicol Pathol* **36**, 345-352, doi:10.1177/0192623307311412 (2008).

269 Okada, M. *et al.* Fenofibrate-induced muscular toxicity is associated with a metabolic shift limited to type-1 muscles in rats. *Toxicol Pathol* **37**, 517-520, doi:10.1177/0192623309336151 (2009).

270 Oberbach, A. *et al.* Altered fiber distribution and fiber-specific glycolytic and oxidative enzyme activity in skeletal muscle of patients with type 2 diabetes. *Diabetes Care* **29**, 895-900 (2006).

271 Simoneau, J. A., Colberg, S. R., Thaete, F. L. & Kelley, D. E. Skeletal muscle glycolytic and oxidative enzyme capacities are determinants of insulin sensitivity and muscle composition in obese women. *FASEB J* **9**, 273-278 (1995).

272 Aguer, C. *et al.* Galactose enhances oxidative metabolism and reveals mitochondrial dysfunction in human primary muscle cells. *PLoS One* **6**, e28536, doi:10.1371/journal.pone.0028536 (2011).

273 Trabado, S. *et al.* The human plasma-metabolome: Reference values in 800 French healthy volunteers; impact of cholesterol, gender and age. *PLoS One* **12**, e0173615, doi:10.1371/journal.pone.0173615 (2017).

274 Gladden, L. B. Lactate metabolism: a new paradigm for the third millennium. *J Physiol* **558**, 5-30, doi:10.1113/jphysiol.2003.058701 (2004).

275 Brooks, G. A. Cell-cell and intracellular lactate shuttles. *J Physiol-London* **587**, 5591-5600, doi:10.1113/jphysiol.2009.178350 (2009).

276 Divakaruni, A. S., Paradyse, A., Ferrick, D. A., Murphy, A. N. & Jastroch, M. Analysis and Interpretation of Microplate-Based Oxygen Consumption and pH

Data. *Method Enzymol* **547**, 309-354, doi:10.1016/B978-0-12-801415-8.00016-3 (2014).

277 Gaster, M., Handberg, A., Beck-Nielsen, H. & Schroder, H. D. Glucose transporter expression in human skeletal muscle fibers. *Am J Physiol-Endoc M* **279**, E529-E538 (2000).

278 Haber, R. S., Weinstein, S. P., Oboyle, E. & Morgello, S. Tissue Distribution of the Human Glut3 Glucose Transporter. *Endocrinology* **132**, 2538-2543, doi:DOI 10.1210/en.132.6.2538 (1993).

279 Stuart, C. A. *et al.* GLUT-3 expression in human skeletal muscle. *Am J Physiol-Endoc M* **279**, E855-E861 (2000).

280 Gaster, M., Beck-Nielsen, H. & Schroder, H. D. Regenerating human muscle fibres express GLUT3 protein. *Pflug Arch Eur J Phy* **445**, 105-114, doi:10.1007/s00424-002-0895-9 (2002).

281 Covington, J. D. *et al.* Effect of serial cell passaging in the retention of fiber type and mitochondrial content in primary human myotubes. *Obesity (Silver Spring)* **23**, 2414-2420, doi:10.1002/oby.21192 (2015).

282 Heden, T. D. *et al.* Greater Oxidative Capacity in Primary Myotubes from Endurance-trained Women. *Med Sci Sports Exerc* **49**, 2151-2157, doi:10.1249/MSS.0000000000001352 (2017).

283 Khodabukus, A. & Baar, K. Contractile and metabolic properties of engineered skeletal muscle derived from slow and fast phenotype mouse muscle. *J Cell Physiol* **230**, 1750-1757, doi:10.1002/jcp.24848 (2015).

284 Bennet, W. M., Connacher, A. A., Scrimgeour, C. M., Smith, K. & Rennie, M. J. Increase in anterior tibialis muscle protein synthesis in healthy man during mixed amino acid infusion: studies of incorporation of [1-13C]leucine. *Clin Sci (Lond)* **76**, 447-454 (1989).

285 Wolfson, R. L. & Sabatini, D. M. The Dawn of the Age of Amino Acid Sensors for the mTORC1 Pathway. *Cell Metab* **26**, 301-309, doi:10.1016/j.cmet.2017.07.001 (2017).

286 Dutchak, P. A. *et al.* Loss of a Negative Regulator of mTORC1 Induces Aerobic Glycolysis and Altered Fiber Composition in Skeletal Muscle. *Cell Rep* **23**, 1907-1914, doi:10.1016/j.celrep.2018.04.058 (2018).

287 Saxton, R. A. & Sabatini, D. M. mTOR Signaling in Growth, Metabolism, and Disease. *Cell* **169**, 361-371, doi:10.1016/j.cell.2017.03.035 (2017).

288 Stegink, L. D. *et al.* Plasma Amino-Acid-Concentrations and Amino-Acid Ratios in Normal Adults and Adults Heterozygous for Phenylketonuria Ingesting a Hamburger and Milk Shake Meal. *Am J Clin Nutr* **53**, 670-675 (1991).

289 Stein, W. H. & Moore, S. The free amino acids of human blood plasma. *J Biol Chem* **211**, 915-926 (1954).

290 Ikenoue, T., Hong, S. & Inoki, K. Monitoring mammalian target of rapamycin (mTOR) activity. *Methods Enzymol* **452**, 165-180, doi:10.1016/S0076-6879(08)03611-2 (2009).

291 Civitarese, A. E. *et al.* Calorie restriction increases muscle mitochondrial biogenesis in healthy humans. *PLoS Med* **4**, e76, doi:10.1371/journal.pmed.0040076 (2007).

292 Chomentowski, P. *et al.* Moderate exercise attenuates the loss of skeletal muscle mass that occurs with intentional caloric restriction-induced weight loss in older, overweight to obese adults. *The journals of gerontology. Series A, Biological sciences and medical sciences* **64**, 575-580, doi:10.1093/gerona/glp007 (2009).

293 Cerletti, M., Jang, Y. C., Finley, L. W., Haigis, M. C. & Wagers, A. J. Short-term calorie restriction enhances skeletal muscle stem cell function. *Cell Stem Cell* **10**, 515-519, doi:10.1016/j.stem.2012.04.002 (2012).

294 Edom, F., Mouly, V., Barbet, J. P., Fiszman, M. Y. & Butlerbrowne, G. S. Clones of Human Satellite Cells Can Express in-Vitro Both Fast and Slow Myosin Heavy-Chains. *Dev Biol* **164**, 219-229, doi:DOI 10.1006/dbio.1994.1193 (1994).

295 Monteiro, R. & Azevedo, I. Chronic inflammation in obesity and the metabolic syndrome. *Mediators Inflamm* **2010**, doi:10.1155/2010/289645 (2010).

296 Dandona, P., Aljada, A., Chaudhuri, A., Mohanty, P. & Garg, R. Metabolic syndrome: a comprehensive perspective based on interactions between obesity, diabetes, and inflammation. *Circulation* **111**, 1448-1454, doi:10.1161/01.CIR.0000158483.13093.9D (2005).

297 DeFronzo, R. A. & Tripathy, D. Skeletal muscle insulin resistance is the primary defect in type 2 diabetes. *Diabetes Care* **32 Suppl 2**, S157-163, doi:10.2337/dc09-S302 (2009).

298 Powers, S. K., Lynch, G. S., Murphy, K. T., Reid, M. B. & Zijdewind, I. Disease-Induced Skeletal Muscle Atrophy and Fatigue. *Med Sci Sports Exerc* **48**, 2307-2319, doi:10.1249/MSS.0000000000000975 (2016).

299 Londhe, P. & Guttridge, D. C. Inflammation induced loss of skeletal muscle. *Bone* **80**, 131-142, doi:10.1016/j.bone.2015.03.015 (2015).

300 Martinez, F. O. & Gordon, S. The M1 and M2 paradigm of macrophage activation: time for reassessment. *F1000Prime Rep* **6**, 13, doi:10.12703/P6-13 (2014).

301 Fleetwood, A. J., Lawrence, T., Hamilton, J. A. & Cook, A. D. Granulocyte-macrophage colony-stimulating factor (CSF) and macrophage CSF-dependent macrophage phenotypes display differences in cytokine profiles and transcription factor activities: implications for CSF blockade in inflammation. *J Immunol* **178**, 5245-5252 (2007).

302 Jaguin, M., Houlbert, N., Fardel, O. & Lecureur, V. Polarization profiles of human M-CSF-generated macrophages and comparison of M1-markers in

classically activated macrophages from GM-CSF and M-CSF origin. *Cell Immunol* **281**, 51-61, doi:10.1016/j.cellimm.2013.01.010 (2013).

303 Portevin, D., Gagneux, S., Comas, I. & Young, D. Human macrophage responses to clinical isolates from the Mycobacterium tuberculosis complex discriminate between ancient and modern lineages. *PLoS Pathog* **7**, e1001307, doi:10.1371/journal.ppat.1001307 (2011).

304 Donath, M. Y. & Shoelson, S. E. Type 2 diabetes as an inflammatory disease. *Nat Rev Immunol* **11**, 98-107, doi:10.1038/nri2925 (2011).

305 Varma, V. *et al.* Muscle inflammatory response and insulin resistance: synergistic interaction between macrophages and fatty acids leads to impaired insulin action. *Am J Physiol Endocrinol Metab* **296**, E1300-1310, doi:10.1152/ajpendo.90885.2008 (2009).

306 Cassol, E., Cassetta, L., Rizzi, C., Alfano, M. & Poli, G. M1 and M2a polarization of human monocyte-derived macrophages inhibits HIV-1 replication by distinct mechanisms. *J Immunol* **182**, 6237-6246, doi:10.4049/jimmunol.0803447 (2009).

307 Sonnet, C. *et al.* Human macrophages rescue myoblasts and myotubes from apoptosis through a set of adhesion molecular systems. *J Cell Sci* **119**, 2497-2507, doi:10.1242/jcs.02988 (2006).

308 Chazaud, B. *et al.* Satellite cells attract monocytes and use macrophages as a support to escape apoptosis and enhance muscle growth. *J Cell Biol* **163**, 1133-1143, doi:10.1083/jcb.200212046 (2003).

309 Mantovani, A. *et al.* The chemokine system in diverse forms of macrophage activation and polarization. *Trends Immunol* **25**, 677-686, doi:10.1016/j.it.2004.09.015 (2004).

310 Atri, C., Guerfali, F. Z. & Laouini, D. Role of Human Macrophage Polarization in Inflammation during Infectious Diseases. *Int J Mol Sci* **19**, doi:10.3390/ijms19061801 (2018).

311 Roszer, T. Understanding the Mysterious M2 Macrophage through Activation Markers and Effector Mechanisms. *Mediators Inflamm* **2015**, 816460, doi:10.1155/2015/816460 (2015).

312 Verreck, F. A. *et al.* Human IL-23-producing type 1 macrophages promote but IL-10-producing type 2 macrophages subvert immunity to (myco)bacteria. *Proc Natl Acad Sci U S A* **101**, 4560-4565, doi:10.1073/pnas.0400983101 (2004).

313 Munoz-Canoves, P., Scheele, C., Pedersen, B. K. & Serrano, A. L. Interleukin-6 myokine signaling in skeletal muscle: a double-edged sword? *FEBS J* **280**, 4131-4148, doi:10.1111/febs.12338 (2013).

314 Podbregar, M., Lainscak, M., Prelovsek, O. & Mars, T. Cytokine response of cultured skeletal muscle cells stimulated with proinflammatory factors depends on differentiation stage. *ScientificWorldJournal* **2013**, 617170, doi:10.1155/2013/617170 (2013).

315 Lang, C. H., Silvis, C., Deshpande, N., Nystrom, G. & Frost, R. A. Endotoxin stimulates in vivo expression of inflammatory cytokines tumor necrosis factor alpha, interleukin-1beta, -6, and high-mobility-group protein-1 in skeletal muscle. *Shock* **19**, 538-546, doi:10.1097/01.shk.0000055237.25446.80 (2003).

316 De Rossi, M., Bernasconi, P., Baggi, F., de Waal Malefyt, R. & Mantegazza, R. Cytokines and chemokines are both expressed by human myoblasts: possible relevance for the immune pathogenesis of muscle inflammation. *Int Immunol* **12**, 1329-1335 (2000).

317 Lumeng, C. N., Bodzin, J. L. & Saltiel, A. R. Obesity induces a phenotypic switch in adipose tissue macrophage polarization. *J Clin Invest* **117**, 175-184, doi:10.1172/JCI29881 (2007).

318 Kintscher, U. *et al.* T-lymphocyte infiltration in visceral adipose tissue: a primary event in adipose tissue inflammation and the development of obesity-mediated insulin resistance. *Arterioscler Thromb Vasc Biol* **28**, 1304-1310, doi:10.1161/ATVBAHA.108.165100 (2008).

319 Walsmith, J. & Roubenoff, R. Cachexia in rheumatoid arthritis. *Int J Cardiol* **85**, 89-99 (2002).

320 Londhe, P. & Davie, J. K. Gamma interferon modulates myogenesis through the major histocompatibility complex class II transactivator, CIITA. *Mol Cell Biol* **31**, 2854-2866, doi:10.1128/MCB.05397-11 (2011).

321 Kalovidouris, A. E., Plotkin, Z. & Graesser, D. Interferon-gamma inhibits proliferation, differentiation, and creatine kinase activity of cultured human muscle cells. II. A possible role in myositis. *J Rheumatol* **20**, 1718-1723 (1993).

322 Li, Y. P. & Reid, M. B. NF-kappaB mediates the protein loss induced by TNF-alpha in differentiated skeletal muscle myotubes. *Am J Physiol Regul Integr Comp Physiol* **279**, R1165-1170, doi:10.1152/ajpregu.2000.279.4.R1165 (2000).

323 Vandanmagsar, B. *et al.* The NLRP3 inflammasome instigates obesity-induced inflammation and insulin resistance. *Nat Med* **17**, 179-188, doi:10.1038/nm.2279 (2011).

324 Di Gregorio, G. B. *et al.* Expression of CD68 and macrophage chemoattractant protein-1 genes in human adipose and muscle tissues: association with cytokine expression, insulin resistance, and reduction by pioglitazone. *Diabetes* **54**, 2305-2313 (2005).

325 Esser, N., Legrand-Poels, S., Piette, J., Scheen, A. J. & Paquot, N. Inflammation as a link between obesity, metabolic syndrome and type 2 diabetes. *Diabetes Res Clin Pract* **105**, 141-150, doi:10.1016/j.diabres.2014.04.006 (2014).

326 de Luca, C. & Olefsky, J. M. Inflammation and insulin resistance. *FEBS Lett* **582**, 97-105, doi:10.1016/j.febslet.2007.11.057 (2008).

327 Remels, A. H., Gosker, H. R., Langen, R. C. & Schols, A. M. The mechanisms of cachexia underlying muscle dysfunction in COPD. *J Appl Physiol (1985)* **114**, 1253-1262, doi:10.1152/japplphysiol.00790.2012 (2013).

328 Remels, A. H., Gosker, H. R., Verhees, K. J., Langen, R. C. & Schols, A. M. TNF-alpha-induced NF-kappaB activation stimulates skeletal muscle glycolytic metabolism through activation of HIF-1alpha. *Endocrinology* **156**, 1770-1781, doi:10.1210/en.2014-1591 (2015).

329 Huffman, K. M. *et al.* Molecular alterations in skeletal muscle in rheumatoid arthritis are related to disease activity, physical inactivity, and disability. *Arthritis Res Ther* **19**, 12, doi:10.1186/s13075-016-1215-7 (2017).

330 Ciaraldi, T. P., Carter, L., Mudaliar, S., Kern, P. A. & Henry, R. R. Effects of tumor necrosis factor-alpha on glucose metabolism in cultured human muscle cells from nondiabetic and type 2 diabetic subjects. *Endocrinology* **139**, 4793-4800, doi:10.1210/endo.139.12.6368 (1998).

331 Bedard, S., Marcotte, B. & Marette, A. Cytokines modulate glucose transport in skeletal muscle by inducing the expression of inducible nitric oxide synthase. *Biochem J* **325 (Pt 2)**, 487-493 (1997).

332 Saisho, Y. Metformin and Inflammation: Its Potential Beyond Glucose-lowering Effect. *Endocr Metab Immune Disord Drug Targets* **15**, 196-205 (2015).

333 Sag, D., Carling, D., Stout, R. D. & Suttles, J. Adenosine 5'-monophosphate-activated protein kinase promotes macrophage polarization to an anti-inflammatory functional phenotype. *J Immunol* **181**, 8633-8641 (2008).

334 Long, D. E. *et al.* Metformin to Augment Strength Training Effective Response in Seniors (MASTERS): study protocol for a randomized controlled trial. *Trials* **18**, 192, doi:10.1186/s13063-017-1932-5 (2017).

335 Hall, D. T. *et al.* The AMPK agonist 5-aminoimidazole-4-carboxamide ribonucleotide (AICAR), but not metformin, prevents inflammation-associated cachectic muscle wasting. *EMBO Mol Med* **10**, doi:10.15252/emmm.201708307 (2018).

336 van Diepen, J. A., Berbee, J. F., Havekes, L. M. & Rensen, P. C. Interactions between inflammation and lipid metabolism: relevance for efficacy of anti-inflammatory drugs in the treatment of atherosclerosis. *Atherosclerosis* **228**, 306-315, doi:10.1016/j.atherosclerosis.2013.02.028 (2013).

337 Kopp, E. & Ghosh, S. Inhibition of NF-kappa B by sodium salicylate and aspirin. *Science* **265**, 956-959 (1994).

338 Phillips, T. & Leeuwenburgh, C. Muscle fiber specific apoptosis and TNF-alpha signaling in sarcopenia are attenuated by life-long calorie restriction. *FASEB J* **19**, 668-670, doi:10.1096/fj.04-2870fje (2005).

Biography

Megan Elizabeth Kondash earned a Bachelor of Science degree in Chemical Engineering from the University of Kansas in May of 2012, graduating with highest distinction. In November of 2017, she received her Master of Science degree in Biomedical Engineering from Duke University. She received a National Science Foundation Graduate Research Fellowship in 2012, and during her time at Duke she was awarded honorable mention for TA of the year in 2016. Her publications include:

1. Zhang, X., Hong, S., Yen, R., **Kondash, M.**, Fernandez, C.E., Truskey, G.A. A system to monitor statin-induced myopathy in individual engineered skeletal muscle myobundles. Lab Chip. 2018;18:2787-2796.
2. **Kondash, M.E.**, Davis, B.N.J., Truskey, G.A. 2017. Optimizing 3D Models of Engineered Skeletal Muscle. Engineering 3D Tissue Test Systems. K.J.L. Burg, D. Dreau and T. Burg. Boca Raton, FL, CRC Press, 321-350 doi: 10.1201/9781315118260-19.
3. Boularaoui, S.M., Abdel-Raouf, K.M.A., Alwahab, N.S.A., **Kondash, M.E.**, Truskey, G.A., Teo, J.C.M., and Christoforou, N. 2017. Efficient transdifferentiation of human dermal fibroblasts into skeletal muscle. J Tissue Eng Regen Med, doi: 10.1002/term.2415.

4. Mellott A.J., **Godsey M.E.**, Shinogle H.E., Moore D.S., Forrest M.L., Detamore M.S. Improving viability and transfection efficiency with human umbilical cord wharton's jelly cells through use of a ROCK inhibitor. Cell Reprogram. 2014;16:91-7.
5. White J.C., **Godsey M.E.**, Bhatia S.R. Perfluorocarbons enhance oxygen transport in alginate-based hydrogels. Polymers for Advanced Technologies. 2014;25:1242-6.
6. **Godsey M.E.**, Suryaprakash S., Leong K.W. Materials innovation for co-delivery of diverse therapeutic cargos. RSC Adv. 2013;3:24794-811.